ERDC/CHL TR-24-12

U.S. ARMY

US Army Corps of Engineers®

ERDC

Coastal and Hydraulics Laboratory

Statistical Analysis of Storm Surge and Seiche Hazards for Lake Erie

Efrain Ramos-Santiago, Norberto C. Nadal-Caraballo, Fabian Garcia-Moreno, Luke A. Aucoin, Meredith L. Carr, Madison C. Yawn, and Jeffrey A. Melby

May 2024

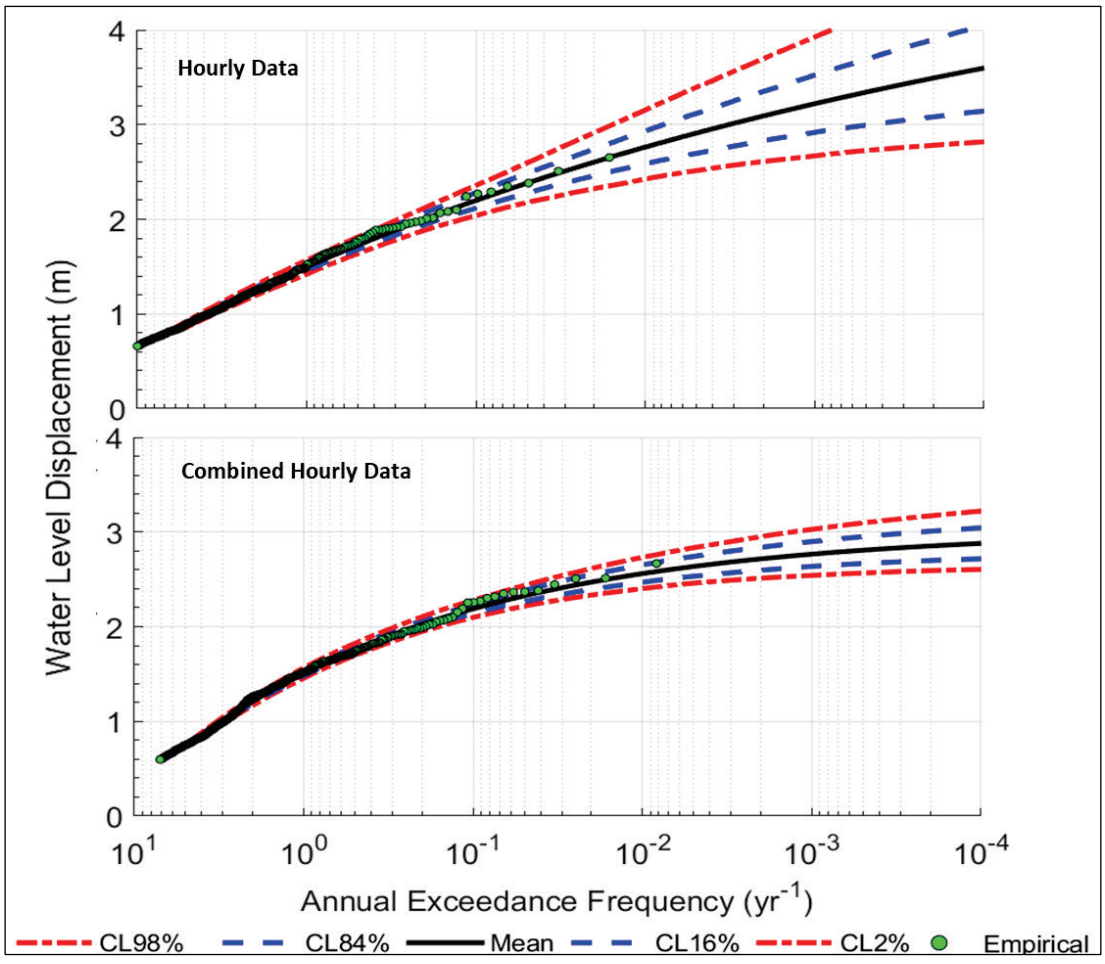

The US Army Engineer Research and Development Center (ERDC) solves the nation's toughest engineering and environmental challenges. ERDC develops innovative solutions in civil and military engineering, geospatial sciences, water resources, and environmental sciences for the Army, the Department of Defense, civilian agencies, and our nation's public good. Find out more at www.erdc.usace.army.mil.

To search for other technical reports published by ERDC, visit the ERDC online library at https://erdclibrary.on.worldcat.org/discovery.

ERDC/CHL TR-24-12
May 2024

Statistical Analysis of Storm Surge and Seiche Hazards for Lake Erie

Efrain Ramos-Santiago, Norberto C. Nadal-Caraballo, Fabian Garcia-Moreno, Luke A. Aucoin, Meredith L. Carr, Madison C. Yawn, and Jeffrey A. Melby

US Army Engineer Research and Development Center (ERDC)
Coastal and Hydraulics Laboratory (CHL)
3909 Halls Ferry Road
Vicksburg, MS 39180-6199

Final Technical Report (TR)

Prepared for US Army Corps of Engineers (USACE)
Detroit District
477 Michigan Ave.
Detroit, MI 48226

Under Labor Charge Code

Abstract

Storm surge and seiche events are generally forced by severe storms, initially resulting in a wind-driven super elevation of water level on one or more sides of a lake (surge) followed by a rebound and periodic oscillation of water levels between opposing sides of the lake (seiche). These events have caused flooding along Lake Erie and significant damages to coastal communities and infrastructure. This study builds upon statistical analysis methods initially developed for the 2012 federal interagency Great Lakes Coastal Flood Study. Using the Coastal Hazards System's stochastic Storm Simulation (StormSim) suite of tools, including the Probabilistic Simulation Technique (PST), and regional frequency model, historical extreme events were assessed in a local frequency analysis and a regional frequency analysis to quantify the annual exceedance frequency (AEF) of WLD events specific to Lake Erie. The objective of this study was to quantify AEFs of storm surge and seiche hazards to provide a better understanding of these events to aid flood mitigation and risk reduction for lakeside properties.

Contents

Figures and Tables

Figures

Tables

Preface

The study summarized in this report was performed to quantify storm surge and seiche hazards in Lake Erie. The study was funded by the US Army Corps of Engineers (USACE), Detroit District, under a Labor Charge Code. The technical monitor for the Detroit District was Mr. Gregory M. Mausolf, project manager.

This work was performed by the Harbors, Entrances, and Structures Branch of the Navigation Division, US Army Engineer Research and Development Center (ERDC), Coastal and Hydraulics Laboratory (CHL). At the time of publication of this report, Mr. Chad R. Bounds was chief, Harbors, Entrances, and Structures Branch; Ms. Patricia M. Tolley was acting chief, Navigation Division; and Dr. Julie D. Rosati was the technical director for Flood and Coastal Risk Management Research and Development. The deputy director of ERDC-CHL was Mr. Keith Flowers, and the director was Dr. Ty V. Wamsley.

COL Christian Patterson was commander of ERDC, and Dr. David W. Pittman was the director.

1 Introduction

1.1 Background

The Great Lakes region, including Lake Erie, is subject to coastal flooding from coastal hazards, such as storm surge, seiche, waves, and ice flows, due to severe weather events and lake levels. As discussed by Melby et al. (2012), high winds from storm events blowing across the surface of a lake can generate extreme wave heights and send water toward the shoreline, causing a temporary super elevation of the lake's water level, known as *storm surge*. When storm surge is observed on one side of a lake, it is usually concurrent with the setdown or lowering of lake levels on the opposite side (Figure 1). This instability in the lake surface is followed by a rebound and a subsequent long-period oscillation of the lake water level, called a *seiche*. This oscillation is often colloquially referred to as the *bathtub effect* (Ohio DPS 2019). More specifically, a seiche is defined as a standing wave formed in an enclosed or semi-enclosed body of water, such as a lake, when strong winds and rapid changes in atmospheric pressure push water from one end of the lake to the other (NOAA 2021). When the wind stops, the water rebounds to the other side of the lake, and the back-and-forth oscillation continues for hours, or even days, as the water attempts to reach equilibrium.

In the Great Lakes, seiche events tend to exhibit relatively short durations and are generally not of concern for the statistical analysis of extreme water levels. This is because seiche levels are of lesser magnitude than the initial storm surge levels and are not accompanied by the extreme wave heights that are coincident with storm surge (Melby et al. 2012). However, Lake Erie has a history of experiencing significant seiche events, particularly when high winds flow southwest to northeast along the lake's long axis. As far back as 1844, a 6.7 m* (22 ft) seiche was noted that breached a 4.3 m (14 ft) high sea wall, causing significant damage to life and property (NOAA 2021). Events that occurred in the 1940s recorded waves ranging from 1.8 to 6.1 m (6 to 20 ft) high (Ohio DPS 2019). More recently, a 3.7 to 4.9 m (12 to 16 ft) seiche was recorded in 2008 that caused flooding in Buffalo, New York (NOAA 2021). The historical effects of this hazard in the

* For a full list of the spelled-out forms of the units of measure used in this document and their conversions, please refer to *US Government Publishing Office Style Manual*, 31st ed. (Washington, DC: US Government Publishing Office, 2016), 248–252 and 345–347, https://www.govinfo.gov/content/pkg/GPO-STYLEMANUAL-2016/pdf/GPO-STYLEMANUAL-2016.pdf.

region demonstrate the importance of understanding and assessing the risks related to these events to prepare for potential flooding.

Figure 1. Seiche event in Lake Erie during the storm of 15 November 2020. (Inset map adapted from USGS, n.d.)

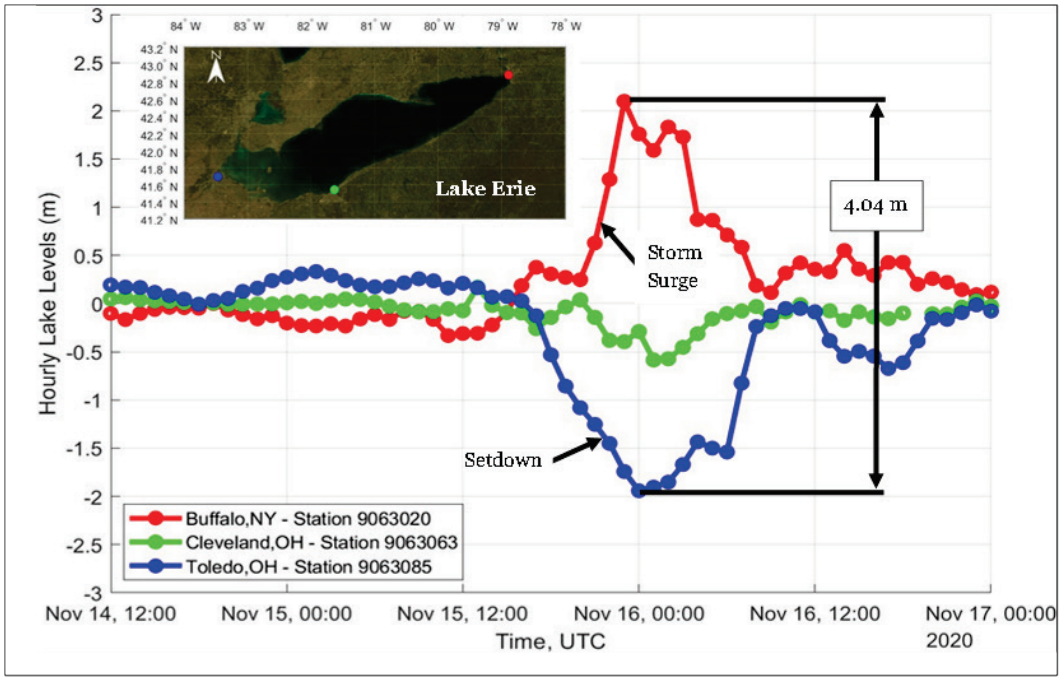

1.2 Objectives

The US Army Engineer Research and Development Center (ERDC), Coastal and Hydraulics Laboratory (CHL), conducted a statistical analysis of available water-level observations in Lake Erie. Specifically, this study sought to quantify storm hazards in isolation from lake levels and to improve such estimates by applying local and regional frequency methods.

1.3 Approach

ERDC-CHL approached this study using progressively more complex methods, each of which provided additional information to better define seiche hazards and increase the certainty of the hazard estimates. First, a spectral analysis was conducted on hourly observations from 14 Lake Erie water-level gauge stations with record lengths of 30 years or more. Spectral analysis was used to identify and isolate specific events based on known physical characteristics. In the spectral analysis, seiche events were identified and isolated at known wave frequencies. However, this effort resulted in multiple sets of potential seiche events and, consequently,

multiple independent hazard curves (i.e., frequency distributions) that did not necessarily prove useful.

Historical water-level data captured not only the magnitude of seiche events but also those of storm surge and other physical hydrodynamic phenomena common to the region. In practice, when examining water-level observations, it is not feasible to completely differentiate between storm surge and seiche events. For a seiche event to occur, it must first be initiated by a storm surge or a similar abnormal rise of water levels elsewhere within the lake. Therefore, this study employed the concept of *water-level displacement* (WLD) that is frequently used by federal agencies, including NOAA. WLD is defined herein as a transient deviation from the lake level at the time of the event, regardless of whether the WLD quantity being identified belongs to the incipient buildup of water (e.g., storm surge) or to the subsequent periodic oscillation of the lake surface (i.e., seiche).

This study builds upon statistical analysis methods initially developed for the 2012 federal interagency Great Lakes Coastal Flood Study (GLCFS; Nadal-Caraballo et al. 2012). Using the Coastal Hazards System's (CHS; https://chs.erdc.dren.mil) stochastic Storm Simulation (StormSim) suite of tools, including the Probabilistic Simulation Technique (PST; formerly Stochastic Storm Simulation, SST), and a regional frequency model (RFM), historical extreme events were assessed in both a local frequency analysis (LFA) and a regional frequency analysis (RFA) to quantify the annual exceedance frequency (AEF) of WLD events specific to Lake Erie. Another objective of this study was to quantify storm hazards in isolation from lake levels. Quantifying WLD hazards independently from lake levels permits the superposition of WLD hazard curves on different lake levels for use in both subannual and long-term risk assessments and in the planning and designing of coastal storm risk management alternatives.

2 Methodology

This section describes the initial approach used to identify and isolate seiche events and the subsequent quantification of WLD hazards in Lake Erie. First, the data used in the study, including sources, frequency, and location, are described. The next subsection covers the established criteria for gauge data selection and the detrending of selected datasets. This is followed by a discussion of the power spectral density (PSD) and filtering process used to isolate seiche events and the approaches used for completing the LFA and RFA.

2.1 Data

The initial analysis used hourly water-level observations from 14 water-level gauge stations with record lengths greater than 30 years located on the perimeter of Lake Erie (Table 1, Figure 2, and Figure 3). NOAA's Center for Operational Oceanographic Products and Services (CO-OPS) maintains the seven gauge stations on the US coastline. Corresponding datasets were retrieved from the "Tides and Currents" website (CO-OPS, n.d.). Data for the seven stations located along the Canadian coastline were retrieved from the Government of Canada's "Marine Environmental Data" (Fisheries and Oceans Canada, n.d.).

The second part of this study considered 11 additional gauge stations that record hourly and shorter record lengths. The RFM was further characterized by including select monthly mean gauge data because some monthly datasets had longer periods of record. These monthly mean data were used to identify potential peak events that occurred outside the period of record or during missing periods of the hourly gauge data. Data recorded until March 2021 were used in these analyses.

A previous interagency study sponsored by FEMA and the US Army Corps of Engineers (USACE; RAMPP 2012) conducted hydrodynamic simulations in Lake Erie using the Advanced Circulation (ADCIRC) model. This study provided virtual water-level observations for 154 storms at 2,202 save points across the region (Figure 4). Hydrodynamic model simulations for storms during the period of 1960 to 2009 used a 15 min temporal resolution. However, model output was only provided for the period of storm-induced hydrographs, resulting in long temporal discontinuities between simulated events. Though the ADCIRC model did not account for

convective events, the model output was used to strengthen the information in the frequency analysis by taking advantage of its temporal and spatial resolutions.

Table 1. Description of water-level gauge stations available around Lake Erie.

Station		Location (Decimal Degrees)		Country	Record Length (Years)
Number	Name	Longitude	Latitude		
11995	Amherstburg, ON	−83.1140	42.1444	Canada	57.6
12005	Bar Point, ON	−83.1150	42.0617		59.1
12065	Kingsville, ON	−82.7348	42.0269		59.1
12120	Point Pelee, ON	−82.5349	41.9666		59.1
12122	Pelee Point East, ON	−82.5072	41.9183		59.1
12250	Erieau, ON	−81.9146	42.2602		59.4
12400	Port Stanley, ON	−81.2137	42.6579		56.4
12710	Port Dover, ON	−80.2015	42.7813		61.3
12865	Port Colborne, ON	−79.2529	42.8744		61.3
9063020	Buffalo, NY	−78.8905	42.8774	United States	61.3
9063028	Sturgeon Point, NY	−79.0473	42.6913		61.3
9063029	Dunkirk, NY	−79.3363	42.4887		0.6
9063032	Barcelona, NY	−79.5936	42.3428		59.1
9063038	Erie, Lake Erie, PA	−80.0925	42.1539		61.3
9063048	Ashtabula, NY	−80.7981	41.9004		0.6
9063053	Fairport, OH	−81.2811	41.7598		45.7
9063063	Cleveland, OH	−81.6355	41.5409		51.2
9063069	Lorain, OH	−82.1753	41.4693		59.1
9063075	Old Woman Creek, NERRS, OH	−82.5144	41.3826		0.4
9063079	Marblehead, OH	−82.7314	41.5436		59.1
9063091	Cooley Creek, Lake Erie, OH	−83.2842	41.6730		0.4
9063085	Toledo, OH	−83.4723	41.6936		54.9
9063087	Monroe, MI	−83.3617	41.8983		59.1
9063090	Fermi Power Plant, MI	−83.2570	41.9600		59.4
9044020	Gibraltar, MI	−83.1867	42.0917		59.4

Figure 2. Data availability for each water-level gauge station listed in Table 1.

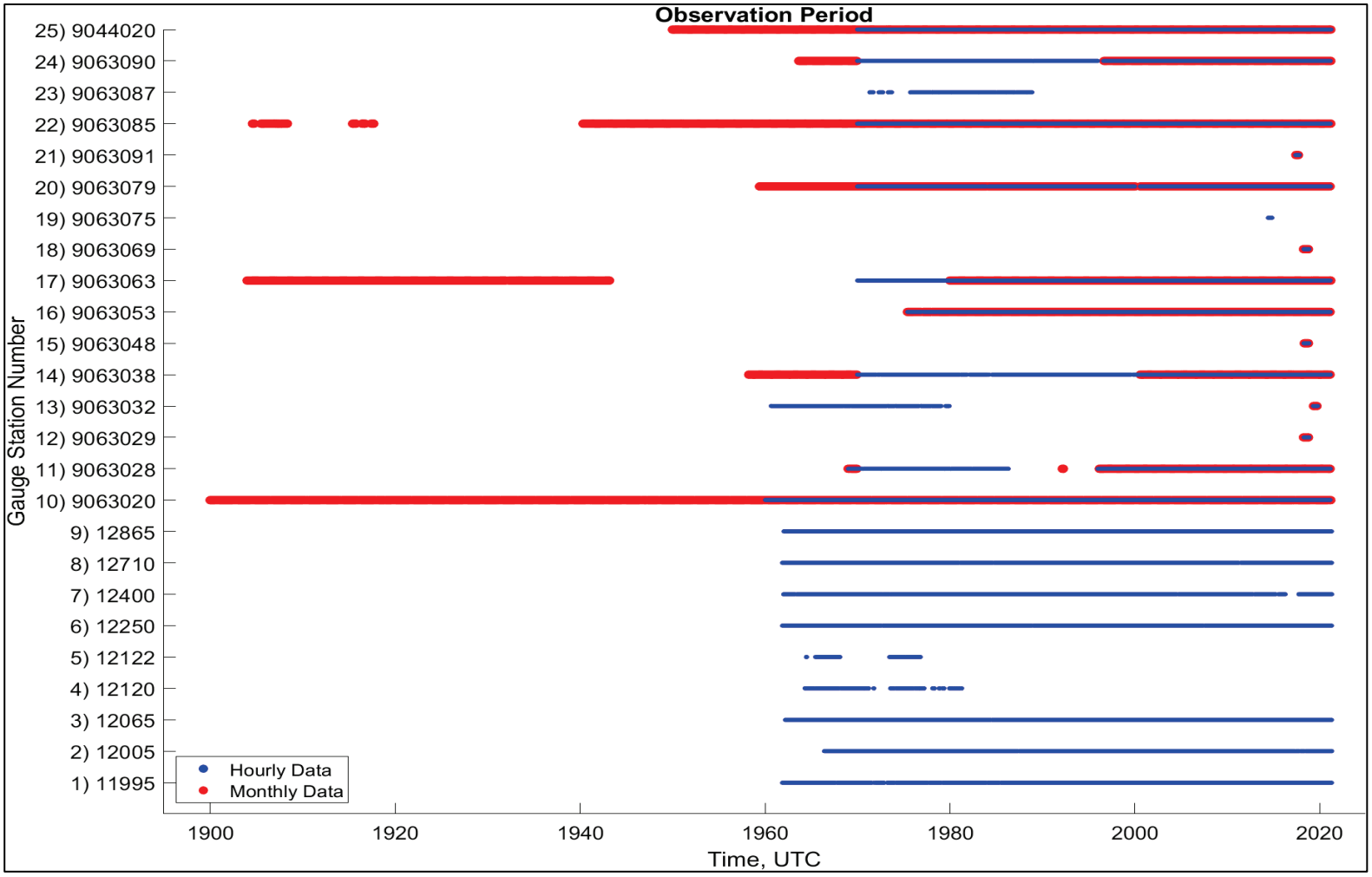

Figure 3. Location of gauge stations listed in Table 1. (Map adapted from USGS, n.d.)

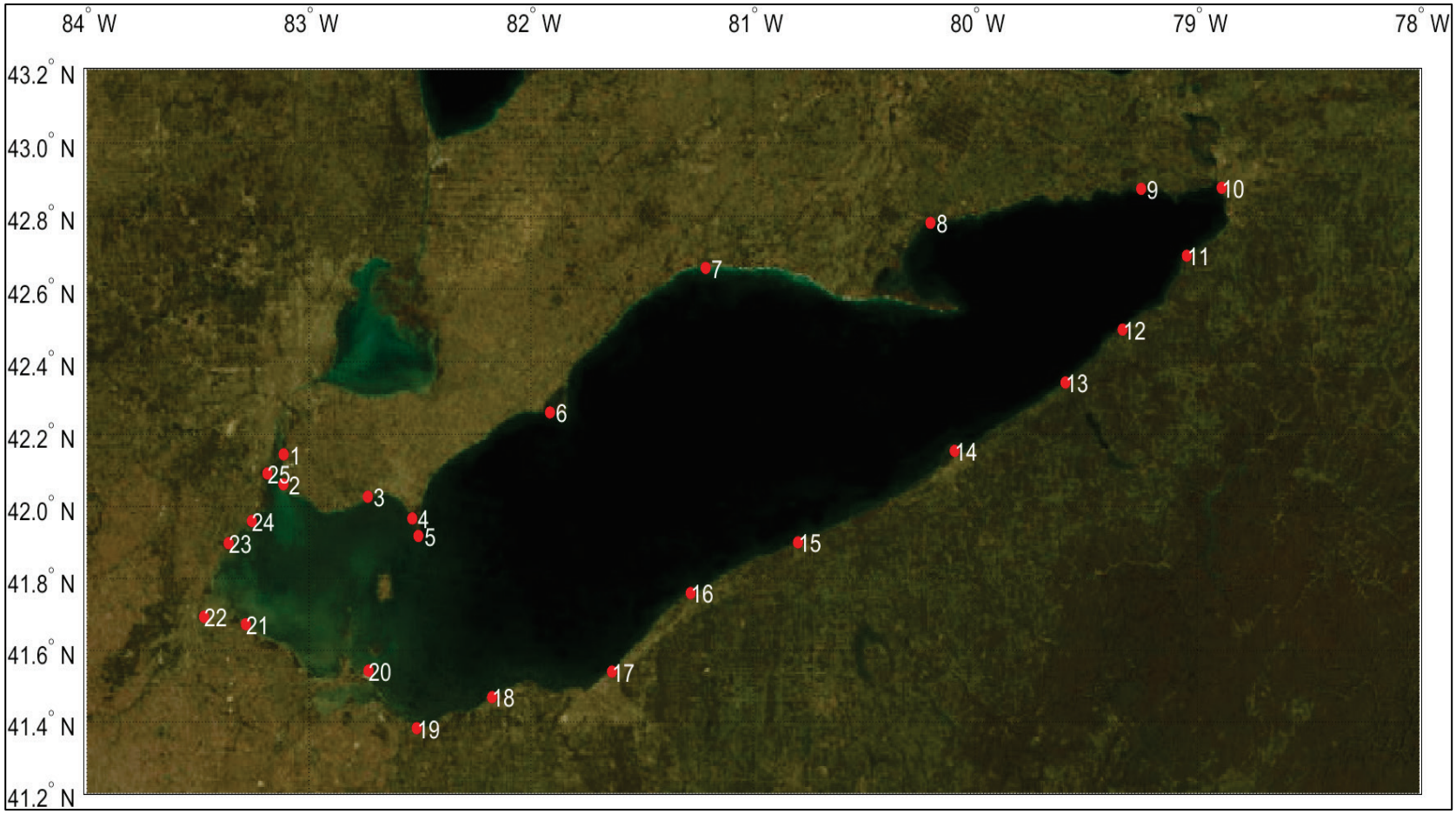

Figure 4. Advanced Circulation (ADCIRC) model save points available around Lake Erie from a previous FEMA–US Army Corps of Engineers (USACE) study (RAMPP 2012). (Map data: Google, Landsat / Copernicus, NOAA 2013.)

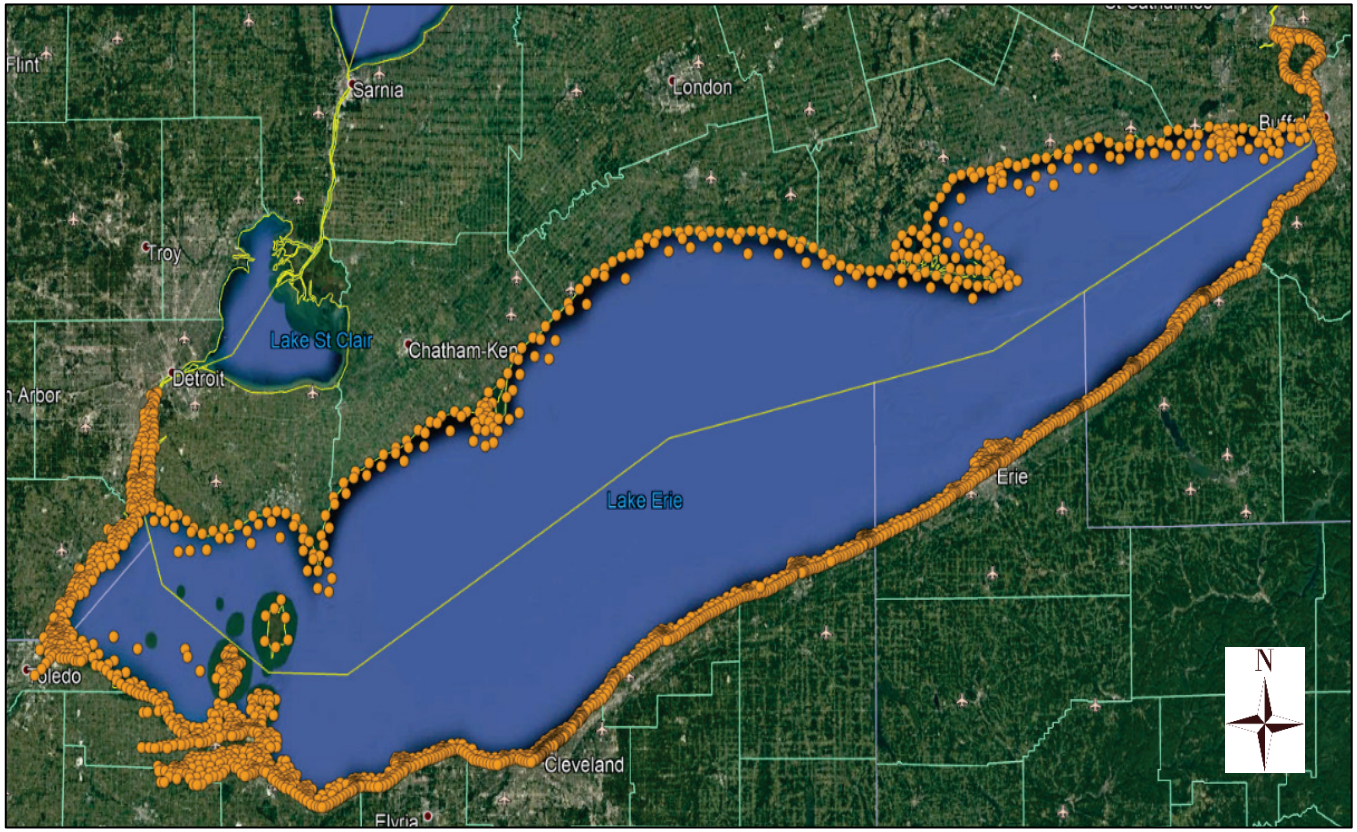

2.2 Water-Level Displacement (WLD)

Lake Erie experiences extreme events other than storm surge and seiche forced by different physical phenomena. Seasonal variabilities of the mean lake level (MLL) also influence the occurrence and effect of hazards. The observed data, in the form of lake levels, therefore represent a mixed storm population that cannot easily be filtered due to the complication of antecedent water levels (similar to prevailing sea state on the coast or base flow in a river). To address the issue of seasonal or varied antecedent water levels, this study translated the historical and simulated records in terms of WLDs. As the variable of interest for this study, the WLD (η_{WLD}) was defined here as the difference between observed values (η) and the average trend ($\bar{\eta}$), or MLL (Figure 5), as follows:

$$\eta_{WLD} = \eta - \bar{\eta}. \quad (1)$$

Figure 5. Computation of water-level displacement (WLD) using Center for Operational Oceanographic Products and Services (CO-OPS) gauge station observations at Toledo, Ohio.

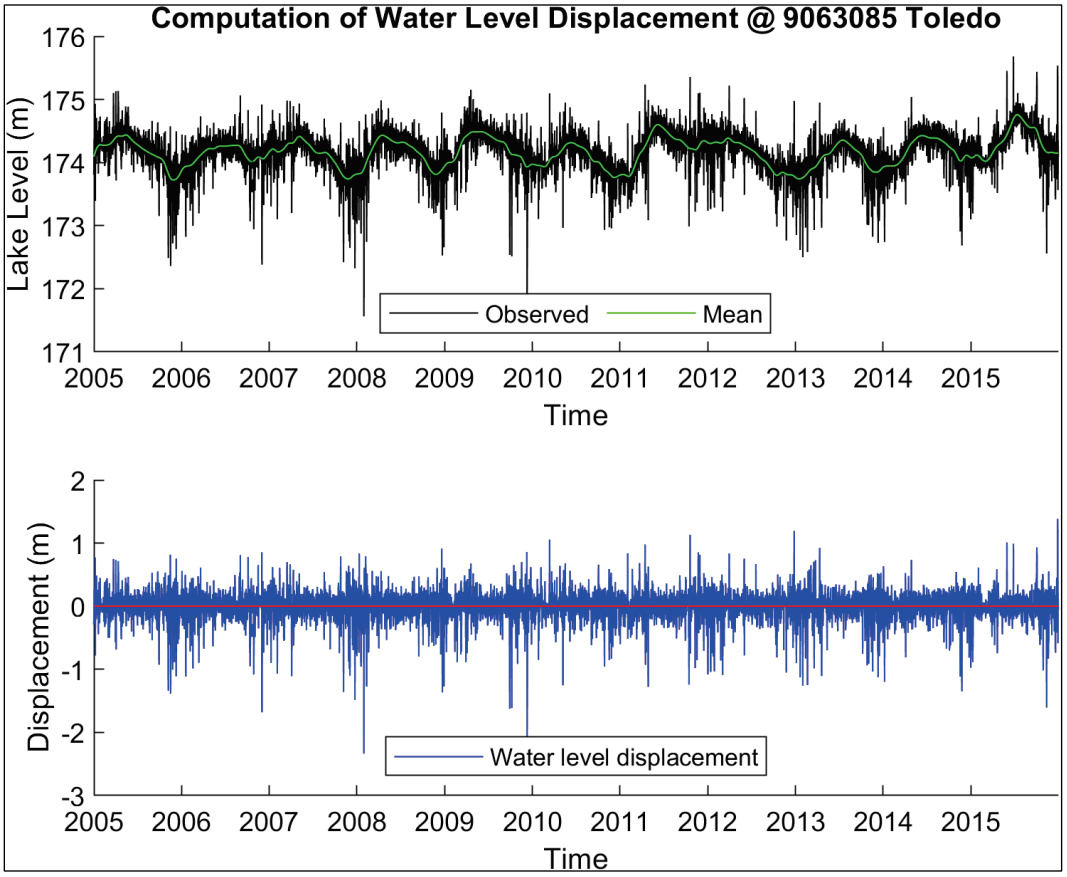

The current study computed the MLL (green line) by applying a 30-day Gaussian window filter (i.e., moving average) to the observed data and assuming independence between WLD events and MLL. Additional research would be needed to characterize any possible minor relationship and its effect on the hazard.

As well as providing a way to allow for mixed storm population filtering, characterizing the risk of flooding in terms of WLD provides additional utility when assessing the risks associated with storm surge and seiche events. For example, during times when MLLs are low on Lake Erie (typically in the winter), the flooding hazard from oscillating water due to WLD events is very low. However, when MLLs are high (e.g., in spring), wind-driven events may cause a large increase in WLD, raising the observed water above that MLL and causing a much higher risk of flooding. Conducting the hazard analysis in terms of WLD allows the results to be used for any MLL that is being observed on Lake Erie (Figure 6).

Figure 6. Sketch of a shoreline with water levels shown in reference to a gauge datum. Lake or gauge water level, mean lake level (MLL), and WLD are shown.

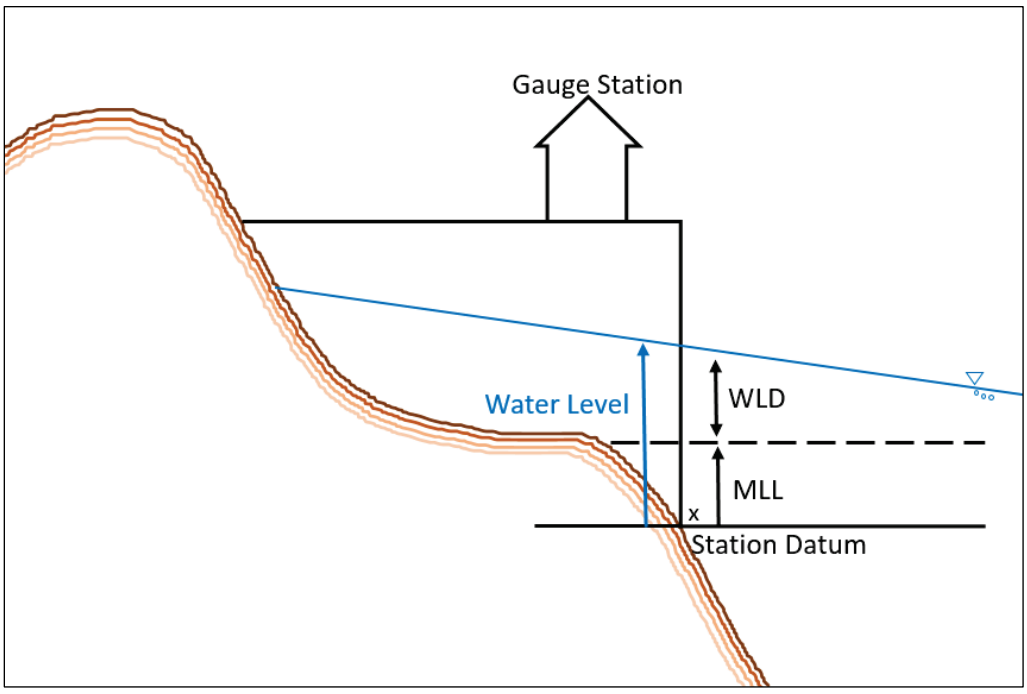

The FEMA study (RAMPP 2012) used an initial lake level as input to the hydrodynamic model for each storm. Water elevations at each of 2,202 save points were recorded as deviations from that initial lake level. To

convert to WLD, the initial lake levels were subtracted from the water elevations for each storm hydrograph.

2.3 Spectral Analysis

A spectral analysis was conducted on the WLD data to identify and separate any potential seiche events. This analysis involved computing the power spectrum for Lake Erie and analyzing the specific frequencies linked to seiche events. Farhadzadeh (2017) studied the low-frequency motion of Lake Erie water levels for both ice-free and ice-covered lake conditions. In the study, periods of free oscillation modes (e.g., 1.7, 2.6, 4.1, and 5.8 cycles per day [CPD]) were computed by analytically solving the equations of motion and continuity for long-standing waves using linear wave theory (Dean and Dalrymple 1991). The analytical results were verified by computing the power spectrum (Figure 7), which exhibited very persistent peaks at the same frequencies as the analytical results. These frequencies served as the foundation for isolating the seiche contribution to the overall WLD. The power spectrum (S_{xx}) is the Fourier transform of the autocorrelation function (R_{xx}) of a random stationary signal, $x(t)$:

$$S_{xx}(f) = \int_{-\infty}^{\infty} R_{xx}(\tau) e^{-2\pi i f \tau} \, d\tau, \tag{2}$$

$$R_{xx}(\tau) = E[x(t)x(t+\tau)] = \int_{-\infty}^{\infty} S_{xx}(f) e^{2\pi i f \tau} df. \tag{3}$$

Figure 7. Power spectrum for selected lake-level gauges with highlighted seiche mode frequencies (*black boxes*).

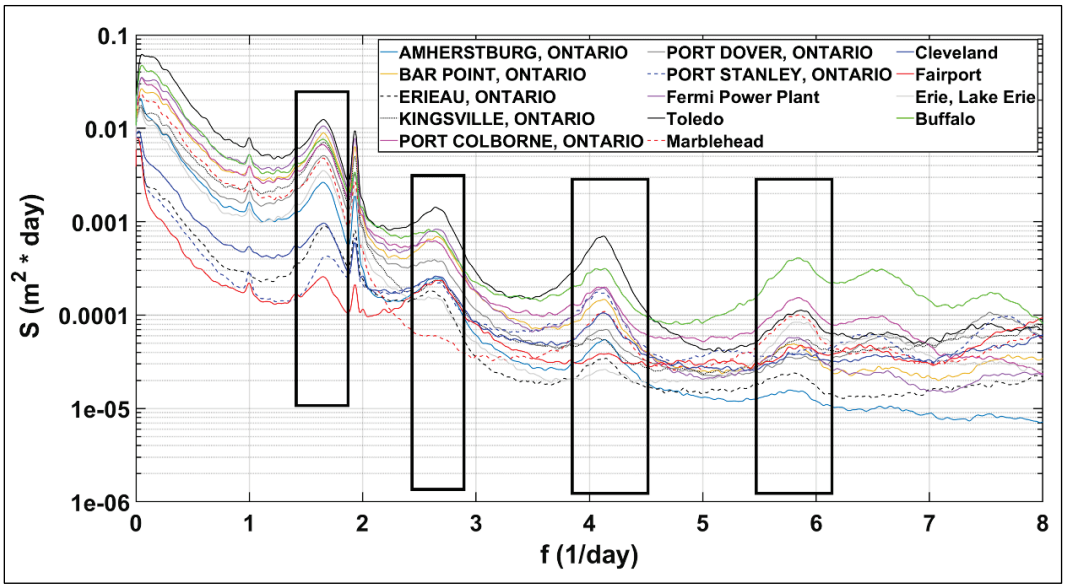

Upon computing the power spectrum, a digital filter was designed using MATLAB's filter designer app (Figure 8). The digital filter designed was an IIR (infinite impulse response) Butterworth filter of order 10 (N) with frequency bounds of Fc1 and Fc2 (Table 2) and a sampling frequency (Fs) of 1 hour. The power gain of an analog Butterworth low-pass filter is expressed as

$$|H_B(j\omega)|^2 = \frac{1}{1+\left(\frac{\omega}{\omega_c}\right)^{2N}}, \tag{4}$$

where ω_c is the cutoff frequency, N is the filter order, and the subscript B indicates the Butterworth transfer function. MATLAB's internal routine utilized state-space transformation and bilinear transformation (with frequency prewarping) to transform the low-pass filter into a band-pass filter (MathWorks 2021). The cutoff frequency was fixed at 3 dB.

Figure 8. MATLAB Filter Designer application user interface.

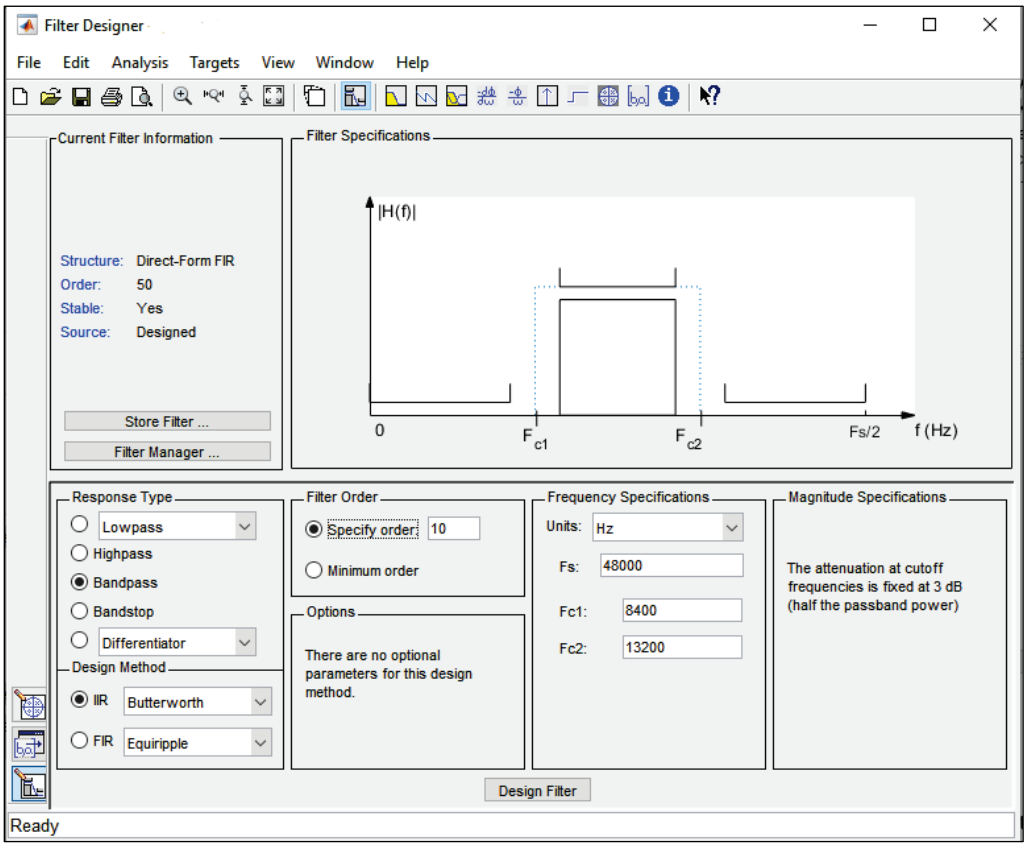

The frequency bounds (Fc1 and Fc2; Table 2) were determined based on two contexts: (1) to comprehend the individual contributions of WLD for each seiching mode (Filter Identifications [IDs] 1–4), and (2) to

comprehend the contribution of WLD from all seiching modes combined (Filter ID 5). The results of the filtering process were subsequently transformed back into the time domain using the inverse Fourier transform to acquire a WLD signal.

Table 2. Filtering methods used in the spectral analysis.

Filter ID	Lower Frequency Limit (CPD, Fc1)	Higher Frequency Limit (CPD, Fc2)
1	1.5367	1.7469
2	2.4886	2.7536
3	3.9736	4.2637
4	5.6122	5.940
5	1.099	6.2

2.4 Local Frequency Analysis (LFA)

This study builds upon statistical analysis methods initially developed for the 2012 GLCFS (Nadal-Caraballo et al. 2012). The CHS stochastic StormSim tool, specifically the PST, was used to conduct LFA to quantify the AEF of WLD events in Lake Erie.

To quantify the probability of storm surge and seiche events, a statistical extreme value analysis, or LFA, was conducted on the WLD. Sampling approaches that can be used to analyze water-level frequency include block maximum series (e.g., annual maximum series) and partial duration series (PDS; i.e., peaks-over-threshold, POT). The POT method is carried out by selecting only independent and identically distributed peaks to avoid counting multiple peaks from a single storm as unique events. A statistical approach based on POT data, known as the empirical simulation technique (EST), was developed by ERDC-CHL in the 1990s (Scheffner et al. 1999). The EST is limited due to its application of nonparametric methods (Borgman 2004), which results in the implementation of splines to complete the fit of low-frequency tails.

However, the CHS StormSim-PST tool developed by ERDC-CHL addresses the limitations of the univariate version of EST because StormSim-PST fits a generalized Pareto distribution (GPD) to complete the low-frequency tail. Described as a bootstrap-based methodology, StormSim-PST utilizes observations or simulations from extreme events, in the form of a POT, as the training set from which to simulate multiple sequences of storm activity and associated responses.

According to extreme value theory (Coles 2001), POT data at the extreme values fit well to a GPD. One challenge of using the POT method is setting an appropriate threshold for fitting the GPD. A large threshold will result in few data points to model the tail of the distribution correctly, but a small threshold will include too many values, producing a high bias. This theory motivated the selection of the GPD for implementation in StormSim-PST. Also, StormSim-PST objectively selects the GPD threshold parameter by employing a mean residual life (MRL) automated threshold detection method (Langousis et al. 2016). The algorithm for the MRL method is as follows:

a. The PDS dataset, X, is sorted in ascending order and used as the initial set of values for the threshold θ.

b. For a given θ, a sample u is defined containing all values in X above the threshold ($X > \theta$). The arithmetic mean (ε) of these excesses is then computed for the sample:

$$\varepsilon = \frac{1}{n}\sum_{i=1}^{n}(u_i - \theta); i = 1,2, \dots, n, \quad (5)$$

where n is the sample size.

c. Assuming that the excesses are independent, a weight (ω) is also computed for the sample:

$$\omega = \frac{N-j}{Var(u-\theta)}, \quad (6)$$

in which N is the size of the dataset X, and j is the rank of each value in the set of θ. Langousis et al. (2016) suggested repeating this step for up to $j = N - 10$ values of θ to ensure a minimum sample size of $n = 10$ excesses for the computation of ε.

d. Afterward, a linear regression model is fitted to a subsample of the set (θ, ε) using the weighted least-squares method and the weighted mean-square error (WMSE) computed from

$$\text{WMSE} = \frac{1}{N_\theta}\sum_{i=1}^{N_\theta}\omega_i\left(\varepsilon_{\text{p},i} - \varepsilon_i\right); i = 1,2, \dots, N_\theta, \quad (7)$$

in which ε_p is the predicted excess, and N_θ is the subsample size. Langousis et al. (2016) suggested repeating this step for up to $j = N - 20$ subsamples of θ to ensure a minimum sample size of $N_\theta = 10$ excesses for the linear fit.

e. The end result of this process is a third set of pairs (θ, WMSE) from which the threshold with a minimum WMSE is selected as the parameter of the GPD.

In the StormSim-PST methodology, when multiple viable local WMSE minima are identified, the annual storm sample rate (or the average number of events sampled per year) is considered an additional criterion for threshold selection. Figure 9 shows an example of the MRL method results for hourly gauge data at Buffalo, New York.

Figure 9. Mean residual life (MRL) method results for the generalized Pareto distribution (GPD) threshold selection using the CO-OPS hourly gauge data at Buffalo, New York.

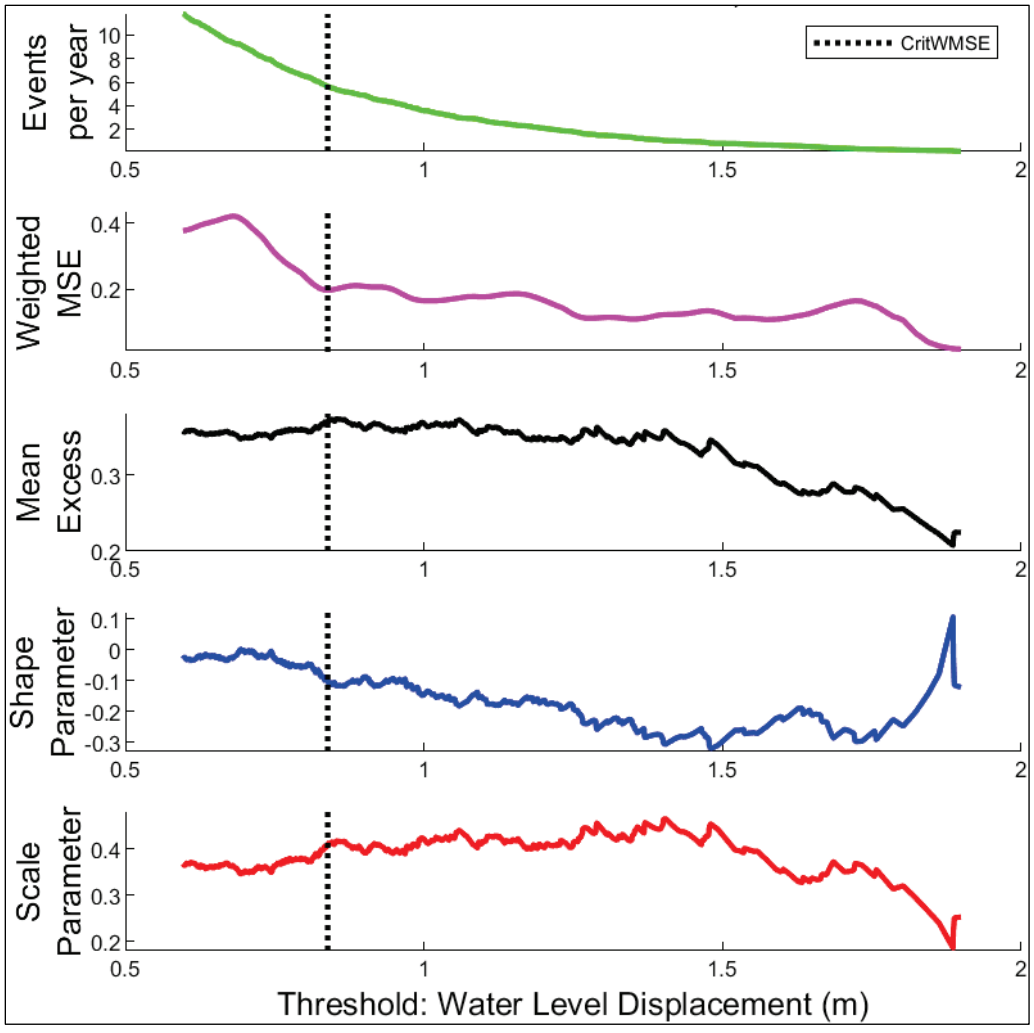

StormSim-PST can output the hazard curve as either annual exceedance probabilities (AEPs) or AEFs. The AEF indicates the expected frequency, in occurrences per year, at which a specific event will meet or surpass a defined threshold (Nadal-Caraballo et al. 2022). By calculating the reciprocal of the AEF, where ARI = 1/AEF, one obtains the average recurrence interval (ARI). The ARI denotes the mean interval between successive occurrences of the event in question, commonly known as the *return period*. Additionally, the intensity of hazards can be expressed through the AEP, which describes the yearly likelihood that a particular event will transpire within any given year. The AEF differs from the AEP, as documented in Nadal-Caraballo et al. (2022). However, the difference between AEF and AEP decreases at the low-frequency tail of the distribution, where events have longer ARI.

The output mean hazard curve and four nonexceedance confidence limits show the probability that Lake Erie will reach or exceed a given WLD value during an average year. As discussed in Section 2.2, the WLD hazard curves produced with the StormSim-PST tool are not dependent on lake levels. Therefore, these curves can be superimposed onto any water level Lake Erie is currently experiencing. For example, Figure 10 shows the hazard curve for the CO-OPS gauge station dataset for Buffalo, New York. The dashed purple lines indicate that the 1% (0.01) chance of exceedance event will cause a WLD of about 2.8 m. If the WLD occurred in the winter, when MLL was low, for example at 173.5 m, the WLD would bring the water level to about 176.3 m. However, if the WLD occurred in the spring, at a high MLL of 174.5 m, the peak of the WLD would be 177.3 m.

This study performed the LFA by applying the StormSim-PST tool to create the hazard curves at each site (i.e., gauge station location). This tool has a built-in POT scheme to sample the observations of WLD, which informs the MRL method. The PST method uses initial user-supplied estimates of interevent time and sample intensity (i.e., events per year) to start its optimization. Interevent time and sample intensity values of 48 hours and 12 annual events, respectively, were deemed acceptable for this application. Resulting hazard curves were expressed as AEF.

Figure 10. Hazard curve for the NOAA gauge station in Buffalo, New York. CL stands for confidence limit.

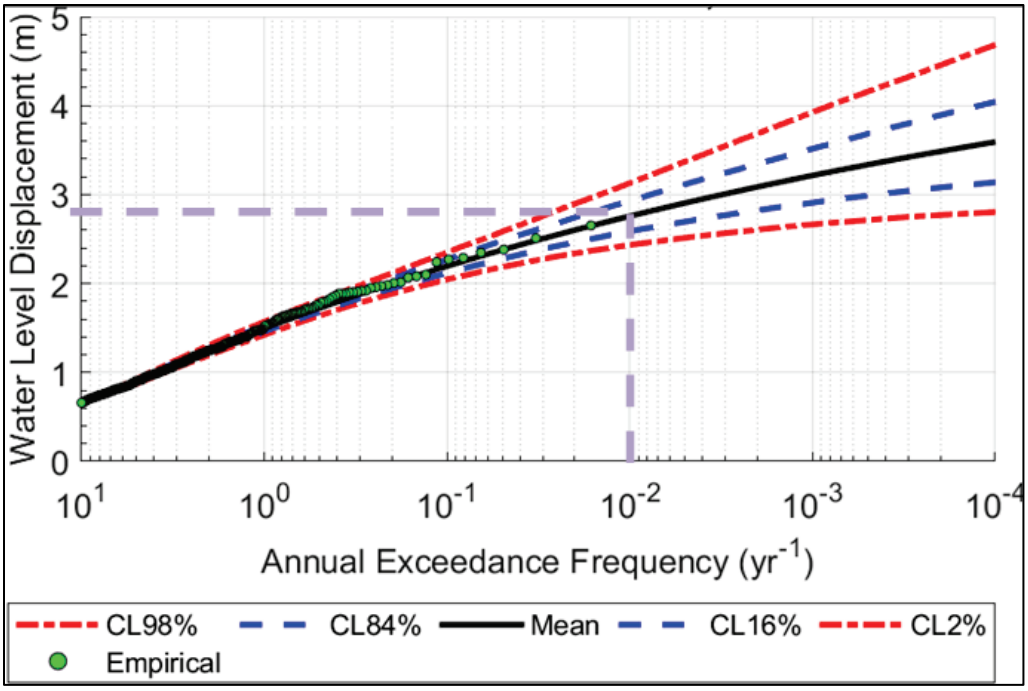

Three versions of LFAs were conducted. The first version used the hourly gauge observations. The second version used combined hourly and monthly gauge observations to assess the effect of expanding the record length in certain locations. Finally, for each gauge station record, the closest save point was identified from the available FEMA-USACE (RAMPP 2012) study, and the LFA was repeated using the PST for those 14 identified save points. The ADCIRC simulations focused on extreme wind events and provided enhanced spatial resolution but excluded convective storms.

2.5 Regional Frequency Analysis (RFA)

To help mitigate any lack of data and increase the representativeness of the hazard estimates for the WLD events among the gauge locations around Lake Erie, an RFA was employed. This consisted of performing the LFA for a site of interest with the StormSim-PST tool and combining that with an RFM (Andreevsky et al. 2020; Hamdi et al. 2018). The RFM approach draws on similarities between neighboring sites to estimate hydrological characteristics at sites with short record lengths or missing data. A site where the hazard is sought is known as a *target site* in this approach.

An empirical spatial extremogram (ESE; Hamdi et al. 2016) was used to delineate a physically homogeneous region centered on a target site. The

ESE is a set of extremal dependence coefficients ($\hat{\rho}$) and is computed as the ratio of the number of simultaneous extreme events at a neighboring site to the number of extreme events at a target site, as follows:

$$\hat{\rho}(X,Y) = \frac{\sum_{i=1}^{D} I\{X(i)>q_x \,\&\, Y(i)>q_y\}}{\sum_{i=1}^{N} I\{X(i)>q_x\}}, \quad (8)$$

in which X and Y are the extreme events at the target and neighboring sites, respectively; and q_x and q_y are the 99% percentile thresholds of the target and neighboring sites, respectively. Figure 11 illustrates the ESE for the CO-OPS gauge station at Toledo, Ohio, as a target site. Based on the dependence coefficient values, a neighborhood threshold (ρ_0) was then chosen to select which stations should belong in the homogeneous region. Only gauges with a dependence coefficient higher than the neighborhood threshold were accepted into the homogeneous region. A large neighborhood threshold will produce a small homogeneous region (i.e., few gauge stations used for the analysis). Conversely, a small neighborhood threshold has the potential to introduce noise (i.e., gauge stations distant from the target site and not affected by the same events) into the region. Accounting for this balance between region size and sample variance, a ρ_0 value of 0.4 was used for this application.

With the initial homogenous region identified (Figure 12 and Figure 13), a linear regression model was established by using the neighbors as predictors. By adding one neighbor at a time, the performance of the model was evaluated through two additional criteria to determine if the farthest neighbors should be kept or removed from the homogeneous region. The first criterion was the Nash-Sutcliffe coefficient (Nash and Sutcliffe 1970), which was used to determine how close the trend of model responses was to a 1:1 relationship compared to the target site record. Following a suggestion from Hamdi et al. (2018), this study removed any neighboring set of linear models with a Nash coefficient less than 0.5 from the homogenous region. In addition, the likelihood ratio test (Wu and Vos 2018) was used to verify the assumption that the farthest neighbor included as a predictor in the linear model improved or belonged to the relationship. The study also removed any linear model not statistically significant at the 5% level. Figure 14 illustrates this neighborhood reduction process for the CO-OPS hourly gauge station data at Toledo, Ohio.

Figure 11. Extremal dependence coefficients for each site neighboring Toledo, Ohio (station number 9063085).

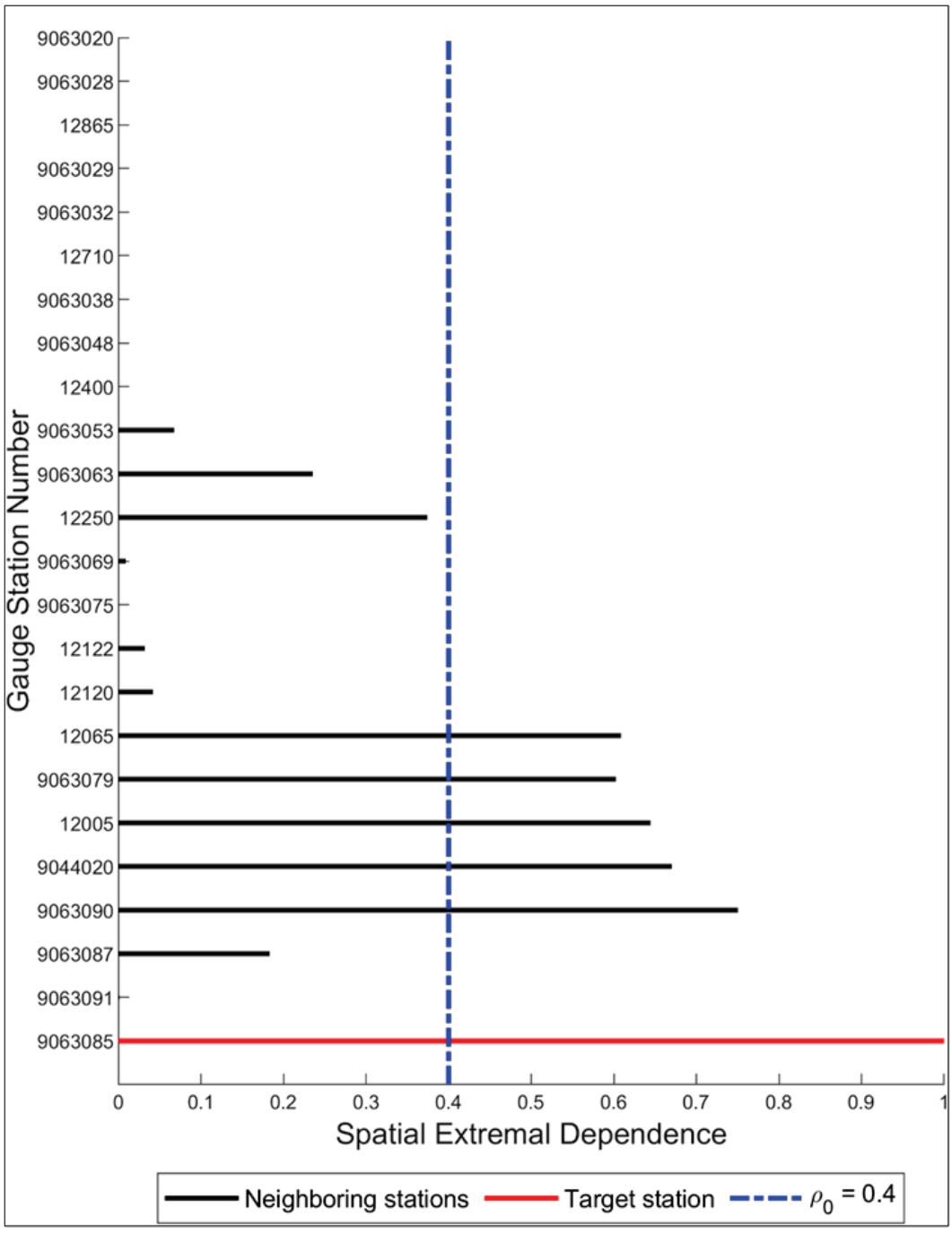

Figure 12. Geographical location of the initial homogeneous region for Toledo, Ohio, as a target site using a neighborhood threshold of 0.4. (Map adapted from USGS, n.d.)

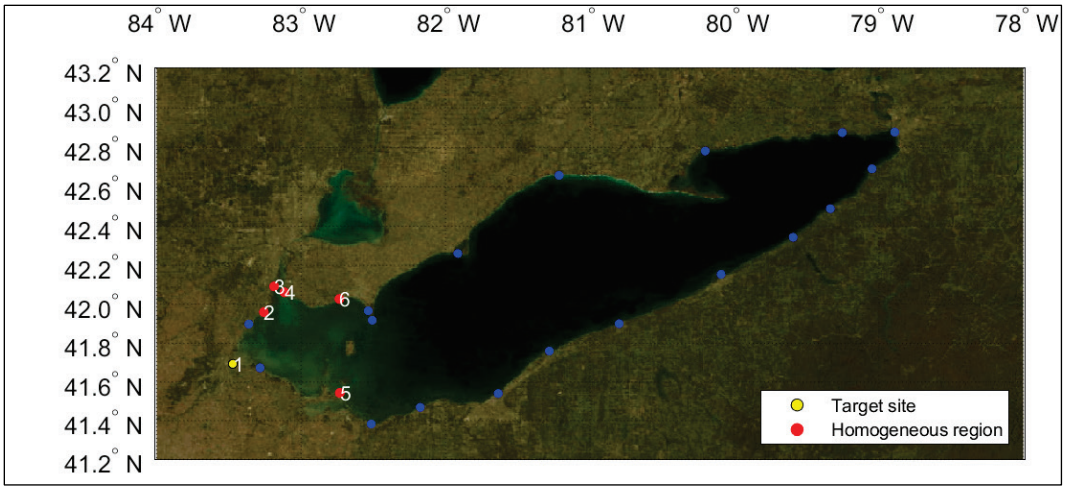

Figure 13. Record length of the initial homogeneous region for Toledo, Ohio, as a target site using a neighborhood threshold of 0.4.

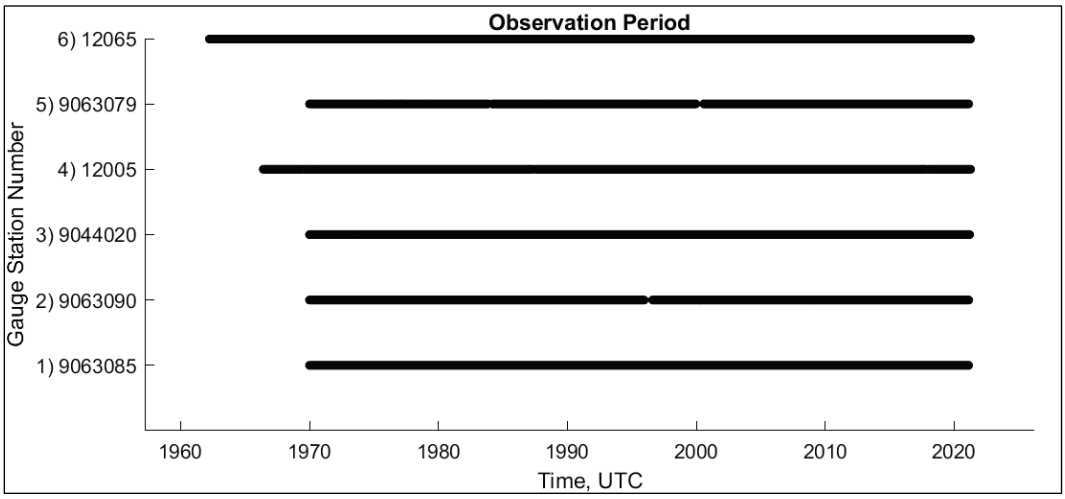

Figure 14. Comparison of linear relationships for different combinations of target-neighbor sites for the CO-OPS gauge station at Toledo, Ohio.

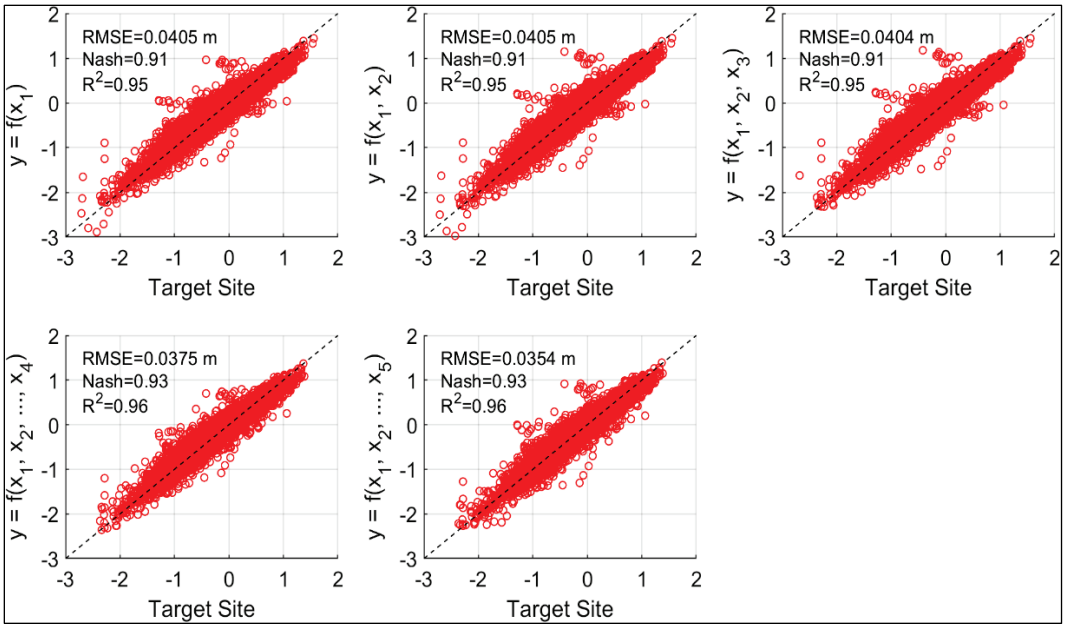

The final homogeneous region consisted of those neighboring sites whose linear relationship with the target site passed the criteria (Figure 15 and Figure 16). If multiple combinations or linear models passed the criteria, as was the case for Toledo, Ohio (Figure 14), preference was given to the combination with the lowest root-mean-square error (RMSE) value. This way, the RFM was established and used to transfer regional information to the target site, filling in any gaps in the time series and extending the period of record if possible (Figure 17). The last step in this process was to perform the frequency analysis by applying the StormSim-PST tool to both the hourly gauge data and the combined hourly and monthly gauge data that were successfully enriched by the RFM.

Figure 15. Final homogeneous region created for Toledo, Ohio, as a target site using a neighborhood threshold of 0.4. (Map adapted from USGS, n.d.)

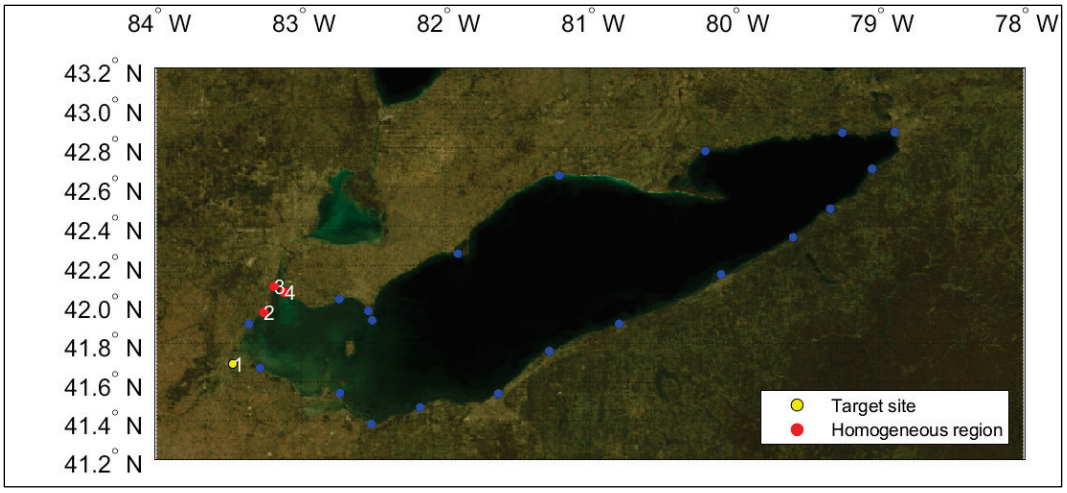

Figure 16. Record length of the final homogeneous region created for Toledo, Ohio, as a target site using a neighborhood threshold of 0.4.

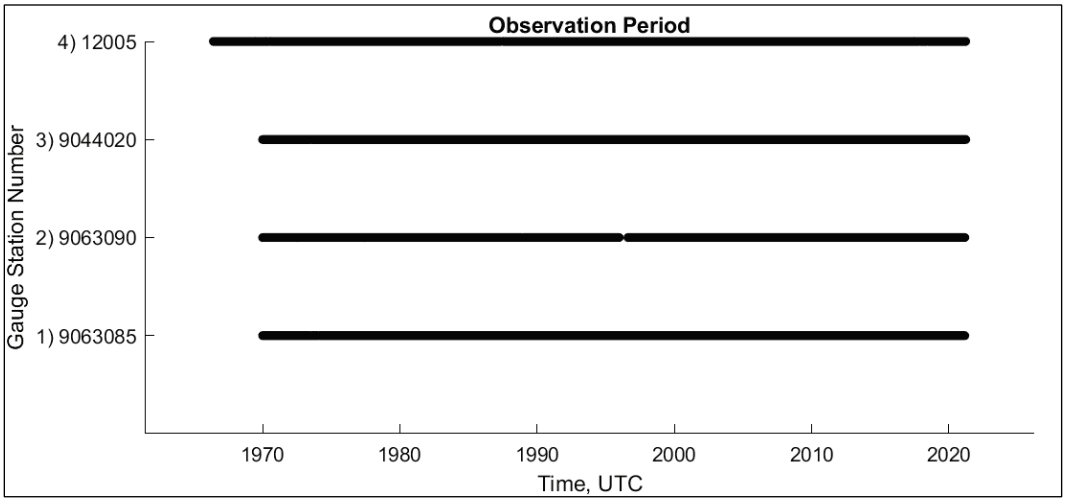

Figure 17. Results of the regional frequency model (RFM) applied for the CO-OPS gauge station 9063085 at Toledo, Ohio.

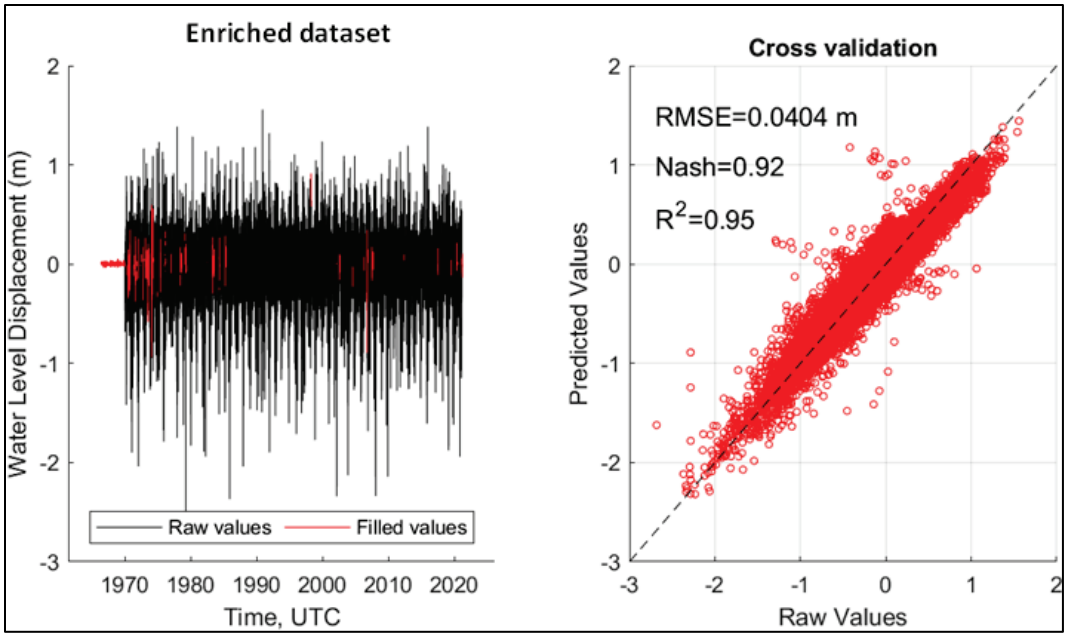

The enhanced gauge station datasets were then used to enrich the data from the 2,202 ADCIRC save points from the previous FEMA-USACE (RAMPP 2012) study. The same process was repeated to develop the RFM, but this time the possible neighboring sites were restricted to the ADCIRC save points closest to the 24 gauge stations. While the ADCIRC model output data were used for developing the RFM, the enhanced gauge station datasets were used as predictors in the data transfer. The intention of this additional experiment was to explore the possibility of transferring extreme events recorded by the gauge station network and forced by physical phenomena not necessarily included in the ADCIRC simulations. Hazard curves for each save point were also computed by applying StormSim-PST.

The nature of the ADCIRC-simulated datasets contributed to an unsuccessful application of the proposed RFM approach to the 2,202 save points. These only included hydrographs for storm-specific time periods over the entire Lake Erie. Because the gaps were within the same time window at all virtual gauges, the RFM could not transfer representative events for enriching target sites. ERDC-CHL modified the approach to instead pair virtual gauges with gauge stations, training the RFM with the gauge stations to then be applied on the ADCIRC datasets. Hazard curves computed with this alternate approach were unrealistic when compared against the gauge stations' hazards.

3 Results

3.1 Spectral Analysis

In Figure 7, the estimated PSD was displayed for each gauge, and the location of the seiche frequency bands was highlighted. The estimated power spectrum displayed a similar pattern to that observed by Farhadzadeh (2017), where the energy density, counterclockwise from Toledo, decreased toward the center of the lake and increased again at the eastern side of the lake. All gauges exhibited prominent peaks at the specified seiche frequencies, indicating the consistency of the methodology.

The designed bandpass filter successfully isolated the spectral density associated with the seiche frequency bounds, resulting in individual seiche WLD datasets. The PSD results indicate the dominant seiche mode for all gauges across Lake Erie, which translates to how the WLD scale between themselves. Figure 18 illustrates the individual WLD contributions for the gauge located at Toledo, Ohio, where the WLD contributions become smaller as we progress through the seiche modes, following the behavior of the power spectrum for Toledo, Ohio (black plot in Figure 7). Moreover, qualitative comparisons reveal that seiche events represent a small percentage of the overall WLD. This finding is consistent across all gauges, although the dominant mode of seiching varies spatially across Lake Erie.

In addition, spectral results for the combined seiche mode of oscillation (Filter ID 5) revealed more significant contributions toward the overall WLD (Figure 19). However, this might not reflect the true nature of the coupling or interaction of these modes but provides an idea of the response given an energy budget.

Figure 18. The individual contributions of each mode of seiching. From *top* to *bottom*: first moment, second moment, third moment, fourth moment, and overall WLD.

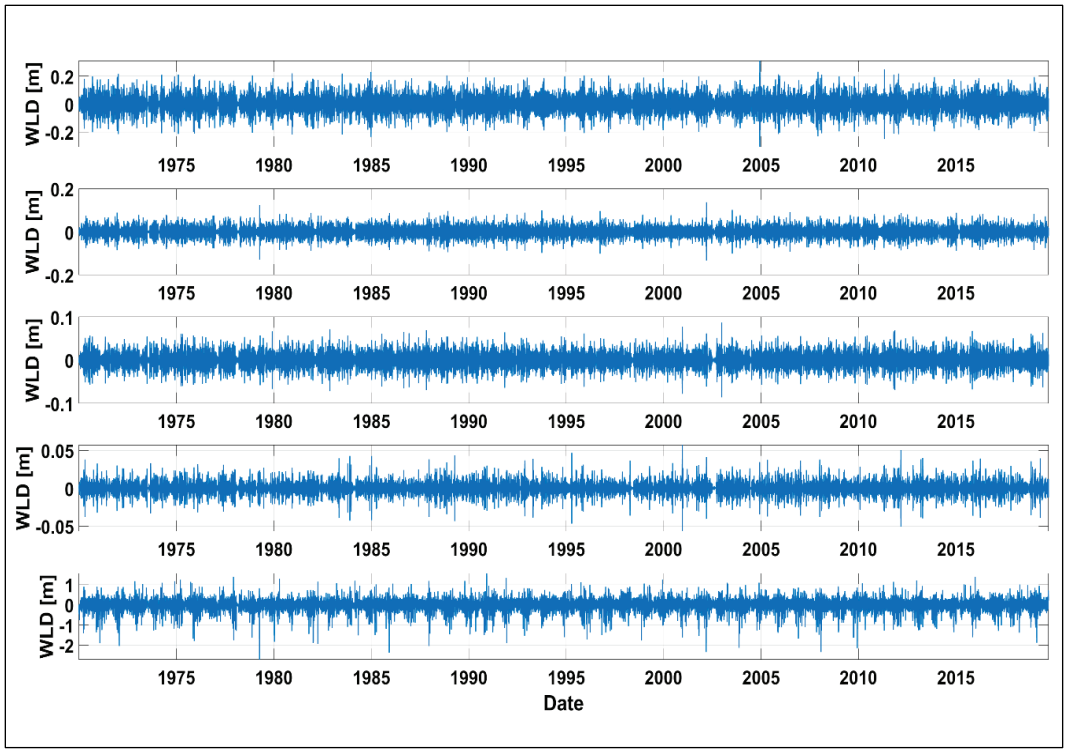

Figure 19. The contributions of the whole frequency band. *Bottom* subplot is the overall WLD.

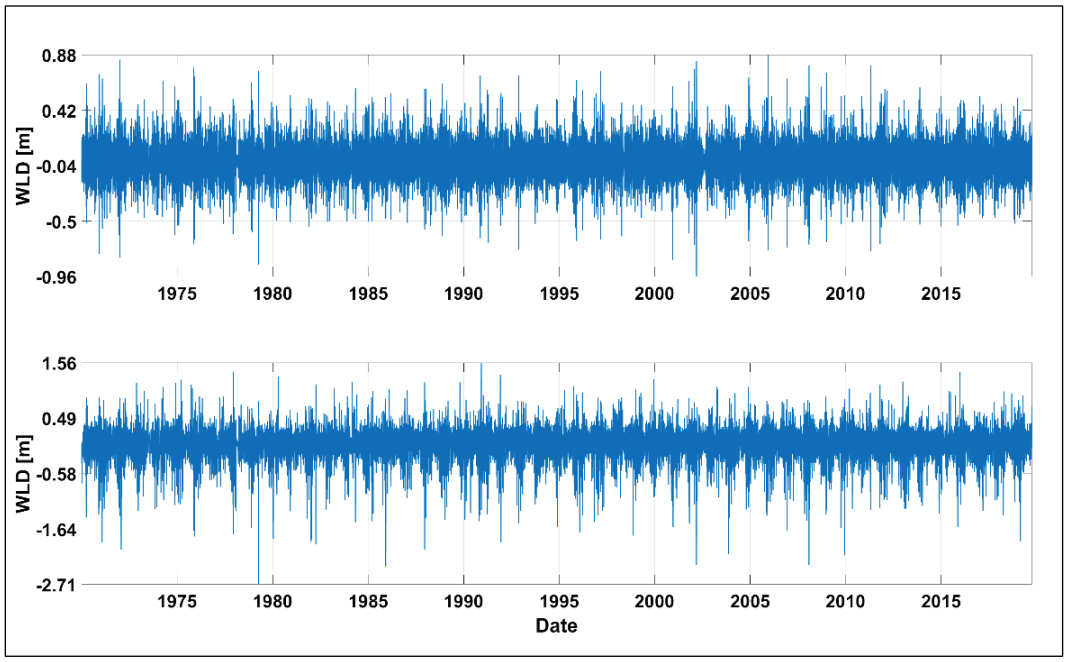

3.2 LFA per Seiche Mode

The results from the PST were consistent with the spectral analysis, as evidenced by the spatial variability of the hazard curves following the PSD behavior. Additionally, the GPD fits agreed with the empirical data, with little variation in confidence levels for most gauges. For example, Toledo had the highest spectral energy for the first three seiche modes among most gauges, resulting in a higher hazard at the tail of the hazard curve for modes 1–3 (Figure 20). Conversely, Buffalo exhibited the highest spectral energy for seiche modes 3–4, leading to a higher hazard at the tail of the hazard curve for modes 3–4 (Figure 21). However, gauges at Buffalo, Marblehead, Bar Point, and Fermi Power Plant had a higher hazard than Toledo for the first mode, suggesting that the filter parameters or frequency bands should be refined to reduce spectral energy not associated with seiches. This is also apparent in the lower hazard for combined seiche modes than for individual modes at Buffalo (Figure 22). LFA results for all gauges can be found in Appendix B.

Figure 20. WLD hazard curve comparison between Seiche Mode 1 (*a*), 2 (*b*), 3 (*c*), and 4 (*d*) for Toledo, Ohio (9063085). Individual figures available in Appendix B. The vertical reference is mean sea level (MSL).

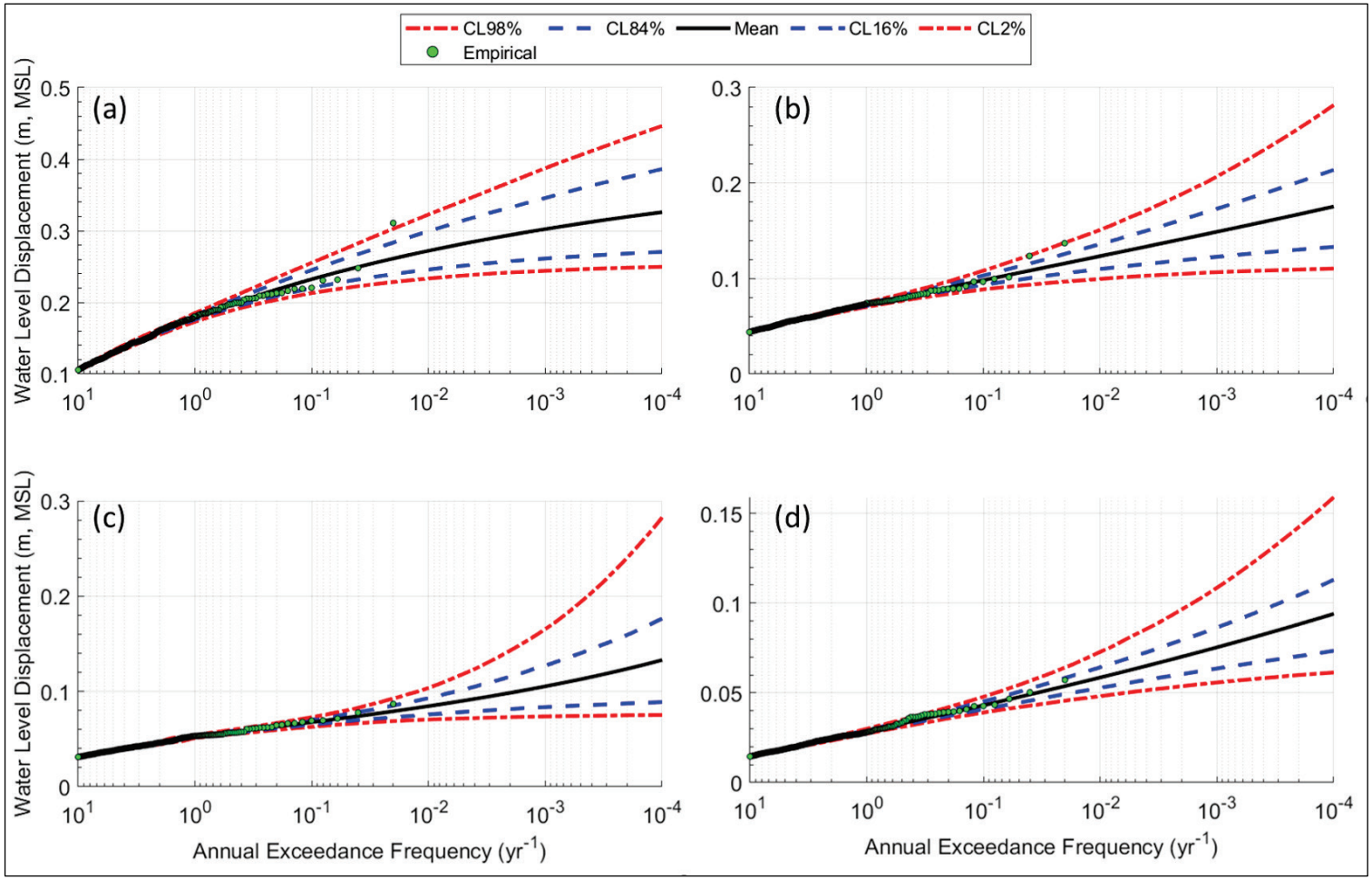

Figure 21. WLD hazard curve comparison between Seiche Mode 1 (*a*), 2 (*b*), 3 (*c*), and 4 (*d*) for Buffalo (9063020). Individual figures available in Appendix B. The vertical reference is MSL.

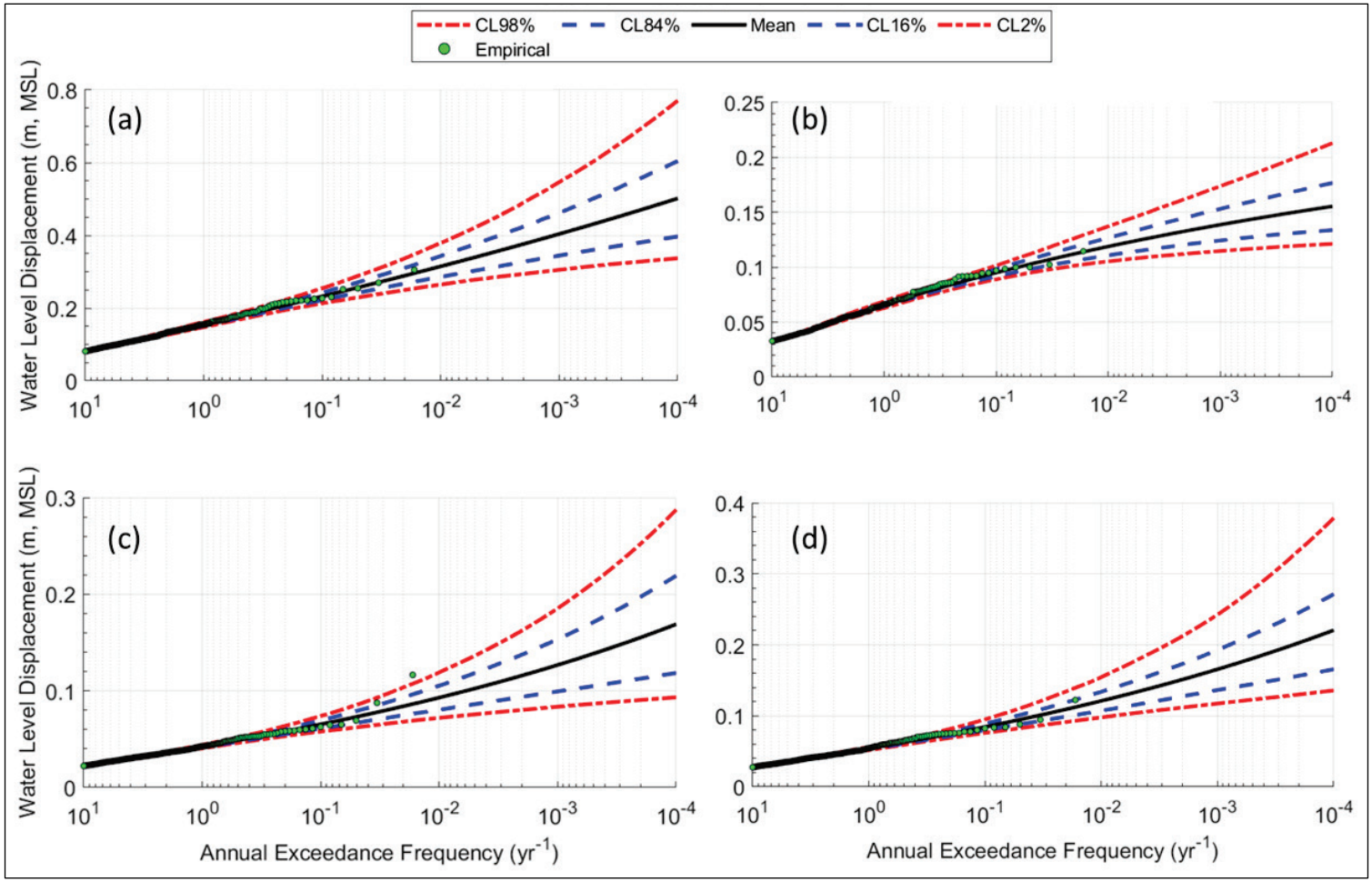

Figure 22. WLD hazard curve comparison of the combined seiche mode for gauges located at the west, center, and east off the lake. Individual figures available in Appendix B. The vertical reference is MSL.

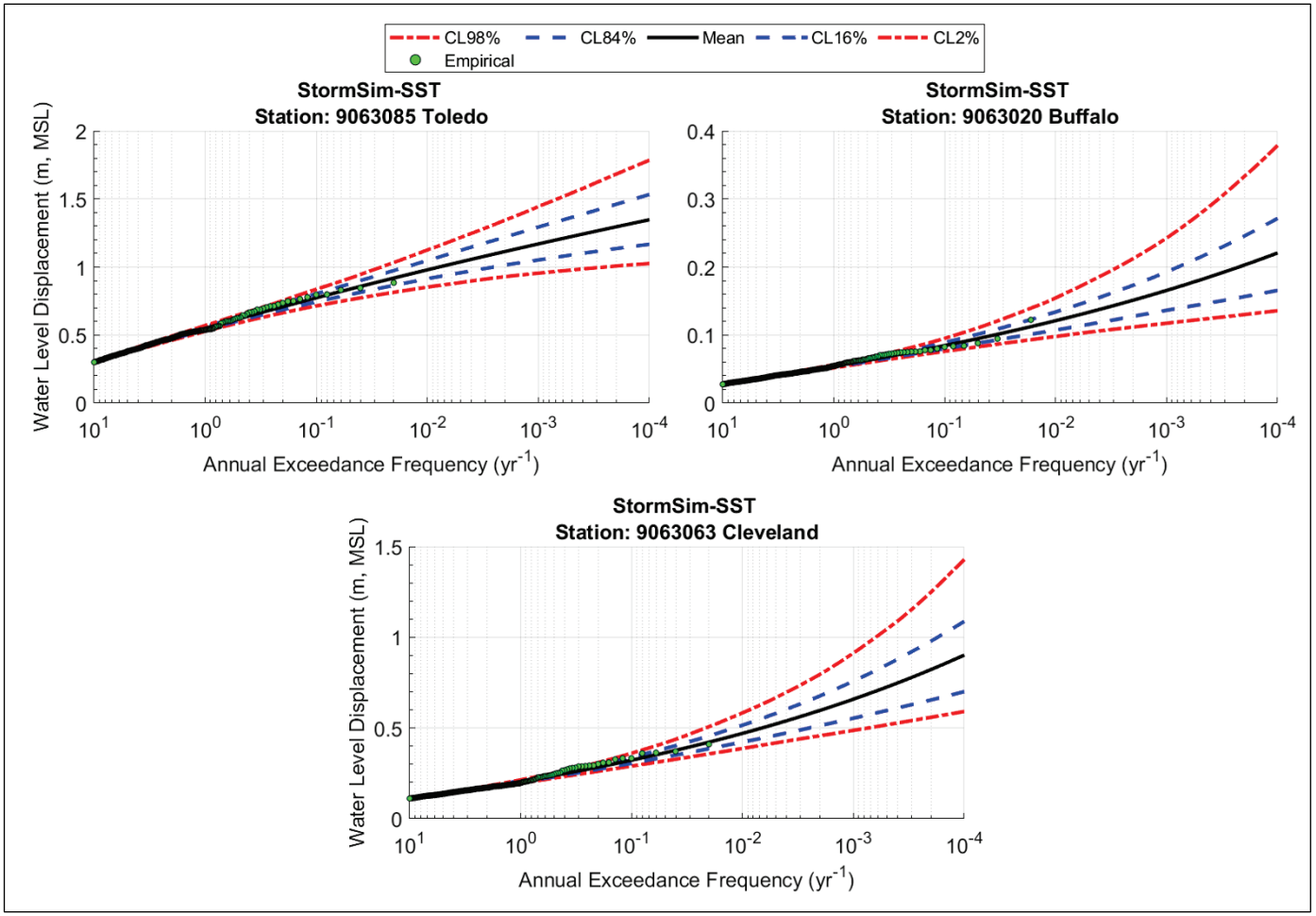

3.3 LFA of WLD Data

The LFA was performed with the hourly and combined datasets at each of the 24 gauges using the StormSim-PST methodology. Figure 23 through Figure 25 compare the hazard curves for the hourly and combined datasets at the Buffalo, Cleveland, and Toledo gauges, respectively. In general, inspection of the hourly and combined hazard curves showed a close agreement between the empirical samples and the GPD fits. However, stark differences were observed in the 96% confidence intervals (CIs), represented by the red dashed lines in the plots, for many gauges, including the three mentioned previously. Nowhere was the discrepancy between the two curves more pronounced than at the Buffalo gauge, where the 96% CI at the hourly curve was over triple that of the combined curve at the 10^{-4} AEF. The difference in variation at the Buffalo gauge was attributed to the record of the combined data beginning 60 years before the record of the hourly data, which greatly increased the size of the POT sample calculated from the combined dataset. The longer record length at the Buffalo gauge resulted in many more low-magnitude WLD events being incorporated into the POT sample from the combined data, hence lowering the low-frequency tail. The 96% CIs of the hazard curves for the hourly and combined datasets also varied at other gauges, such as the Cleveland and Toledo gauges, that had large record-length differences. Stations where the hazards of the two datasets were nearly identical tended to be cases where the record length of the combined dataset was only marginally longer than the record length of the hourly dataset. Figure 2, which compares the record length of the combined data to the length of the hourly data, is a good indicator of whether the LFA results of the hourly and combined datasets will be different. Table 3 contains the summary of the numerical values of the LFA at the three gauges.

Figure 23. Local frequency analysis (LFA) results for the hourly (*top*) and combined (*bottom*) datasets from the CO-OPS gauge station 9063020 at Buffalo, New York.

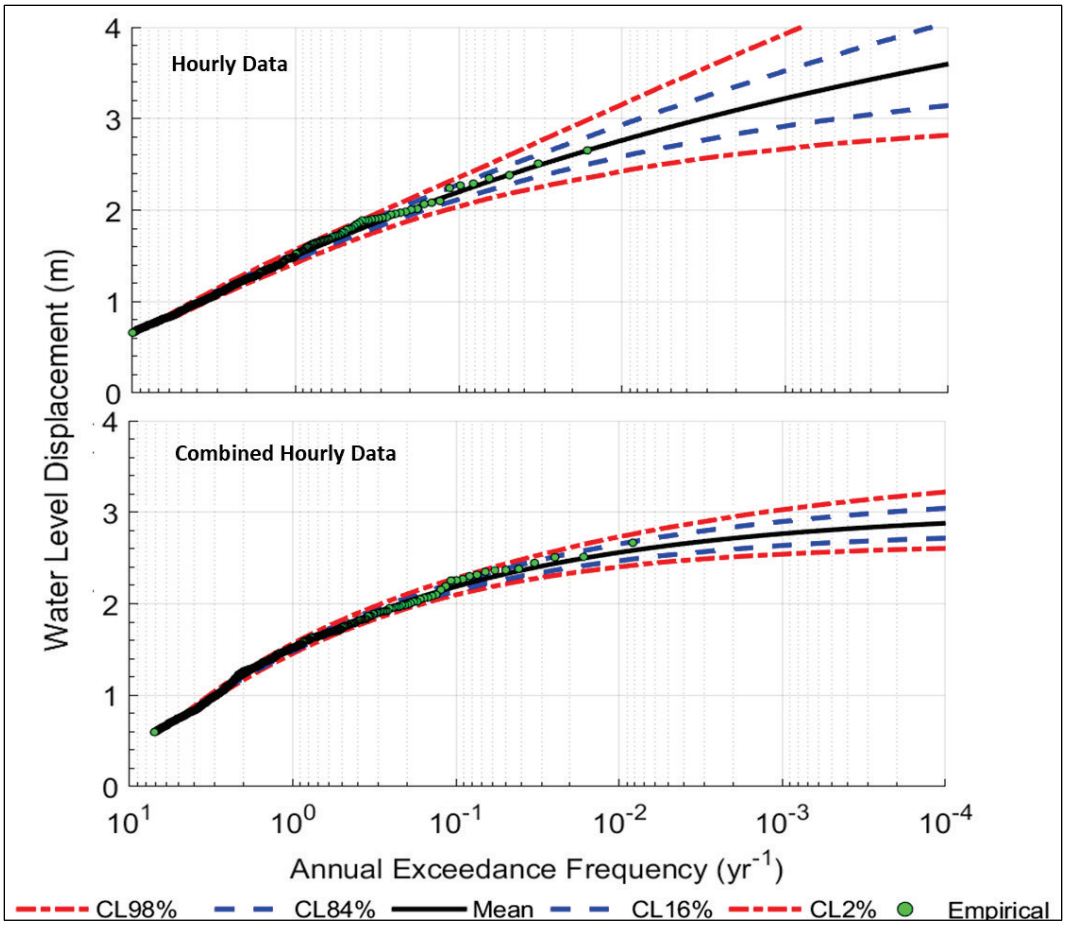

Figure 24. LFA results for the hourly (*top*) and combined (*bottom*) datasets from the CO-OPS gauge station 9063063 at Cleveland, Ohio.

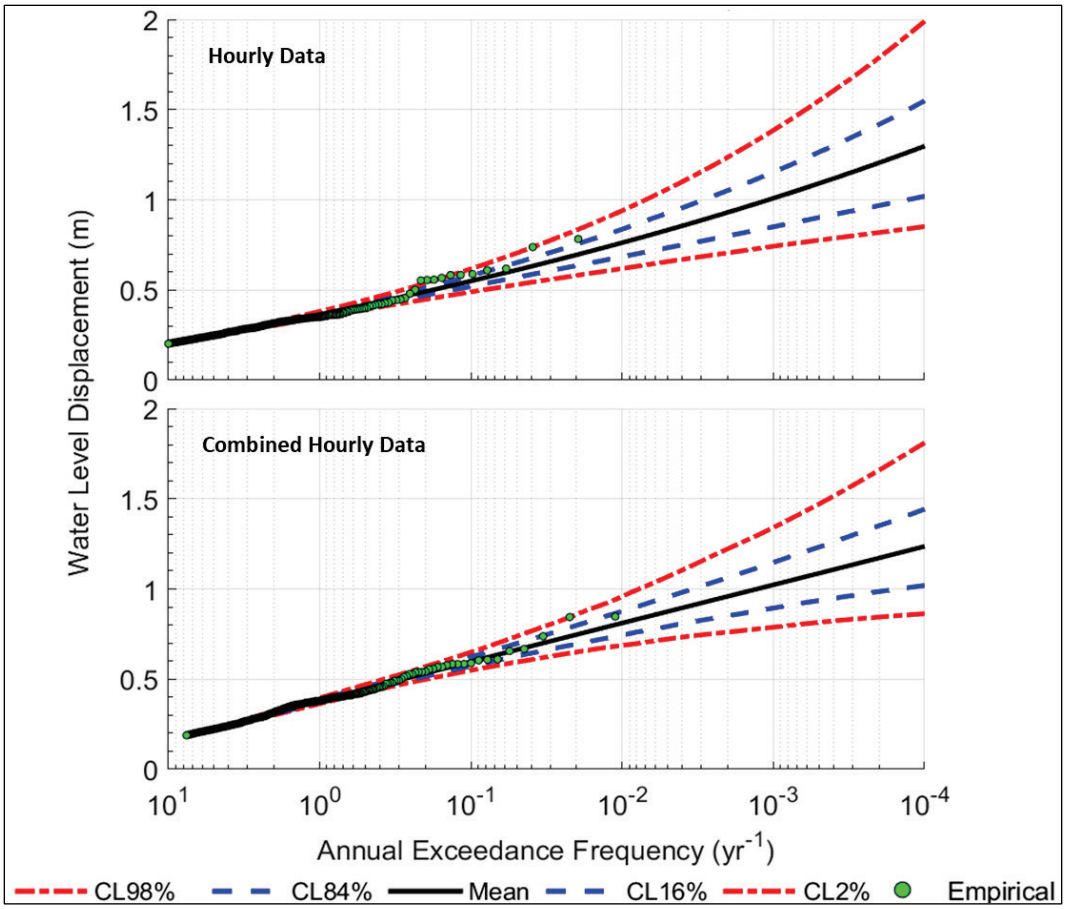

Figure 25. LFA results for the hourly (*top*) and combined (*bottom*) datasets from the CO-OPS gauge station 9063085 at Toledo, Ohio.

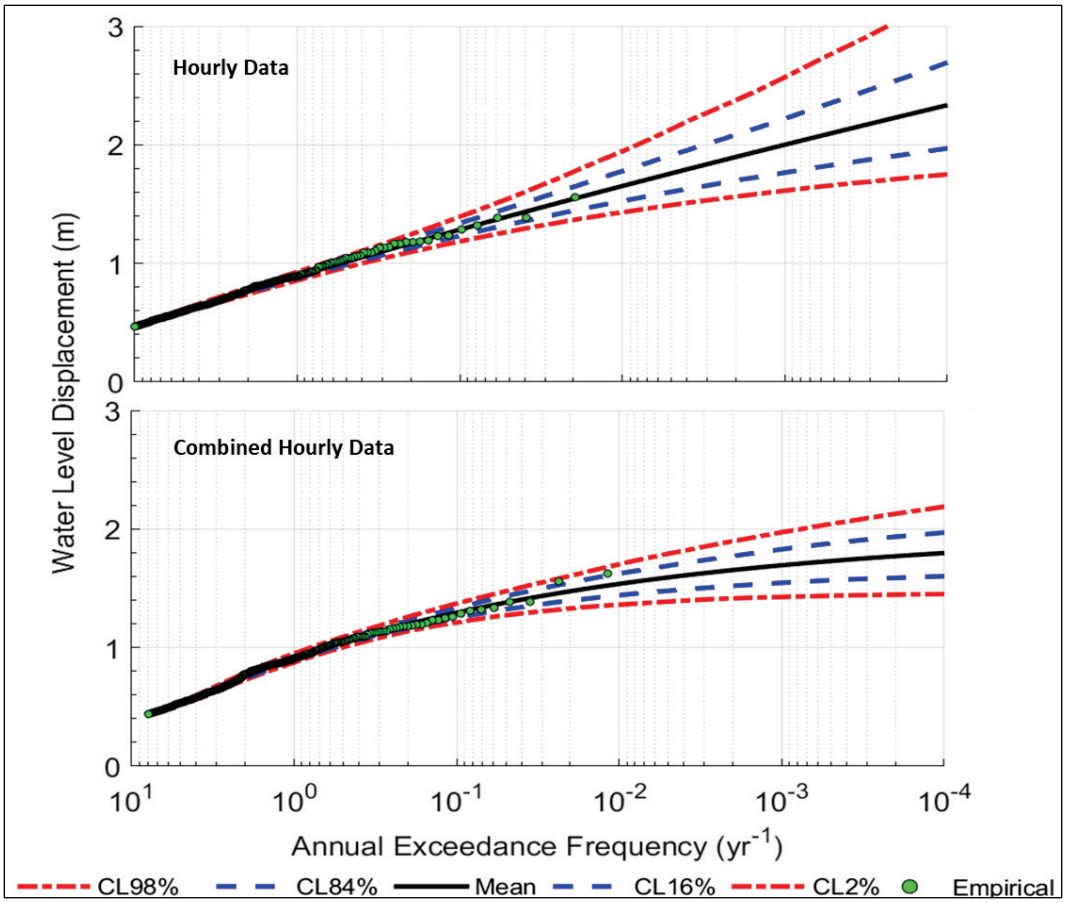

Selected results from the combined datasets at the 10^{-2} AEF will be discussed. The WLD hazard at Buffalo was 2.558 m, compared to 0.811 m at the Cleveland gauge and 1.526 m at the Toledo gauge. Examining the values at the other gauges showed a trend of increasing WLD from the southwest to the northeast corners of Lake Erie, and indeed, the largest hazard values at the 10^{-2} AEF were observed at Buffalo, New York. Hazard also increased from southwest to northeast at the Canadian gauges. The minimum and maximum hazards observed at the 10^{-2} AEF were 0.611 m at the Port Pelee, Ontario, gauge and 2.268 m at Kingsville, Ontario, respectively.

Table 3. Results of LFAs using hourly and combined datasets for selected CO-OPS gauge stations.

AEP	AEF	ID 9063085—Toledo		ID 9063063—Cleveland		ID 9063020—Buffalo	
		Hourly	Comb. Hourly	Hourly	Comb. Hourly	Hourly	Comb. Hourly
1	10	0.469	0.397	0.202	0.171	0.661	0.466
0.99	5	0.600	0.534	0.249	0.223	0.900	0.748
0.86	2	0.769	0.756	0.313	0.312	1.251	1.212
0.63	1	0.892	0.911	0.365	0.379	1.495	1.512
0.4	0.5	1.013	1.044	0.418	0.445	1.723	1.761
0.2	0.2	1.169	1.194	0.491	0.532	2.001	2.027
0.1	0.1	1.284	1.289	0.550	0.597	2.195	2.189
0.05	0.05	1.397	1.372	0.611	0.662	2.377	2.325
0.02	0.02	1.543	1.466	0.695	0.747	2.600	2.470
0.01	0.01	1.651	1.526	0.762	0.811	2.757	2.558
0.005	0.005	1.757	1.579	0.832	0.875	2.905	2.632
0.002	0.002	1.895	1.638	0.930	0.959	3.086	2.712
0.001	0.001	1.997	1.677	1.008	1.023	3.215	2.761
0.0005	0.0005	2.098	1.711	1.091	1.087	3.335	2.801
0.0002	0.0002	2.229	1.750	1.205	1.171	3.485	2.845
0.0001	0.0001	2.327	1.775	1.297	1.236	3.591	2.872

3.4 RFA of WLD Data

The RFM enriched the WLD datasets at 16 of the 24 CO-OPS gauges used in the study. Reasons for the RFM not processing the other 8 CO-OPS gauges include lack of data and the ESE rejection of the neighbors (i.e., nonhomogenous regions). The RFM was applied in two separate runs: the first used hourly data, and the second used the combined (hourly with monthly events) data. To quantify the error and goodness-of-fit of the model, validation metrics were calculated for each run by comparing the existing gauge data to the predictions from the RFM. The largest RMSE was only 0.04 m, while the average across the 16 gauges was 0.02 m, proving the low-variance quality of the RFM. In addition, the proportion of variance in the data explained by the model, or R-square, was greater than 90% at 12 of the gauges. The only gauge at which the RFM had a suboptimal goodness-of-fit of 64% was the Erieau, Ontario, station. Figure 26 suggests that the RFM was probably unnecessary at the gauge because the data gaps accounted for 1.04% of the record length.

Figure 26. Results of the RFM applied for gauge station 12250 at Erieau, Ontario. The RFM filled 1.04% of the WLD values at the gauge.

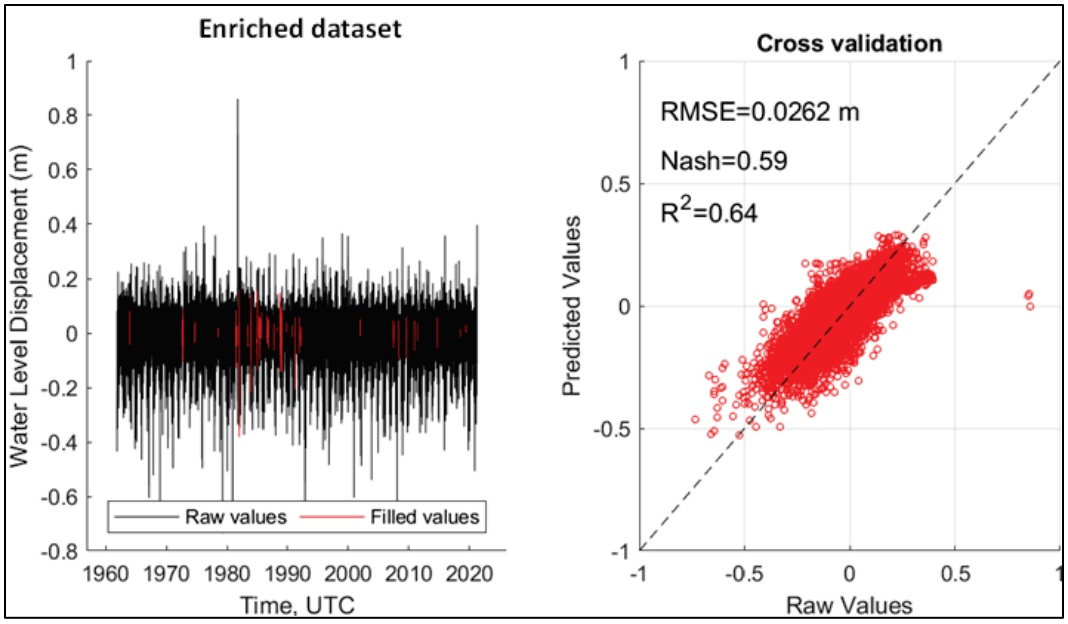

The greatest utility of the RFM was that it effectively enriched datasets at gauges that had sparse temporal resolution, including (1) short record length, (2) decades of inactive status, and (3) large gaps in the historical record. Figure 27 shows the results and validation metrics of the RFM at three gauges that had at least one of these issues: the Lorain (Ohio), Pelee Point East (Ontario), and Sturgeon Point (New York) gauges.

Figure 27. RFM results for gauge stations 12122 (Pelee Point East, Ontario), 9063028 (Sturgeon Point, New York), and 9063069 (Lorain, Ohio).

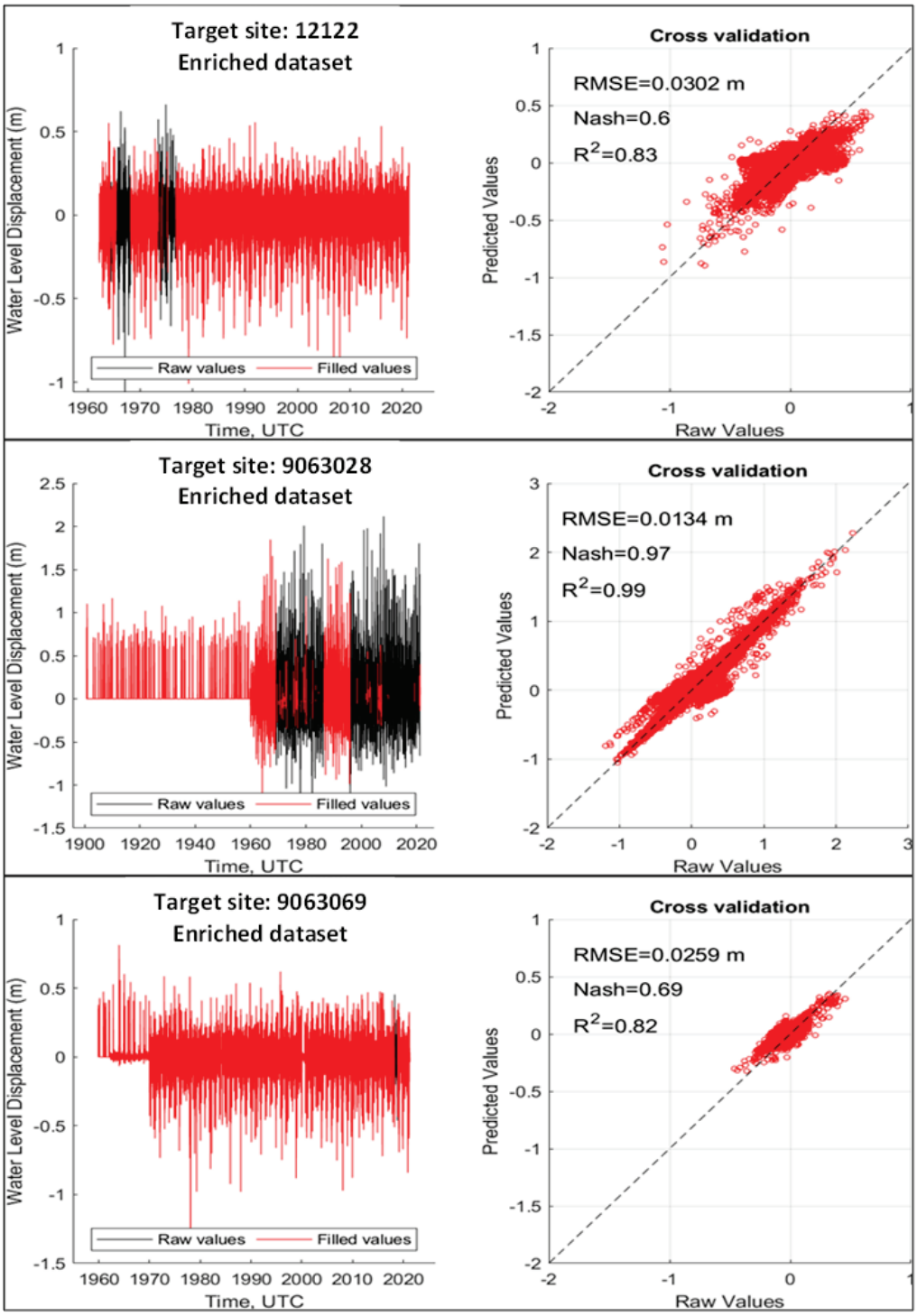

The RFM was implemented with the methodology described in Section 2.5, and the model outputs (i.e., enriched timeseries datasets) were input into the StormSim-PST tool to conduct the RFA. A four-way comparison was made with the best estimates of the WLD hazard from the (1) LFA run

with the hourly data, (2) LFA run with the combined data, (3) RFA run with the hourly data, and (4) RFA run with the combined data.

Figure 28 through Figure 30 show the comparisons at CO-OPS stations, respectively, at Buffalo, New York; Lorain, Ohio; and Toledo, Ohio. The RFA could not be performed at the Cleveland, Ohio, gauge, so the results at the nearby Lorain gauge were examined instead. Inspection of the comparative plots and hazard results showed some cases where the results of the analyses were similar. The agreement of the analyses was best illustrated at the Buffalo station, where the hazard curves of the RFA, represented by the red and magenta curves, were essentially the same as the black and blue curves of the LFA. Buffalo had a nearly complete historical record of data from 1960 to 2020, so the RFM only filled a tiny portion of the record, resulting in nearly identical POT samples computed by StormSim-PST in the two analyses. At the Toledo gauge, which also had a robust period of record, the RFA and the LFA also showed close agreement. The conclusion was that the RFA mirrored the LFA whenever the data enrichment performed by the RFM filled only a small proportion of the record length. However, the close agreement between the RFA and the LFA was not observed at gauges where the RFM drastically augmented the record lengths. At the Lorain gauge, the RFM was able to extend the data record by over 1,000%, so the POT sample generated by the RFA had over 700 events, while only 6 were computed in the LFA. Therefore, the RFA enabled a more conservative approximation of the low-frequency tail of the hazard, as shown in Figure 29. Table 4 summarized the WLD hazards at the Toledo, Lorain, and Buffalo gauges for the RFA using the combined datasets. At the 10^{-2} AEF, the WLD hazards were 1.530 m, 0.698 m, and 2.565 m for the respective gauges. At the 10^{-3} AEF for Lorain, WLD hazards were 0.805 m in the RFA and 1.283 m in the LFA, which was a significant difference.

Figure 28. Comparison of regional frequency analysis (RFA) to LFA results for hourly (HH) and combined (HHMM) datasets of the CO-OPS gauge station 9063020 at Buffalo, New York.

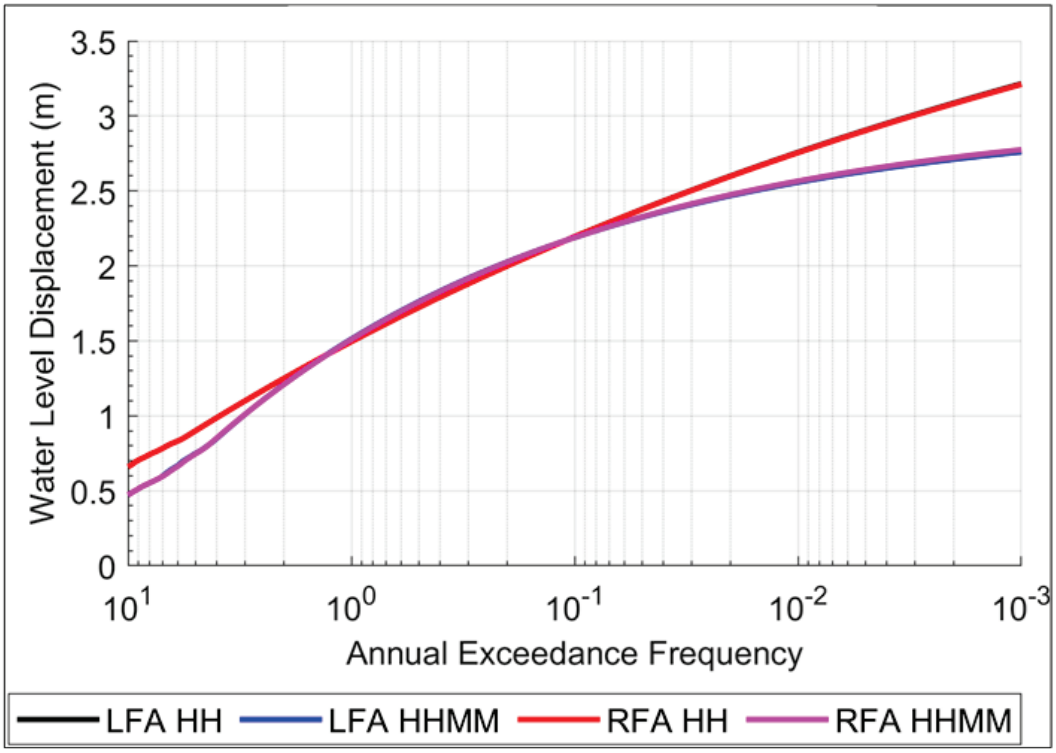

Figure 29. Comparison of RFA to LFA results for the hourly and combined datasets of CO-OPS gauge station 9063069 at Lorain, Ohio.

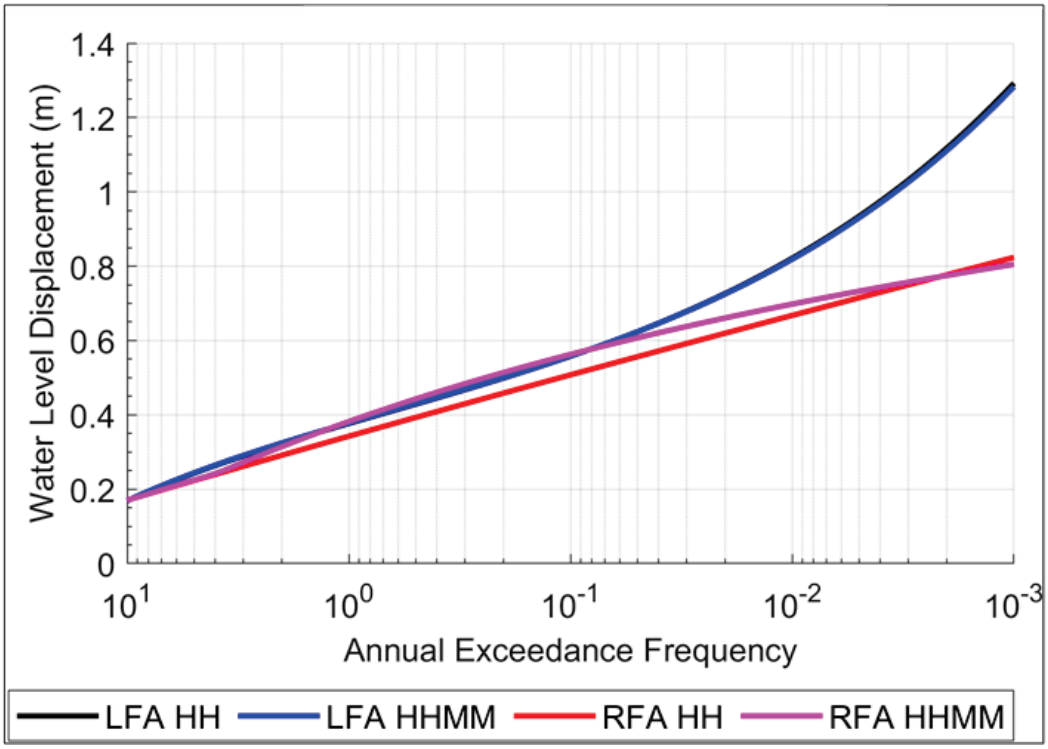

Figure 30. Comparison of RFA to LFA results for the hourly and combined datasets for CO-OPS gauge station 9063085 at Toledo, Ohio.

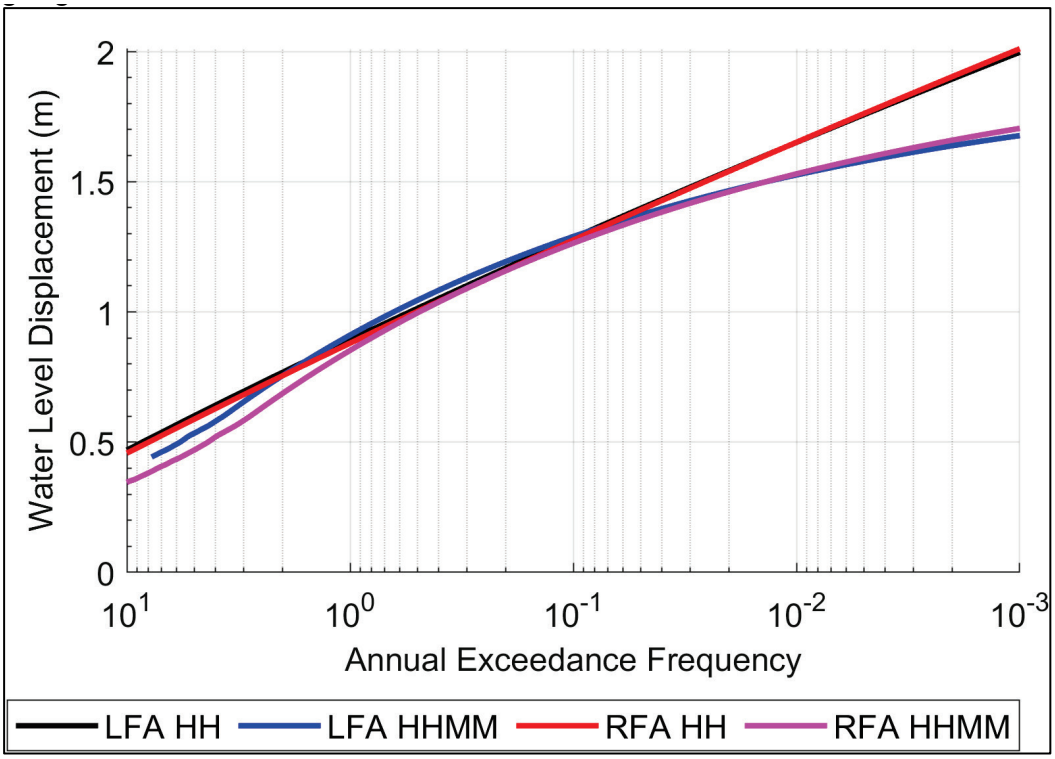

Table 4. Results of RFA using hourly and combined datasets for selected CO-OPS gauge stations.

AEP	AEF	ID 9063085—Toledo		ID 9063069—Lorain		ID 9063020—Buffalo	
		Hourly	Comb. Hourly	Hourly	Comb. Hourly	Hourly	Comb. Hourly
1	10	0.458	0.346	0.170	0.171	0.660	0.472
0.99	5	0.588	0.469	0.223	0.224	0.899	0.746
0.86	2	0.756	0.688	0.291	0.315	1.250	1.211
0.63	1	0.880	0.852	0.342	0.382	1.494	1.509
0.4	0.5	1.002	0.996	0.393	0.443	1.722	1.758
0.2	0.2	1.159	1.158	0.459	0.514	2.000	2.026
0.1	0.1	1.276	1.264	0.508	0.563	2.194	2.190
0.05	0.05	1.391	1.356	0.556	0.607	2.376	2.327
0.02	0.02	1.540	1.461	0.620	0.661	2.599	2.474
0.01	0.01	1.651	1.530	0.668	0.698	2.755	2.565
0.005	0.005	1.761	1.590	0.715	0.733	2.902	2.641
0.002	0.002	1.904	1.659	0.777	0.775	3.083	2.723
0.001	0.001	2.010	1.705	0.824	0.805	3.211	2.774
0.0005	0.0005	2.116	1.745	0.870	0.833	3.331	2.816
0.0002	0.0002	2.253	1.790	0.931	0.869	3.480	2.862
0.0001	0.0001	2.357	1.821	0.978	0.894	3.586	2.891

4 Conclusions and Recommendations

The goal of this study was to develop a replicable methodology to identify and quantify the hazard imposed by storm surge and seiche events in Lake Erie. In this study, WLD was used as the variable of interest to evaluate storm hazards, including both storm surge and seiche events, that can produce significant flooding on Lake Erie. Additionally, the resulting WLD hazard curves can be superimposed onto the lake level that Lake Erie is experiencing at the time to produce a tangible real-time hazard estimate. This study built upon statistical analysis methods initially developed for the 2012 federal interagency GLCFS (Nadal-Caraballo et al. 2012). Using the StormSim-PST tool and an RFM, historical extreme events were assessed in both an LFA and an RFA to quantify the AEF of WLD events specific to Lake Erie.

Hourly and monthly water-level observations from NOAA and Canadian gauge stations were used in conjunction with the hydrodynamic (ADCIRC) simulations from GLCFS to quantify the hazard imposed by the WLD events. After an LFA was conducted using StormSim-PST, an RFA was performed to increase the robustness of the WLD hazard estimates. This involved implementing an RFM methodology in MATLAB and applying it to gauge data for transfer of missing events to each target site. Then, the StormSim-PST tool was applied to the resulting enriched datasets. The following analyses were successfully completed as part of this study:

1. Spectral analysis of hourly data at 14 gauge stations with record lengths longer than 30 years
2. LFA of hourly data per seiche mode
3. LFA of hourly data at 25 gauge stations
4. LFA of combined hourly and monthly data at 25 gauge stations
5. RFA of the enriched hourly data at 16 gauge stations
6. RFA of the enriched combined hourly and monthly data at 16 gauge stations

Characterizing the forcing mechanisms behind Lake Erie's seiches could help improve the hazard analysis. High-fidelity modeling of continuous data is recommended as an approach to explore those forcing mechanisms. In addition, expanding the capabilities of the proposed RFM to include other physical parameters could improve the definition of the

homogeneous regions. Some of these forcing parameters could be wind direction and speed, bathymetry or depth, and river discharge.

References

Andreevsky, M., Y. Hamdi, S. Griolet, P. Bernardara, and R. Frau. 2020. "Regional Frequency Analysis of Extreme Storm Surges Using the Extremogram Approach." *Natural Hazards and Earth System Sciences* 20 (6): 1,705–1,717. https://doi.org/10.5194/nhess-20-1705-2020.

Borgman, L. E. 2004. "New Nonparametric Methods in Risk Analysis Based on Resampling Techniques and Empirical Simulation." In *Civil Engineering in the Oceans VI*, edited by M. J. Briggs and M. E. McCormick, 1–30. Reston, VA: American Society of Civil Engineers. https://doi.org/10.1061/40775(182)1.

Coles, S. 2001. *An Introduction to Statistical Modeling of Extreme Values*. Lecture Notes in Control and Information Sciences. New York, NY: Springer. https://books.google.com/books?id=2nugUEaKqFEC.

CO-OPS (Center for Operational Oceanographic Products and Services). n.d. "High and Low Water Conditions." *NOAA Tides and Currents*. Accessed June 1, 2021. https://tidesandcurrents.noaa.gov/.

Dean, R. G., and R. A. Dalrymple. 1991. *Water Wave Mechanics for Engineers and Scientists*. Advanced Series on Ocean Engineering, Vol. 2. Hackensack, NJ: World Scientific. https://doi.org/10.1142/1232.

Farhadzadeh, A. 2017. "A Study of Lake Erie Seiche and Low Frequency Water Level Fluctuations in the Presence of Surface Ice." *Ocean Engineering* 135: 117–136. https://doi.org/10.1016/j.oceaneng.2017.02.027.

Fisheries and Oceans Canada. n.d. "Marine Environmental Data." Accessed June 1, 2021. https://meds-sdmm.dfo-mpo.gc.ca/isdm-gdsi/index-eng.html.

Hamdi, Y., C.-M. Duluc, L. Bardet, and V. Rebour. 2016. "Use of the Spatial Extremogram to Form a Homogeneous Region Centered on a Target Site for the Regional Frequency Analysis of Extreme Storm Surges." *International Journal of Safety and Security Engineering* 6 (4): 777–781. https://doi.org/10.2495/SAFE-V6-N4-777-781.

Hamdi, Y., C.-M. Duluc, L. Bardet, and V. Rebour. 2018. "Development of a Target-Site-Based Regional Frequency Model Using Historical Information." *Natural Hazards* 98 (3): 895–913. https://doi.org/10.1007/s11069-018-3237-8.

Langousis, A., A. Mamalakis, M. Puliga, and R. Deidda. 2016. "Threshold Detection for the Generalized Pareto Distribution: Review of Representative Methods and Application to the NOAA NCDC Daily Rainfall Database." *Water Resources Research* 52 (4): 2,659–2,681. https://doi.org/10.1002/2015WR018502.

MathWorks. 2021. "MATLAB and Signal Processing Toolbox Release 2021a." https://www.mathworks.com/help/signal/index.html.

Melby, J. A., N. C. Nadal-Caraballo, Y. Pagan-Albelo, and B. A. Ebersole. 2012. *Wave Height and Water Level Variability on Lakes Michigan and St. Clair*. ERDC/CHL TR-12-23. Vicksburg, MS: US Army Engineer Research and Development Center, Coastal and Hydraulics Laboratory. http://hdl.handle.net/11681/7641.

Nadal-Caraballo, N. C., J. A. Melby, and B. A. Ebersole. 2012. *Statistical Analysis and Storm Sampling Approach for Lakes Michigan and St. Clair: Great Lakes Coastal Flood Study, 2012 Federal Inter-Agency Initiative*. ERDC/CHL TR-12-19. Vicksburg, MS: US Army Engineer Research and Development Center, Coastal and Hydraulics Laboratory. https://erdc-library.erdc.dren.mil/jspui/simple-search?query=1011362.

Nadal-Caraballo, N. C., M. C. Yawn, L. A. Aucoin, M. L. Carr, J. A. Melby, E. Ramos-Santiago, V. M. Gonzalez, et al. 2022. *Coastal Hazards System–Louisiana (CHS-LA)*. ERDC/CHL TR-22-16. Vicksburg, MS: US Army Engineer Research and Development Center, Coastal and Hydraulics Laboratory. http://dx.doi.org/10.21079/11681/45286.

Nash, J. E., and J. V. Sutcliffe. 1970. "River Flow Forecasting through Conceptual Models Part I—A Discussion of Principles." *Journal of Hydrology* 10 (3): 282–290. https://doi.org/10.1016/0022-1694(70)90255-6.

NOAA (National Oceanic and Atmospheric Administration). 2021. "What Is a Seiche?" https://oceanservice.noaa.gov/facts/seiche.html.

Ohio DPS (Ohio Department of Public Safety). 2019. *State of Ohio Enhanced Hazard Mitigation Plan*. Columbus, OH: Ohio DPS. https://sharpp.dps.ohio.gov/OhioSHARPP/Documents/OhioMitigationPlan/2014/Section_28_Seiche_Coastal_Flooding.pdf.

RAMPP (Risk Assessment, Mapping, and Planning Partners). 2012. *Lake Erie Storm Surge Study*. Chicago, IL: FEMA. https://chs.erdc.dren.mil/Library/CHS_Studies/FEMA_RiskMAP_GreatLakesStudy/Publications/Lake_Erie_Final_Rampp_Report.pdf.

Scheffner, N. W., J. E. Clausner, A. Militello, L. E. Borgman, B. L. Edge, and P. J. Grace. 1999. *Use and Application of the Empirical Simulation Technique: User's Guide*. Technical Report CHL-99-21. Vicksburg, MS: US Army Engineer Waterways Experiment Station. http://hdl.handle.net/11681/7478.

USGS (United States Geological Survey). "The National Map: National Hydrography Dataset." *National Map*. https://basemap.nationalmap.gov/.

Wu, Q., and P. Vos. 2018. "Inference and Prediction." In *Computational Analysis and Understanding of Natural Languages: Principles, Methods and Applications*, edited by V. N. Gudivada and C. R. Rao, 111–172. Amsterdam, Netherlands: Elsevier. https://doi.org/10.1016/bs.host.2018.06.004.

Appendix A: Spectral Analysis Results

Figure A-1 through Figure A-28 show the spectral analysis results.

Figure A-1. Water-level displacement (WLD) time series computed after filtering the power spectrum for Amherstburg, Ontario (11995). From *top* to *bottom*, the axes show WLD time series using Filter Identifications (IDs) 1–4 (frequency bands containing seiching modes) and the unfiltered signal.

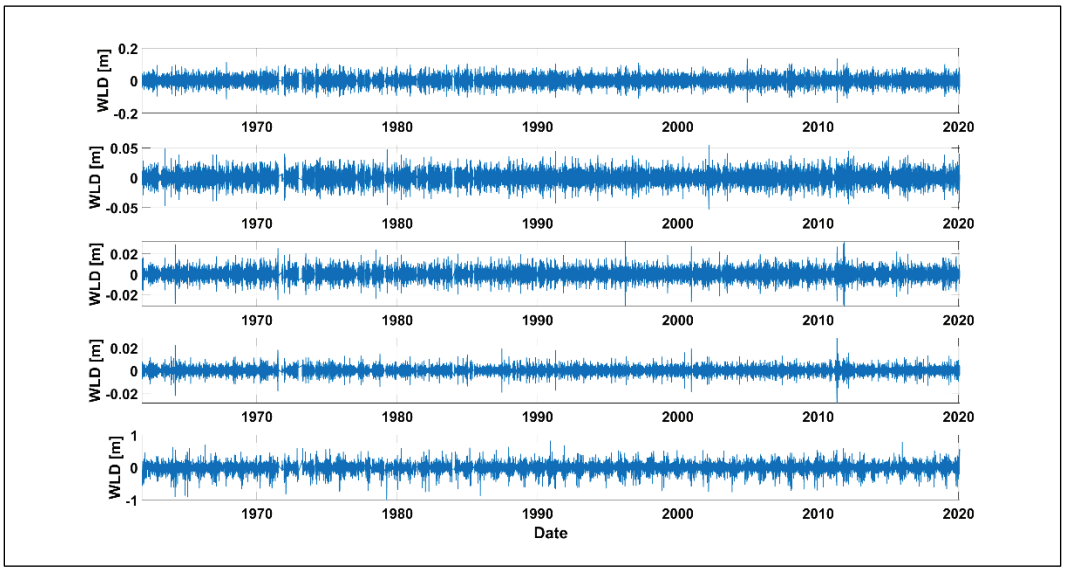

Figure A-2. WLD time series computed after filtering the power spectrum for Amherstburg, Ontario (11995). *Top* axes show WLD contributions by the combined seiching modes (Filter ID 5), and *bottom* axes show the unfiltered signal.

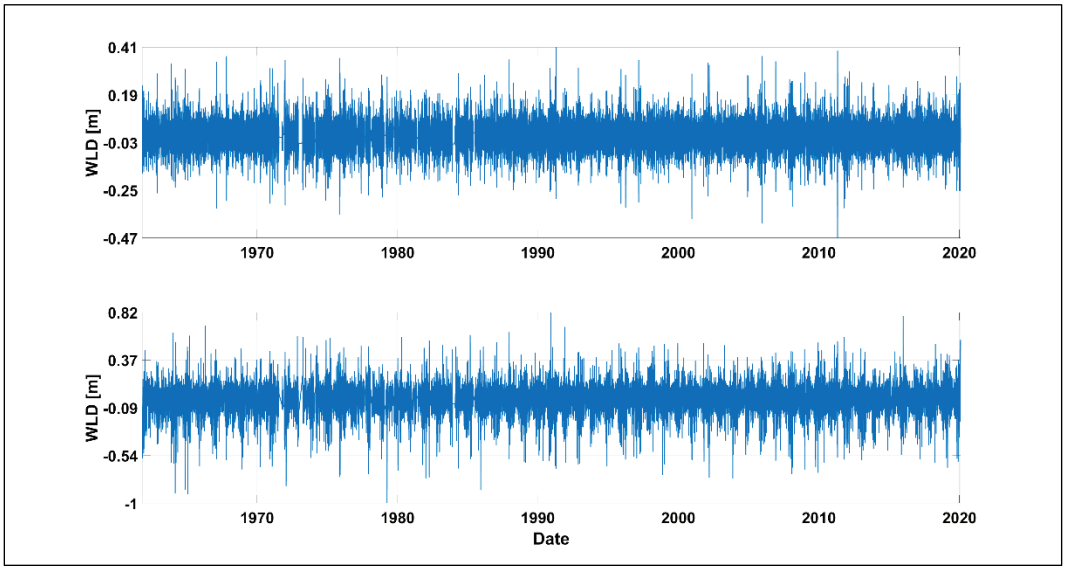

Figure A-3. WLD time series computed after filtering the power spectrum for Bar Point, Ontario (12005). From *top* to *bottom*, the axes show WLD time series using Filter IDs 1–4 (frequency bands containing seiching modes) and the unfiltered signal.

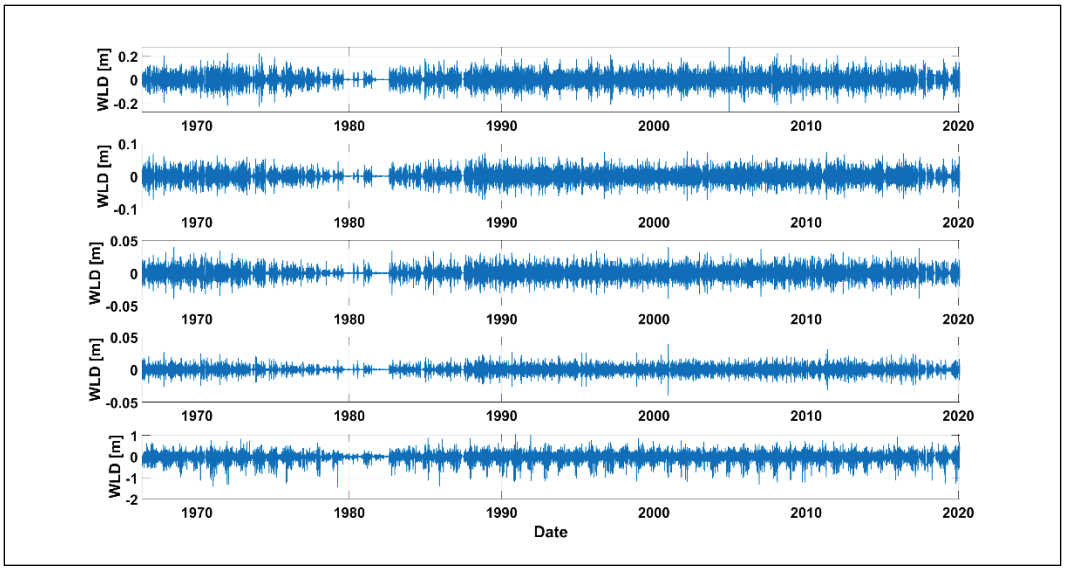

Figure A-4. WLD time series computed after filtering the power spectrum for Bar Point, Ontario (12005). *Top* axes show WLD contributions by the combined seiching modes (Filter ID 5), and *bottom* axes show the unfiltered signal.

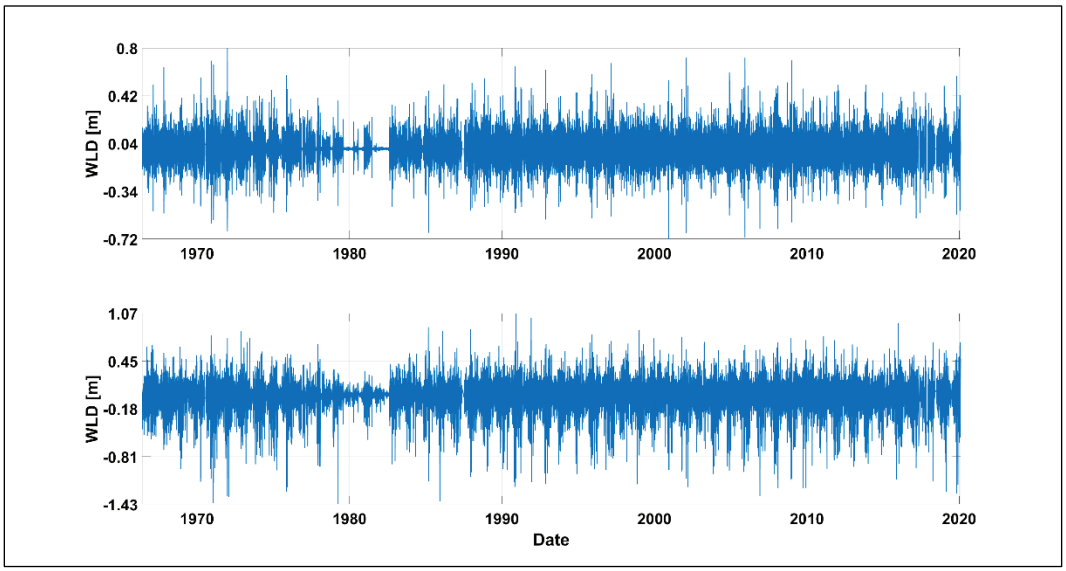

Figure A-5. WLD time series computed after filtering the power spectrum for Erieau, Ontario (12250). From *top* to *bottom*, the axes show WLD time series using Filter IDs 1–4 (frequency bands containing seiching modes) and the unfiltered signal.

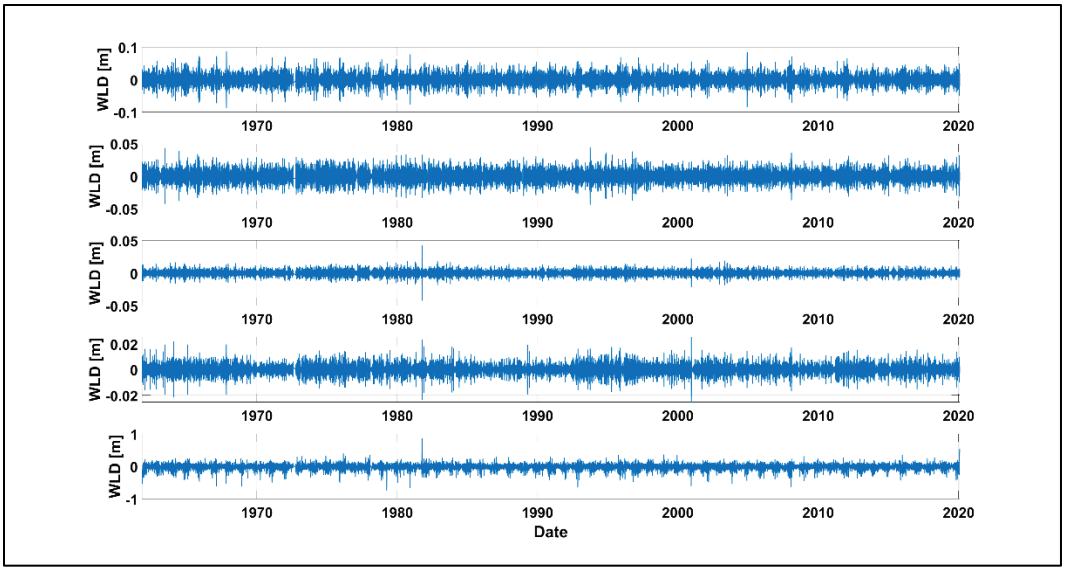

Figure A-6. WLD time series computed after filtering the power spectrum for Erieau, Ontario (12250). *Top* axes show WLD contributions by the combined seiching modes (Filter ID 5), and *bottom* axes show the unfiltered signal.

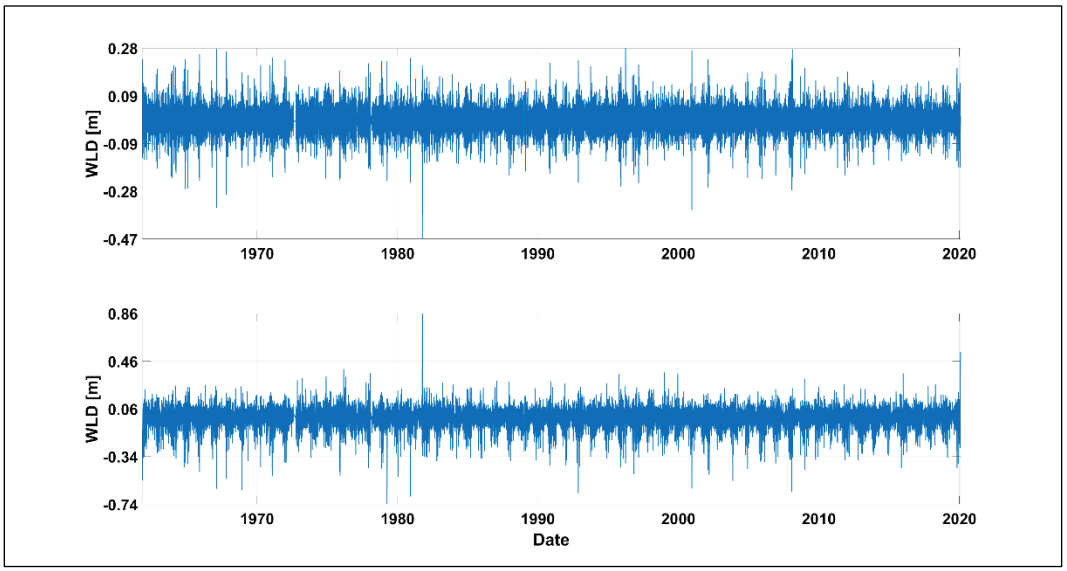

Figure A-7. WLD time series computed after filtering the power spectrum for Kingsville, Ontario (12065). From *top* to *bottom*, the axes show WLD time series using Filter IDs 1–4 (frequency bands containing seiching modes) and the unfiltered signal.

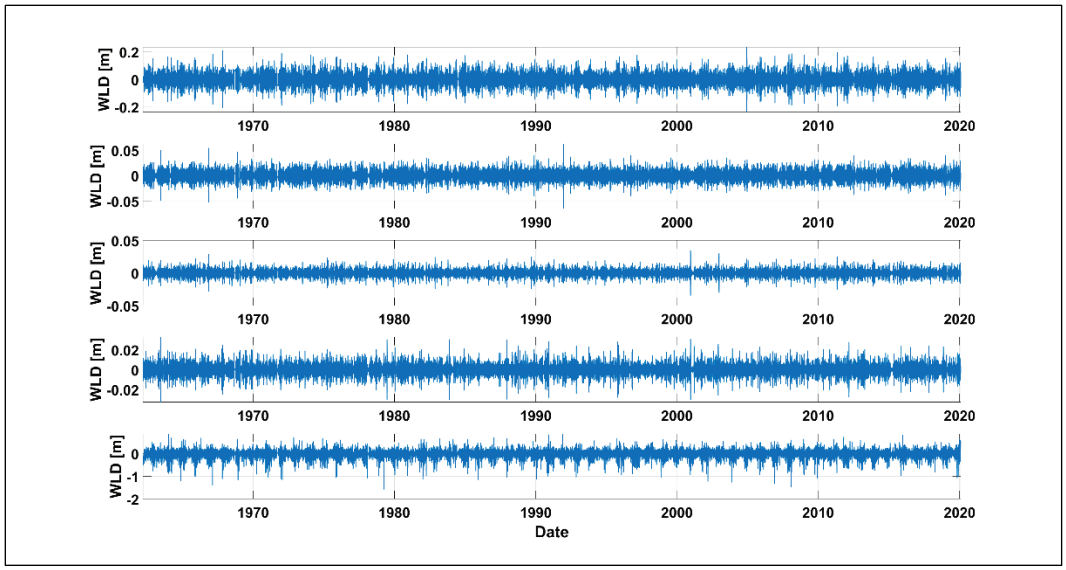

Figure A-8. WLD time series computed after filtering the power spectrum for Kingsville, Ontario (12065). *Top* axes show WLD contributions by the combined seiching modes (Filter ID 5), and *bottom* axes show the unfiltered signal.

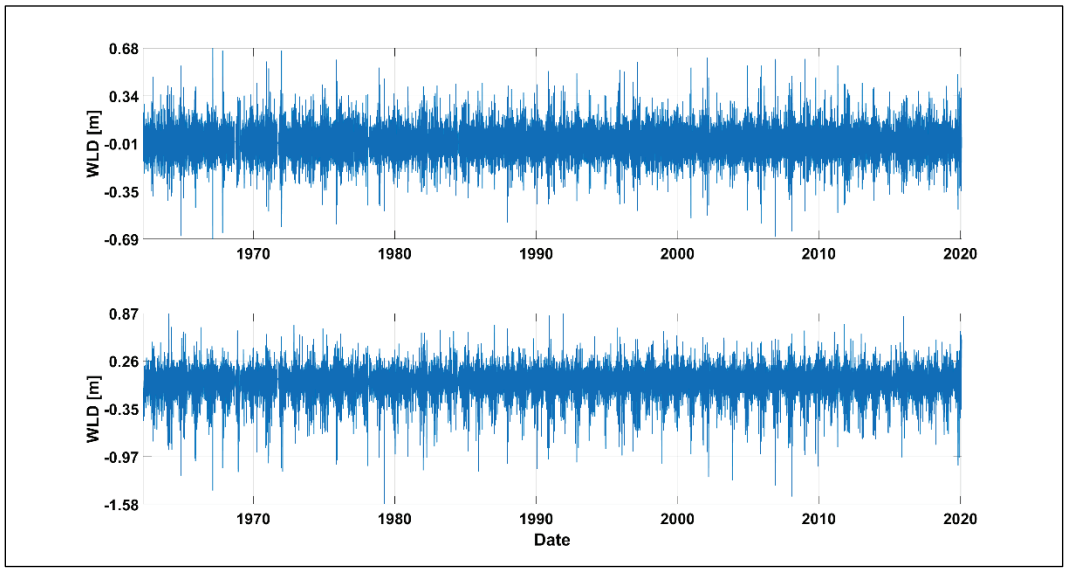

Figure A-9. WLD time series computed after filtering the power spectrum for Port Colborne, Ontario (12865). From *top* to *bottom*, the axes show WLD time series using Filter IDs 1–4 (frequency bands containing seiching modes) and the unfiltered signal.

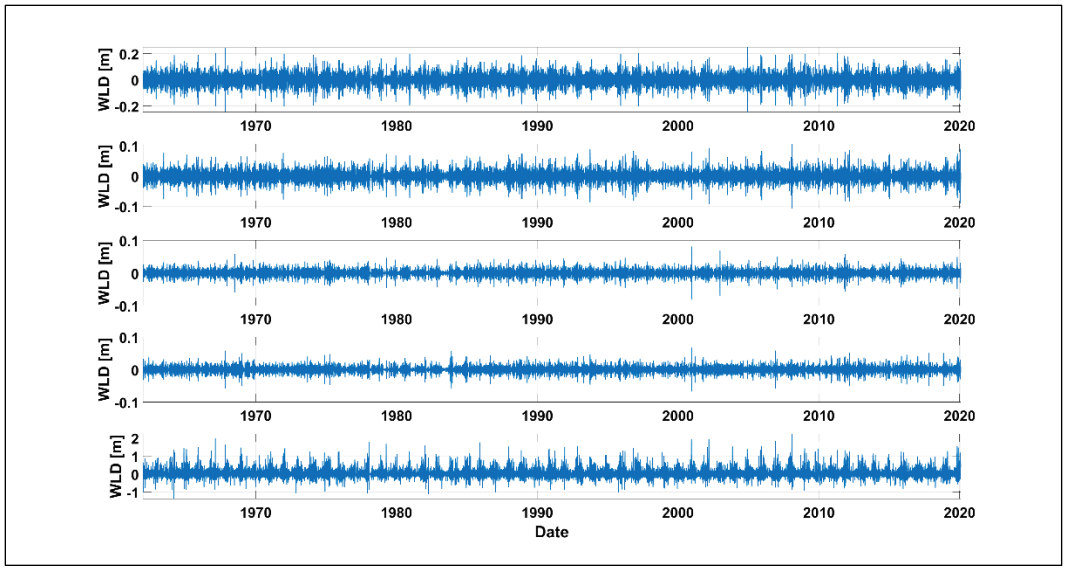

Figure A-10. WLD time series computed after filtering the power spectrum for Port Colborne, Ontario (12865). *Top* axes show WLD contributions by the combined seiching modes (Filter ID 5), and *bottom* axes show the unfiltered signal.

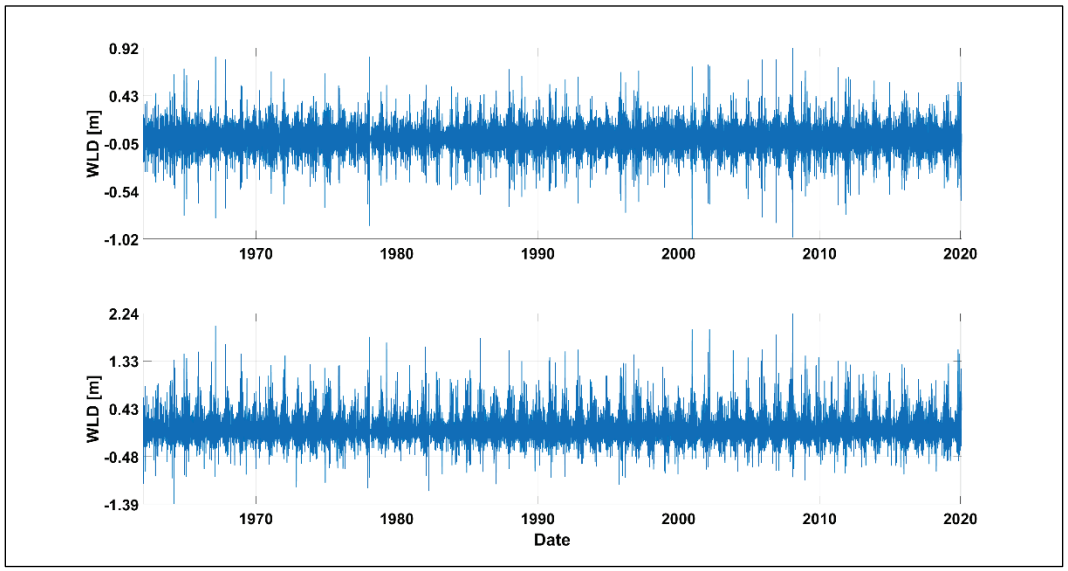

Figure A-11. WLD time series computed after filtering the power spectrum for Port Dover, Ontario (12710). From *top* to *bottom*, the axes show WLD time series using Filter IDs 1–4 (frequency bands containing seiching modes) and the unfiltered signal.

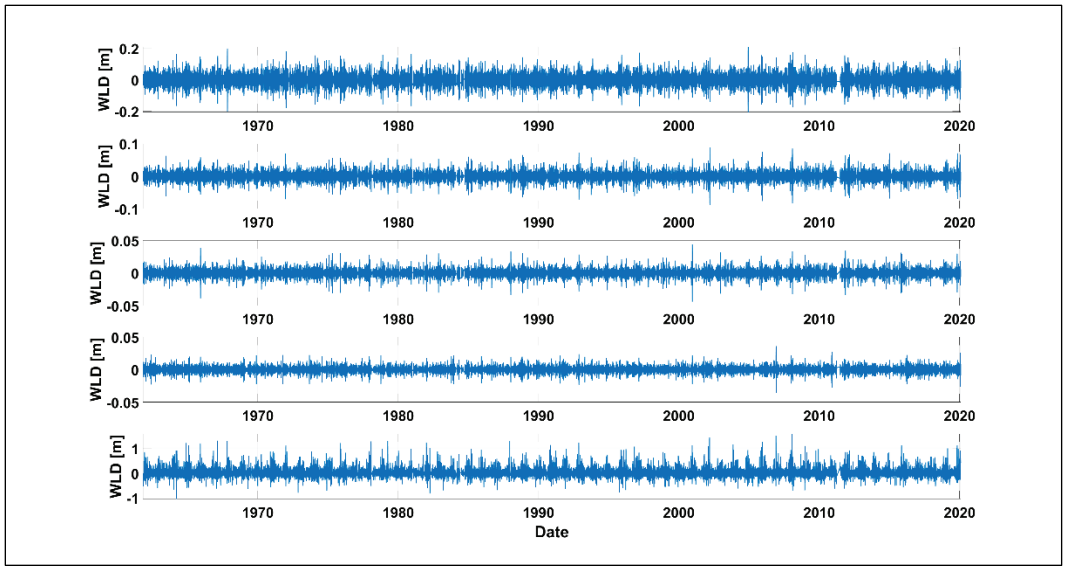

Figure A-12. WLD time series computed after filtering the power spectrum for Port Dover, Ontario (12710). *Top* axes show WLD contributions by the combined seiching modes (Filter ID 5), and *bottom* axes show the unfiltered signal.

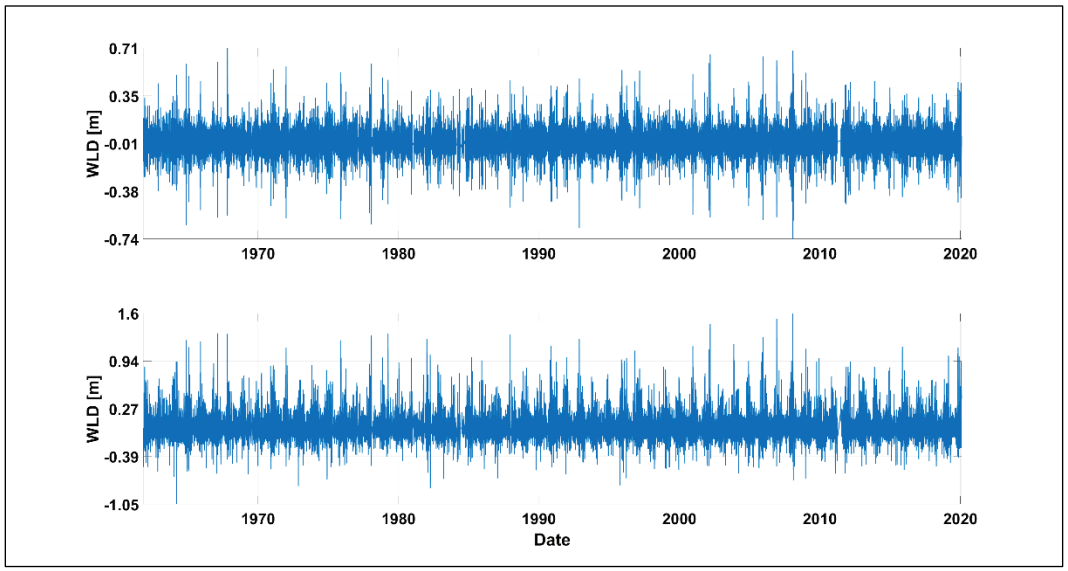

Figure A-13. WLD time series computed after filtering the power spectrum for Port Stanley, Ontario (12400). From *top* to *bottom*, the axes show WLD time series using Filter IDs 1–4 (frequency bands containing seiching modes) and the unfiltered signal.

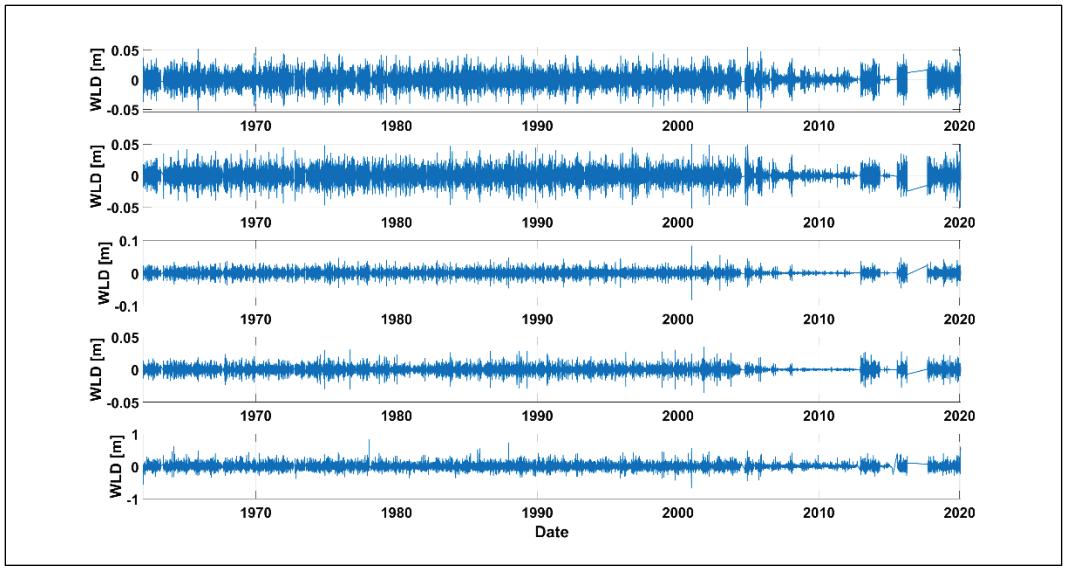

Figure A-14. WLD time series computed after filtering the power spectrum for Port Stanley, Ontario (12400). *Top* axes show WLD contributions by the combined seiching modes (Filter ID 5), and *bottom* axes show the unfiltered signal.

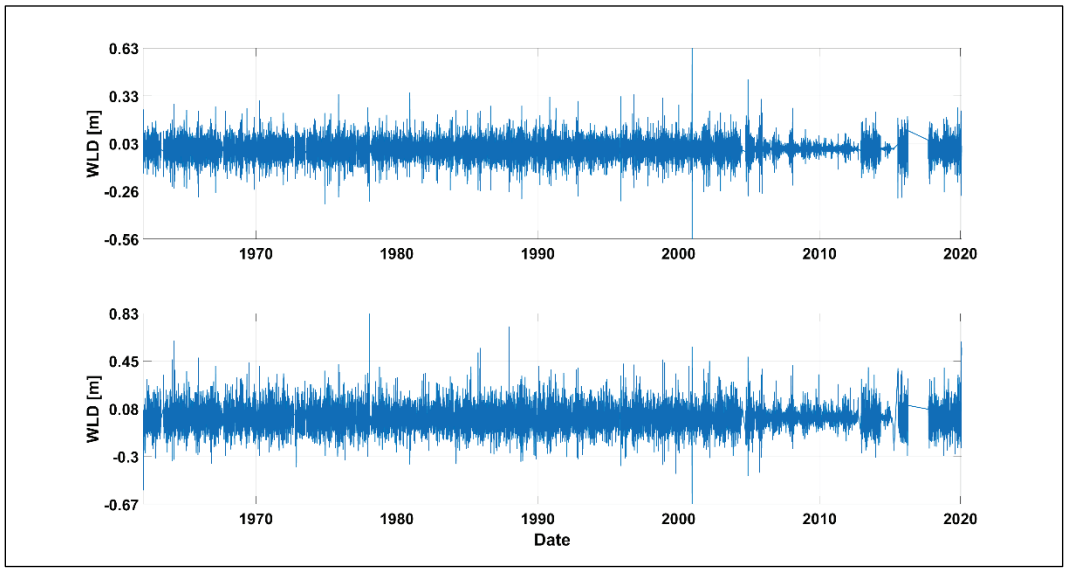

Figure A-15. WLD time series computed after filtering the power spectrum for Fermi Power Plant (9063090). From *top* to *bottom*, the axes show WLD time series using filter IDs 1–4 (frequency bands containing seiching modes) and the unfiltered signal.

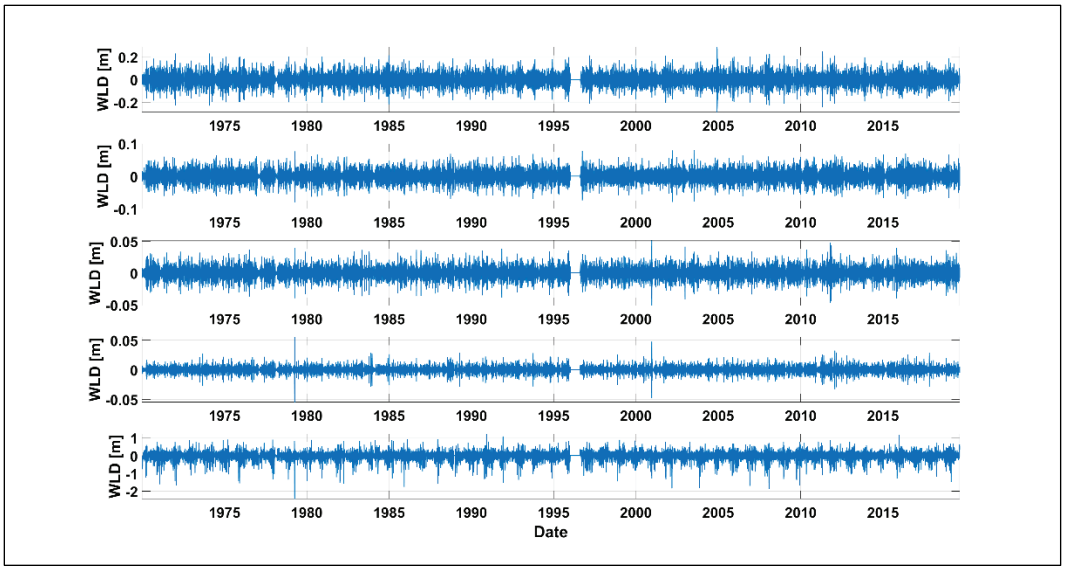

Figure A-16. WLD time series computed after filtering the power spectrum for Fermi Power Plant (9063090). *Top* axes show WLD contributions by the combined seiching modes (Filter ID 5), and *bottom* axes show the unfiltered signal.

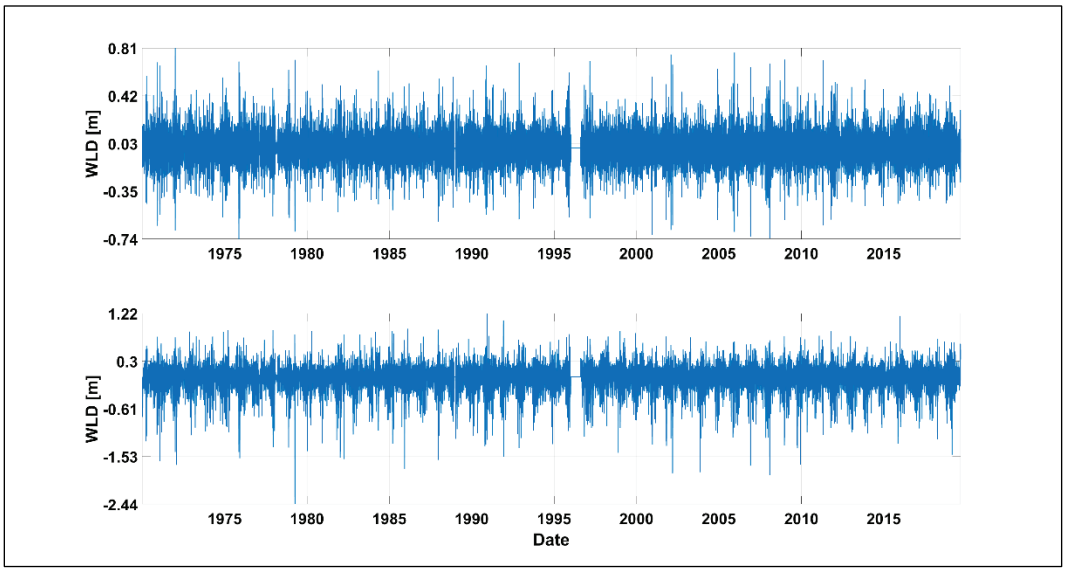

Figure A-17. WLD time series computed after filtering the power spectrum for Toledo (9063085). From *top* to *bottom*, the axes show WLD time series using Filter IDs 1–4 (frequency bands containing seiching modes) and the unfiltered signal.

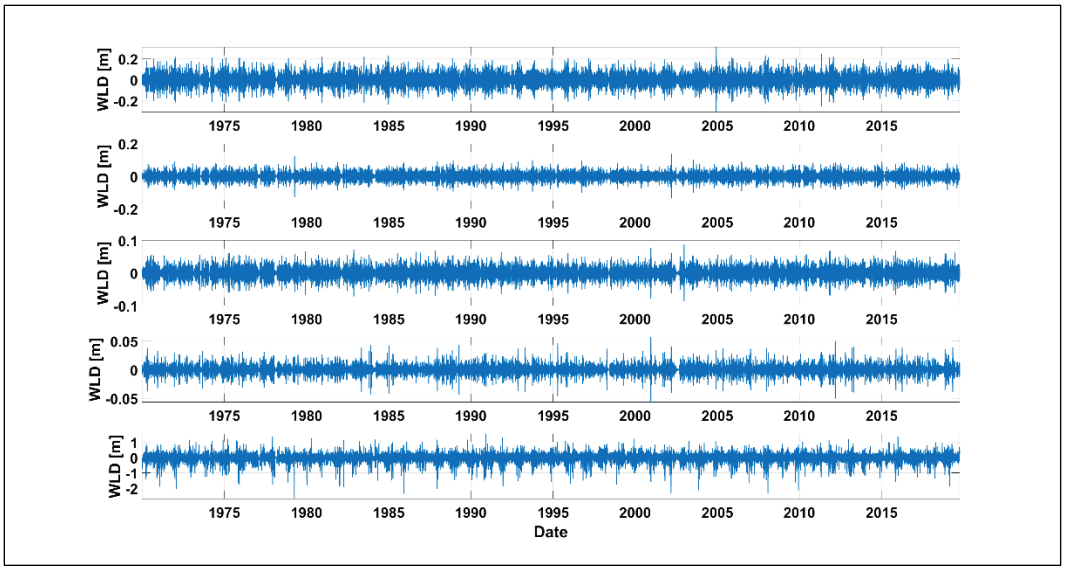

Figure A-18. WLD time series computed after filtering the power spectrum for Toledo (9063085). *Top* axes show WLD contributions by the combined seiching modes (Filter ID 5), and *bottom* axes show the unfiltered signal.

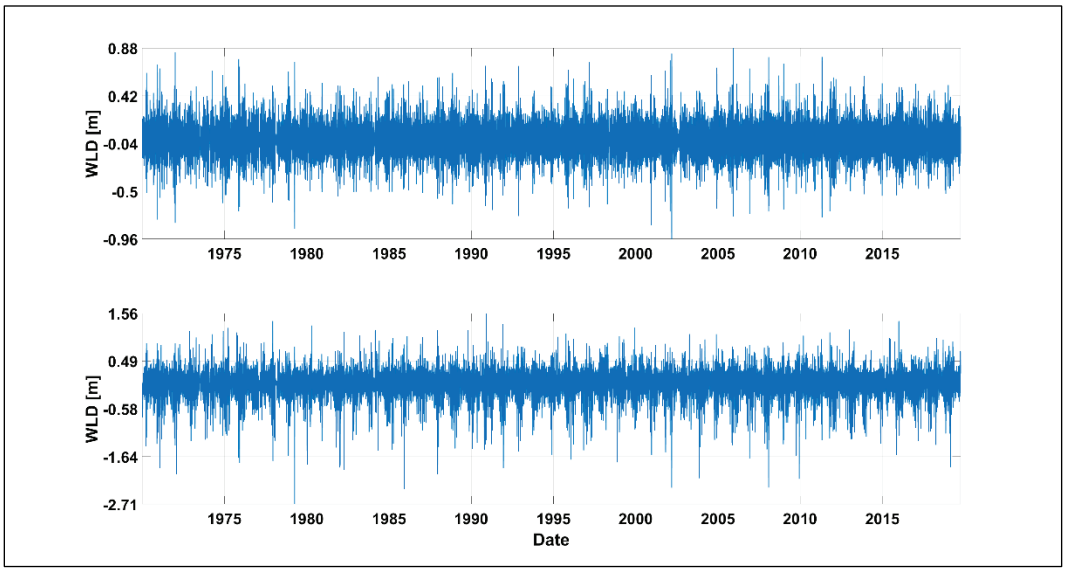

Figure A-19. WLD time series computed after filtering the power spectrum for Marblehead (9063079). From *top* to *bottom*, the axes show WLD time series using Filter IDs 1–4 (frequency bands containing seiching modes) and the unfiltered signal.

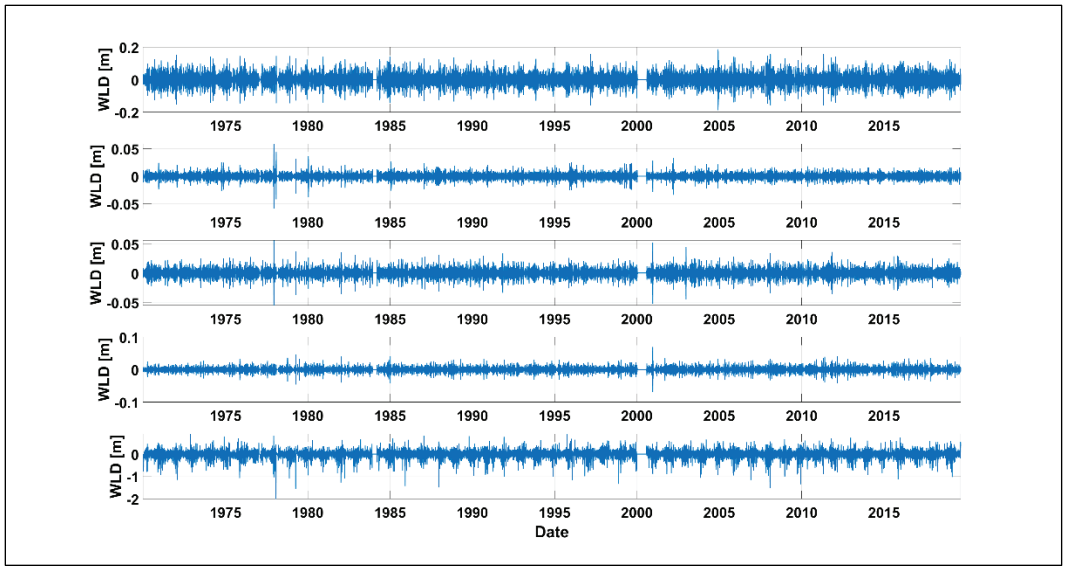

Figure A-20. WLD time series computed after filtering the power spectrum for Marblehead (9063079). *Top* axes show WLD contributions by the combined seiching modes (Filter ID 5), and *bottom* axes show the unfiltered signal.

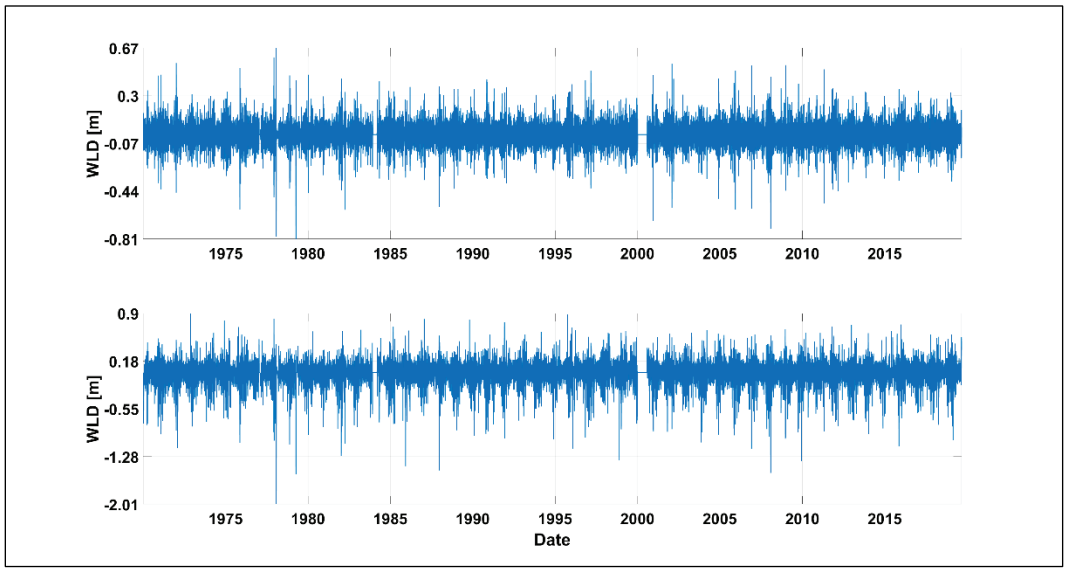

Figure A-21. WLD time series computed after filtering the power spectrum for Cleveland (9063063). From *top* to *bottom*, the axes show WLD time series using Filter IDs 1–4 (frequency bands containing seiching modes) and the unfiltered signal.

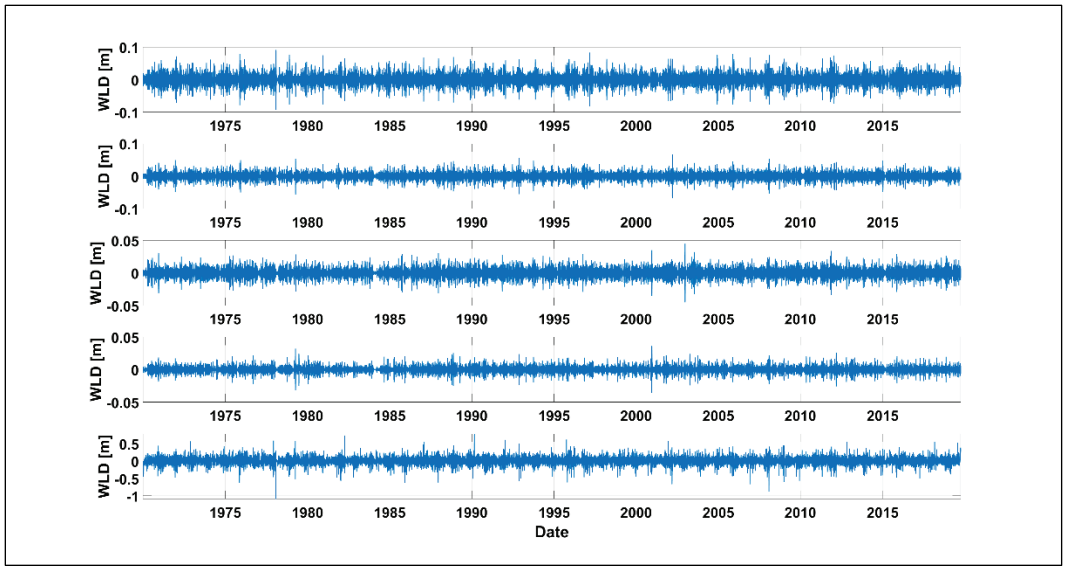

Figure A-22. WLD time series computed after filtering the power spectrum for Cleveland (9063063). *Top* axes show WLD contributions by the combined seiching modes (Filter ID 5), and *bottom* axes show the unfiltered signal.

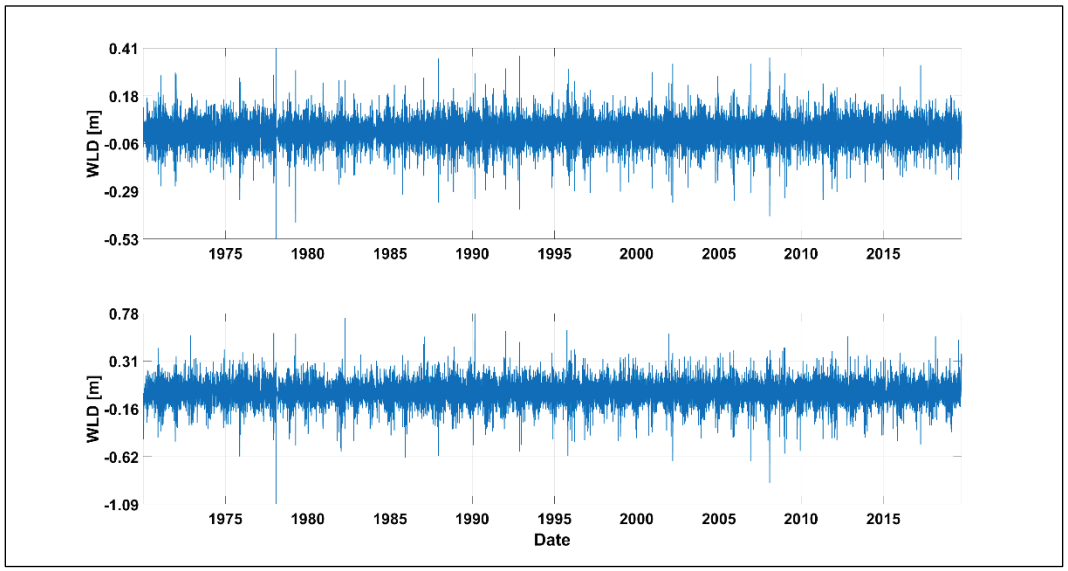

Figure A-23. WLD time series computed after filtering the power spectrum for Fairport (9063053). From *top* to *bottom*, the axes show WLD time series using Filter IDs 1–4 (frequency bands containing seiching modes) and the unfiltered signal.

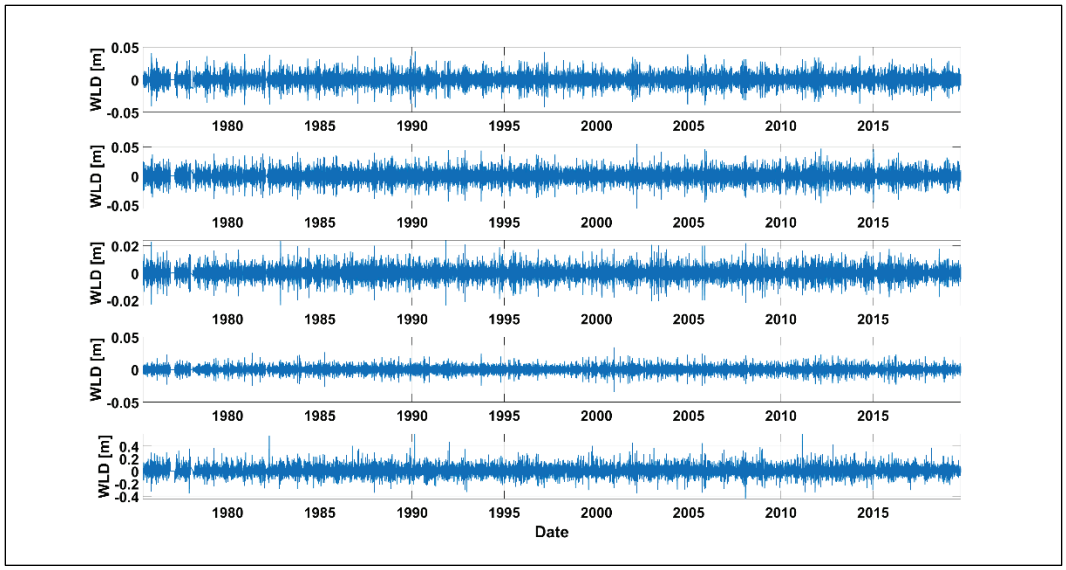

Figure A-24. WLD time series computed after filtering the power spectrum for Fairport (9063053). *Top* axes show WLD contributions by the combined seiching modes (Filter ID 5), and *bottom* axes show the unfiltered signal.

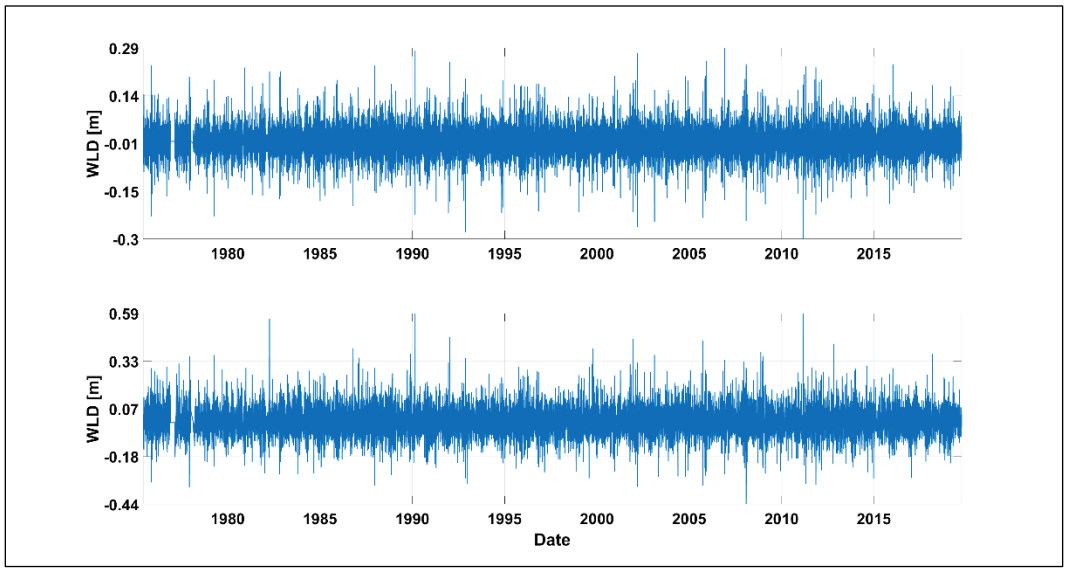

Figure A-25. WLD time series computed after filtering the power spectrum for Erie, Lake Erie (9063038). From *top* to *bottom*, the axes show WLD time series using Filter IDs 1–4 (frequency bands containing seiching modes) and the unfiltered signal.

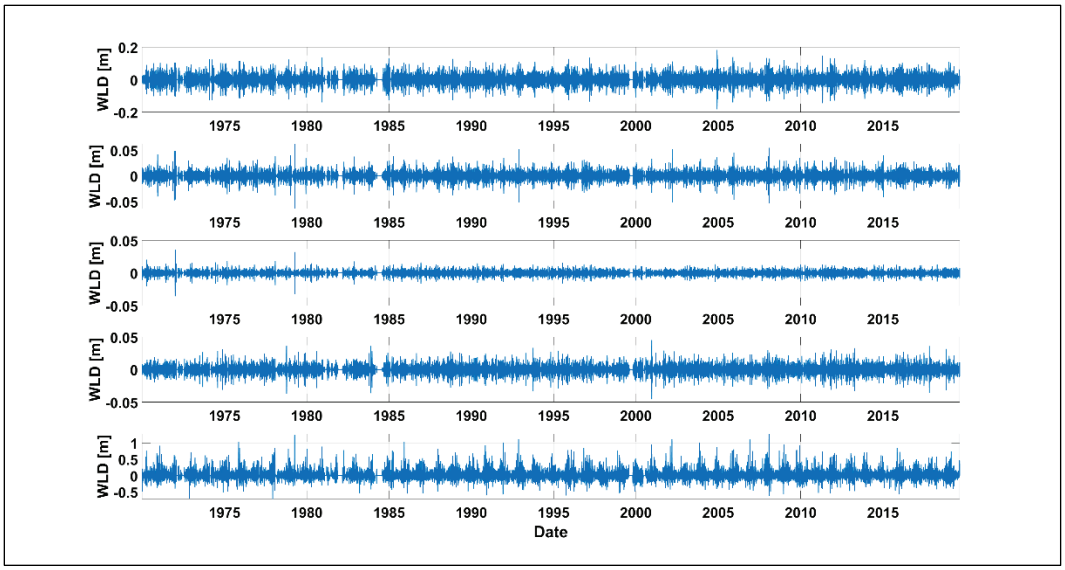

Figure A-26. WLD time series computed after filtering the power spectrum for Erie, Lake Erie (9063038). *Top* axes show WLD contributions by the combined seiching modes (Filter ID 5), and *bottom* axes show the unfiltered signal.

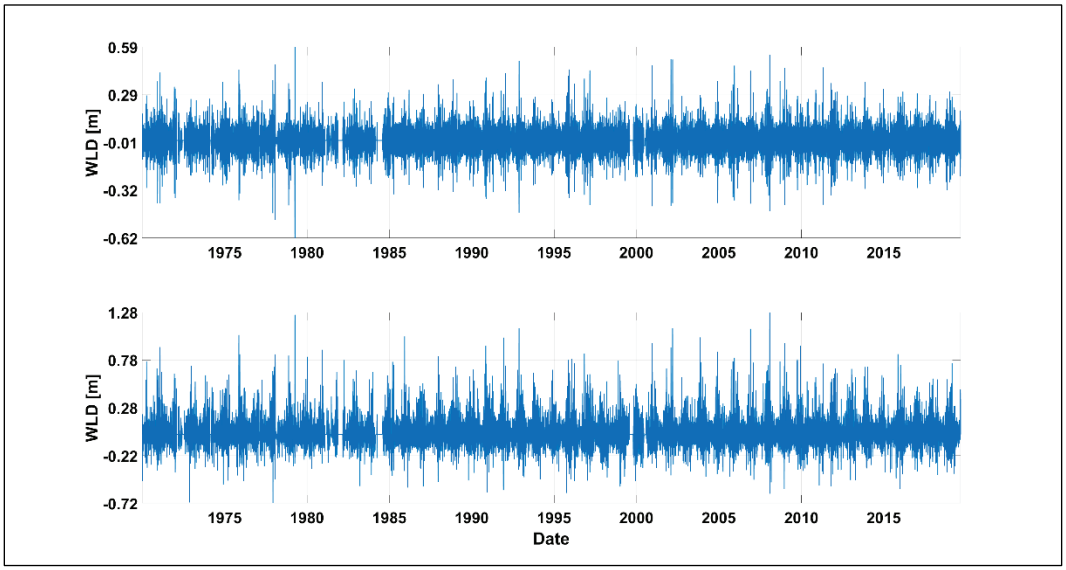

Figure A-27. WLD time series computed after filtering the power spectrum for Buffalo (9063020). From *top* to *bottom*, the axes show WLD time series using Filter IDs 1–4 (frequency bands containing seiching modes) and the unfiltered signal.

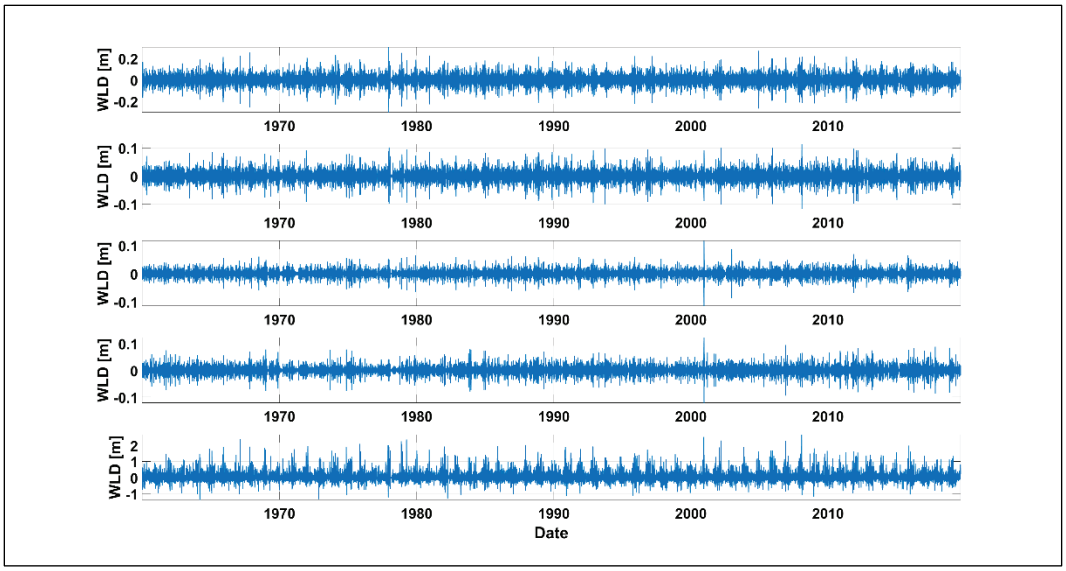

Figure A-28. WLD time series computed after filtering the power spectrum for Buffalo (9063020). *Top* axes show WLD contributions by the combined seiching modes (Filter ID 5), and *bottom* axes show the unfiltered signal.

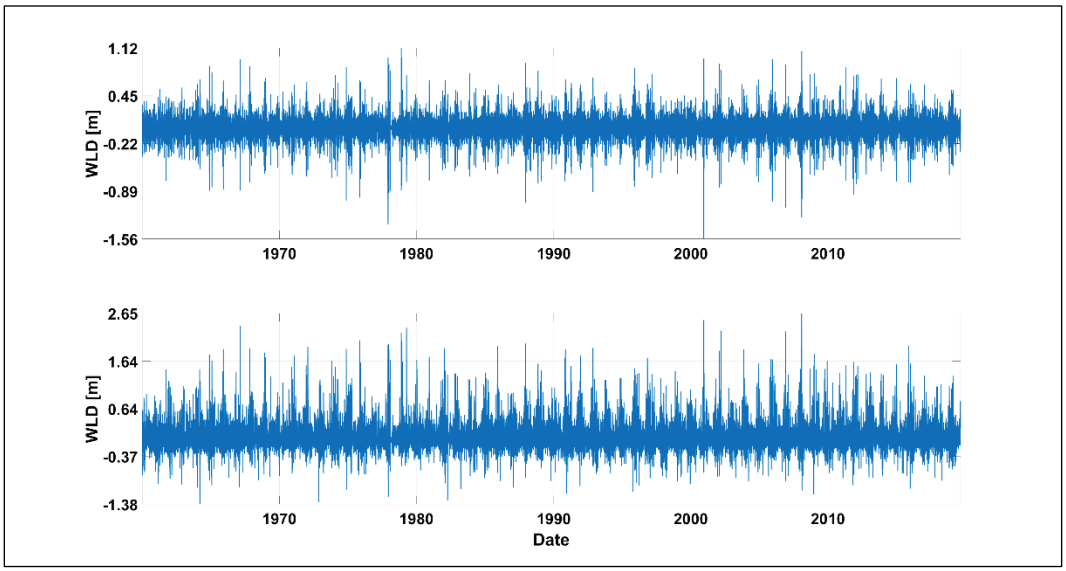

Appendix B: Local Frequency Analysis (LFA) Results per Seiche Mode

Figure B-1 through Figure B-70 show the local frequency analysis (LFA) results per seiche mode.

Figure B-1. WLD hazard curve for Seiche Mode 1 (Filter ID 1) for Amherstburg, Ontario (11995).

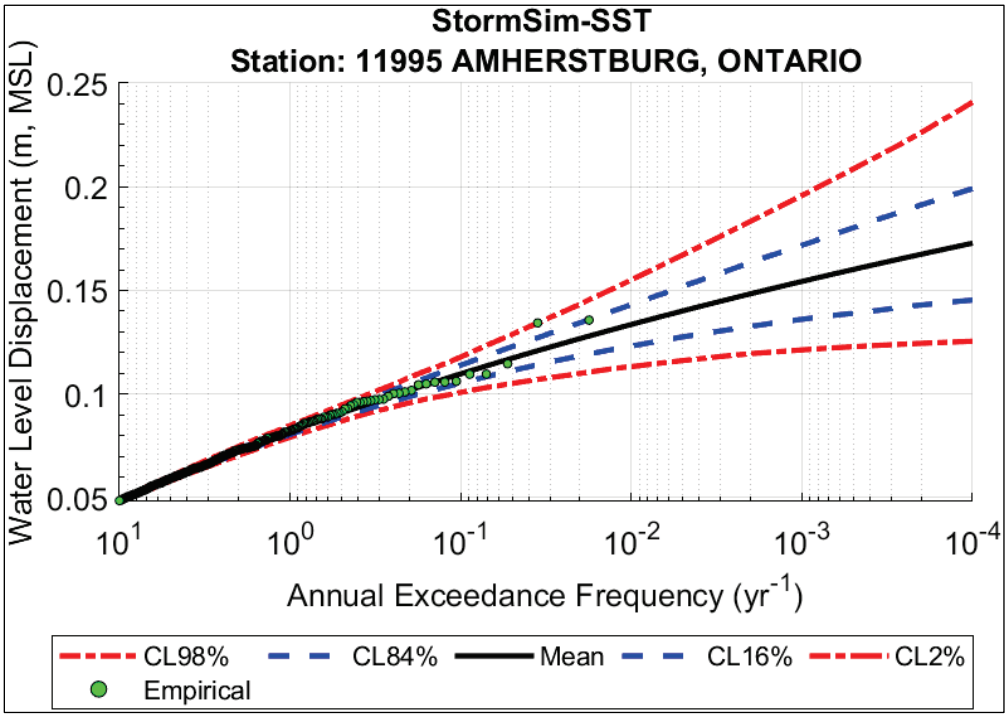

Figure B-2. WLD hazard curve for Seiche Mode 2 (Filter ID 2) for Amherstburg, Ontario (11995).

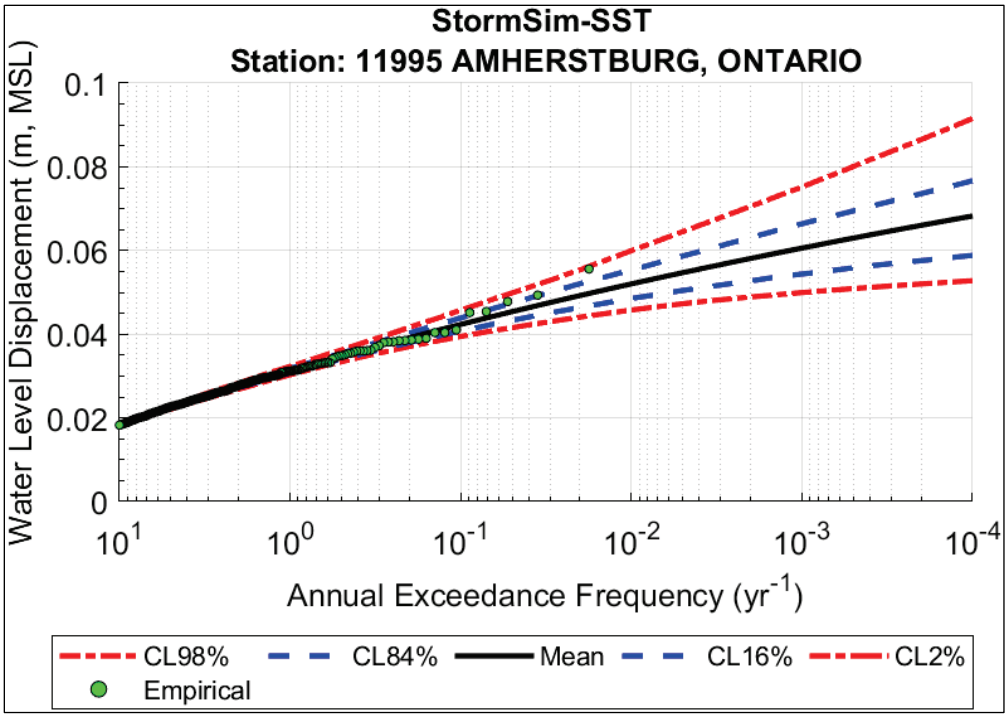

Figure B-3. WLD hazard curve for Seiche Mode 3 (Filter ID 3) for Amherstburg, Ontario (11995).

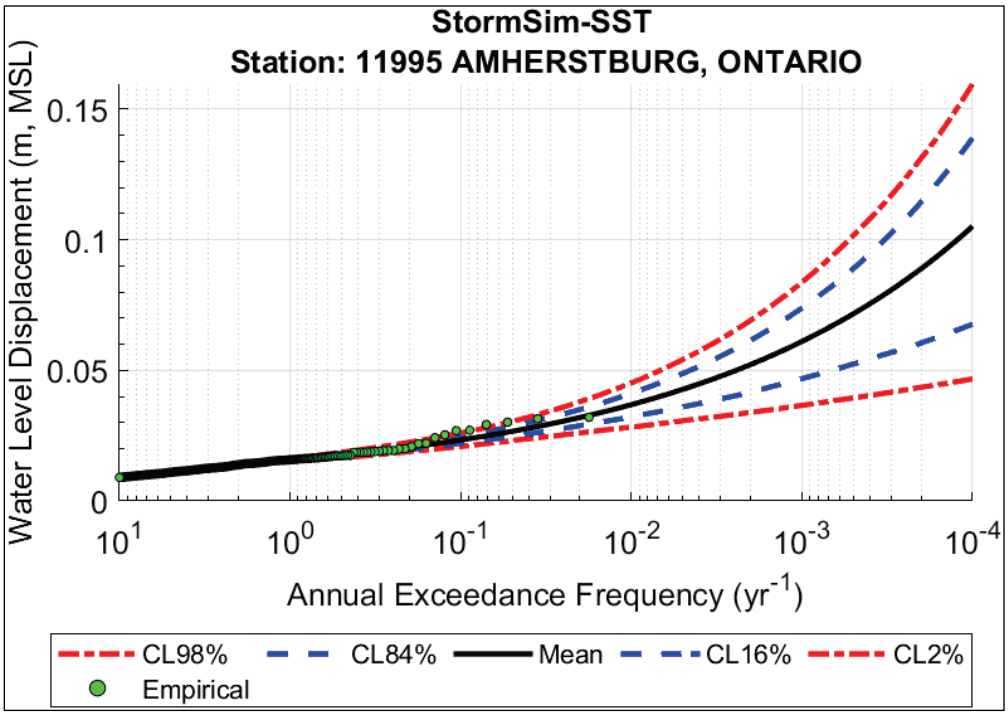

Figure B-4. WLD hazard curve for Seiche Mode 4 (Filter ID 4) for Amherstburg, Ontario (11995).

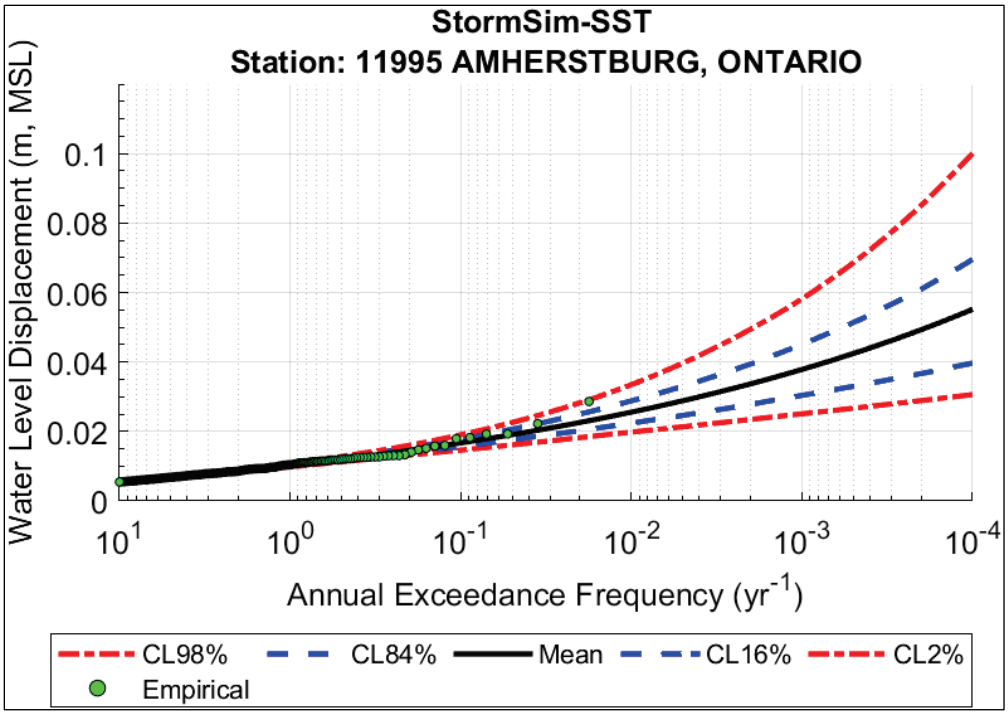

Figure B-5. Combined seiche modes (Filter ID 5) WLD hazard curve for Amherstburg, Ontario (11995).

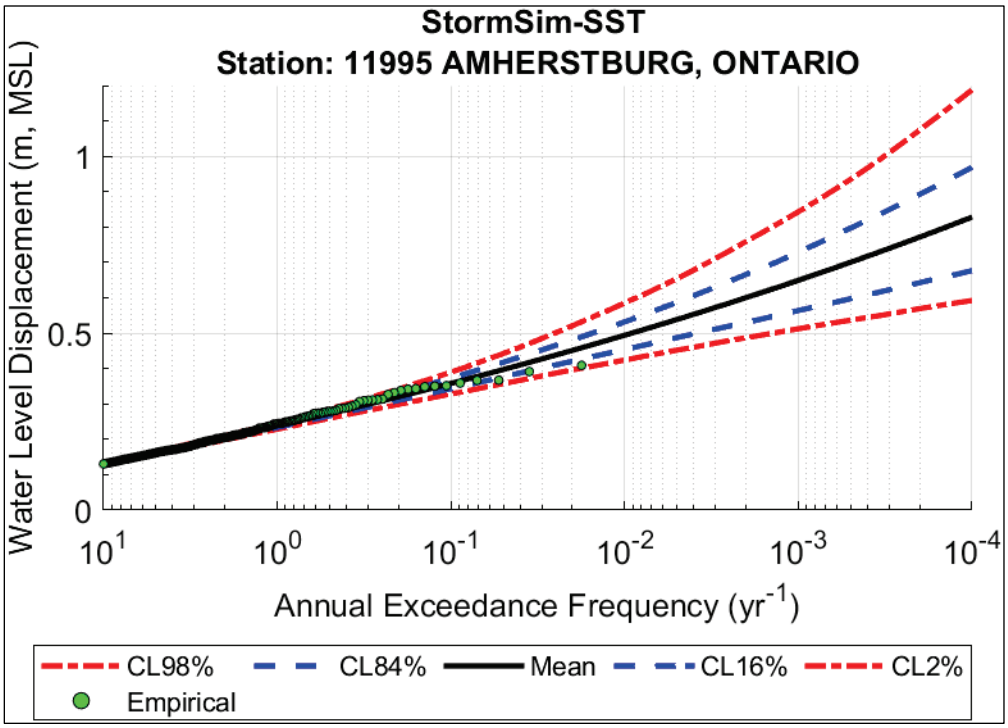

Figure B-6. WLD hazard curve for Seiche Mode 1 (Filter ID 1) for Bar Point, Ontario (12005).

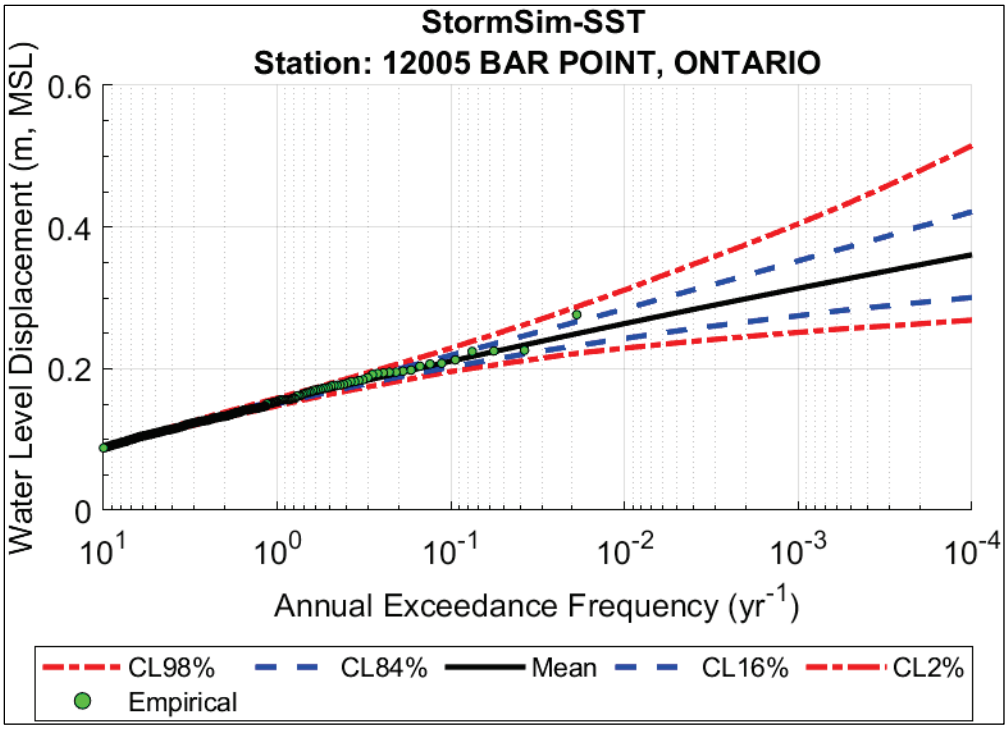

Figure B-7. WLD hazard curve for Seiche Mode 2 (Filter ID 2) for Bar Point, Ontario (12005).

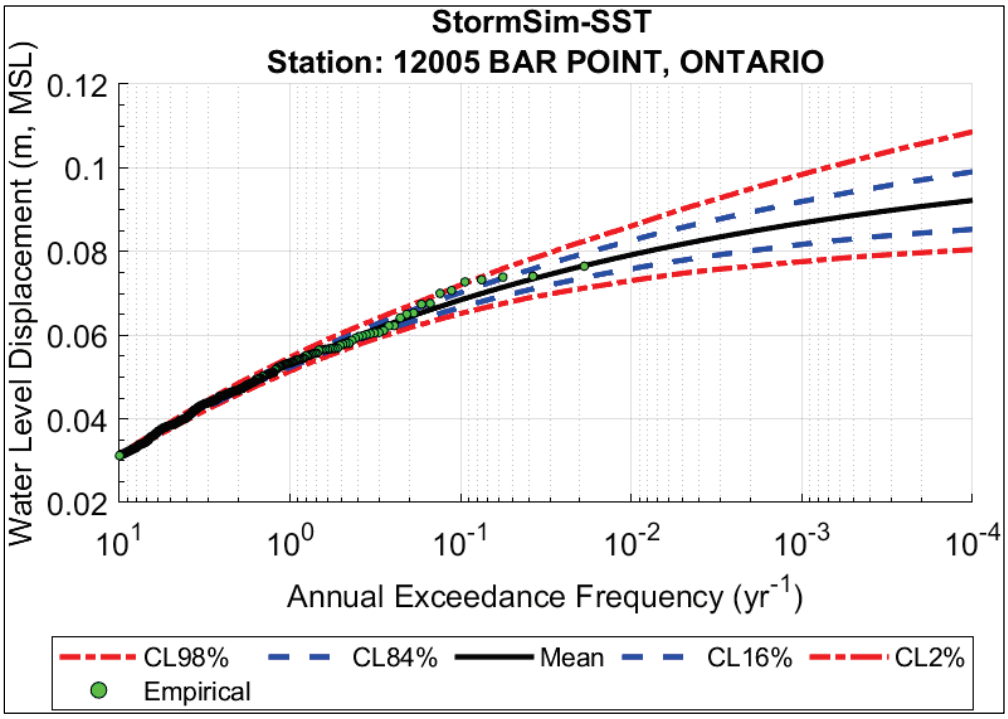

Figure B-8. WLD hazard curve for Seiche Mode 3 (Filter ID 3) for Bar Point, Ontario (12005).

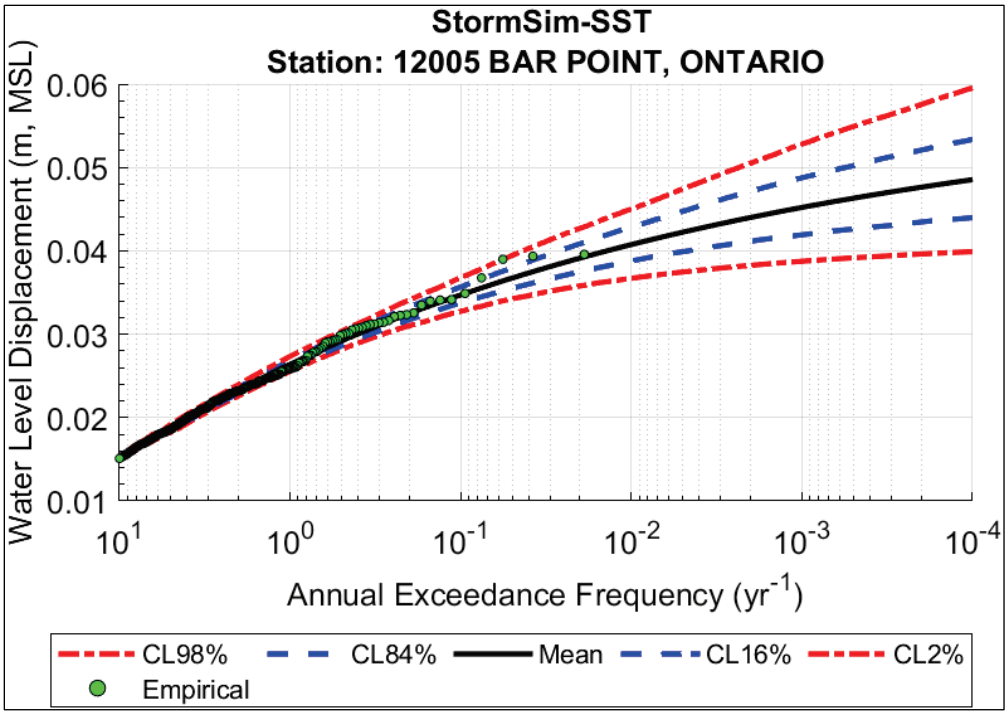

Figure B-9. WLD hazard curve for Seiche Mode 4 (Filter ID 4) for Bar Point, Ontario (12005).

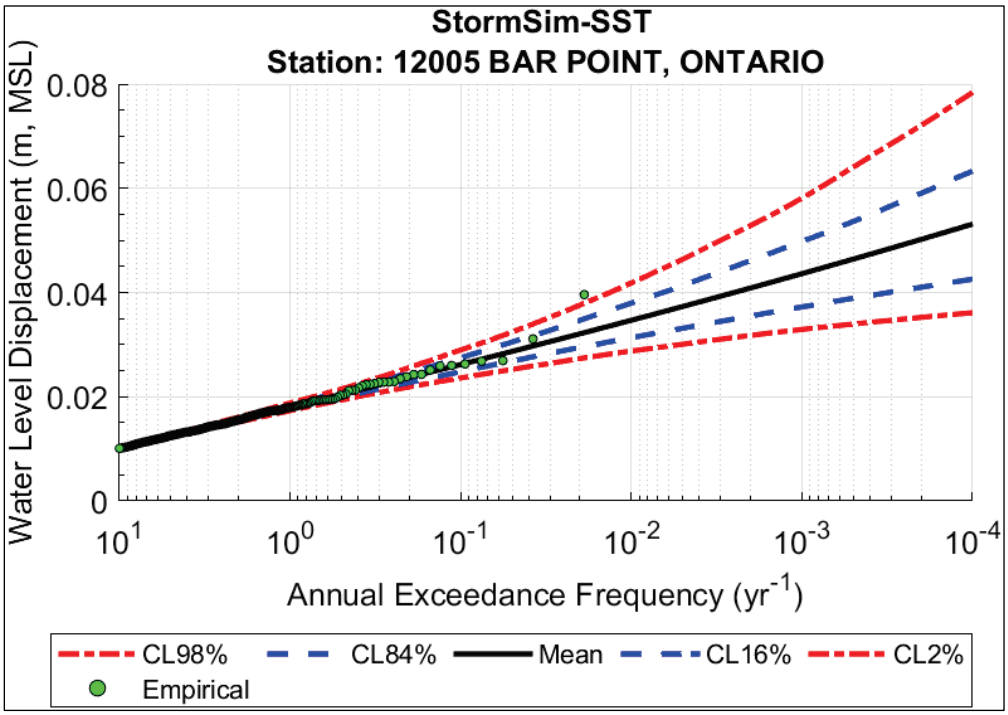

Figure B-10. Combined seiche modes (Filter ID 5) WLD hazard curve for Bar Point, Ontario (12005).

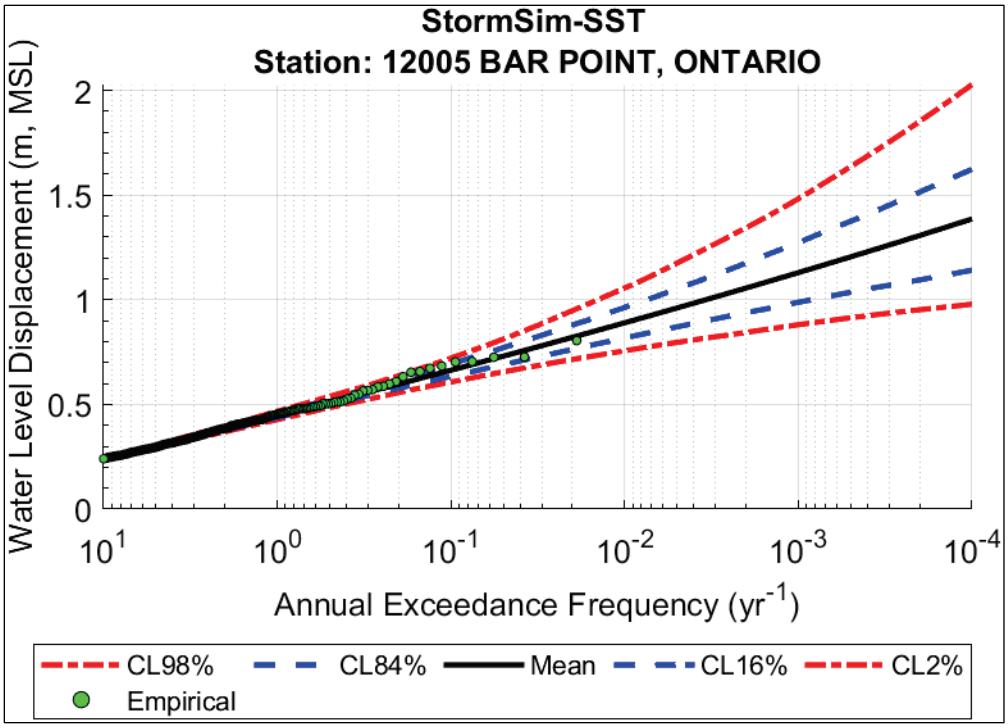

Figure B-11. WLD hazard curve for Seiche Mode 1 (Filter ID 1) for Erieau, Ontario (12250).

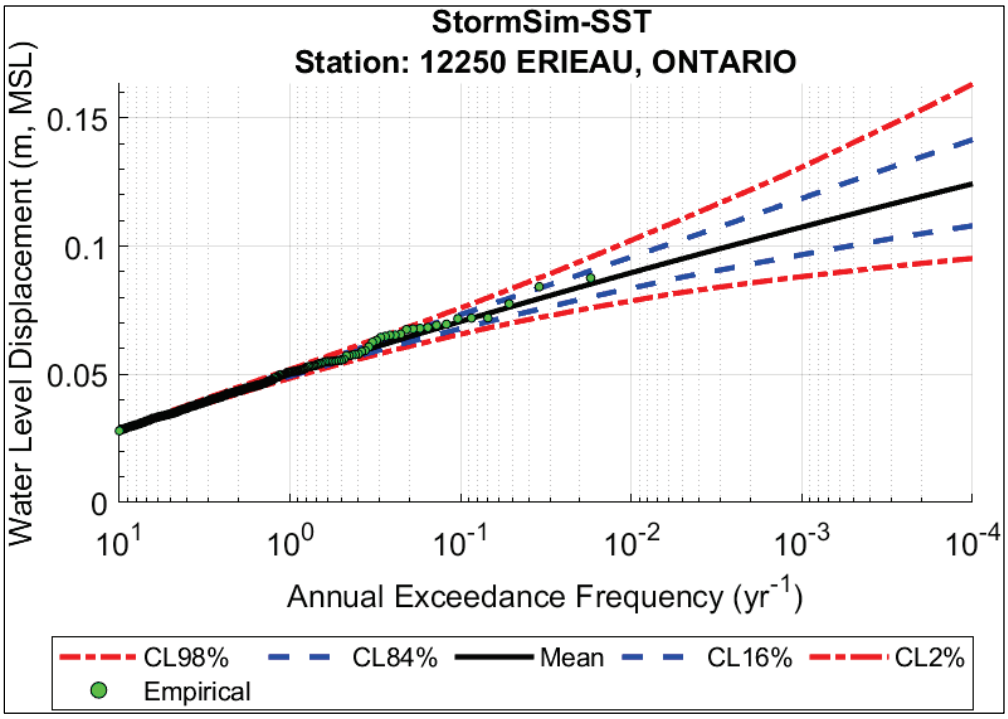

Figure B-12. WLD hazard curve for Seiche Mode 2 (Filter ID 2) for Erieau, Ontario (12250).

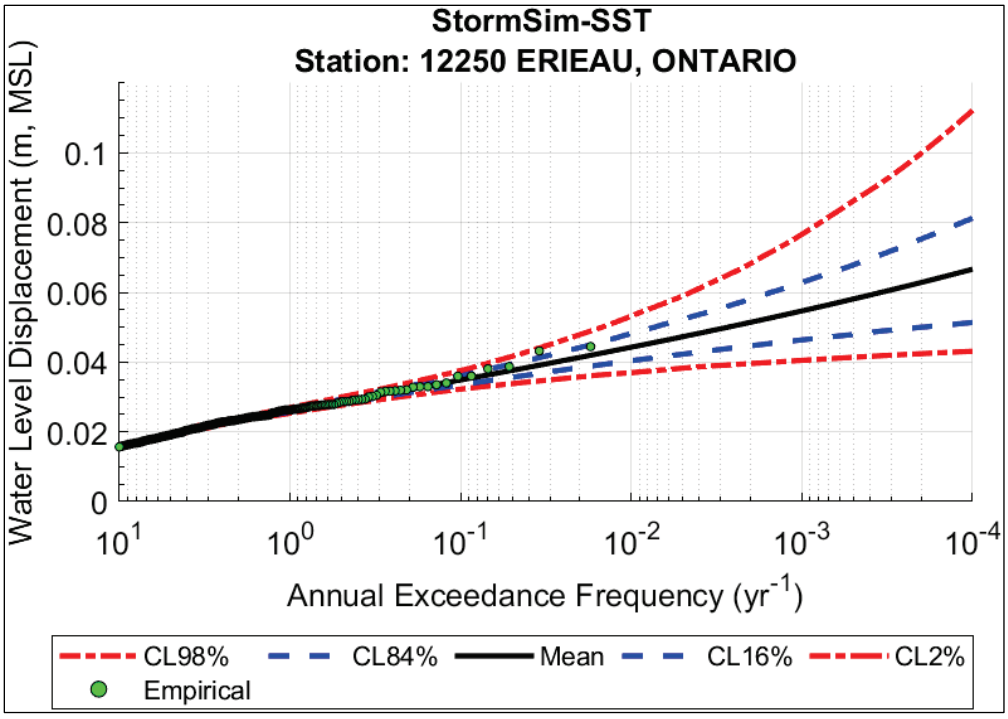

Figure B-13. WLD hazard curve for Seiche Mode 3 (Filter ID 3) for Erieau, Ontario (12250).

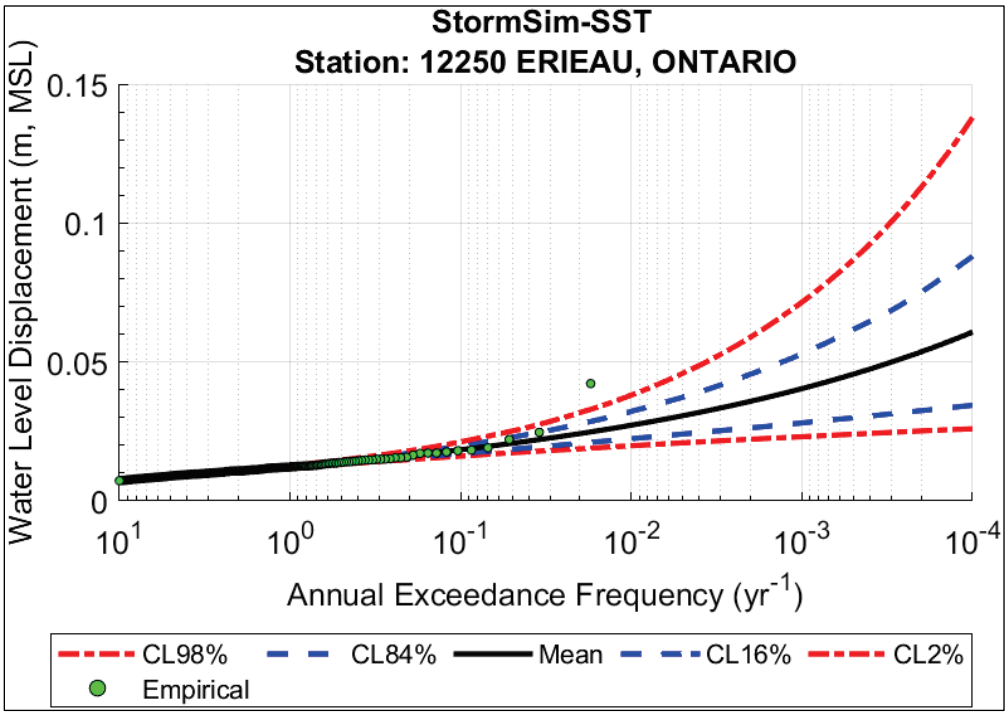

Figure B-14. WLD hazard curve for Seiche Mode 4 (Filter ID 4) for Erieau, Ontario (12250).

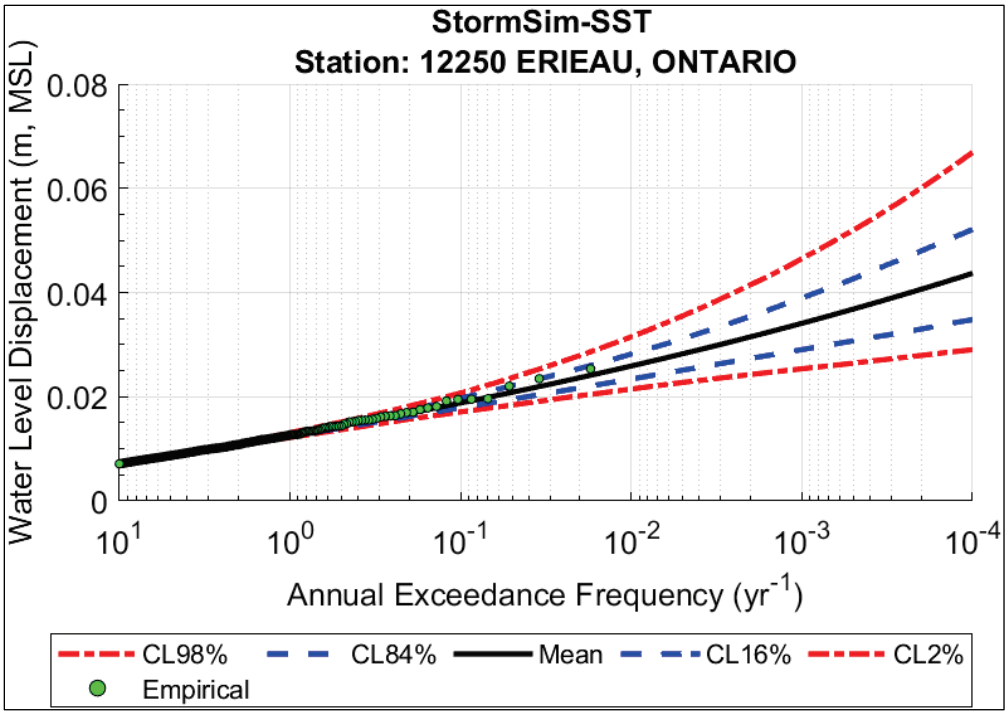

Figure B-15. Combined seiche modes (Filter ID 5) WLD hazard curve for Erieau, Ontario (12250).

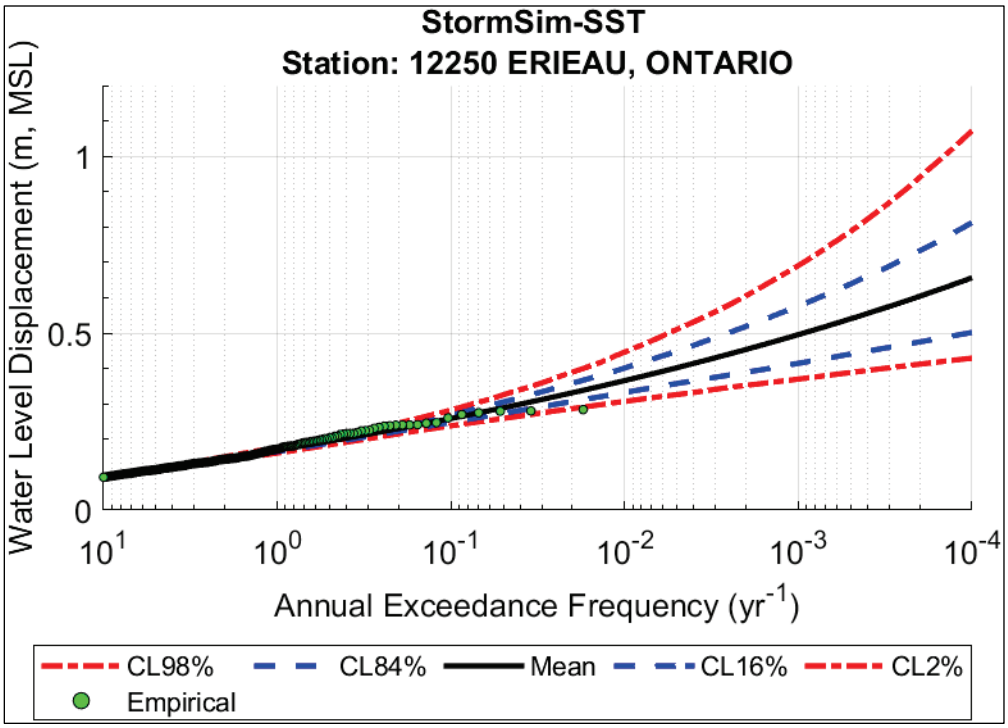

Figure B-16. WLD hazard curve for Seiche Mode 1 (Filter ID 1) for Kingsville, Ontario (12065).

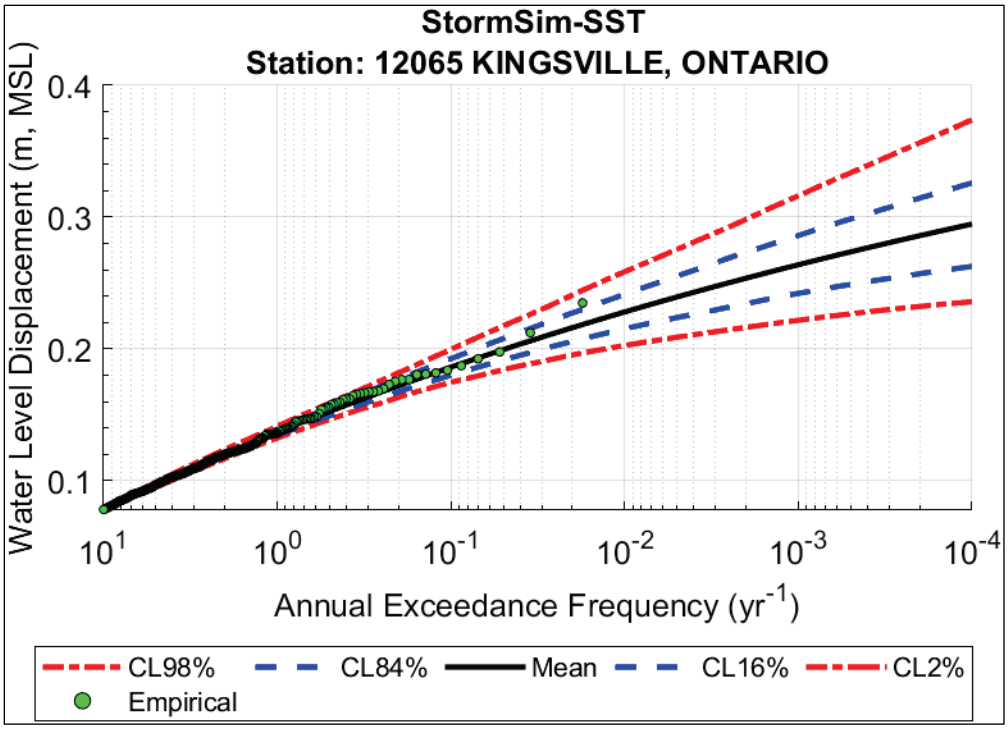

Figure B-17. WLD hazard curve for Seiche Mode 2 (Filter ID 2) for Kingsville, Ontario (12065).

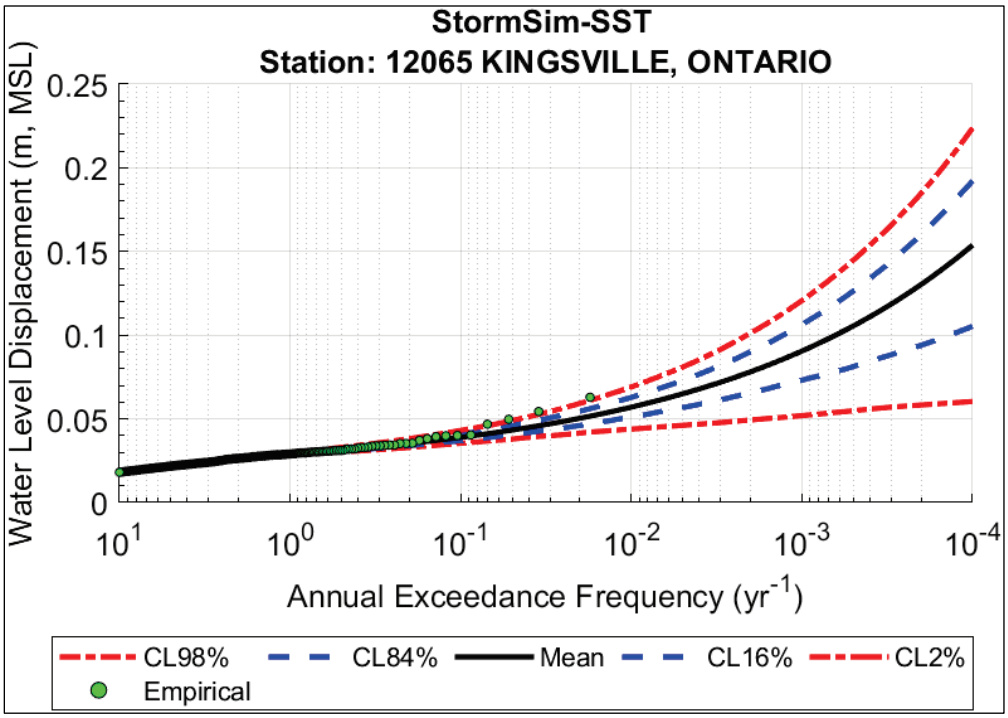

Figure B-18. WLD hazard curve for Seiche Mode 3 (Filter ID 3) for Kingsville, Ontario (12065).

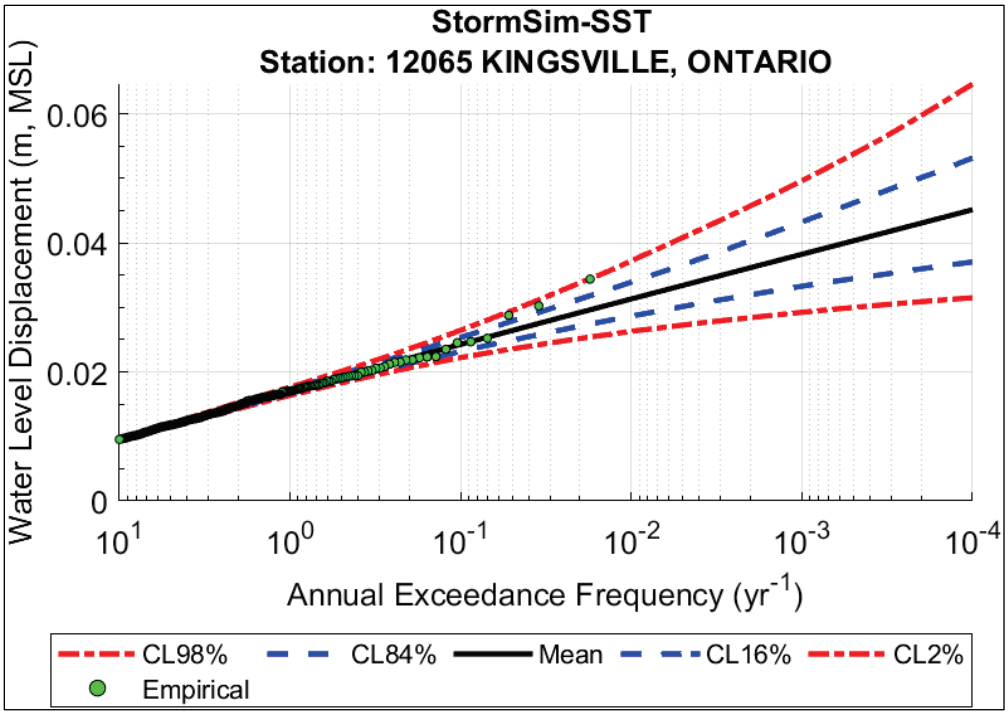

Figure B-19. WLD hazard curve for Seiche Mode 4 (Filter ID 4) for Kingsville, Ontario (12065).

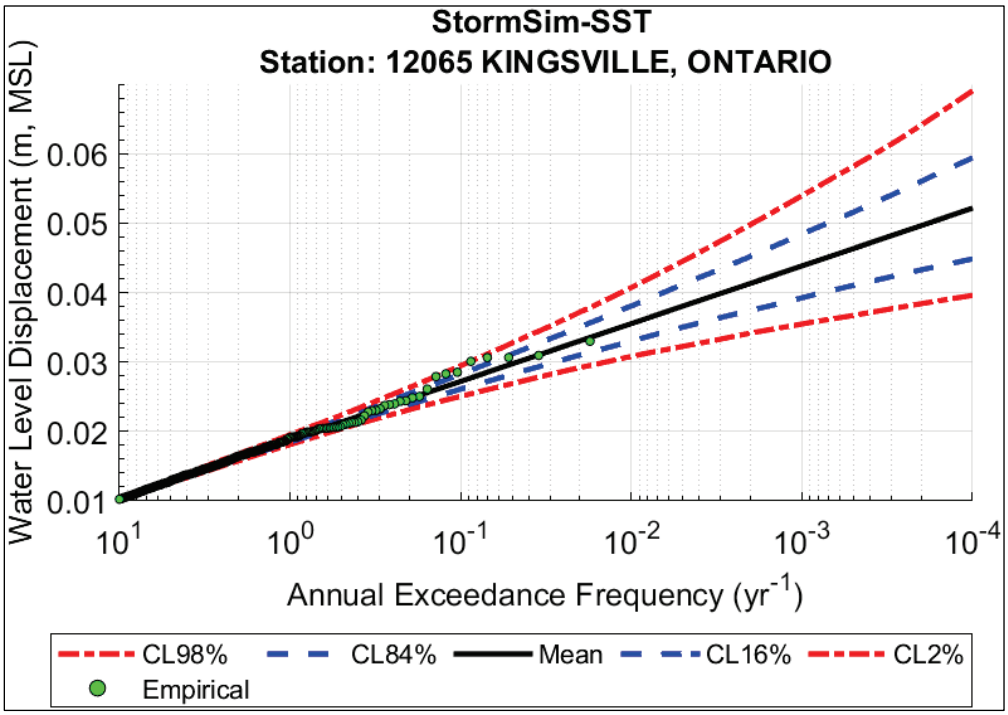

Figure B-20. Combined seiche modes (Filter ID 5) WLD hazard curve for Kingsville, Ontario (12065).

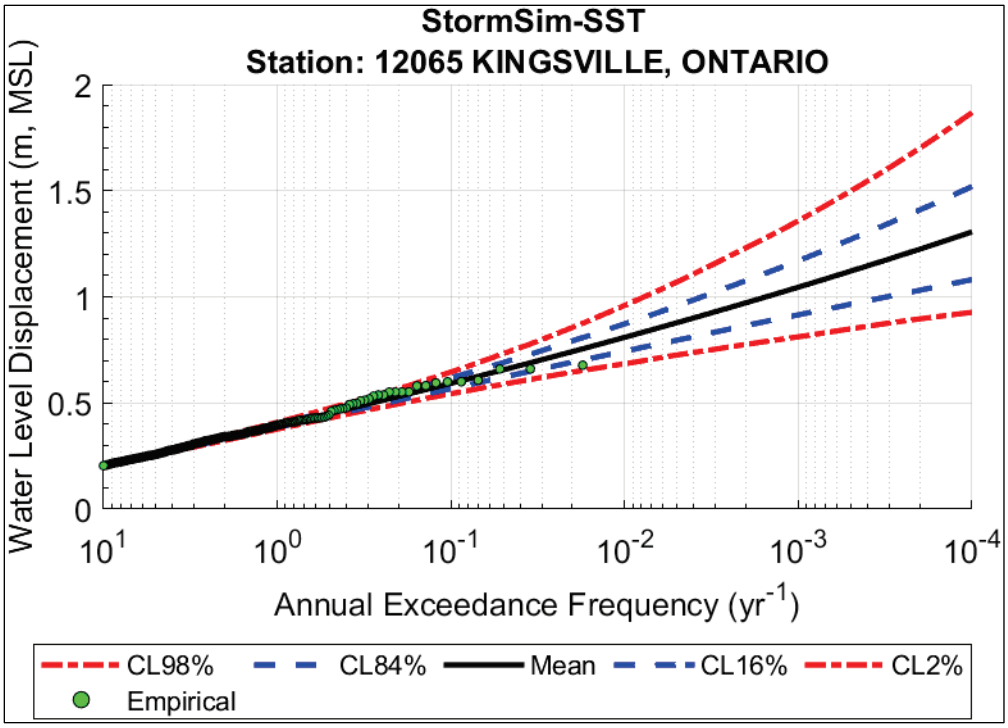

Figure B-21. WLD hazard curve for Seiche Mode 1 (Filter ID 1) for Port Colborne, Ontario (12865).

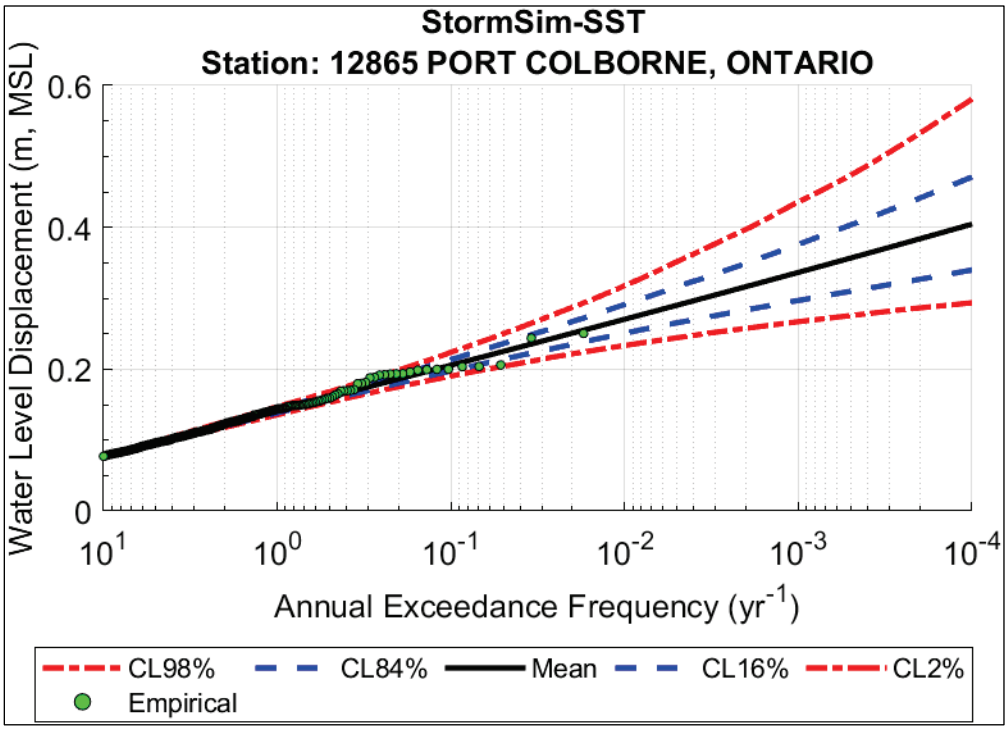

Figure B-22. WLD hazard curve for Seiche Mode 2 (Filter ID 2) for Port Colborne, Ontario (12865).

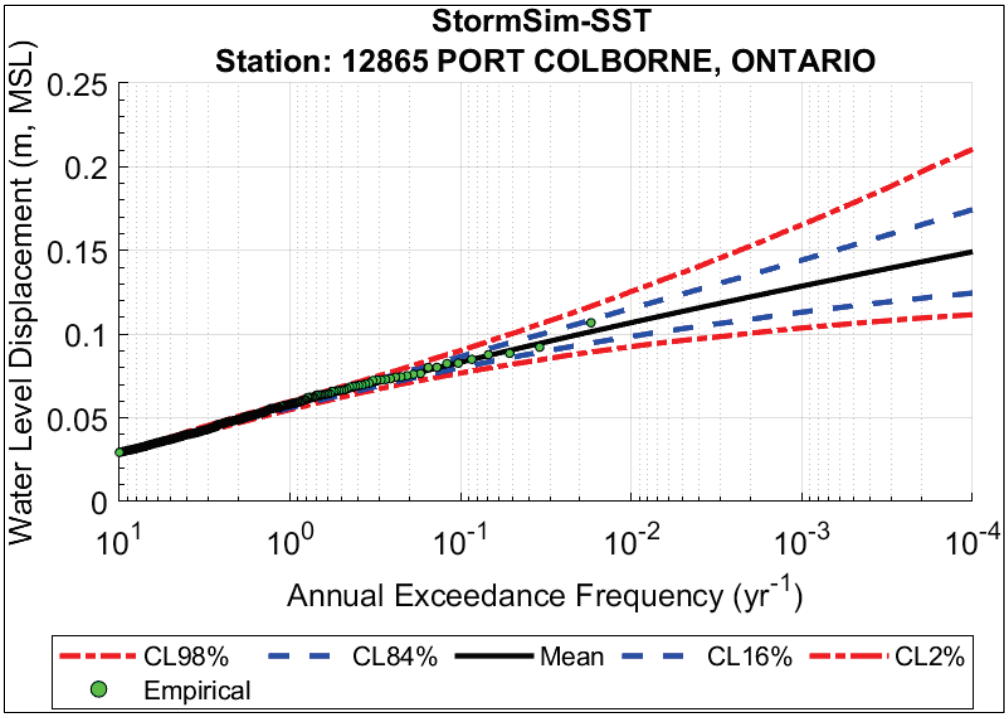

Figure B-23. WLD hazard curve for Seiche Mode 3 (Filter ID 3) for Port Colborne, Ontario (12865).

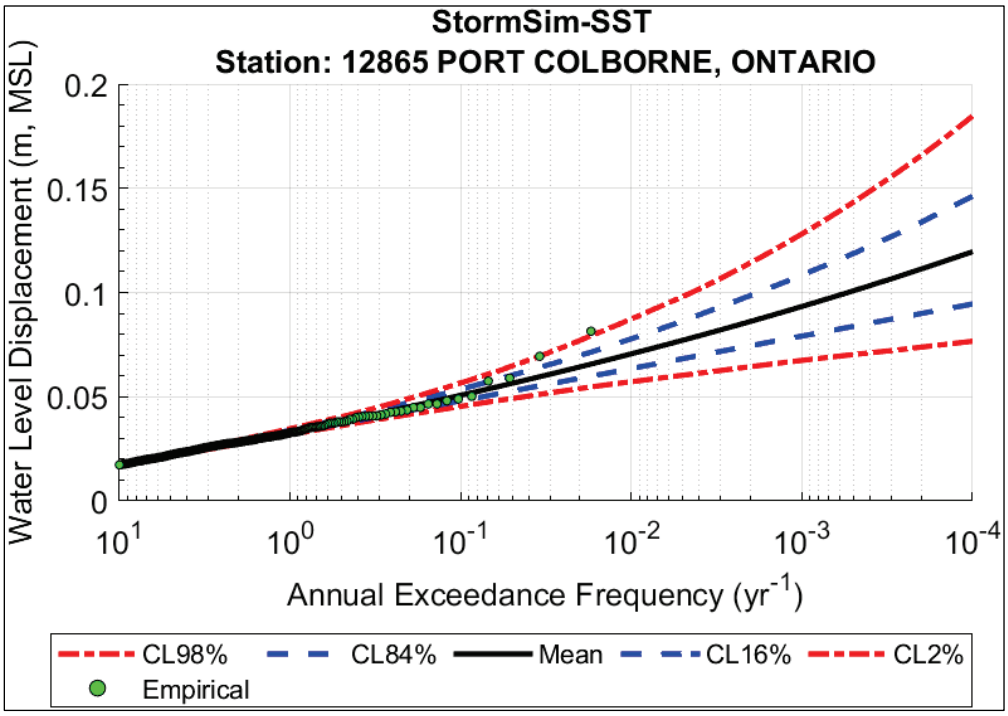

Figure B-24. WLD hazard curve for Seiche Mode 4 (Filter ID 4) for Port Colborne, Ontario (12865).

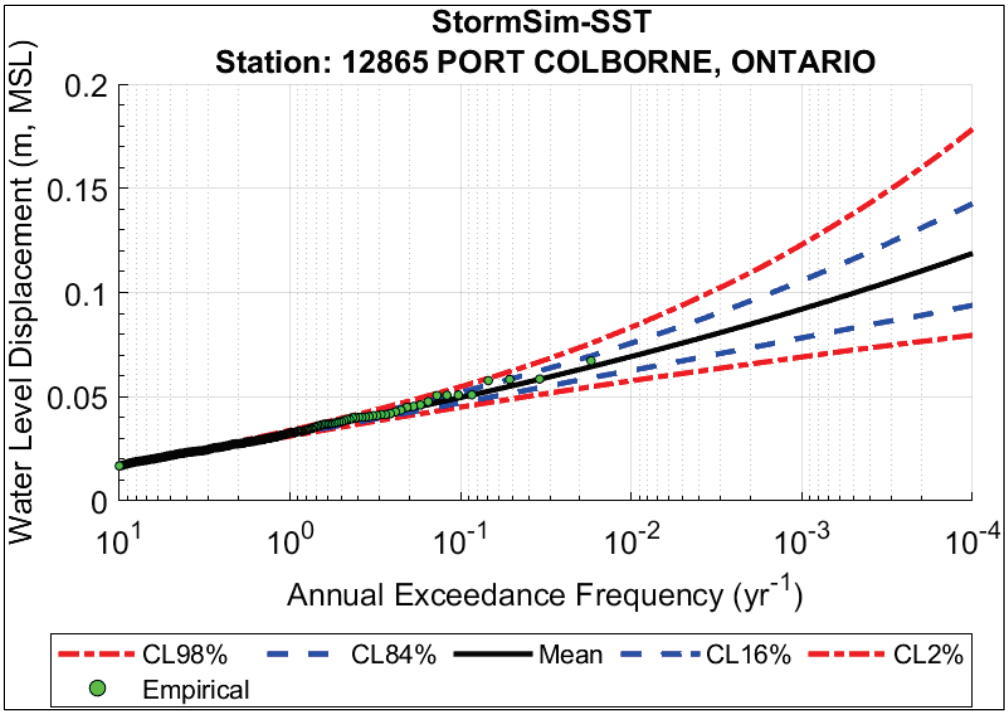

Figure B-25. Combined seiche modes (Filter ID 5) WLD hazard curve for Port Colborne, Ontario (12865).

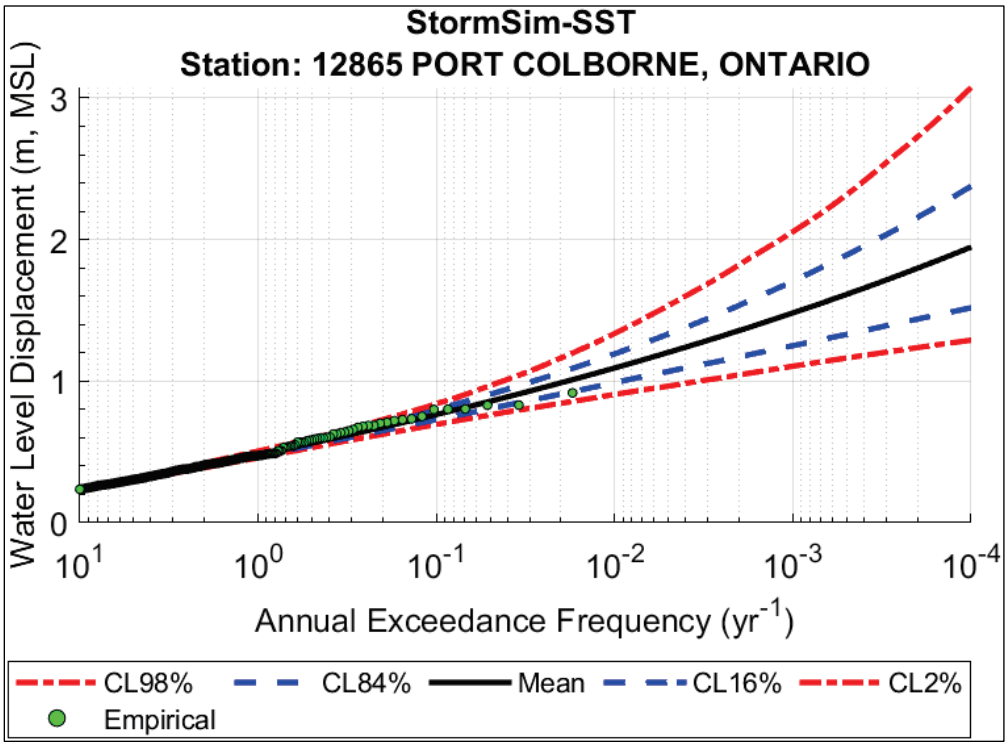

Figure B-26. WLD hazard curve for Seiche Mode 1 (Filter ID 1) Port Dover, Ontario (12710).

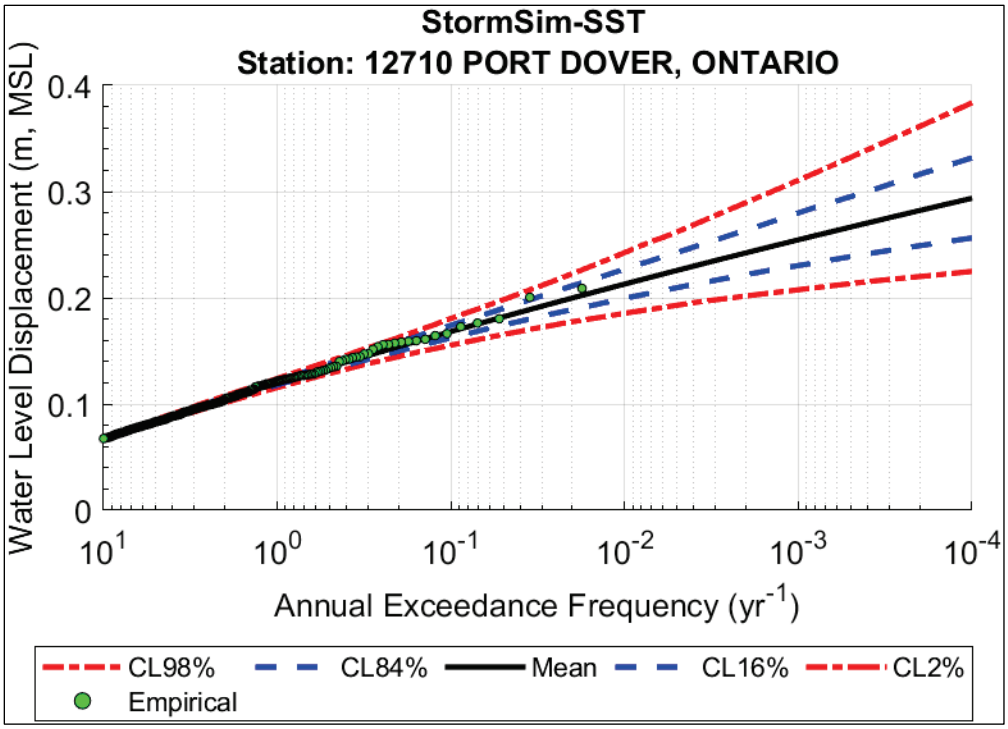

Figure B-27. WLD hazard curve for Seiche Mode 2 (Filter ID 2) for Port Dover, Ontario (12710).

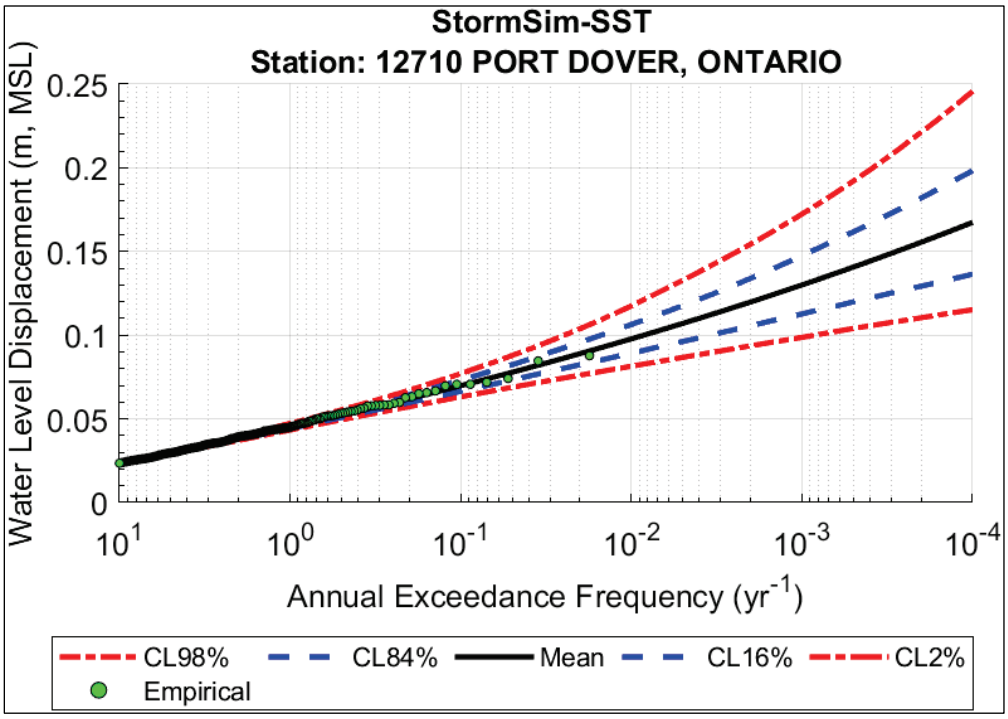

Figure B-28. WLD hazard curve for Seiche Mode 3 (Filter ID 3) for Port Dover, Ontario (12710).

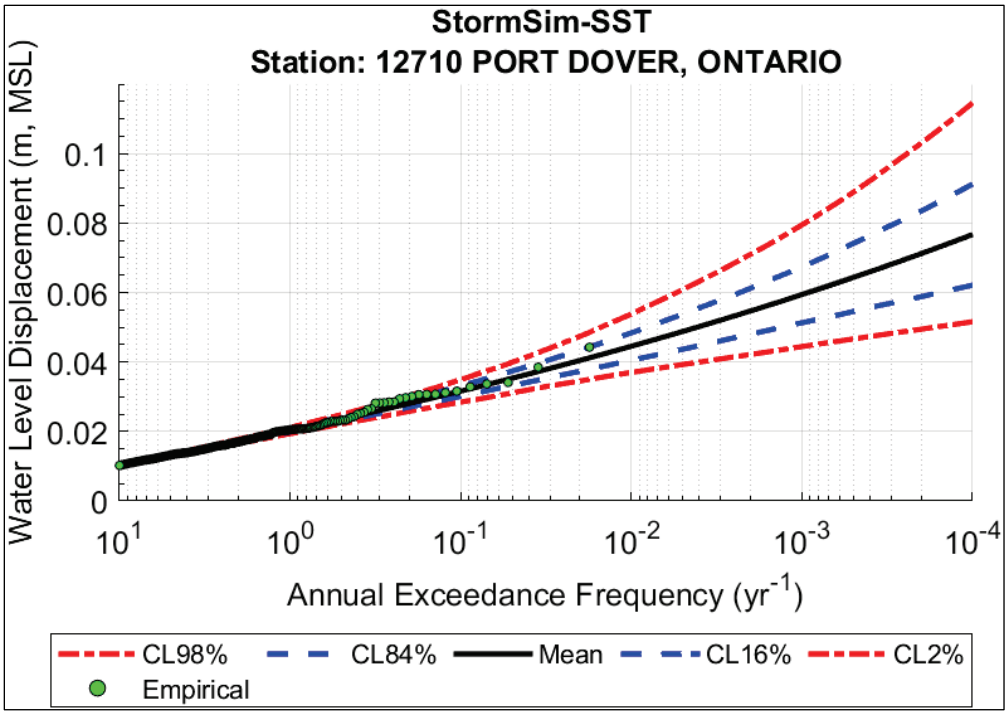

Figure B-29. WLD hazard curve for Seiche Mode 4 (Filter ID 4) for Port Dover, Ontario (12710).

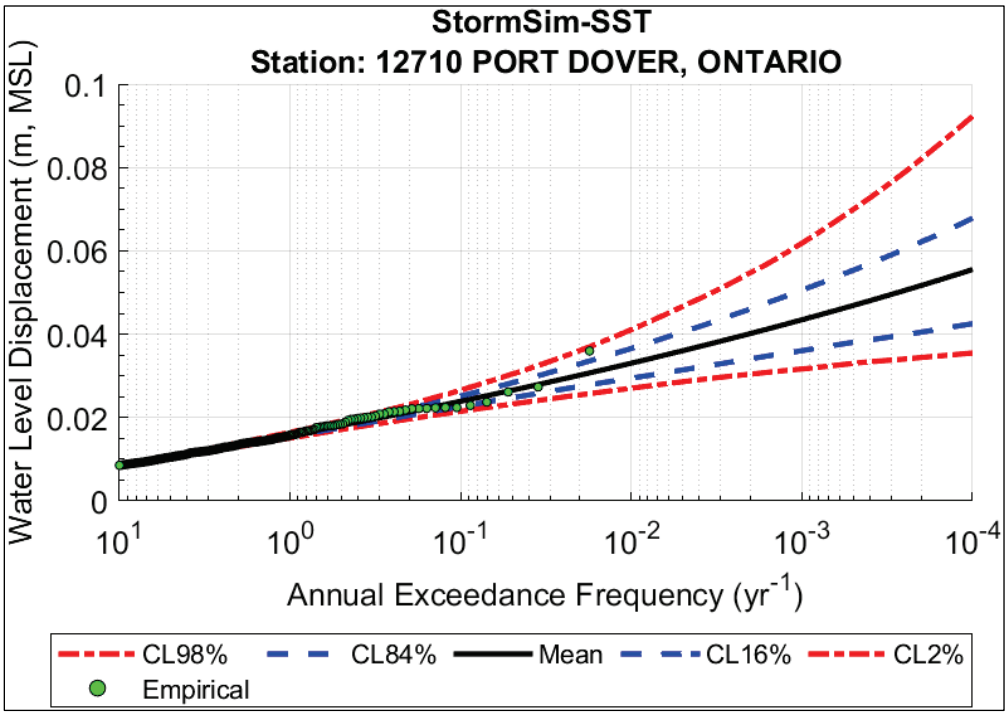

Figure B-30. Combined seiche modes (Filter ID 5) WLD hazard curve for Port Dover, Ontario (12710).

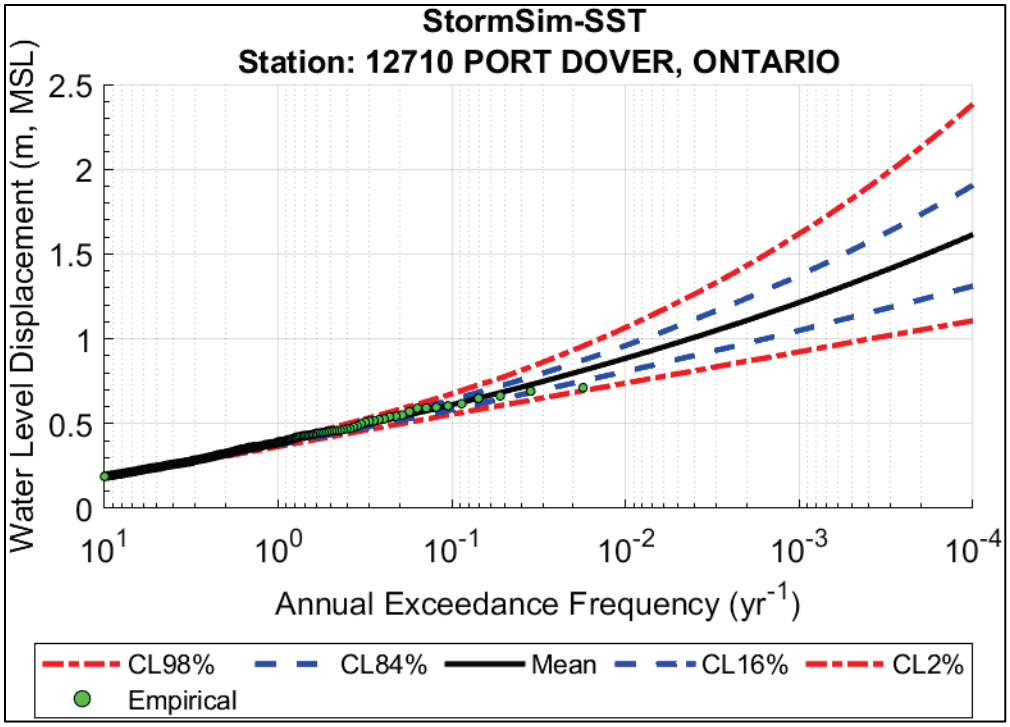

Figure B-31. WLD hazard curve for Seiche Mode 1 (Filter ID 1) for Port Stanley, Ontario (12400).

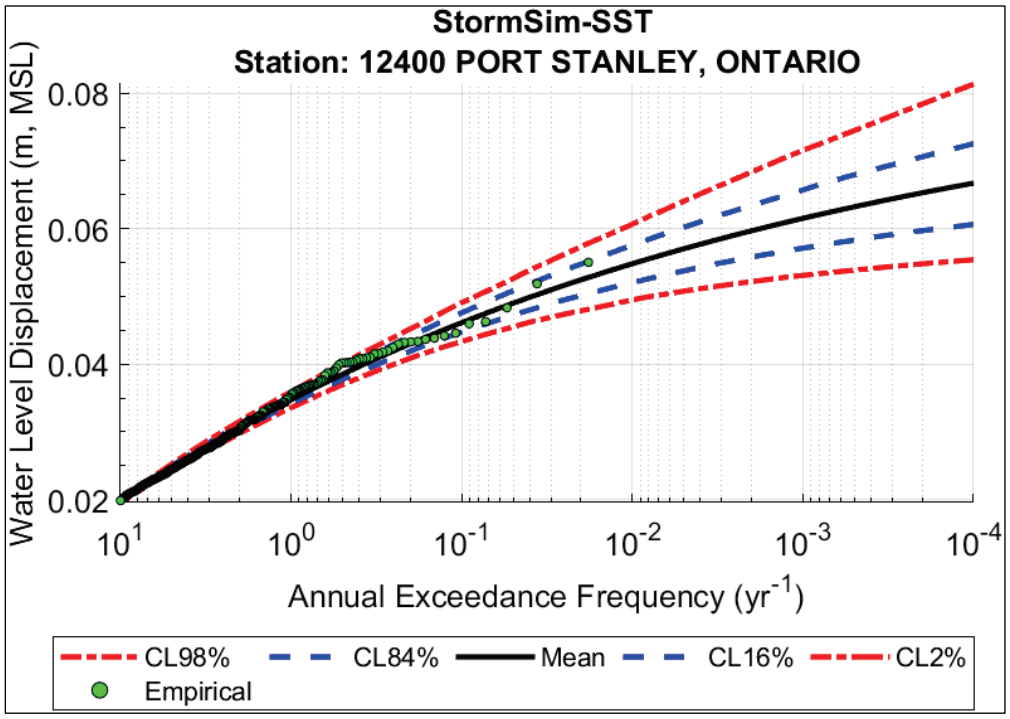

Figure B-32. WLD hazard curve for Seiche Mode 2 (Filter ID 2) for Port Stanley, Ontario (12400).

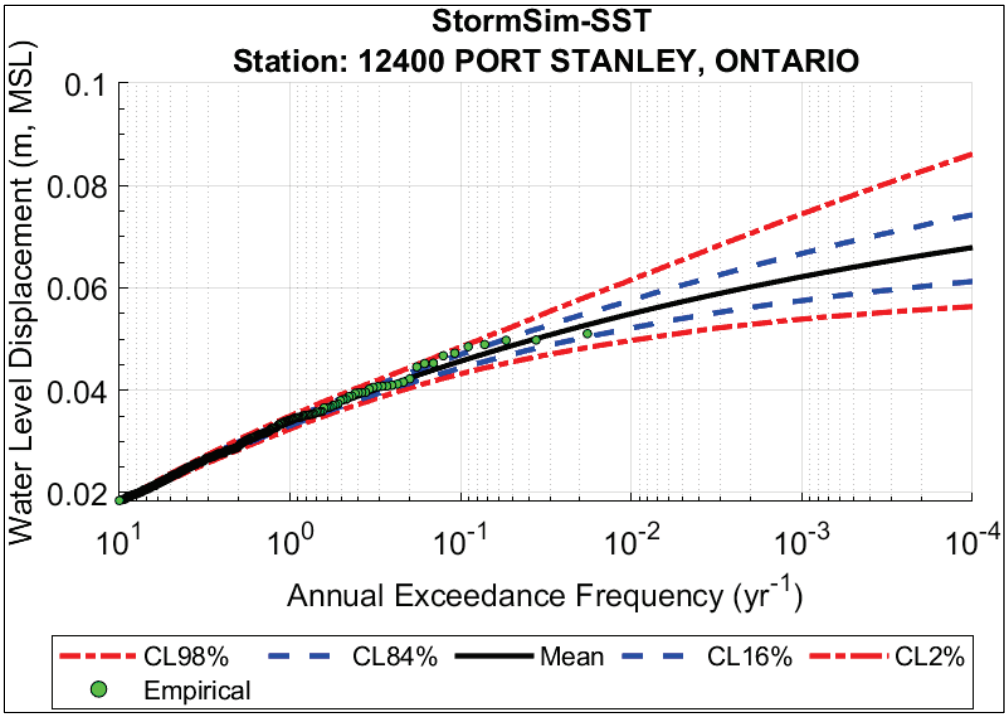

Figure B-33. WLD hazard curve for Seiche Mode 3 (Filter ID 3) for Port Stanley, Ontario (12400).

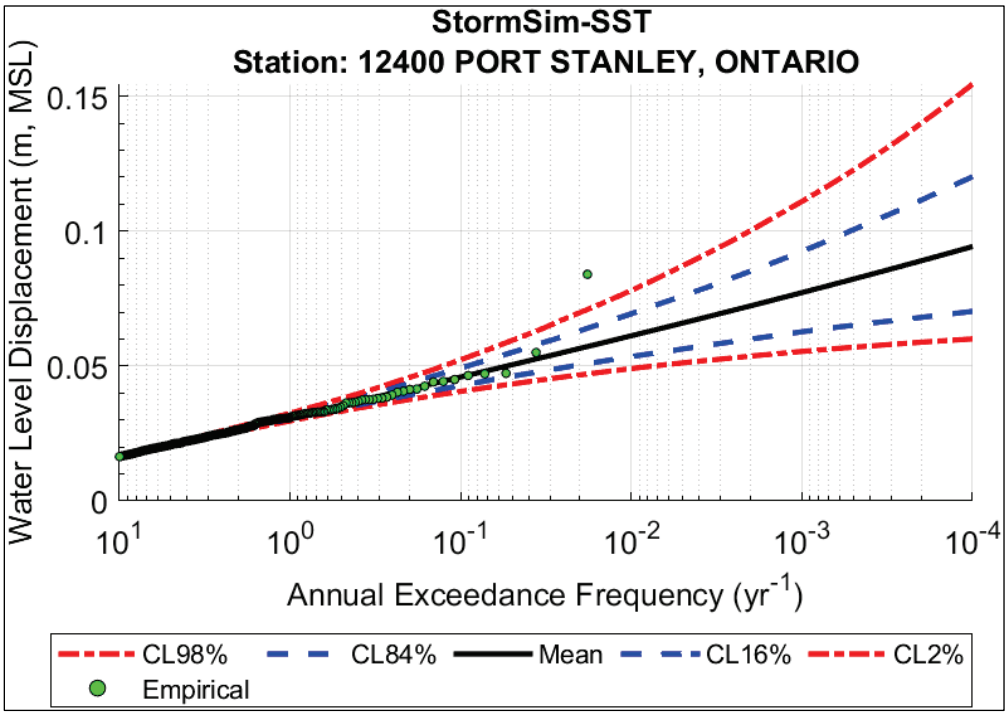

Figure B-34. WLD hazard curve for Seiche Mode 4 (Filter ID 4) for Port Stanley, Ontario (12400).

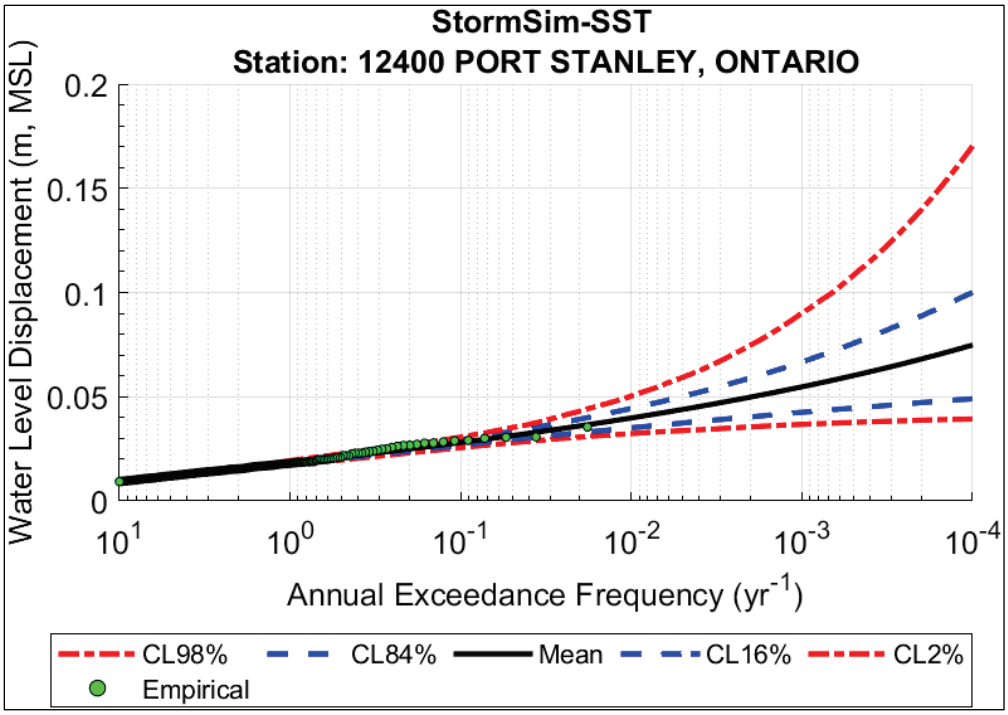

Figure B-35. Combined seiche modes (Filter ID 5) WLD hazard curve for Port Stanley, Ontario (12400).

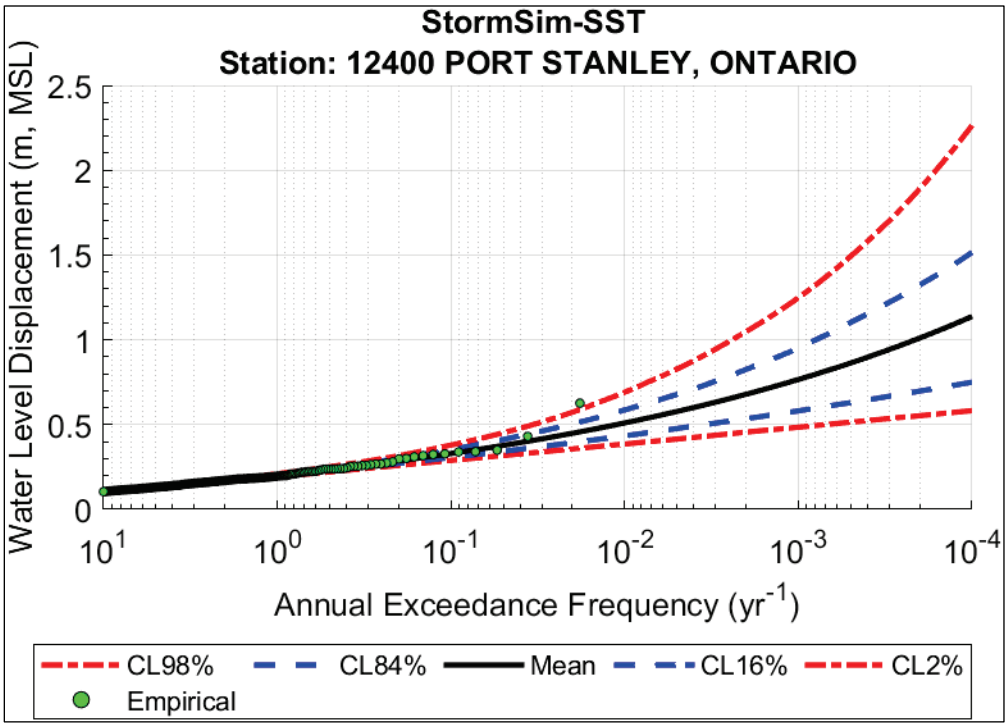

Figure B-36. WLD hazard curve for Seiche Mode 1 (Filter ID 1) for Fermi Power Plant (9063090).

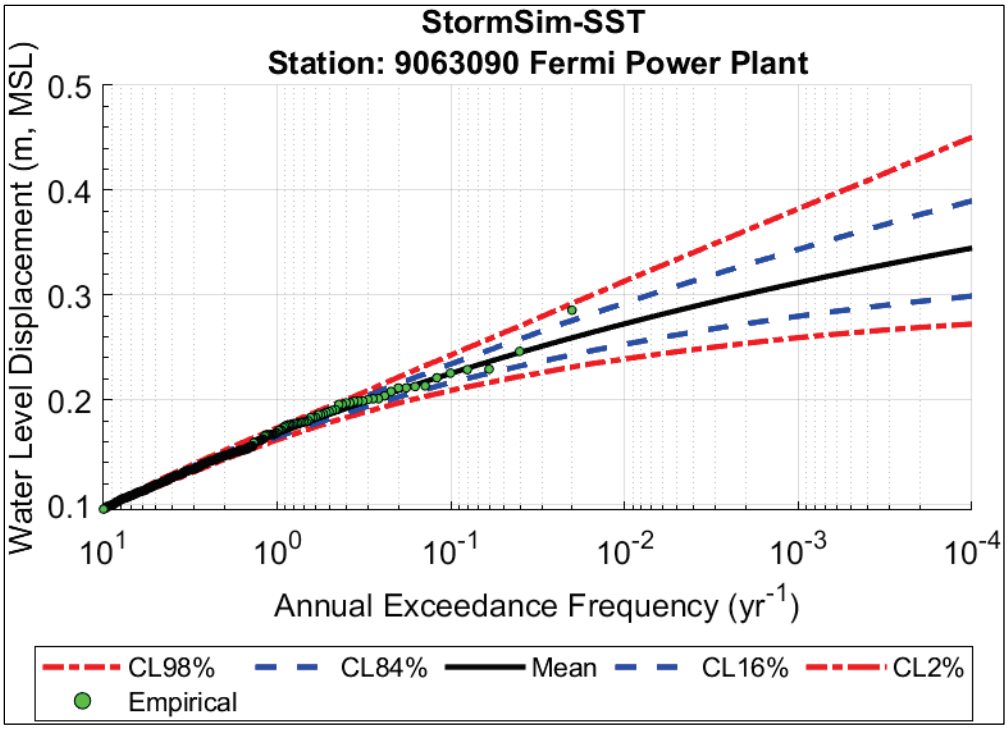

Figure B-37. WLD hazard curve for Seiche Mode 2 (Filter ID 2) for Fermi Power Plant (9063090).

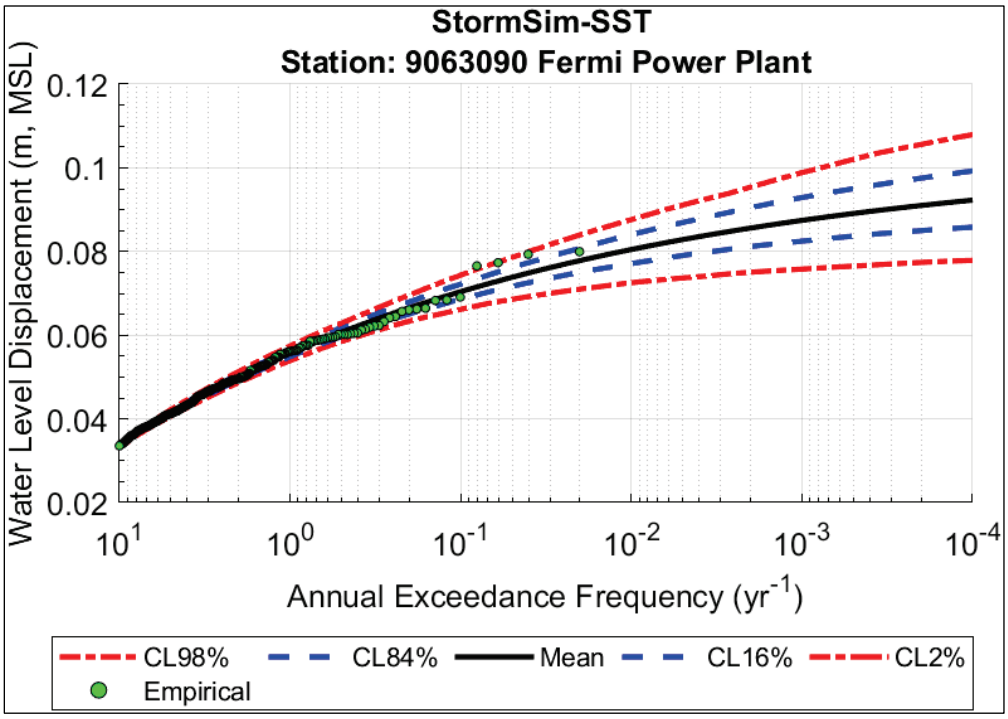

Figure B-38. WLD hazard curve for Seiche Mode 3 (Filter ID 3) for Fermi Power Plant (9063090).

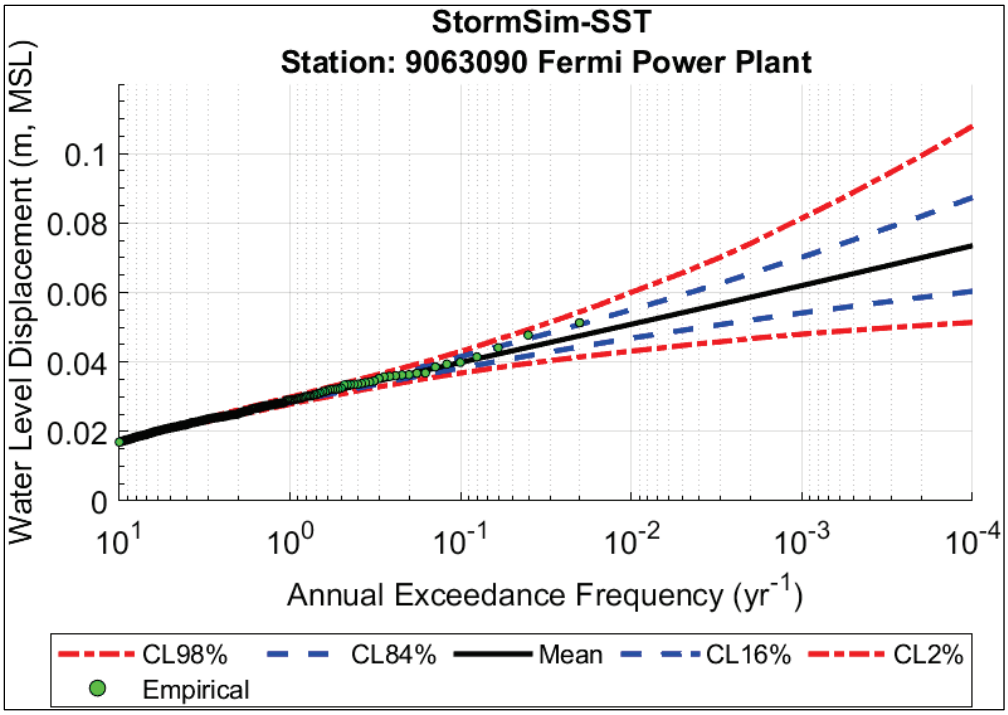

Figure B-39. WLD hazard curve for Seiche Mode 4 (Filter ID 4) for Fermi Power Plant (9063090).

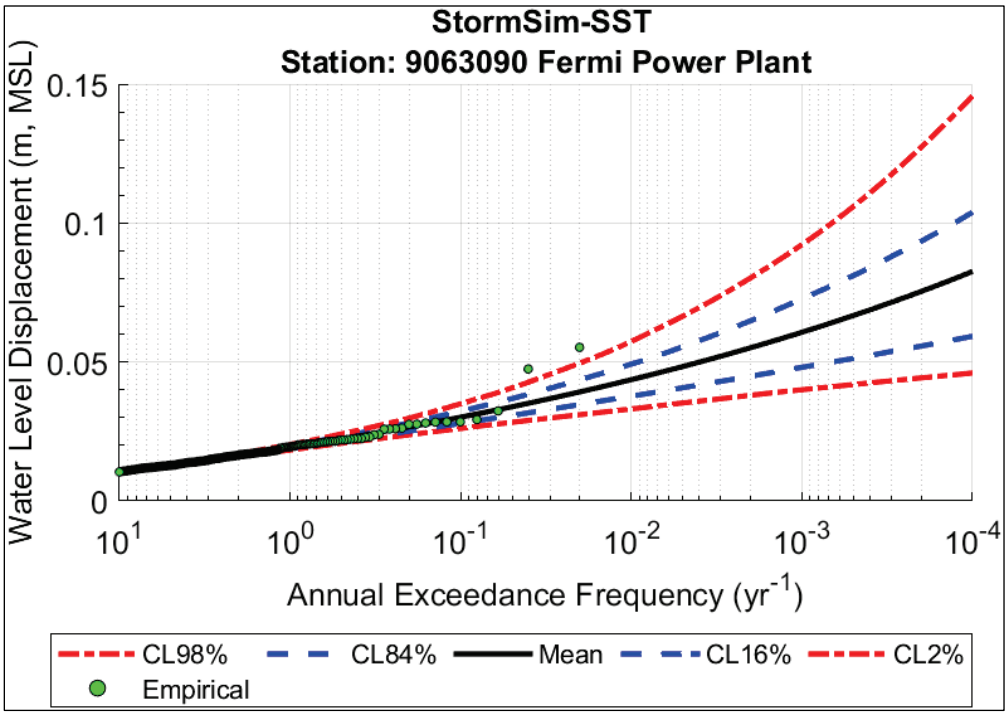

Figure B-40. Combined seiche modes (Filter ID 5) WLD hazard curve for Fermi Power Plant (9063090).

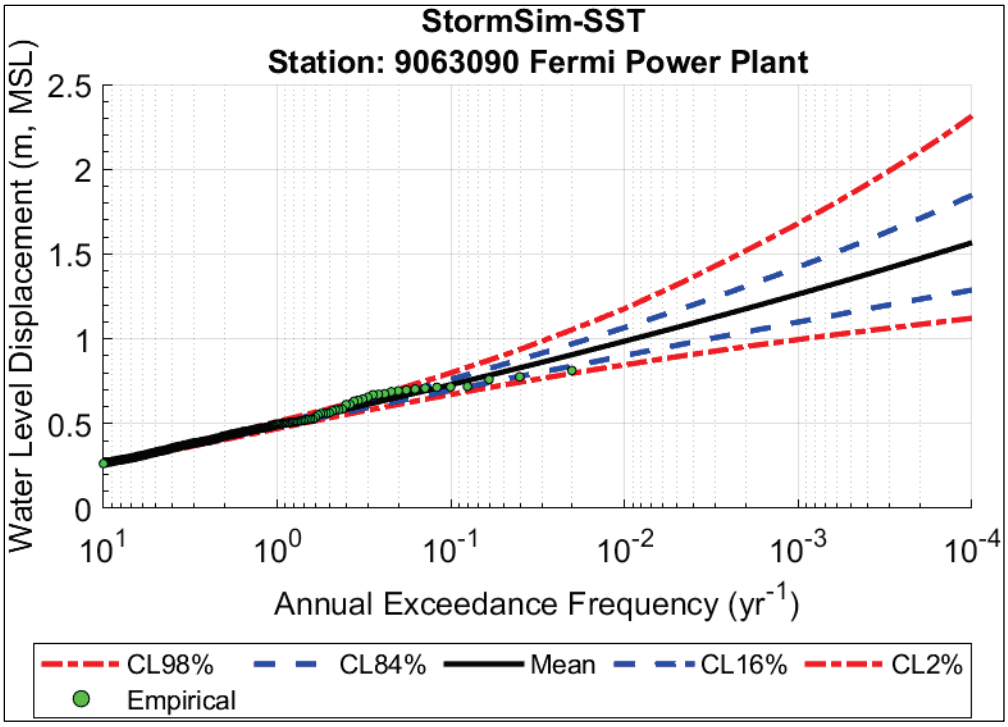

Figure B-41. WLD hazard curve for Seiche Mode 1 (Filter ID 1) for Marblehead (9063079).

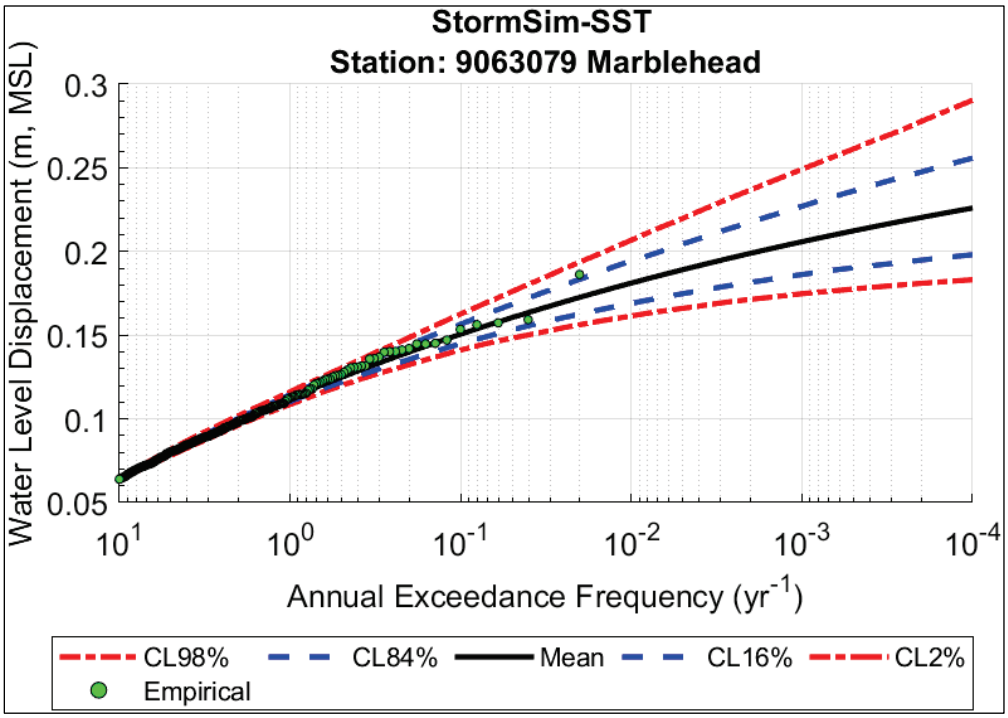

Figure B-42. WLD hazard curve for Seiche Mode 2 (Filter ID 2) for Marblehead (9063079).

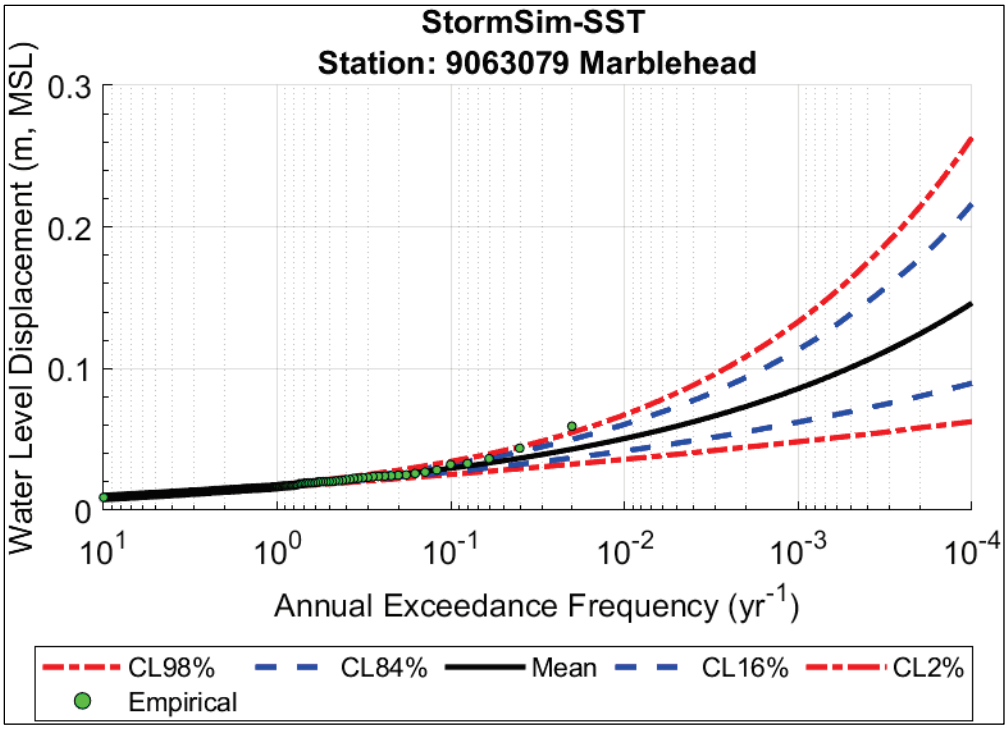

Figure B-43. WLD hazard curve for Seiche Mode 3 (Filter ID 3) Marblehead (9063079).

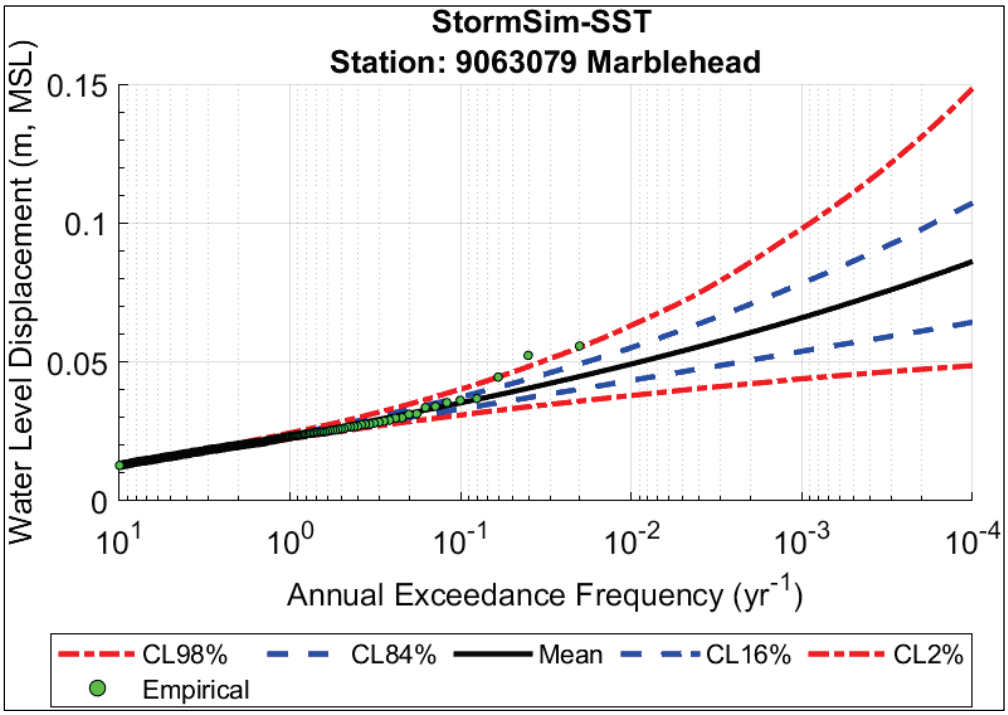

Figure B-44. WLD hazard curve for Seiche Mode 4 (Filter ID 4) for Marblehead (9063079).

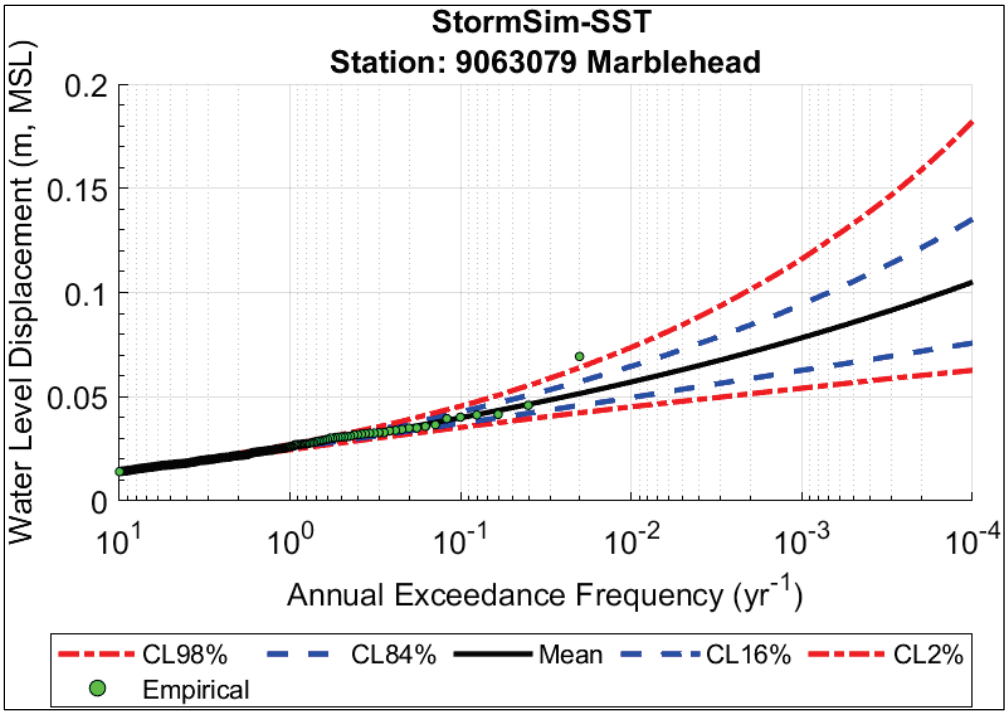

Figure B-45. Combined seiche modes (Filter ID 5) WLD hazard curve for Marblehead (9063079).

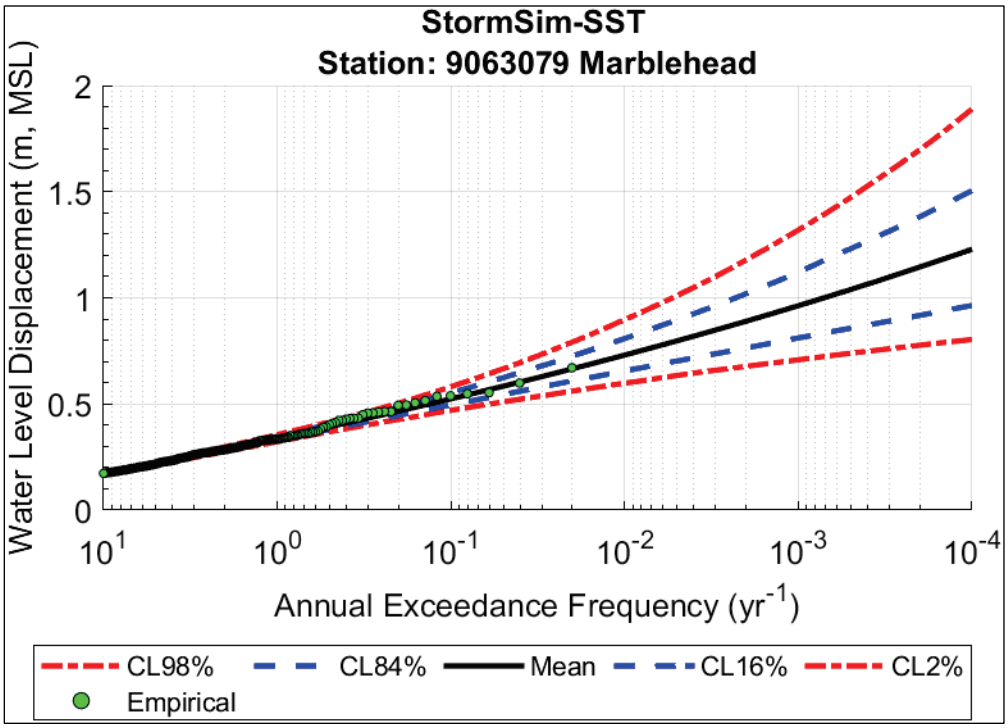

Figure B-46. WLD hazard curve for Seiche Mode 1 (Filter ID 1) for Cleveland (9063063).

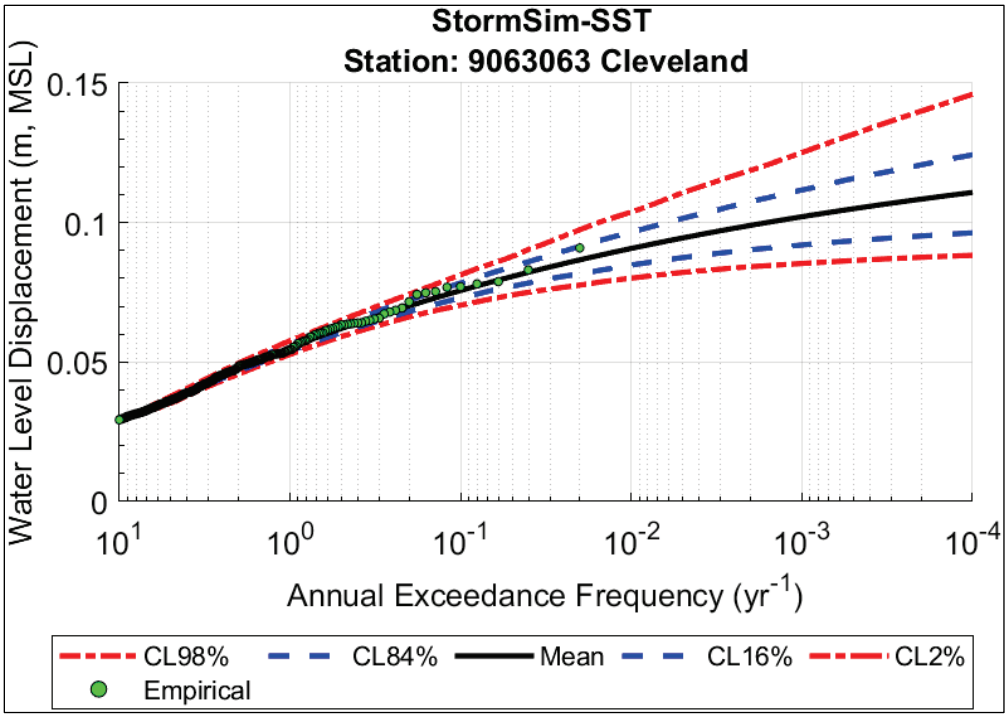

Figure B-47. WLD hazard curve for Seiche Mode 2 (Filter ID 2) for Cleveland (9063063).

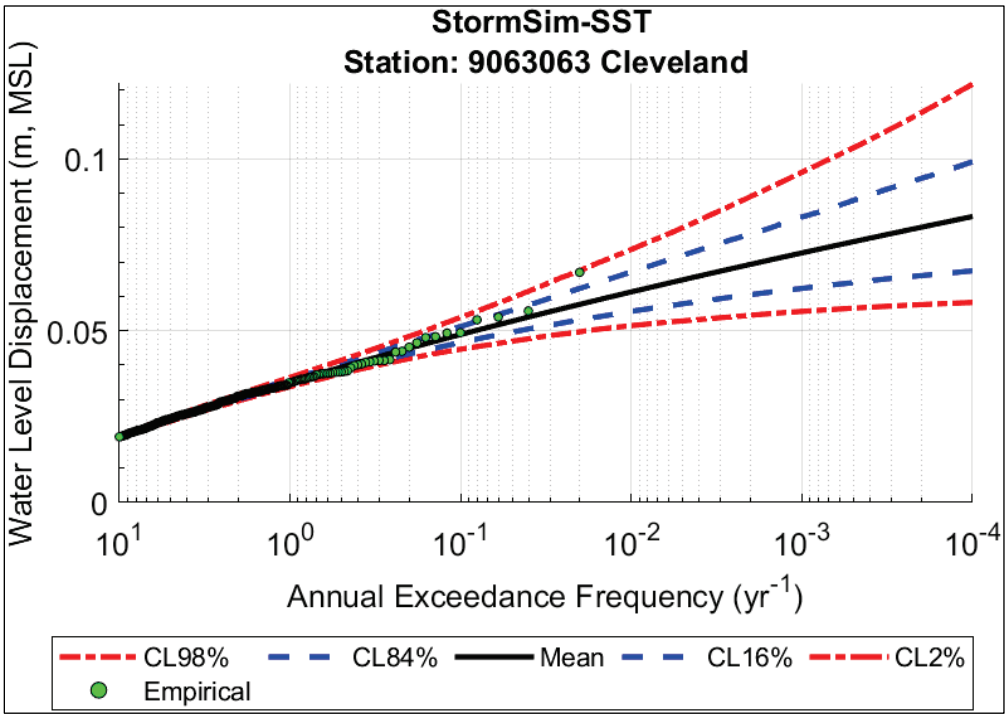

Figure B-48. WLD hazard curve for Seiche Mode 3 (Filter ID 3) for Cleveland (9063063).

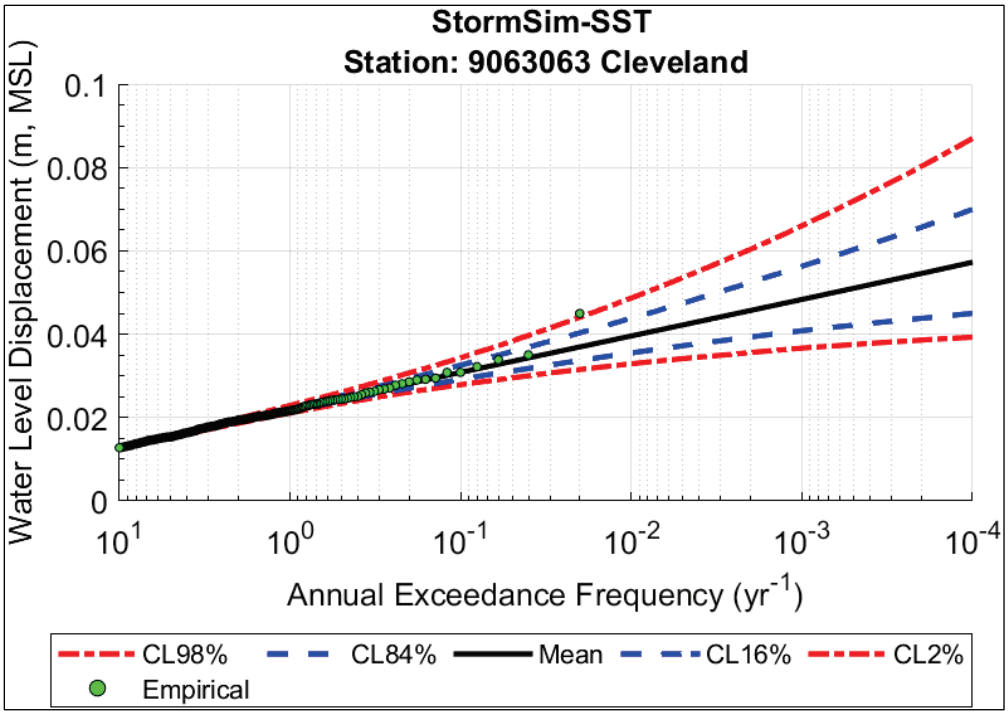

Figure B-49. WLD hazard curve for Seiche Mode 4 (Filter ID 4) for Cleveland (9063063).

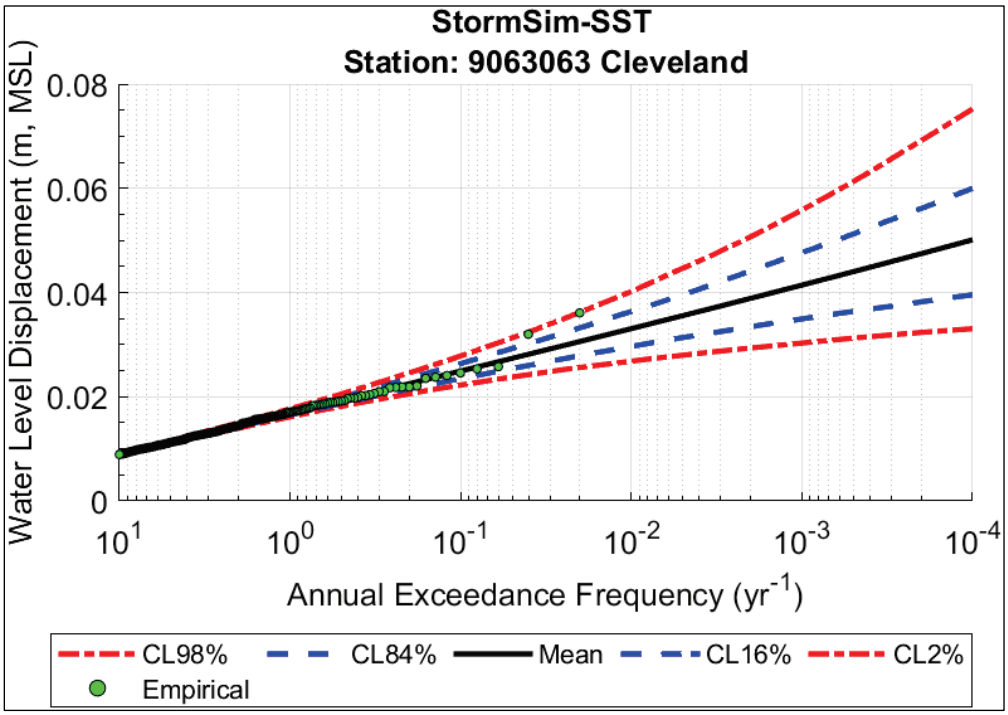

Figure B-50. Combined seiche modes (Filter ID 5) WLD hazard curve for Cleveland (9063063).

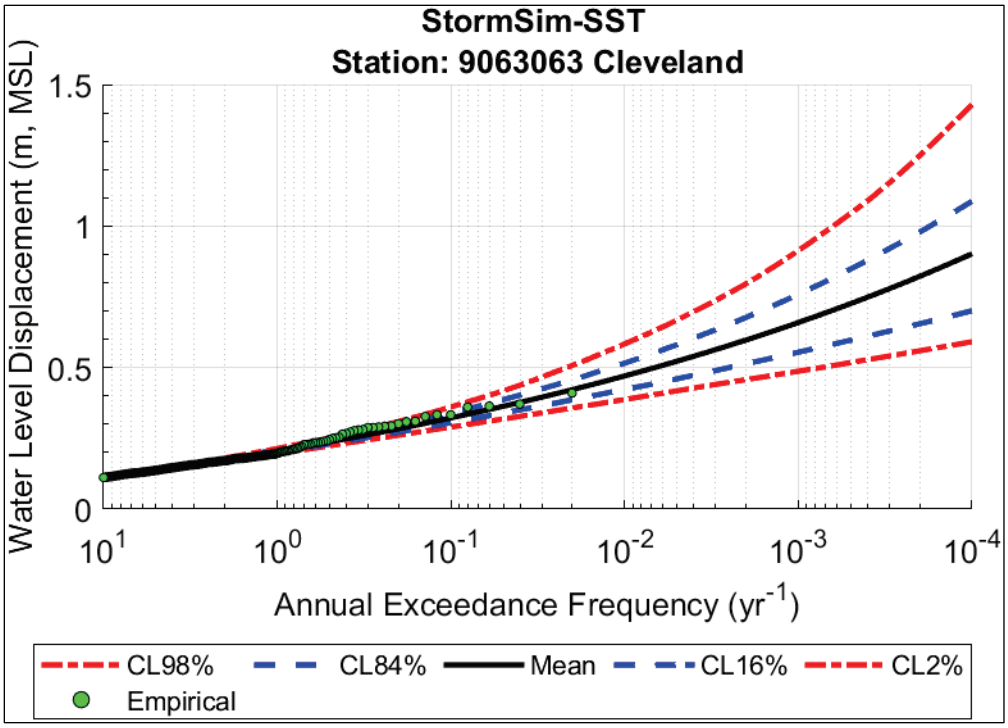

Figure B-51. WLD hazard curve for Seiche Mode 1 (Filter ID 1) for Fairport (9063053).

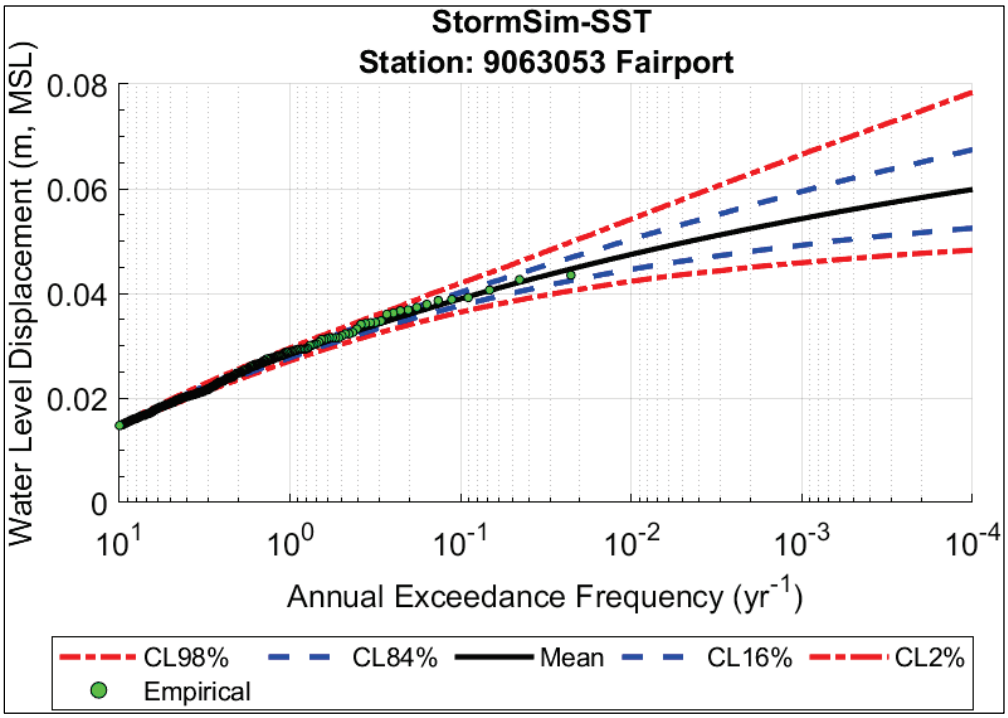

Figure B-52. WLD hazard curve for Seiche Mode 2 (Filter ID 2) for Fairport (9063053).

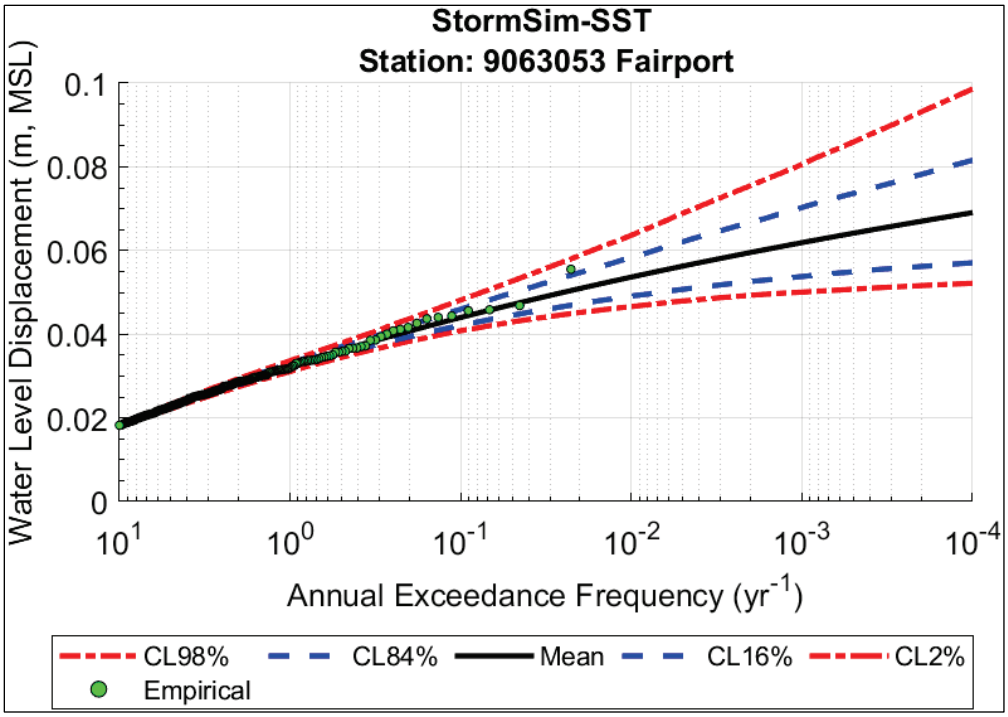

Figure B-53. WLD hazard curve for Seiche Mode 3 (Filter ID 3) for Fairport (9063053).

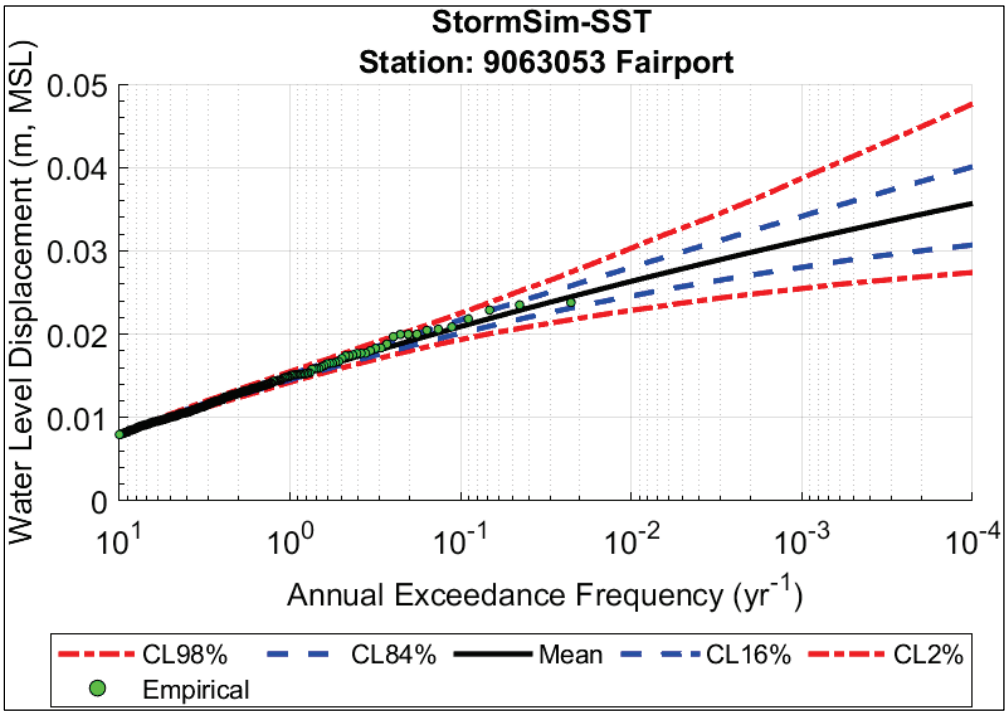

Figure B-54. WLD hazard curve for Seiche Mode 4 (Filter ID 4) for Fairport (9063053).

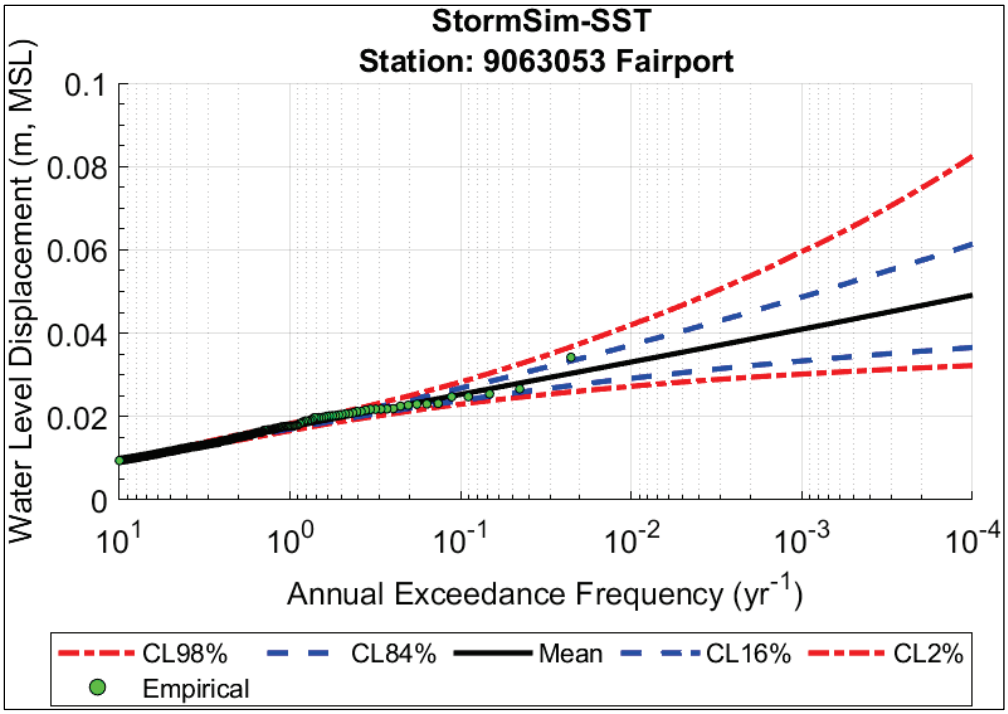

Figure B-55. Combined seiche modes (Filter ID 5) WLD hazard curve for Fairport (9063053).

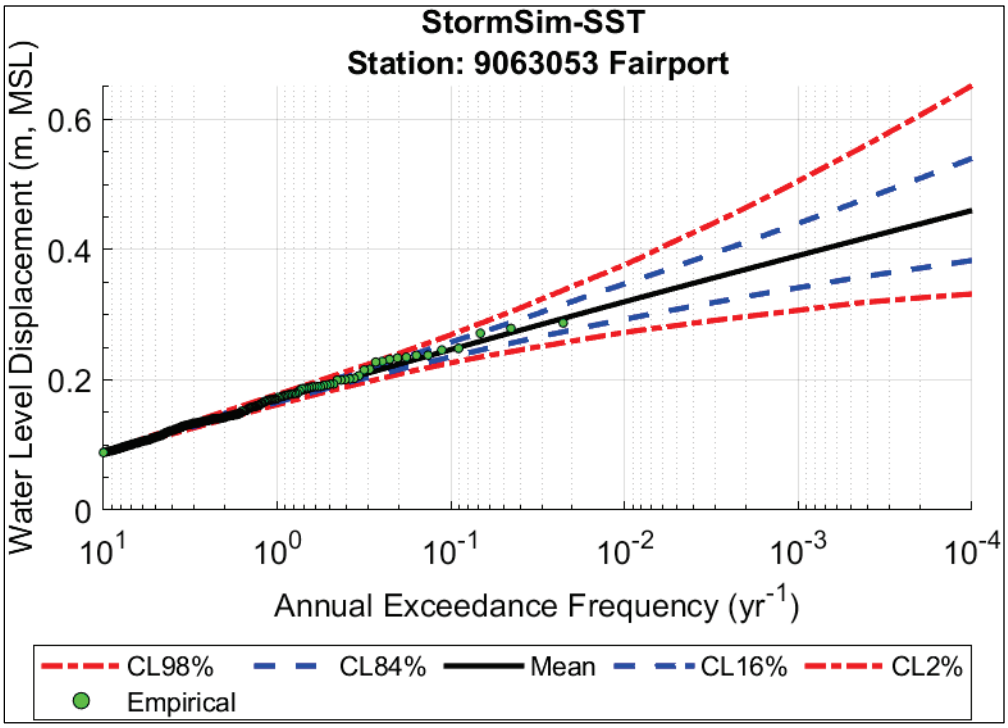

Figure B-56. WLD hazard curve for Seiche Mode 1 (Filter ID 1) for Erie, Lake Erie (9063038).

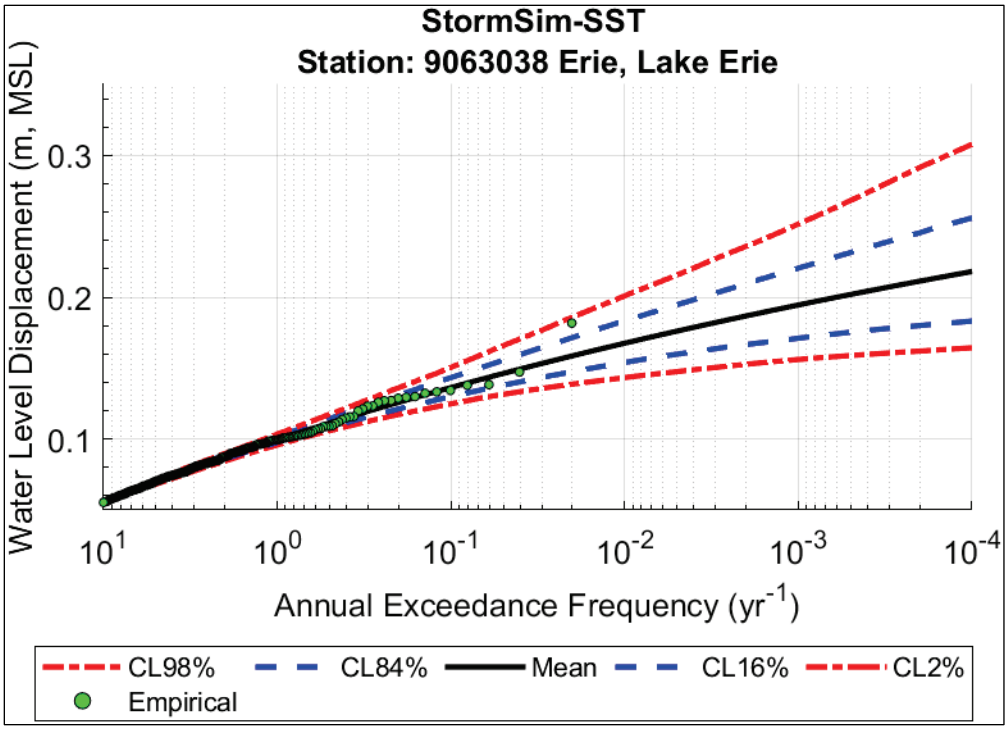

Figure B-57. WLD hazard curve for Seiche Mode 2 (Filter ID 2) for Erie, Lake Erie (9063038).

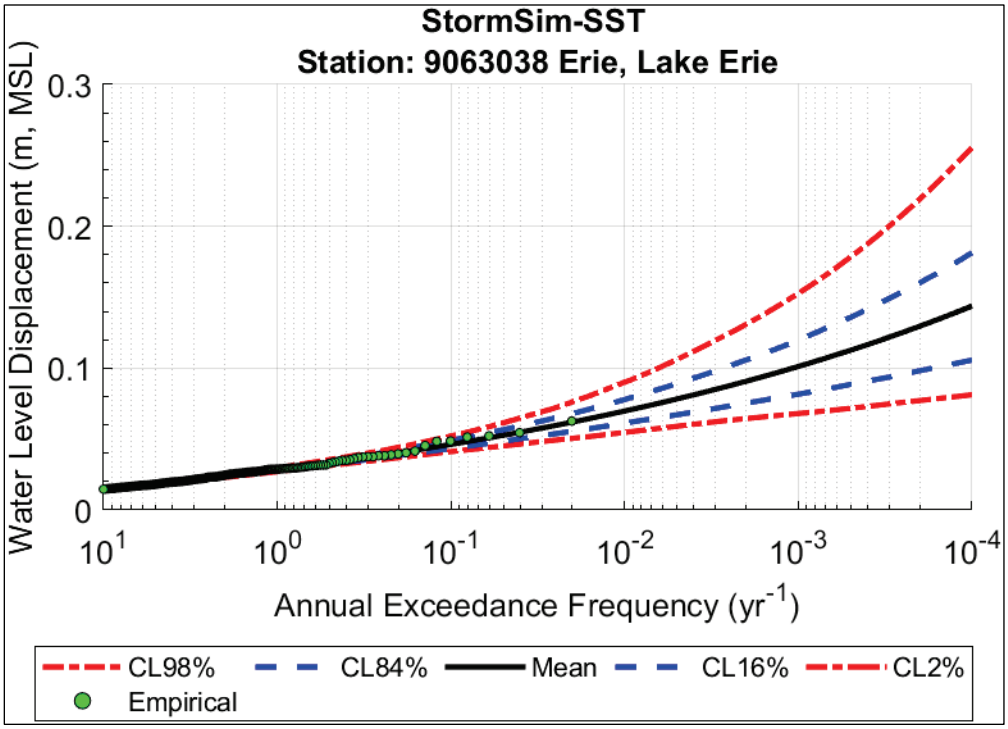

Figure B-58. WLD hazard curve for Seiche Mode 3 (Filter ID 3) for Erie, Lake Erie (9063038).

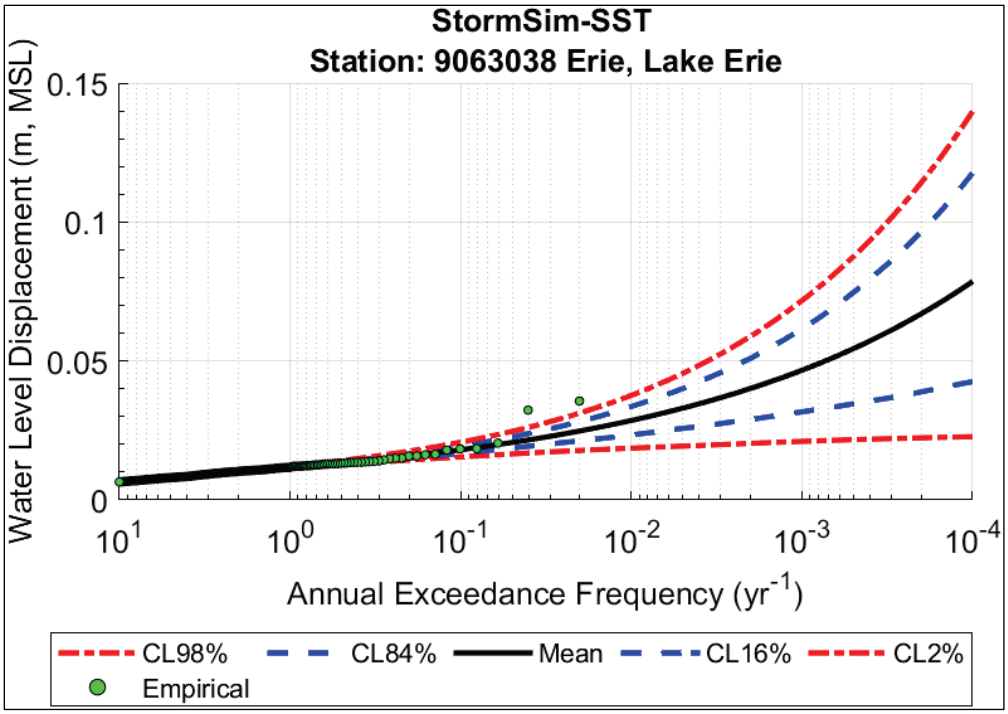

Figure B-59. WLD hazard curve for Seiche Mode 4 (Filter ID 4) for Erie, Lake Erie (9063038).

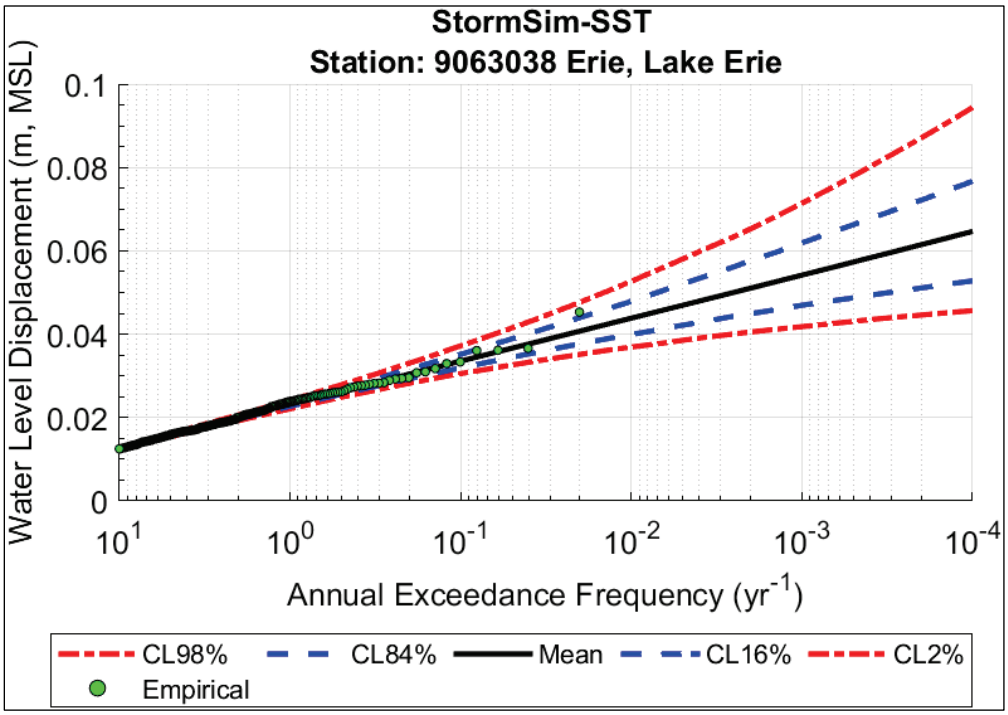

Figure B-60. Combined seiche modes (Filter ID 5) WLD hazard curve for Erie, Lake Erie (9063038).

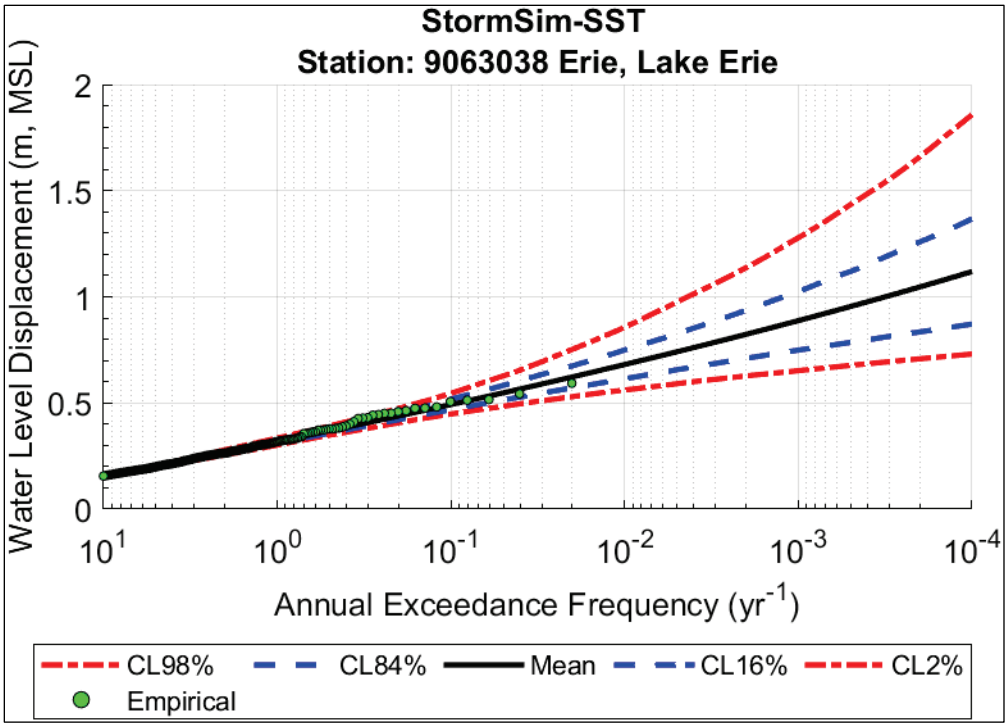

Figure B-61. WLD hazard curve for Seiche Mode 1 (Filter ID 1) for Buffalo (9063020).

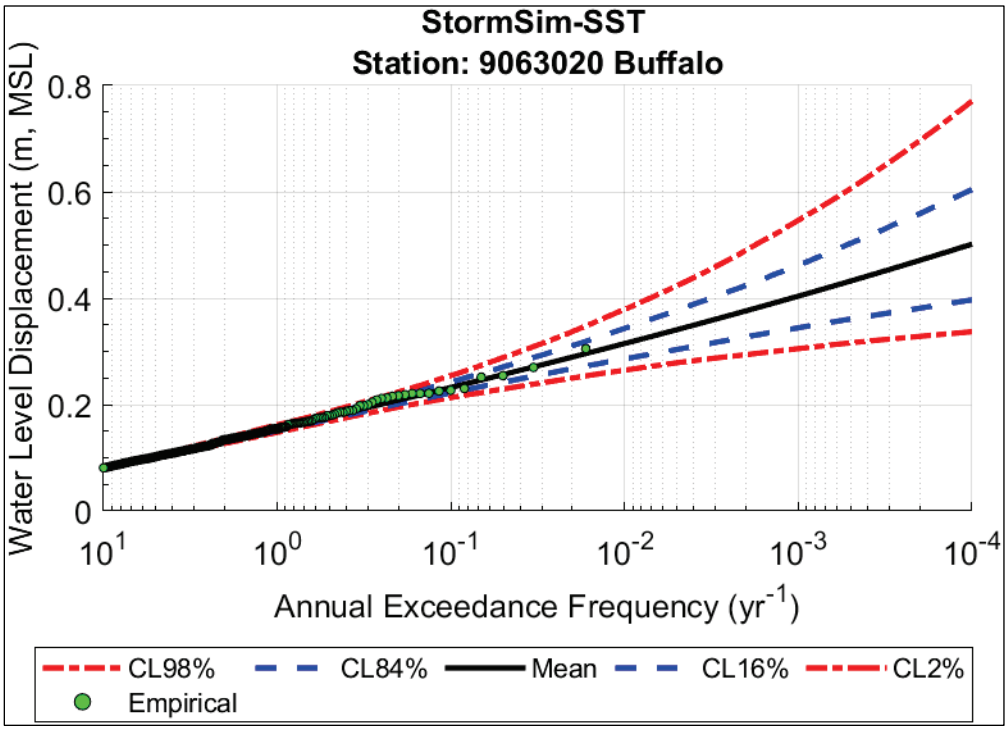

Figure B-62. WLD hazard curve for Seiche Mode 2 (Filter ID 2) for Buffalo (9063020).

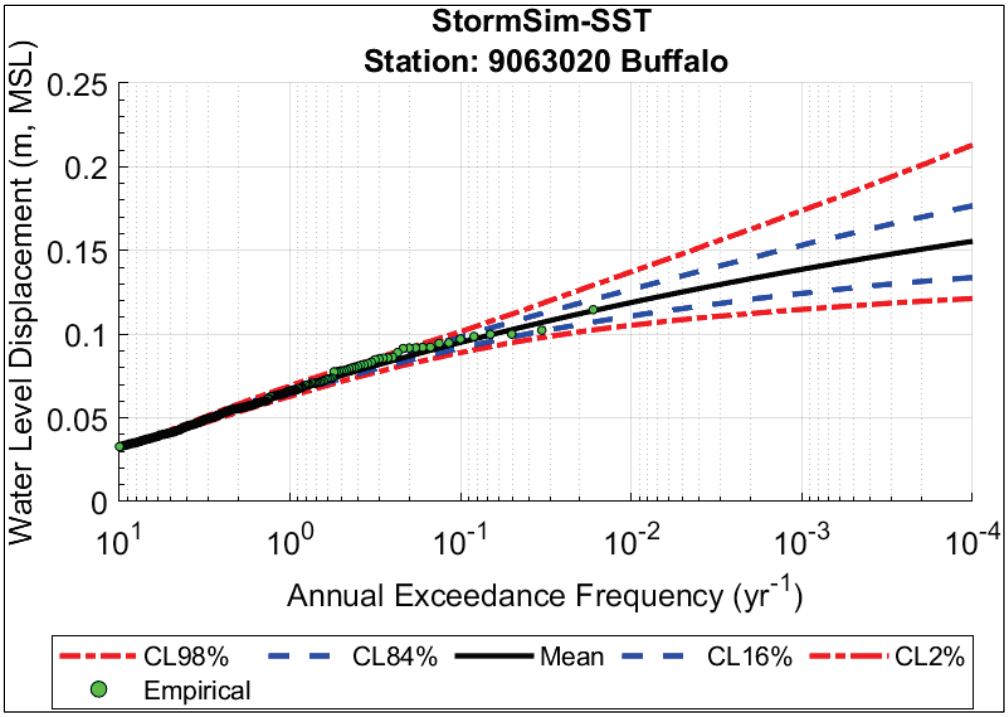

Figure B-63. WLD hazard curve for Seiche Mode 3 (Filter ID 3) for Buffalo (9063020).

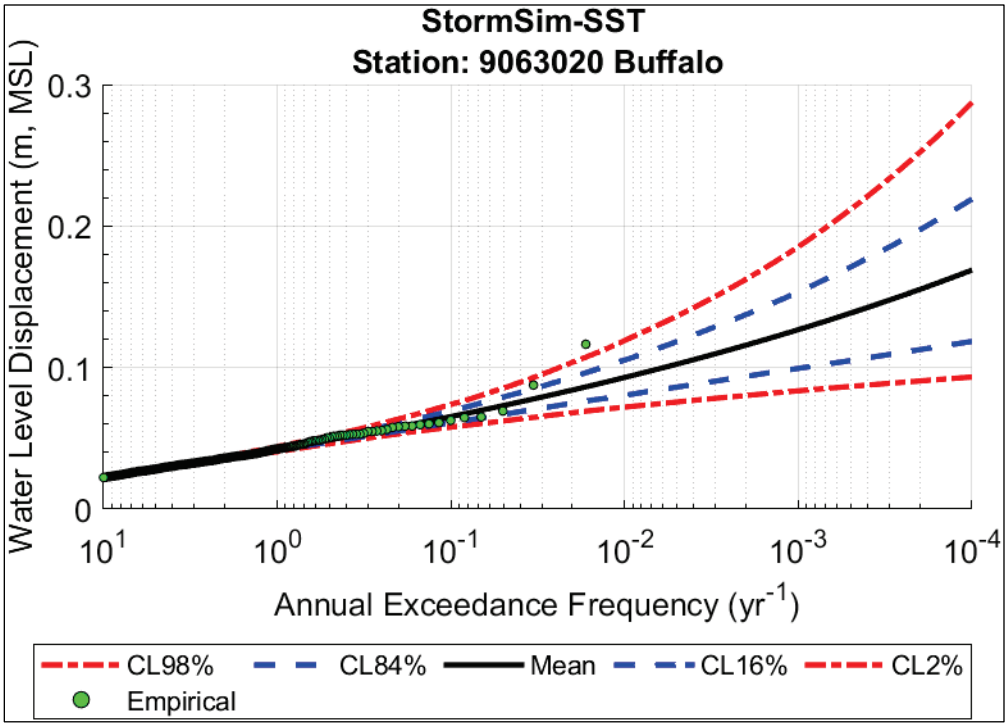

Figure B-64. WLD hazard curve for Seiche Mode 4 (Filter ID 4) for Buffalo (9063020).

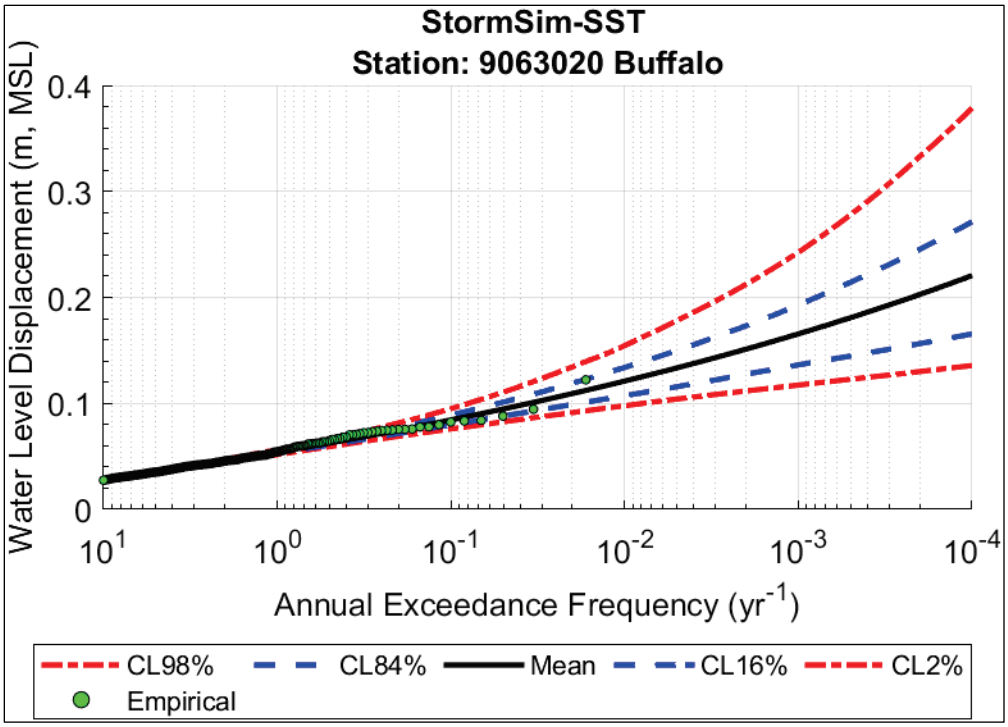

Figure B-65. Combined seiche modes (Filter ID 5) WLD hazard curve for Buffalo (9063020).

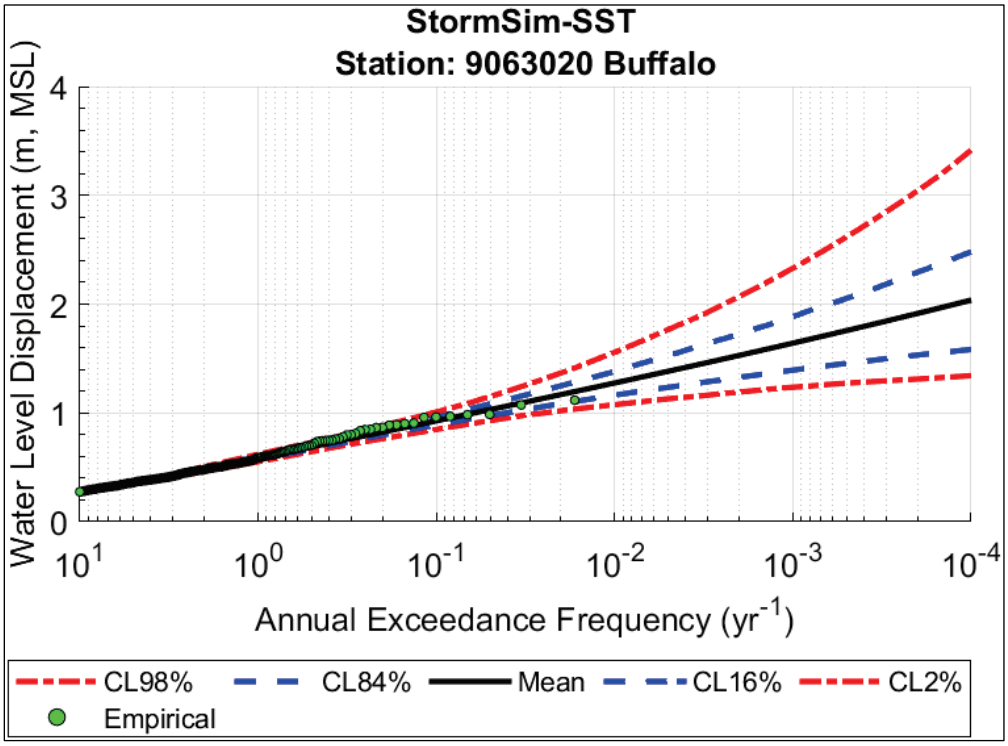

Figure B-66. WLD hazard curve for Seiche Mode 1 (Filter ID 1) for Toledo (9063085)

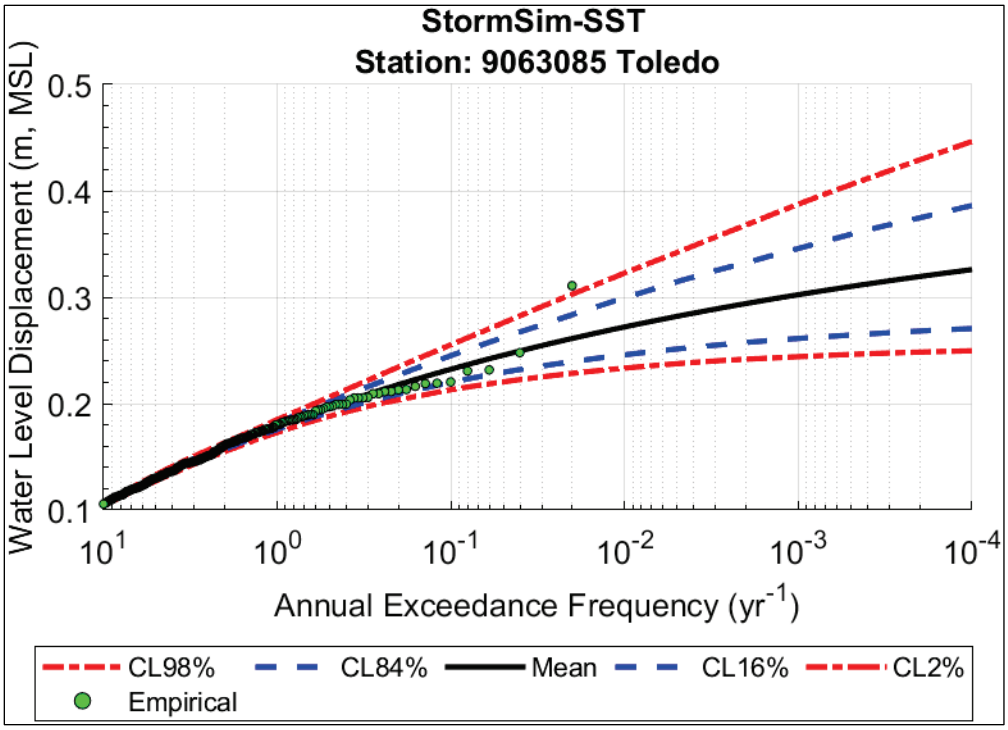

Figure B-67. WLD hazard curve for Seiche Mode 2 (Filter ID 2) for Toledo (9063085).

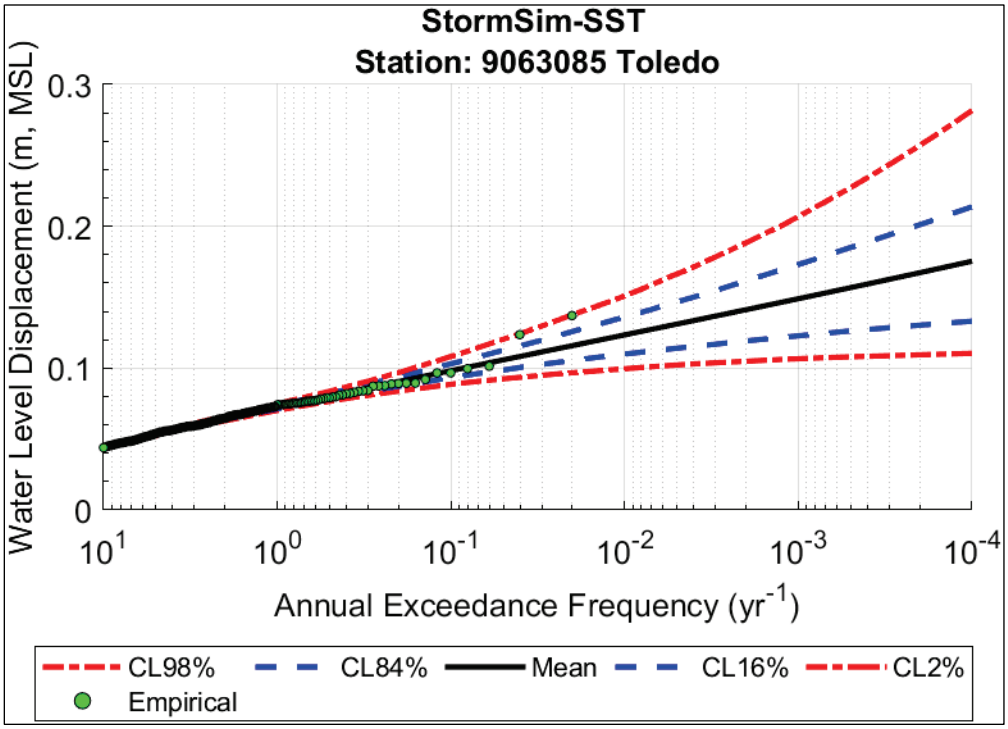

Figure B-68. WLD hazard curve for Seiche Mode 3 (Filter ID 3) for Toledo (9063085).

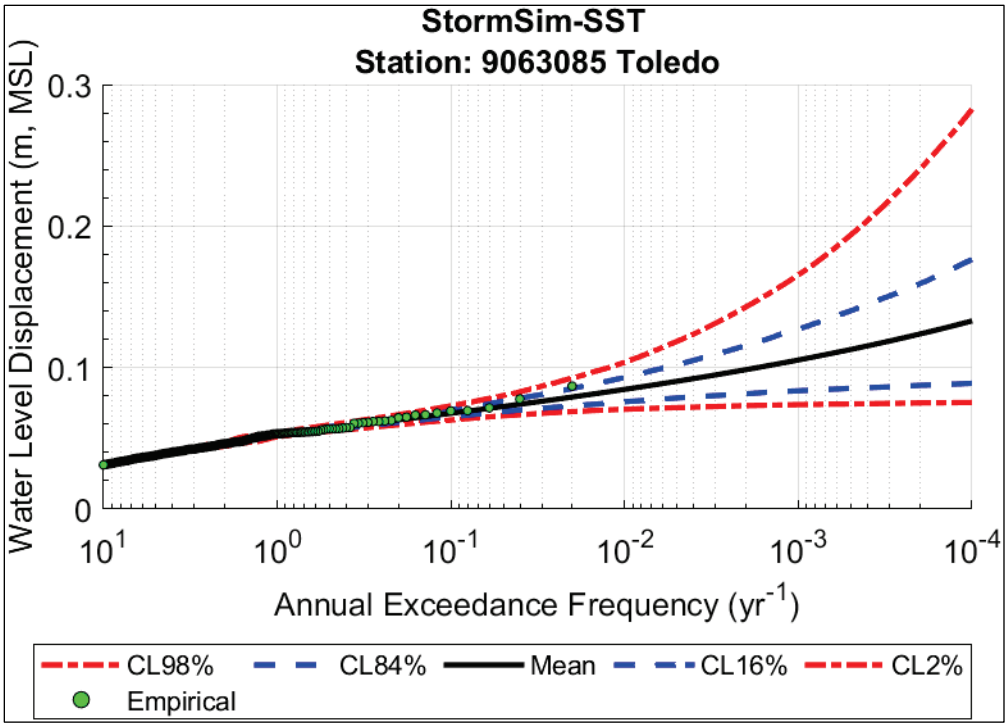

Figure B-69. WLD hazard curve for Seiche Mode 4 (Filter ID 4) for Toledo (9063085).

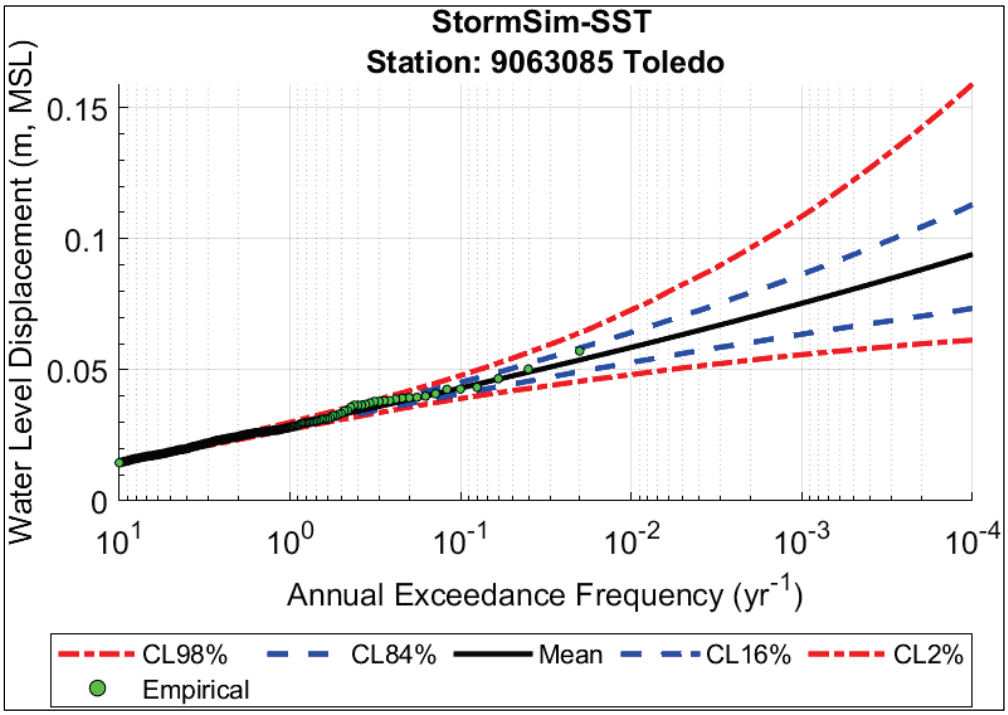

Figure B-70. Combined seiche modes (Filter ID 5) WLD hazard curve for Toledo (9063085).

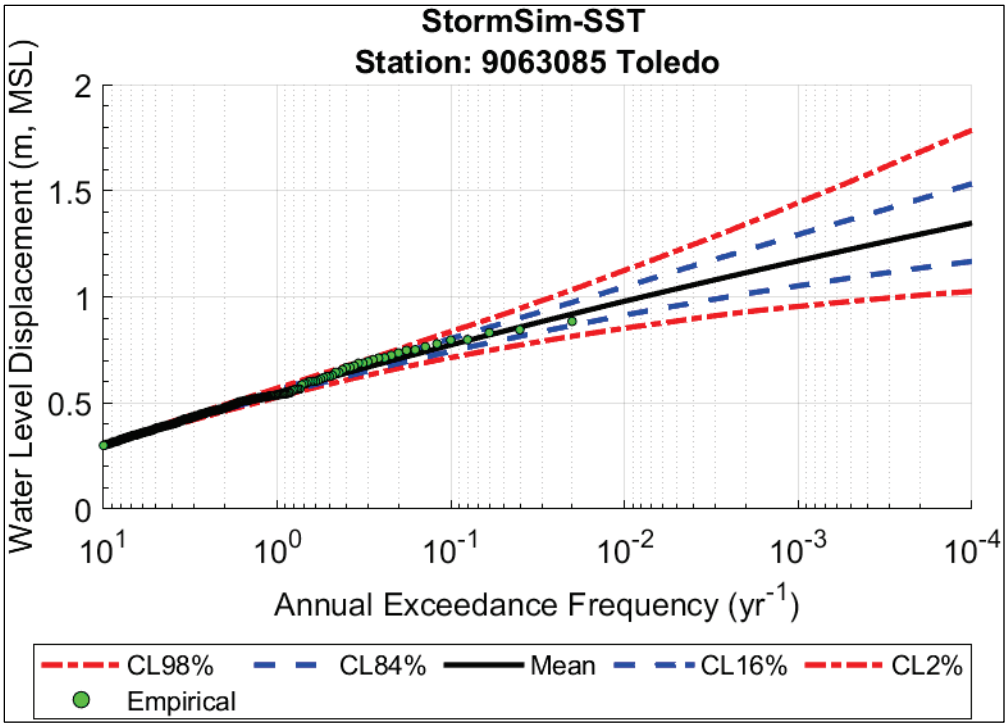

Appendix C: LFA Results Using Hourly Gauge Data

Figure C-1 through Figure C-17 show the LFA results using hourly gauge data.

Figure C-1. Local frequency analysis (LFA) hazard curve (hourly data) at Point Bar, Ontario.

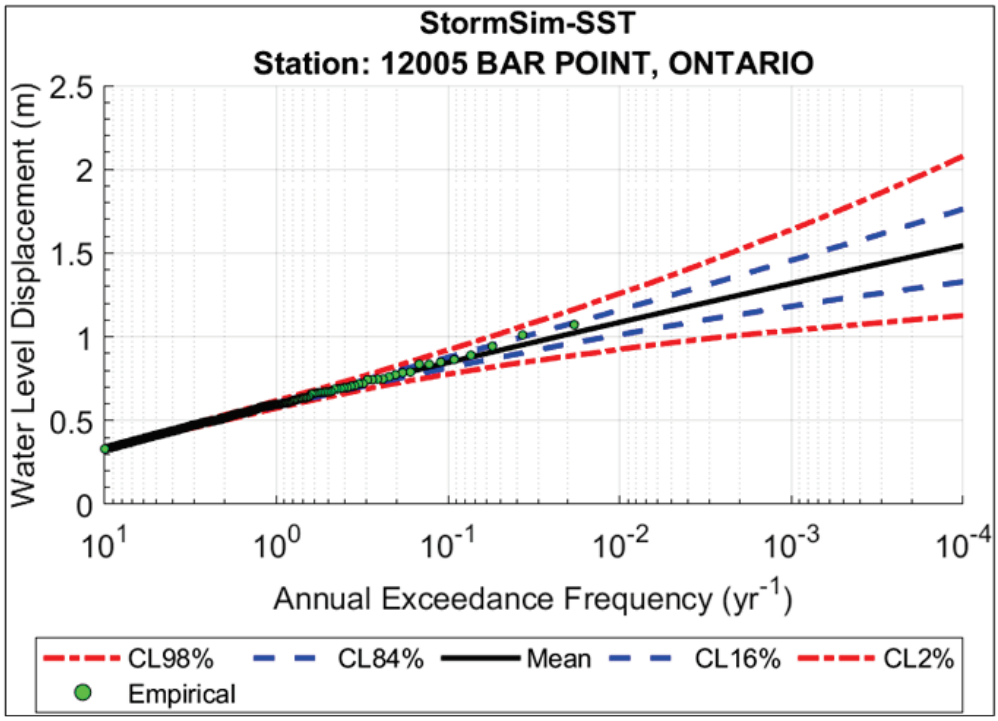

Figure C-2. LFA hazard curve (hourly data) at Kingsville, Ontario.

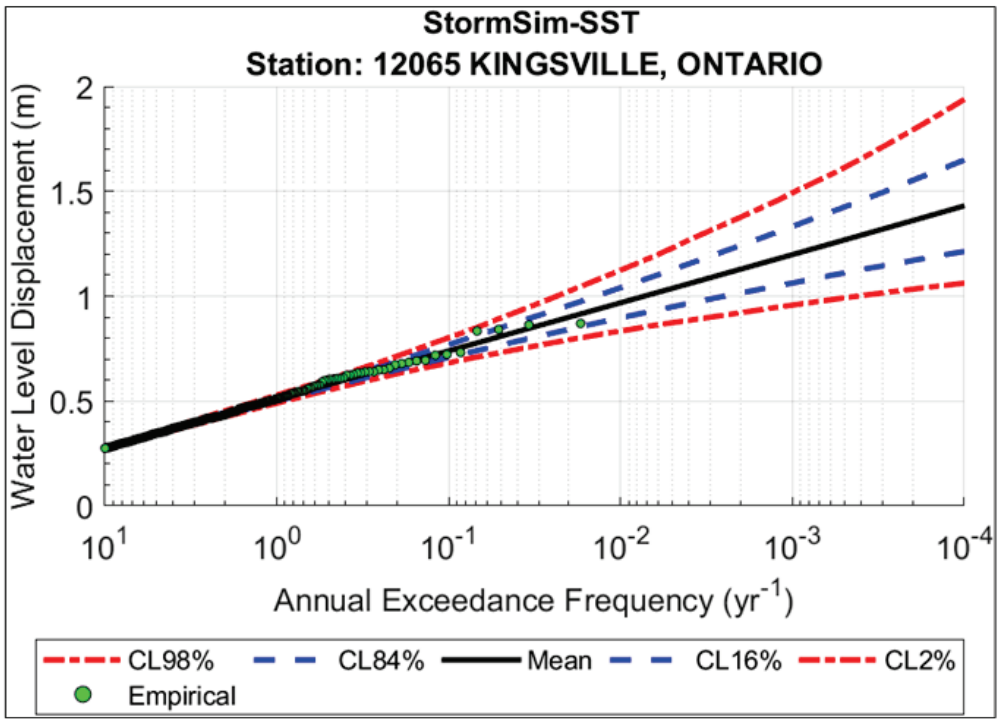

Figure C-3. LFA hazard curve (hourly data) at Point Pelee, Ontario.

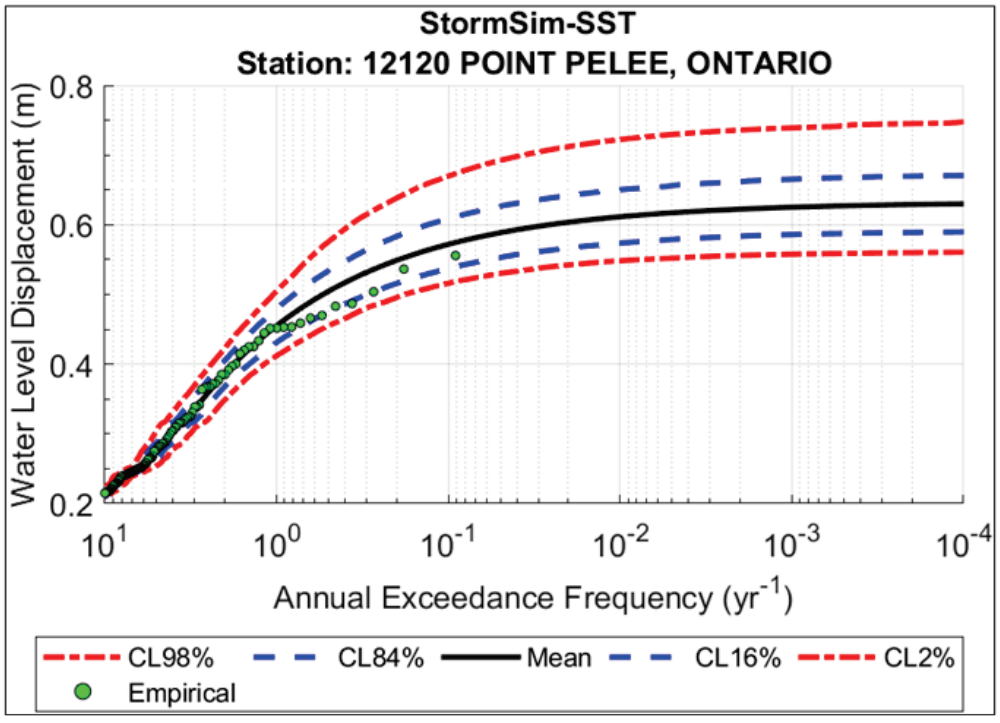

Figure C-4. LFA hazard curve (hourly data) at Point Pelee East, Ontario.

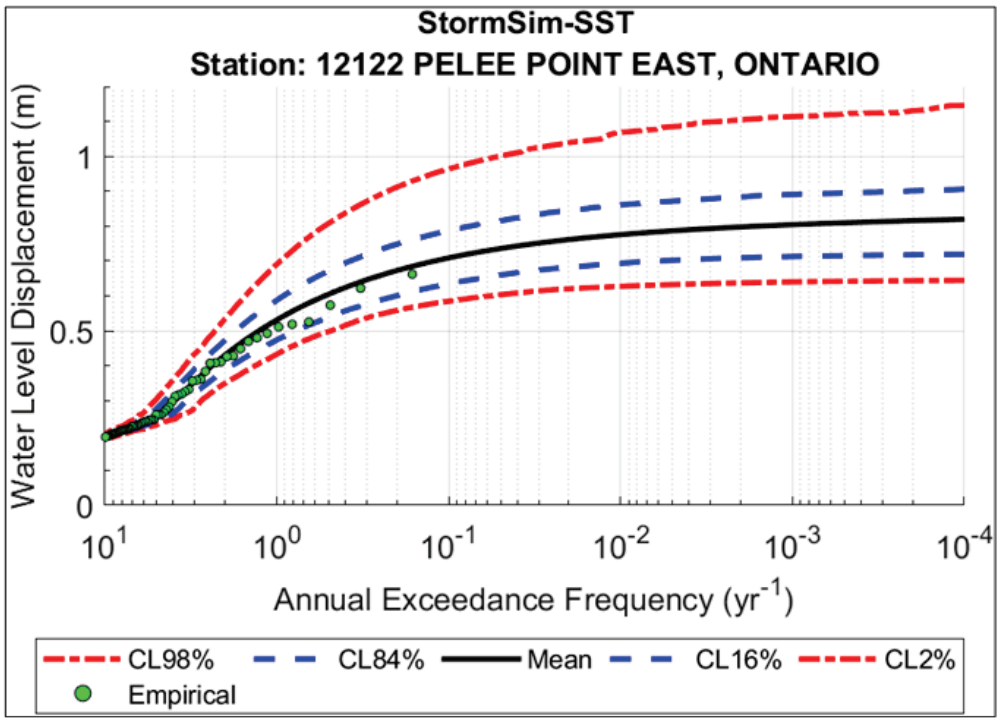

Figure C-5. LFA hazard curve (hourly data) at Erieau, Ontario.

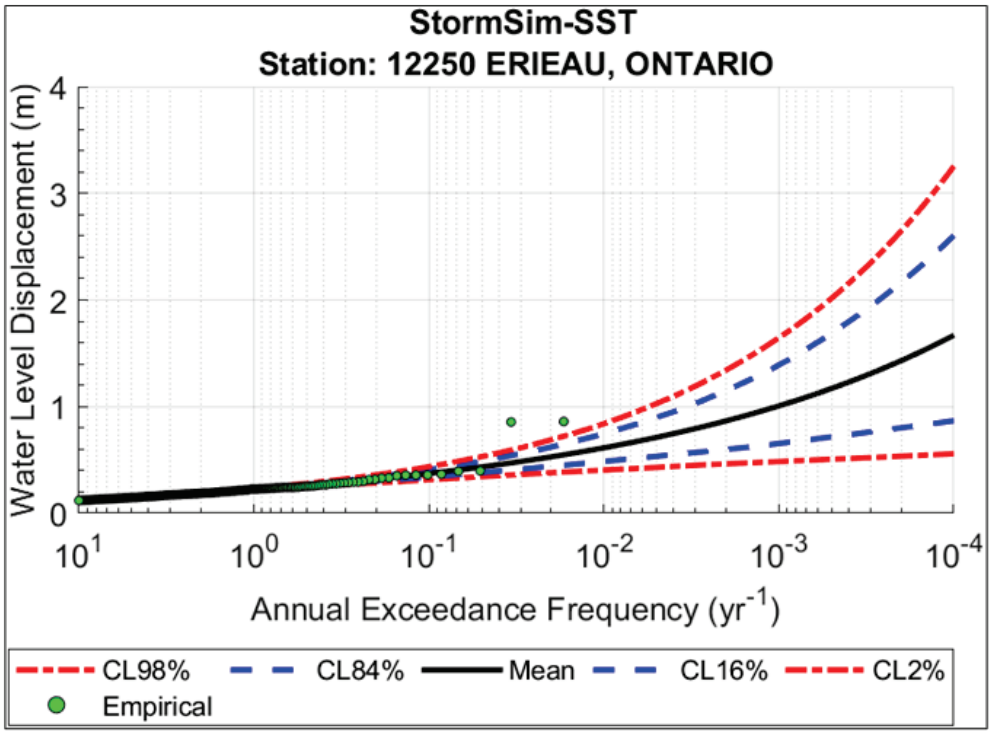

Figure C-6. LFA hazard curve (hourly data) at Port Stanley, Ontario.

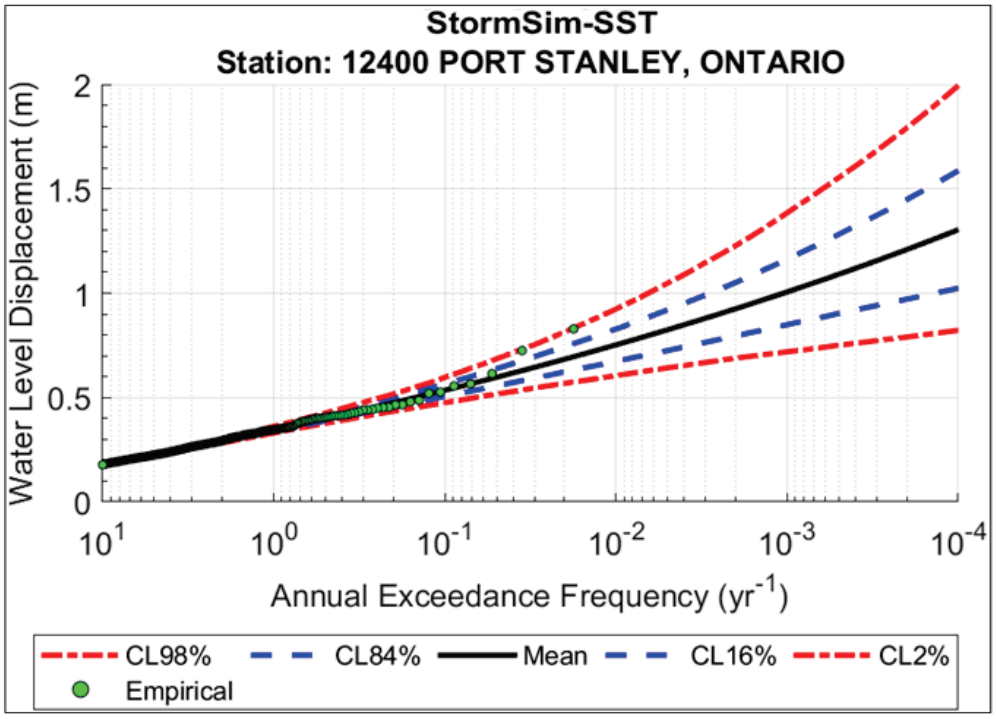

Figure C-7. LFA hazard curve (hourly data) at Port Dover, Ontario.

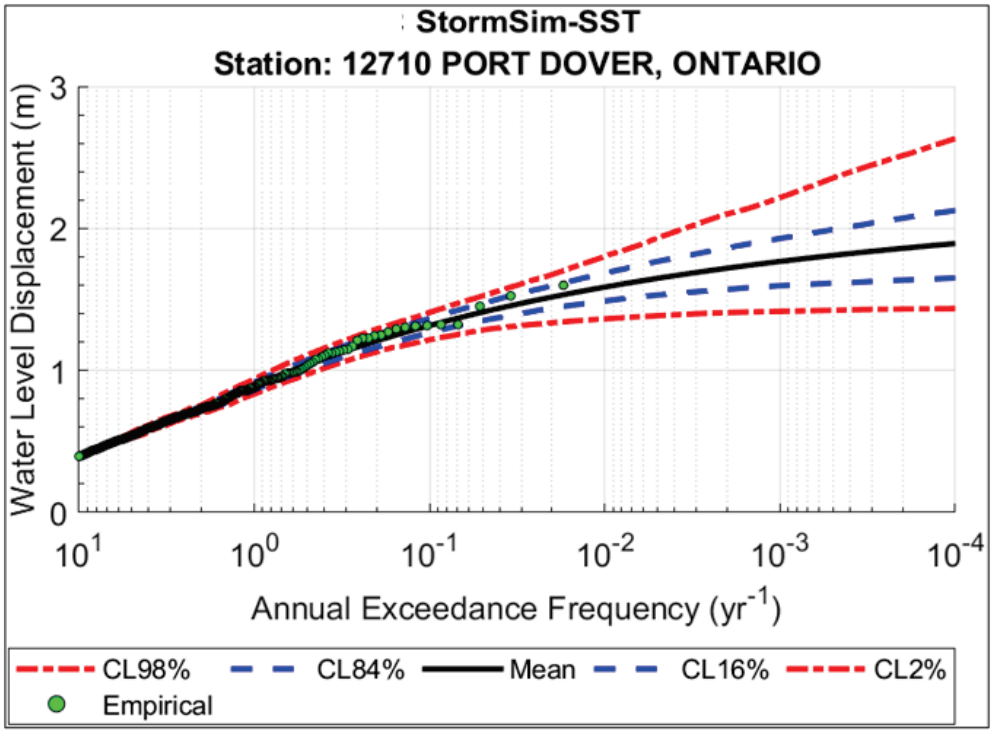

Figure C-8. LFA hazard curve (hourly data) at Port Colborne, Ontario.

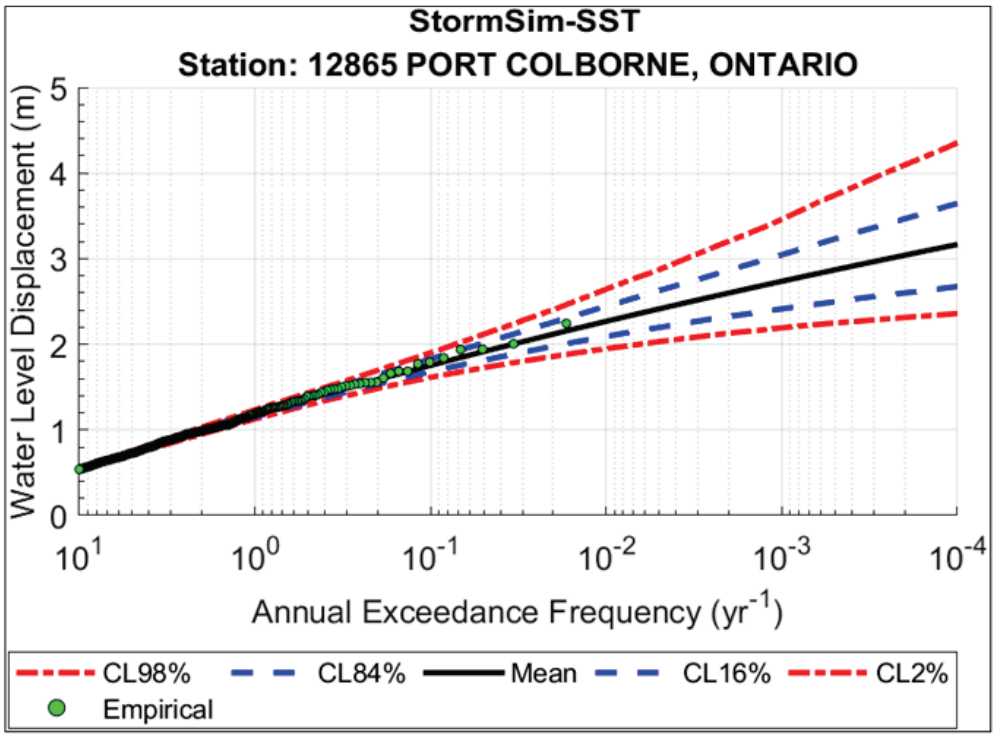

Figure C-9. LFA hazard curve (hourly data) at Gibraltar, Michigan.

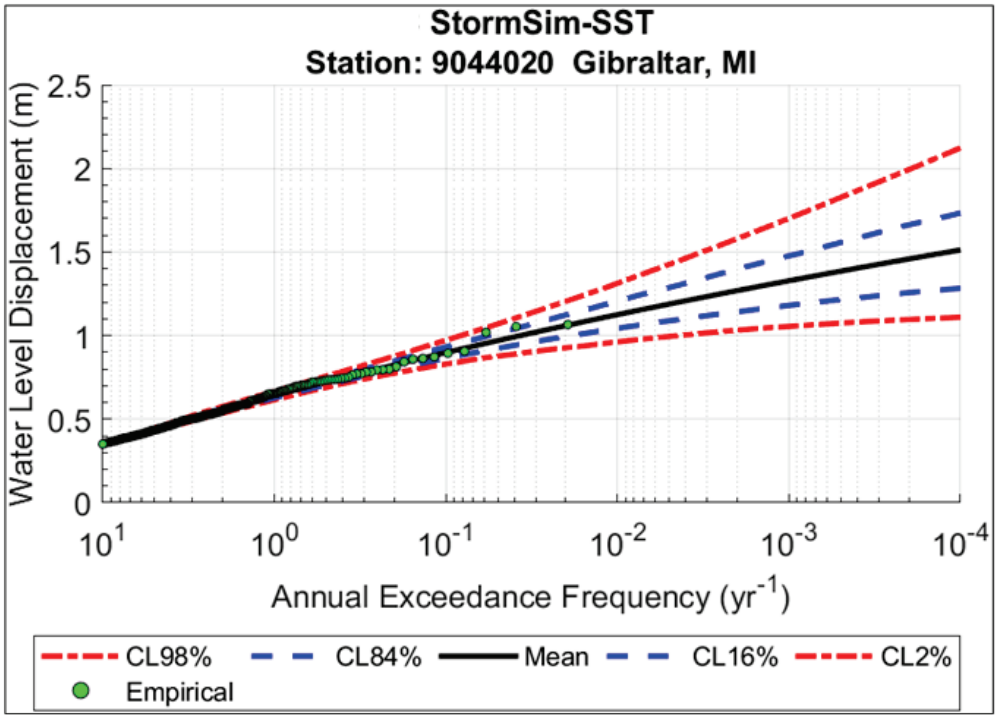

Figure C-10. LFA hazard curve (hourly data) at Buffalo, New York.

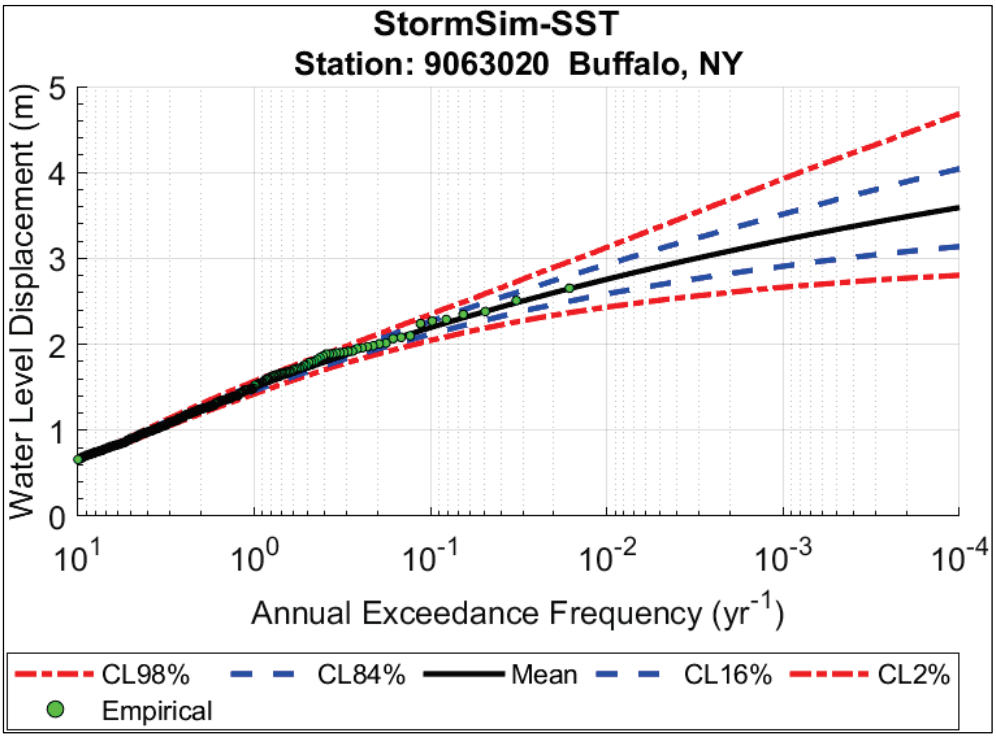

Figure C-11. LFA hazard curve (hourly data) at Sturgeon Point, New York.

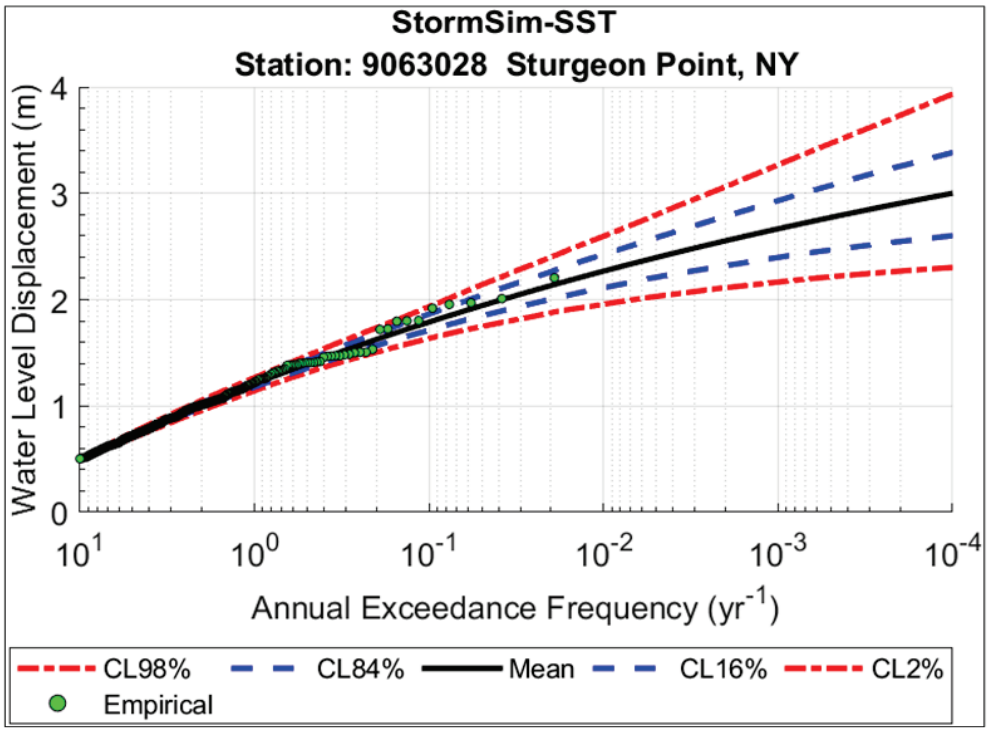

Figure C-12. LFA hazard curve (hourly data) at Barcelona, New York.

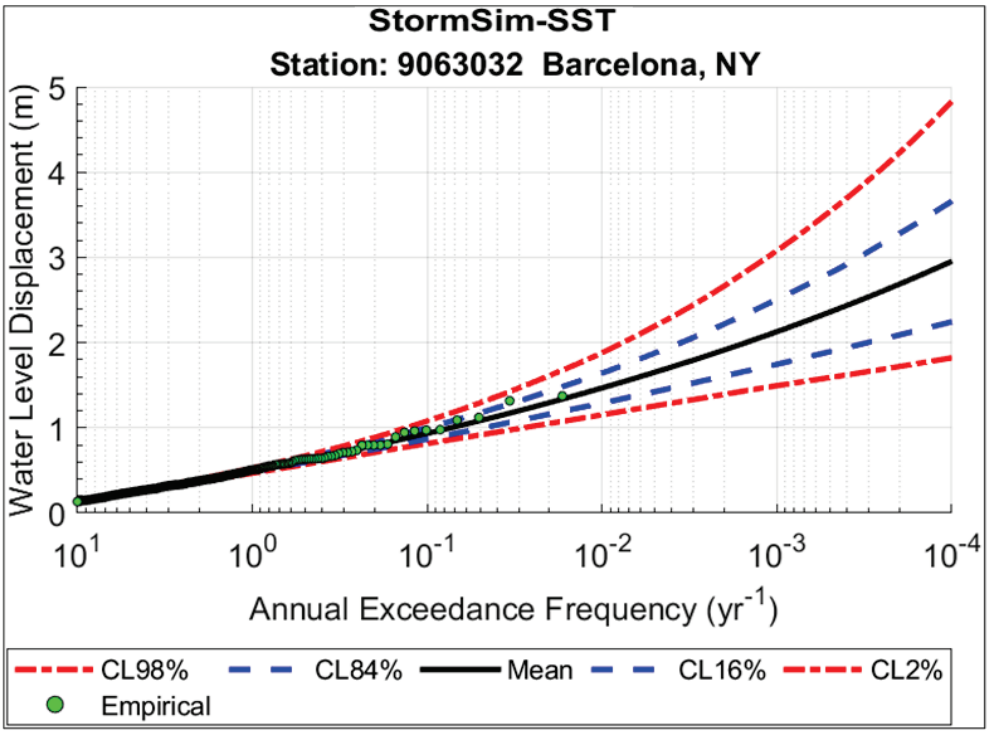

Figure C-13. LFA hazard curve (hourly data) at Erie, Pennsylvania.

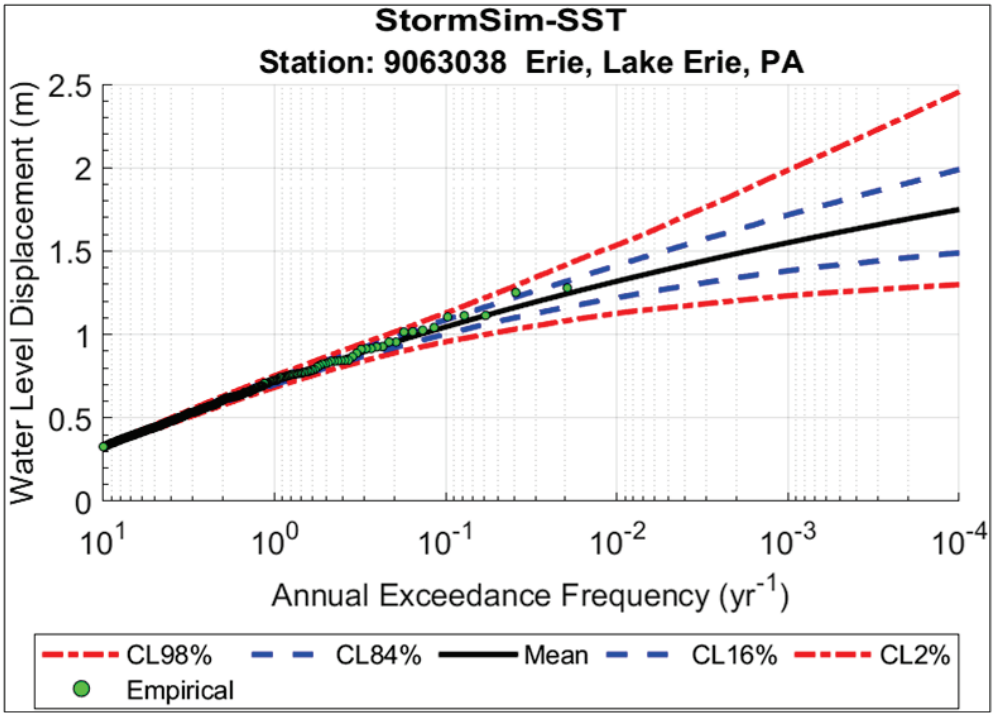

Figure C-14. LFA hazard curve (hourly data) at Fairport, Ohio.

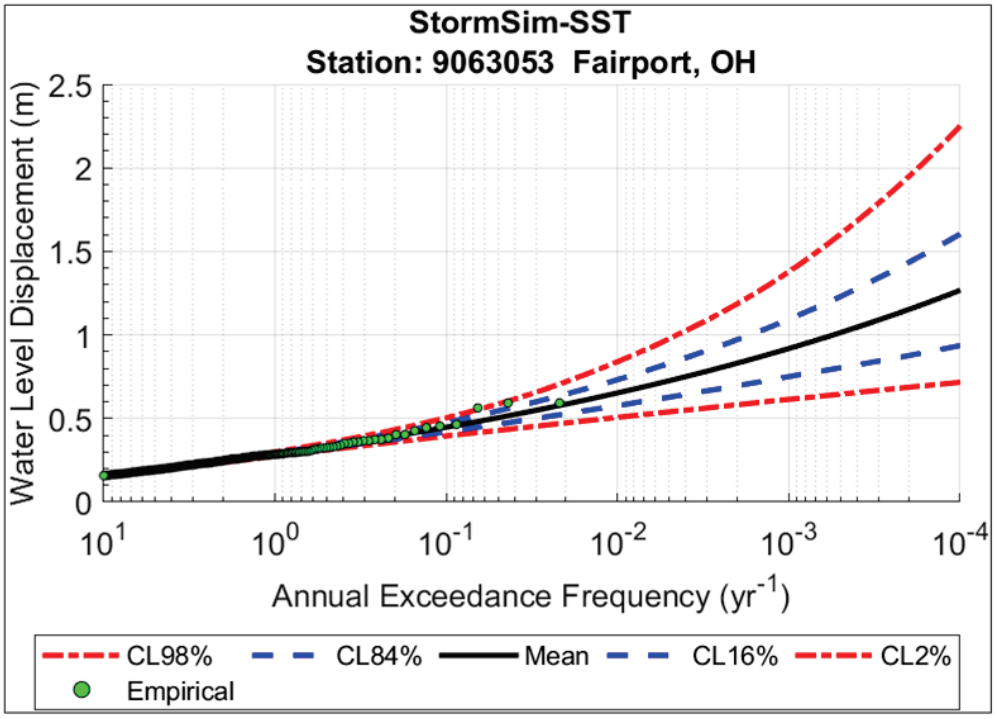

Figure C-15. LFA hazard curve (hourly data) at Marblehead, Ohio.

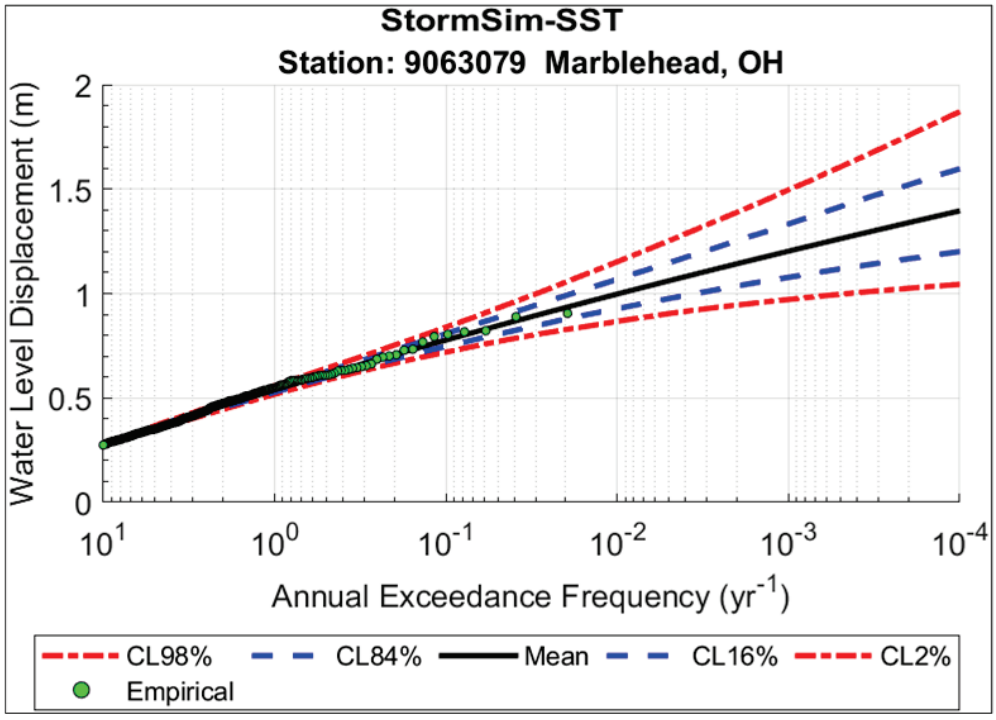

Figure C-16. LFA hazard curve (hourly data) at Monroe, Michigan.

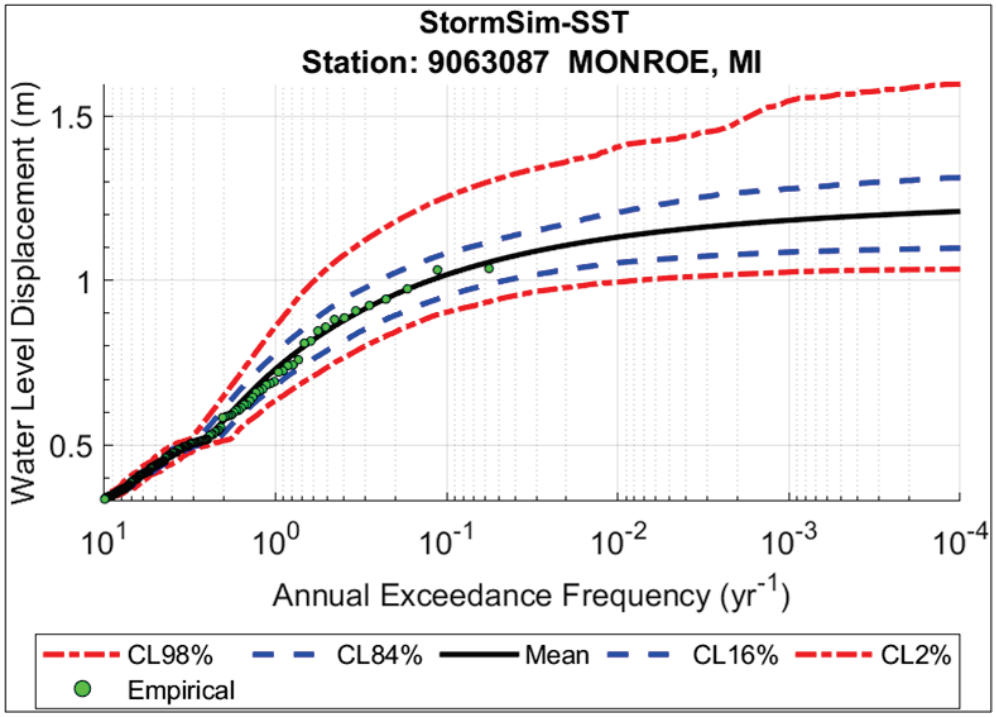

Figure C-17. LFA hazard curve (hourly data) at Fermi Power Plant, Michigan.

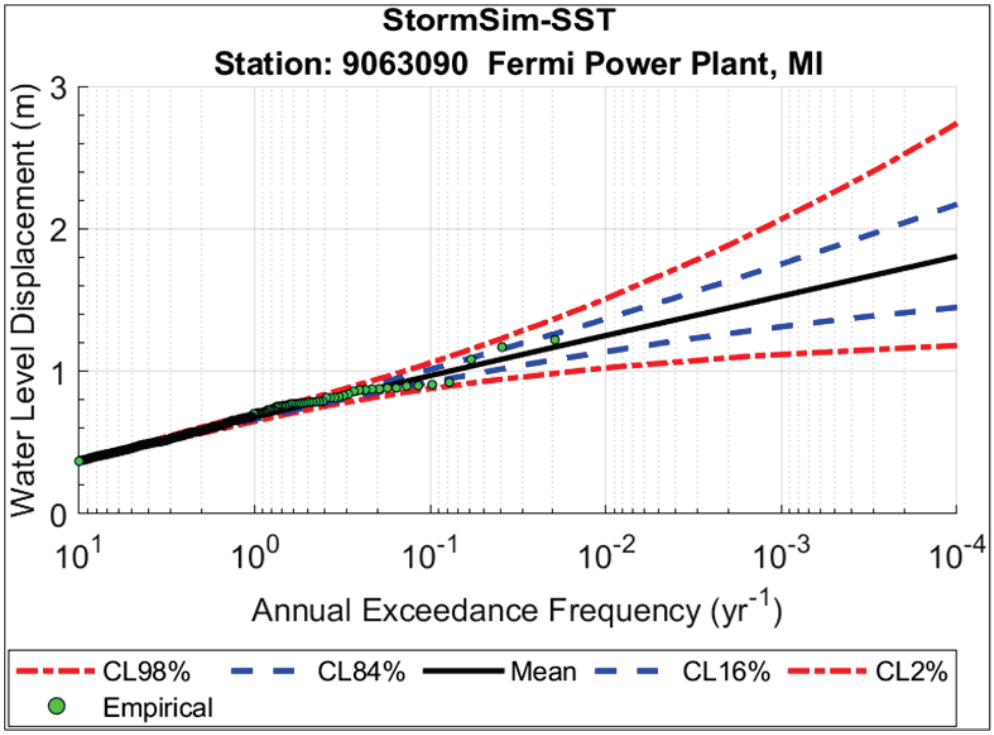

Appendix D: LFA Results Using Combined Hourly Gauge Data

Figure D-1 through Figure D-7 show the LFA results using combined hourly gauge data.

Figure D-1. LFA hazard curve (combined hourly data) at Gibraltar, Michigan.

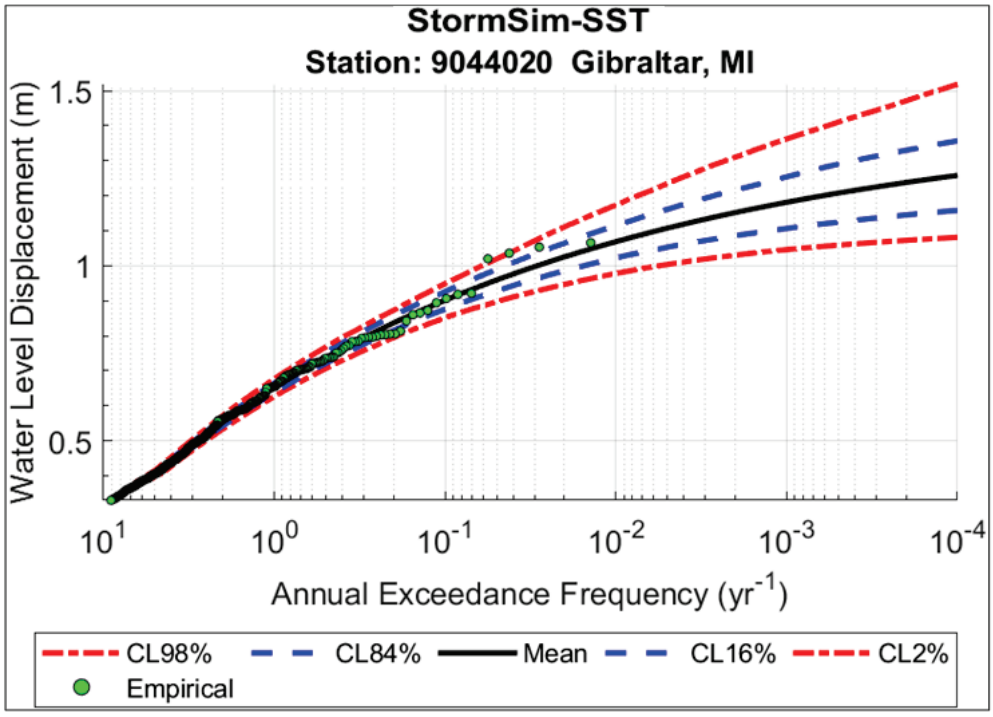

Figure D-2. LFA hazard curve (combined hourly data) at Sturgeon Point, New York.

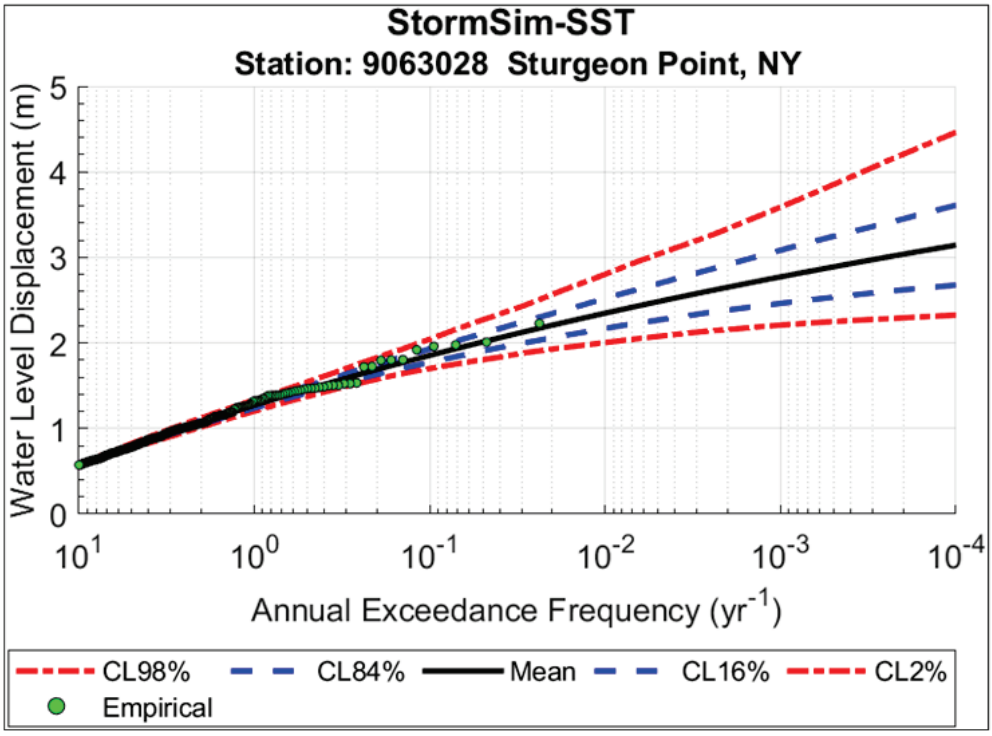

Figure D-3. LFA hazard curve (combined hourly data) at Barcelona, New York.

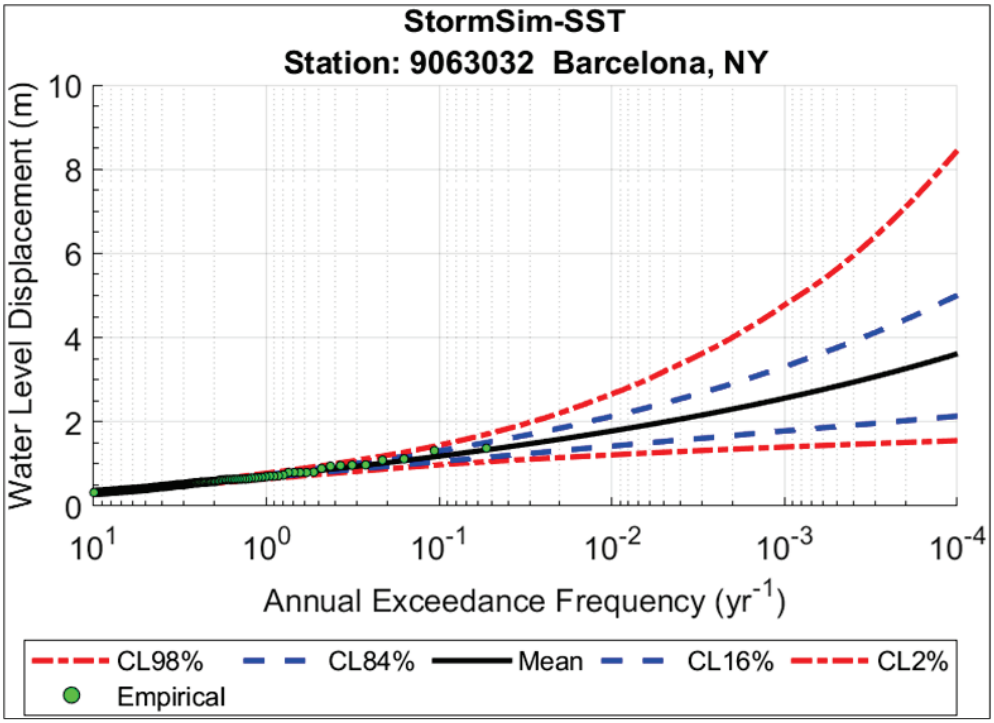

Figure D-4. LFA hazard curve (combined hourly data) at Erie, Pennsylvania.

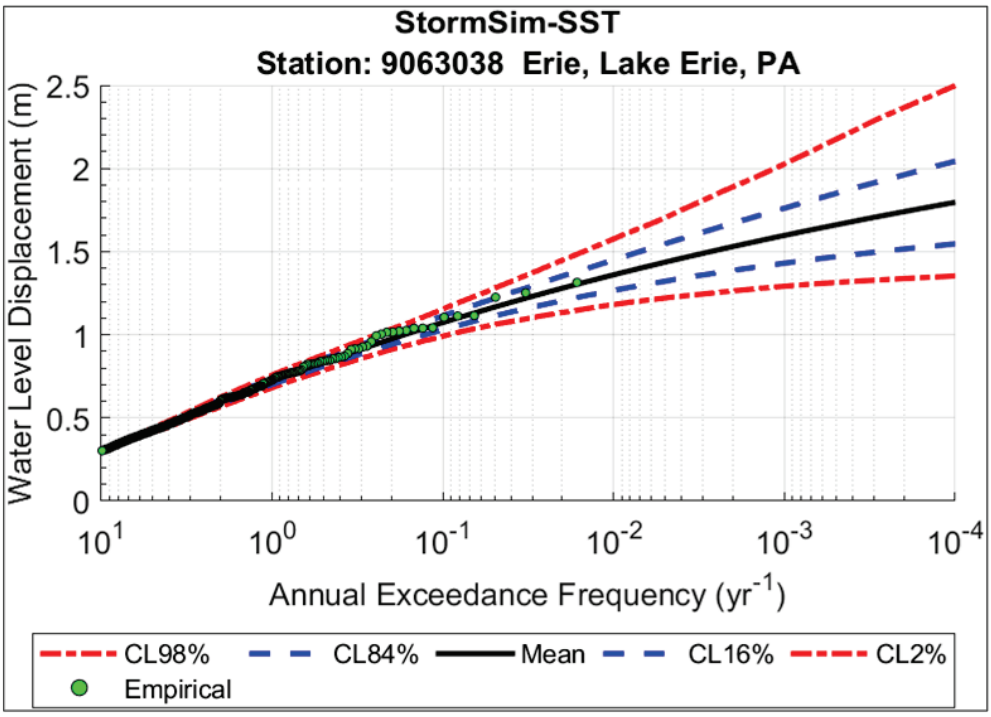

Figure D-5. LFA hazard curve (combined hourly data) at Fairport, Ohio.

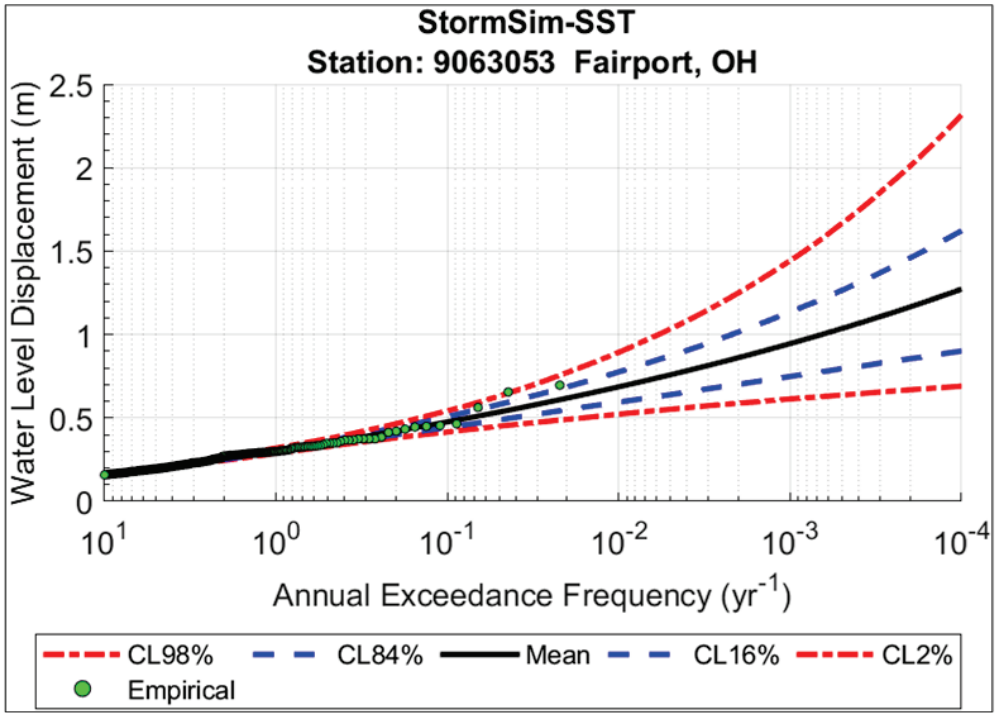

Figure D-6. LFA hazard curve (combined hourly data) at Marblehead, Ohio.

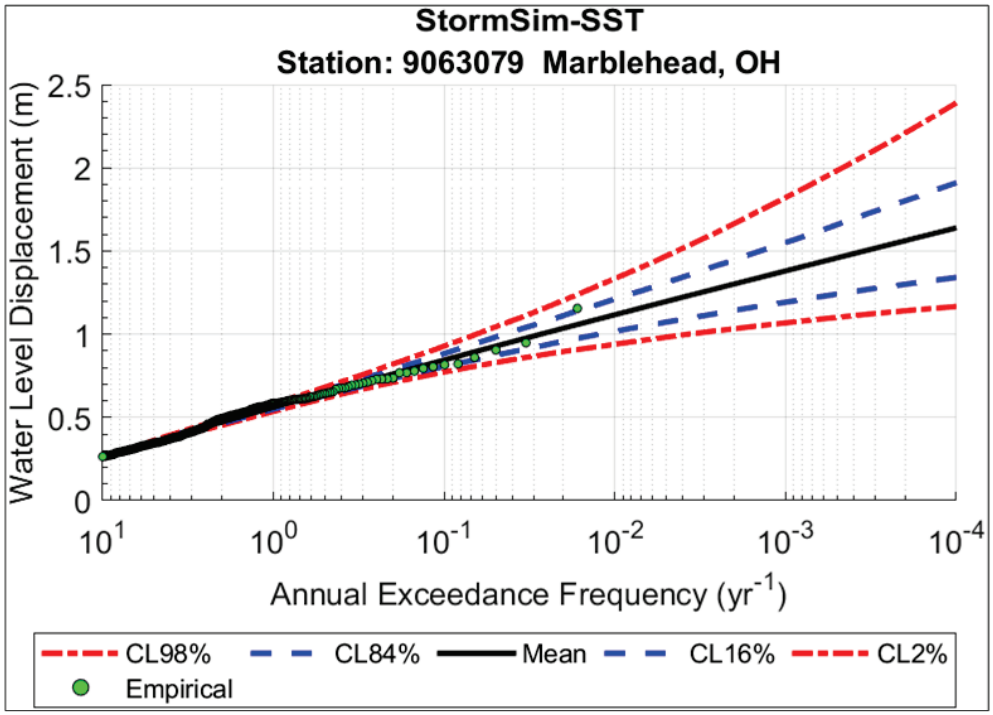

Figure D-7. LFA hazard curve (combined hourly data) at Fermi Power Plant, Michigan.

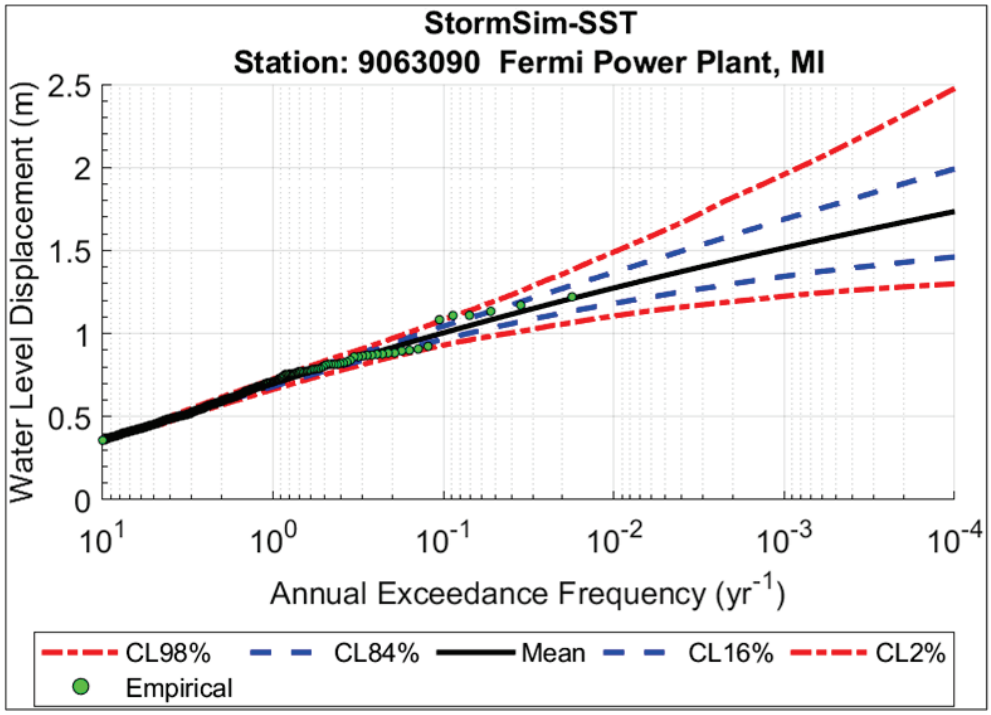

Appendix E: Regional Frequency Analysis (RFA) Results Using Hourly Gauge Data

Figure E-1 through Figure E-17 show the regional frequency analysis (RFA) results using hourly gauge data.

Figure E-1. Regional frequency analysis (RFA) hazard curve (hourly data) at Bar Point, Ontario.

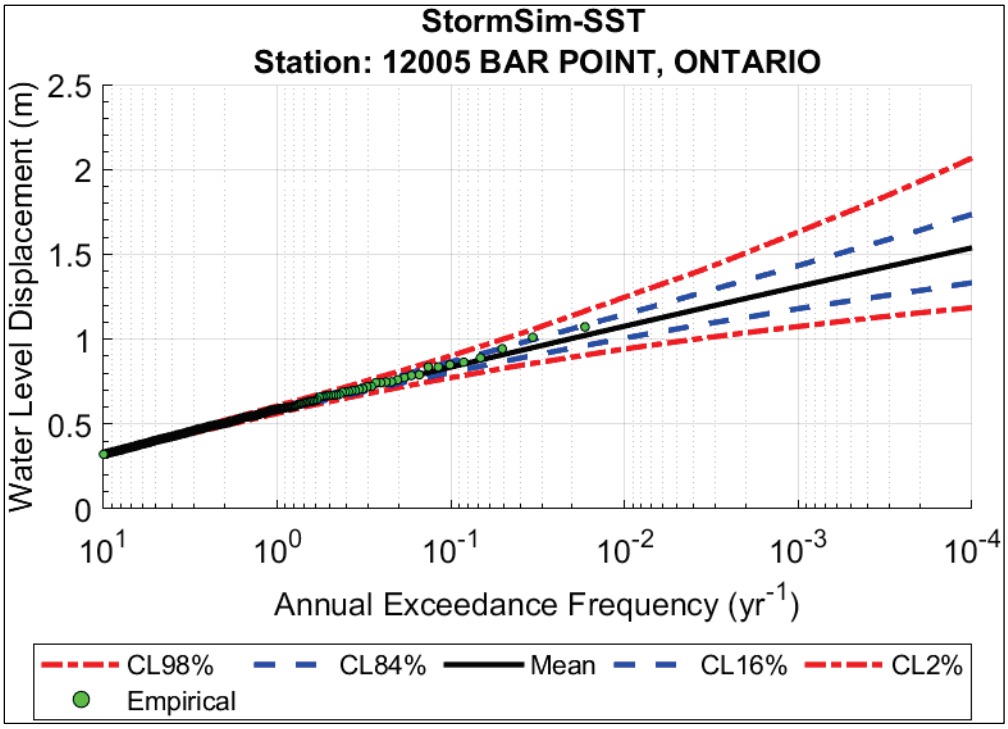

Figure E-2. RFA hazard curve (hourly data) at Kingsville, Ontario.

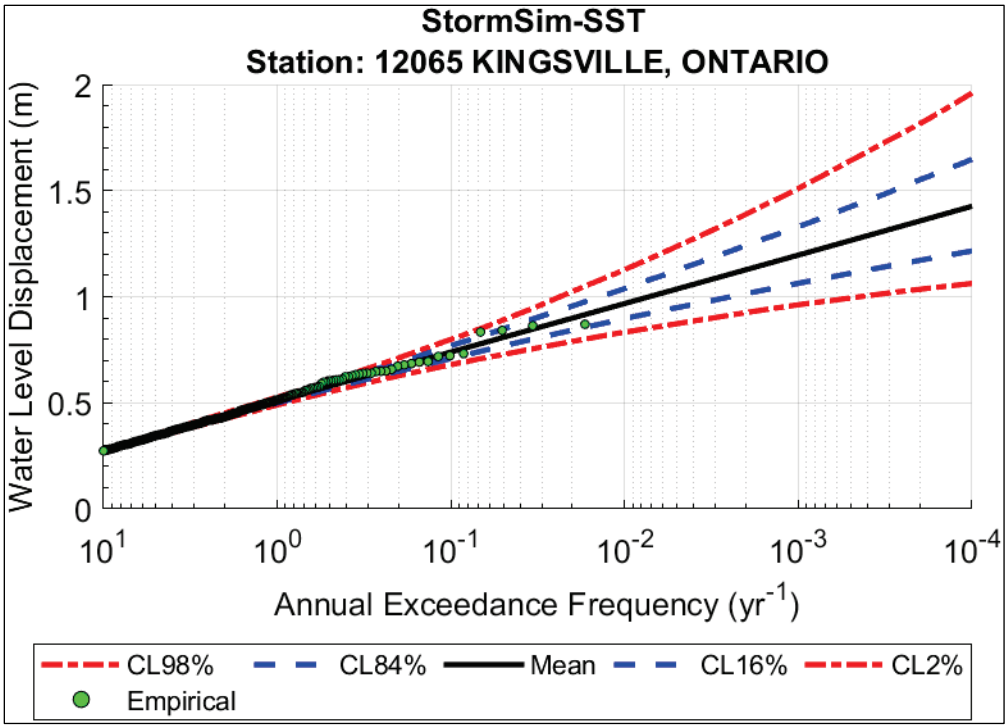

Figure E-3. RFA hazard curve (hourly data) at Point Pelee, Ontario.

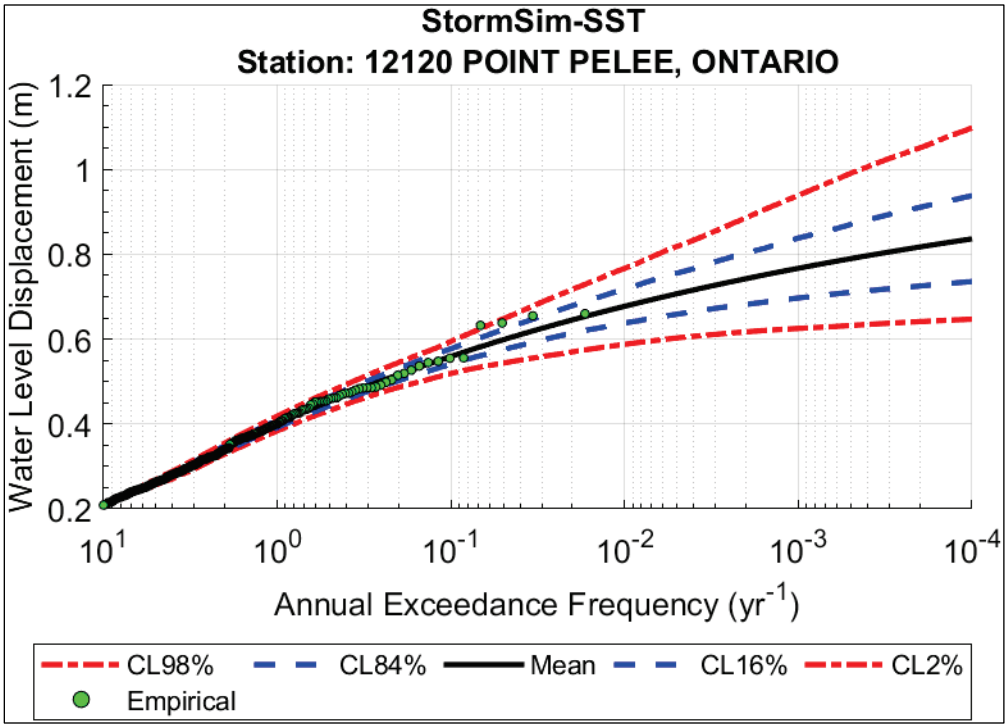

Figure E-4. RFA hazard curve (hourly data) at Point Pelee East, Ontario.

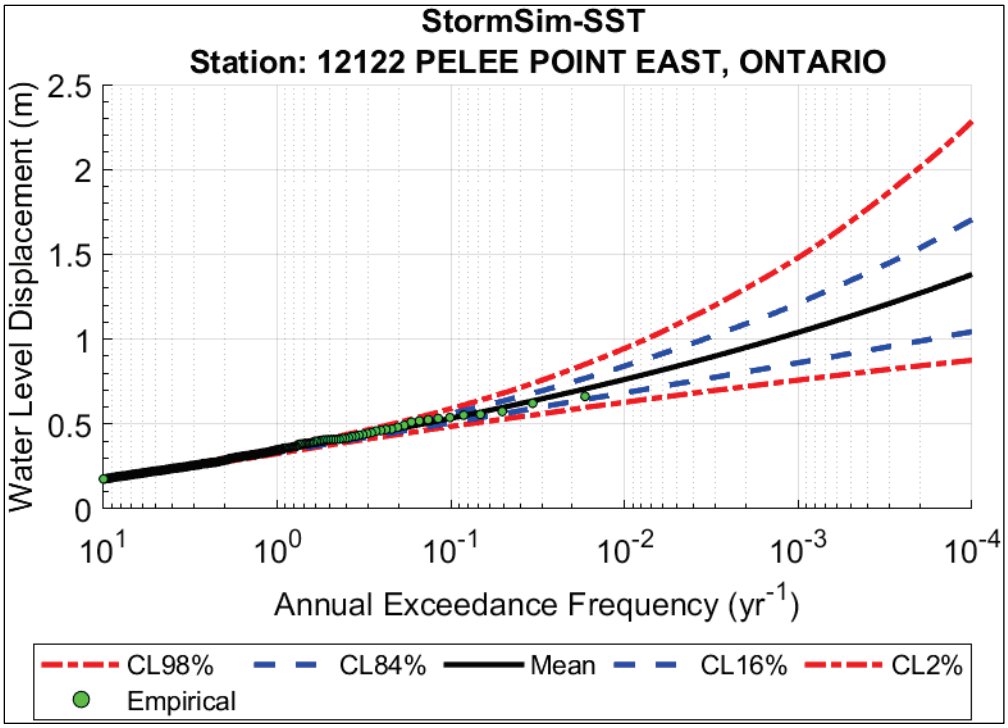

Figure E-5. RFA hazard curve (hourly data) at Erieau, Ontario.

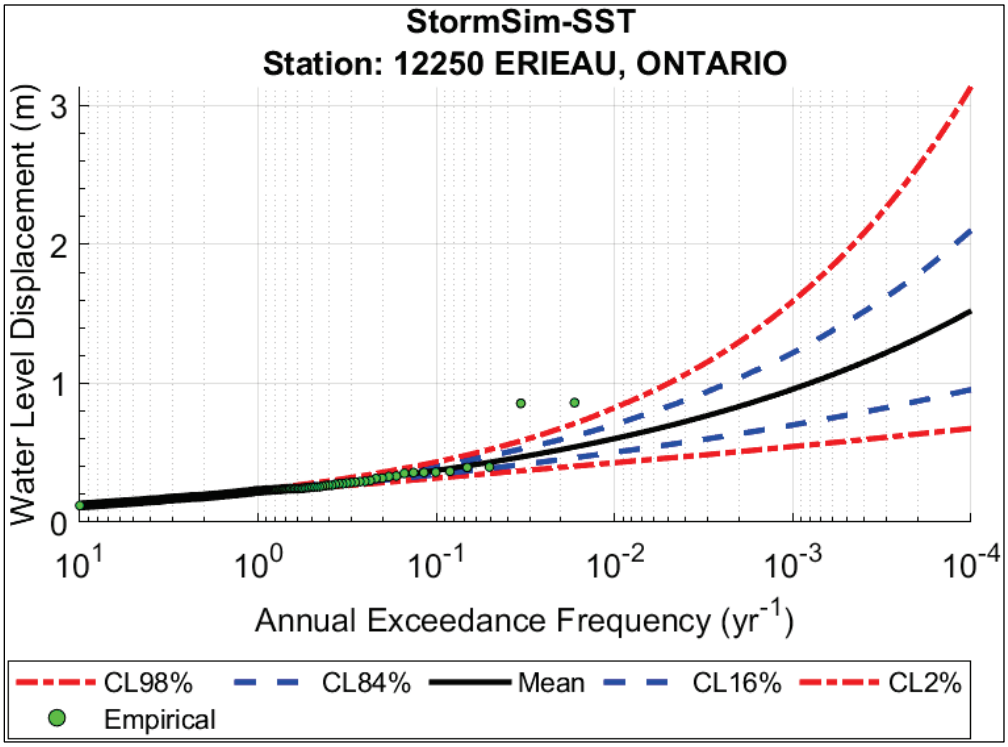

Figure E-6. RFA hazard curve (hourly data) at Port Stanley, Ontario.

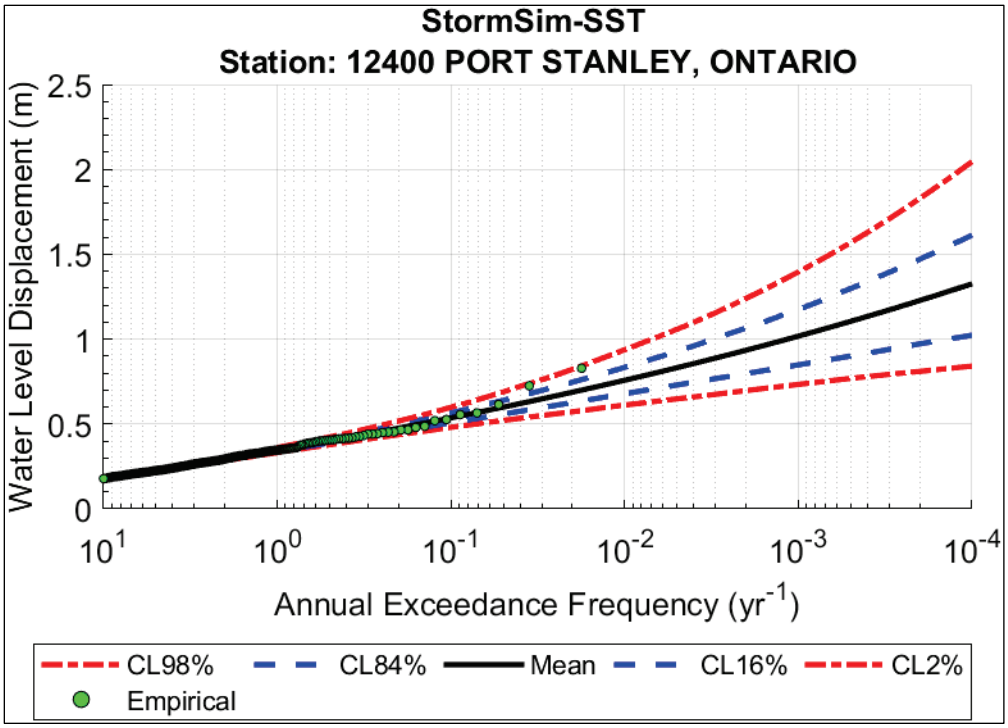

Figure E-7. RFA hazard curve (hourly data) at Port Dover, Ontario.

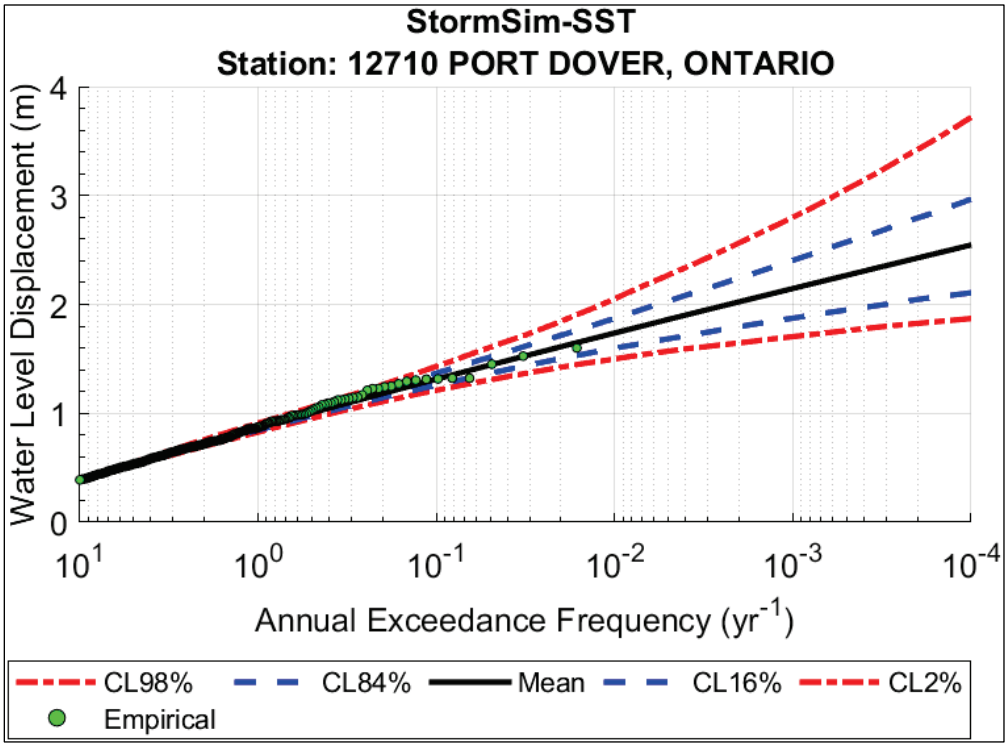

Figure E-8. RFA hazard curve (hourly data) at Port Colborne, Ontario.

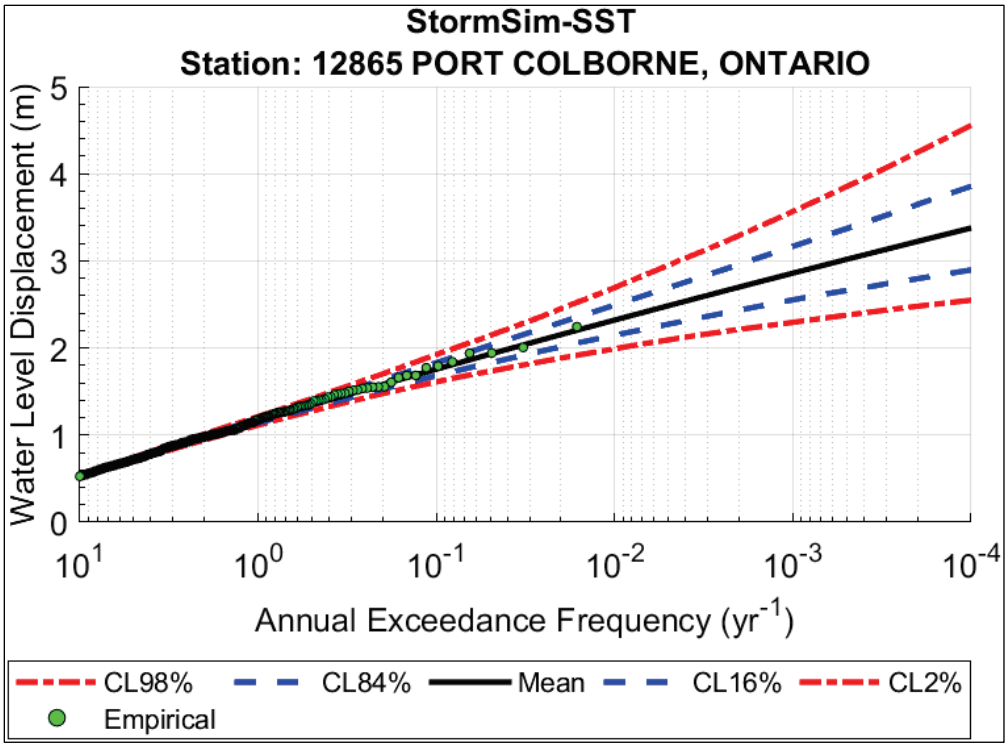

Figure E-9. RFA hazard curve (hourly data) at Gibraltar, Michigan.

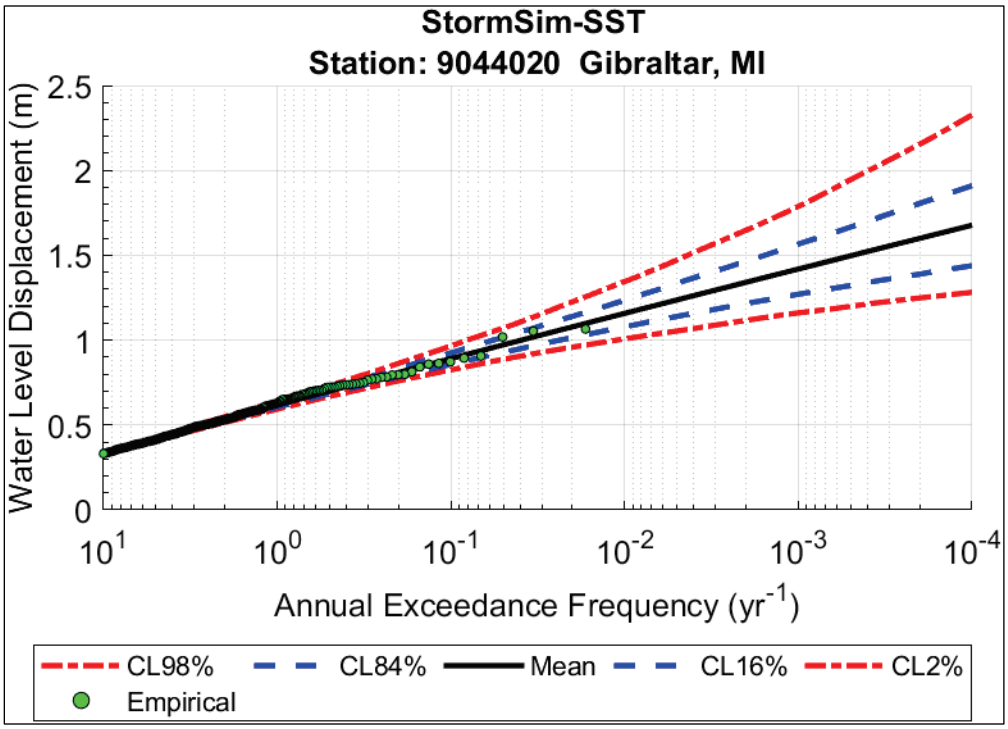

Figure E-10. RFA hazard curve (hourly data) at Sturgeon Point, New York.

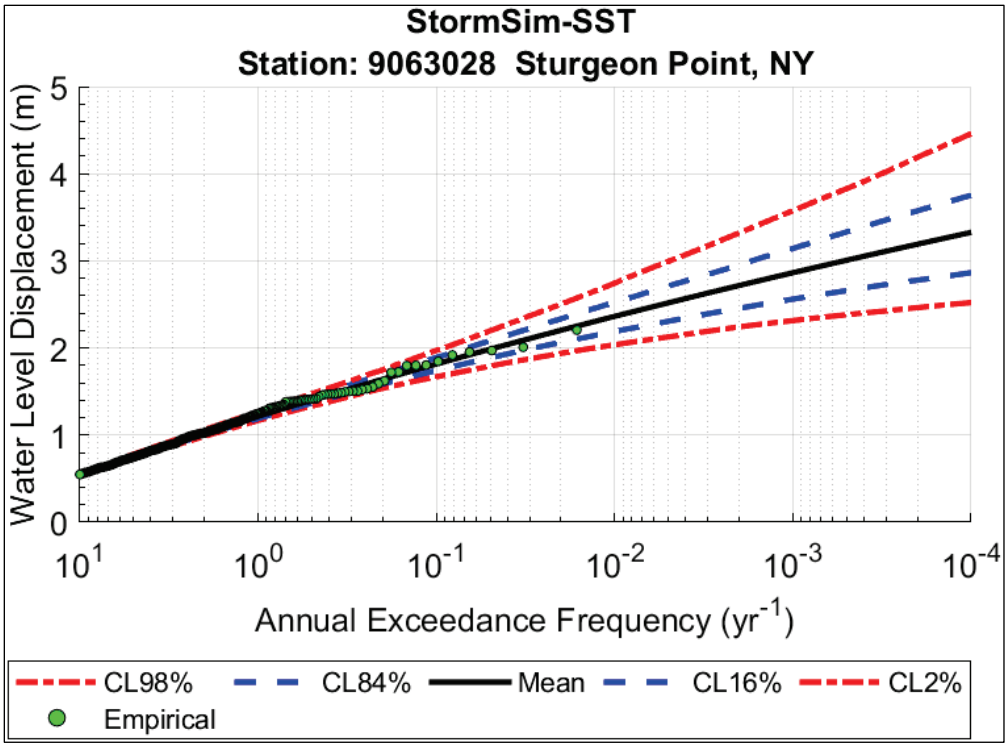

Figure E-11. RFA hazard curve (hourly data) at Barcelona, New York.

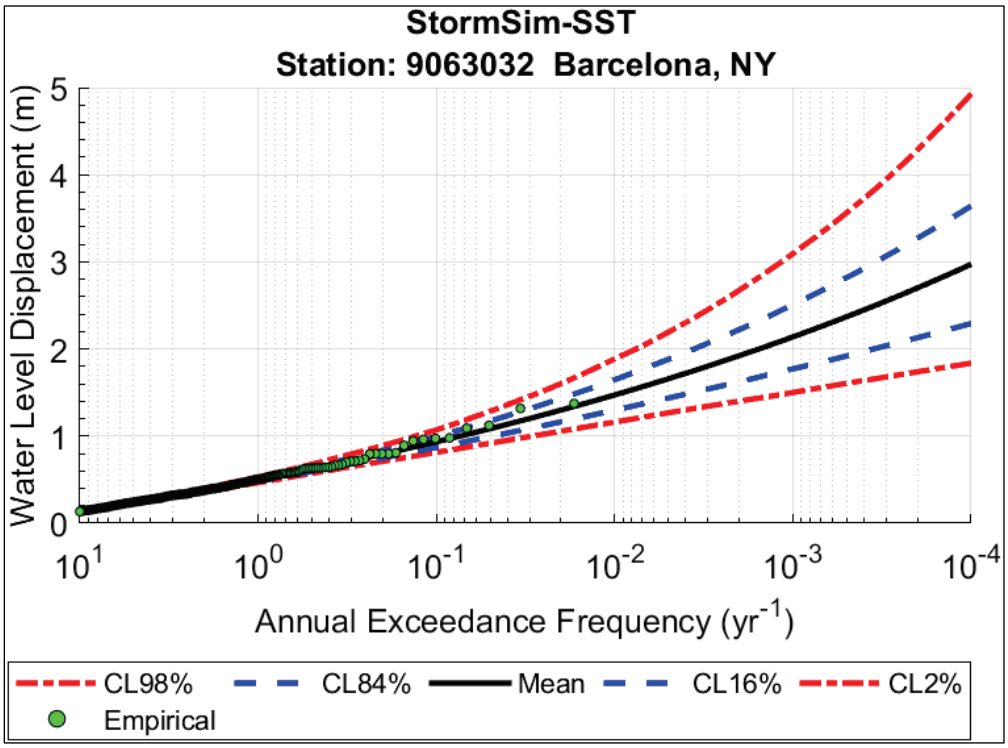

Figure E-12. RFA hazard curve (hourly data) at Erie, Pennsylvania.

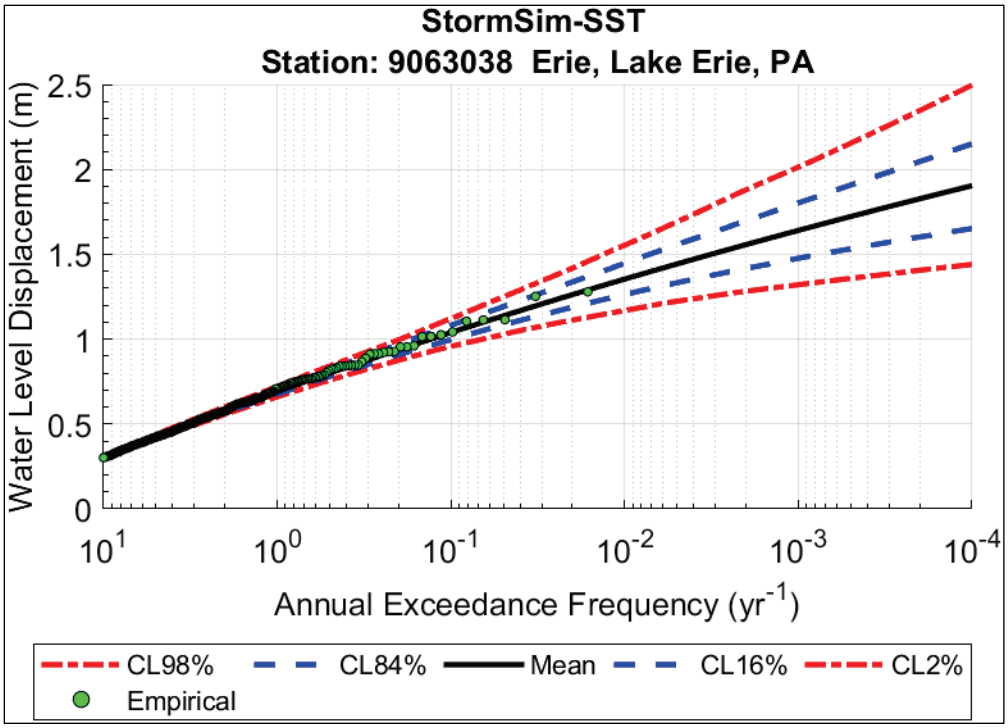

Figure E-13. RFA hazard curve (hourly data) at Fairport, Ohio.

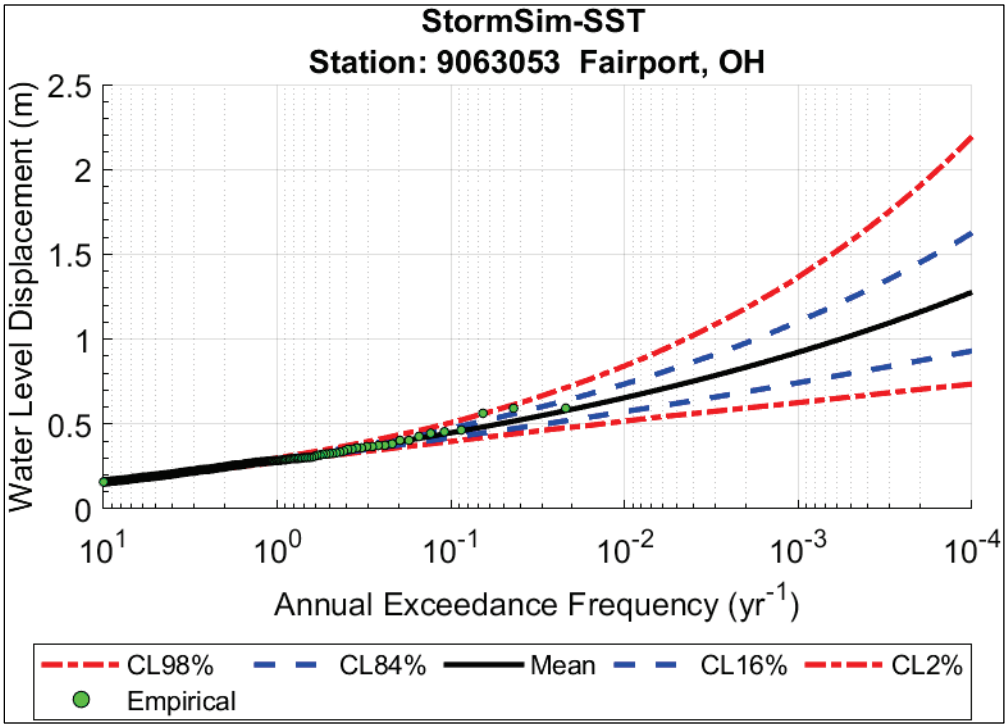

Figure E-14. RFA hazard curve (hourly data) at Lorain, Ohio.

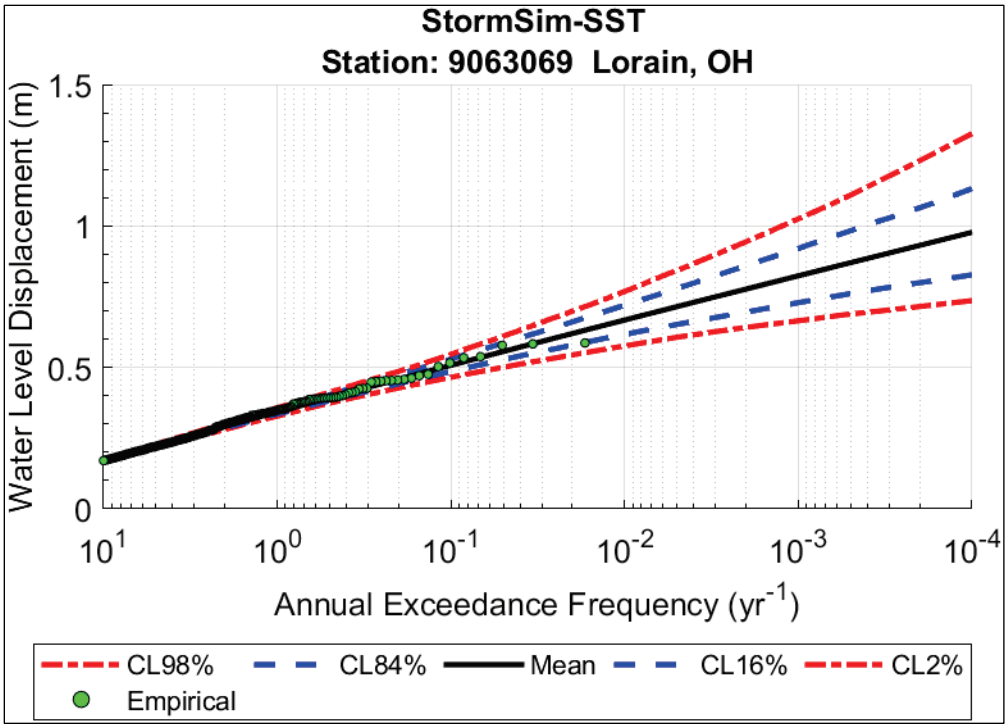

Figure E-15. RFA hazard curve (hourly data) at Marblehead, Ohio.

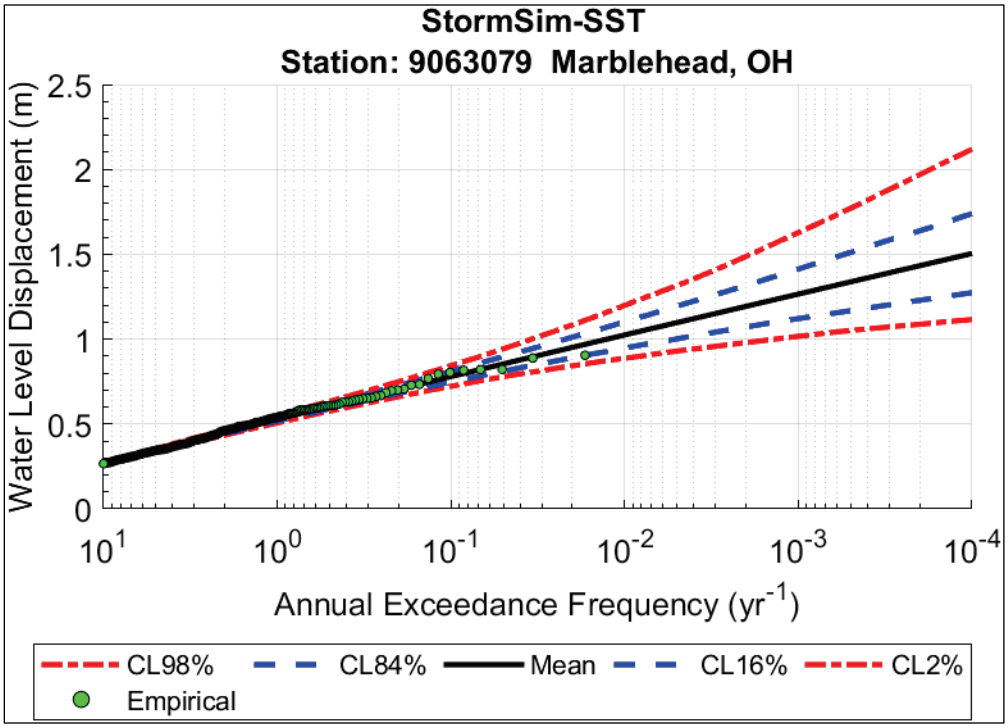

Figure E-16. RFA hazard curve (hourly data) at Monroe, Michigan.

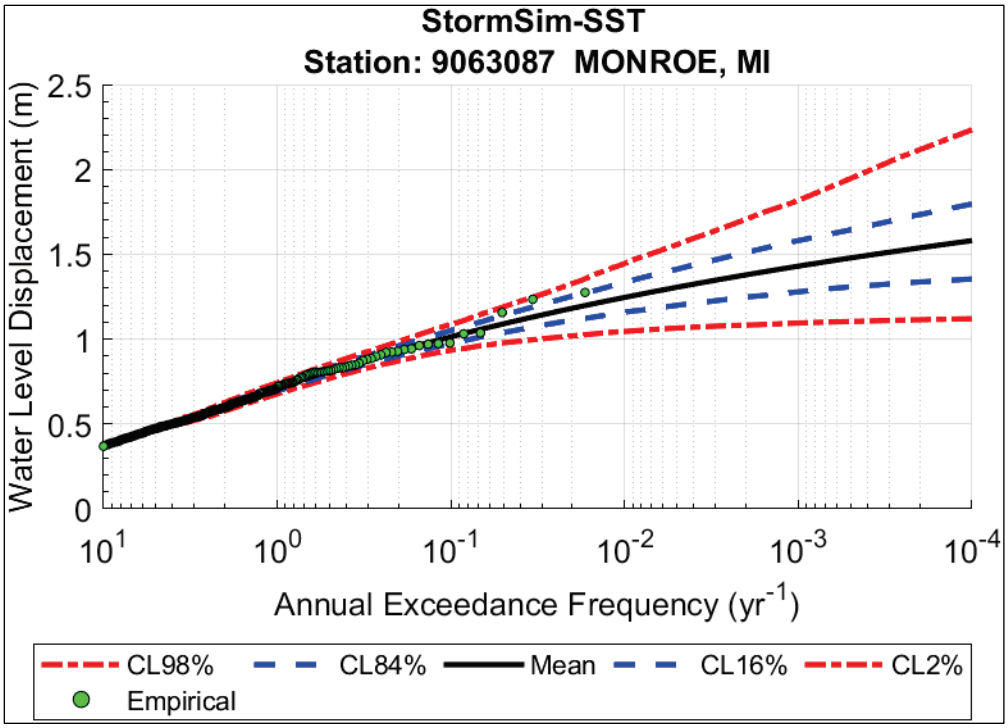

Figure E-17. RFA hazard curve (hourly data) at Fermi Power Plant, Michigan.

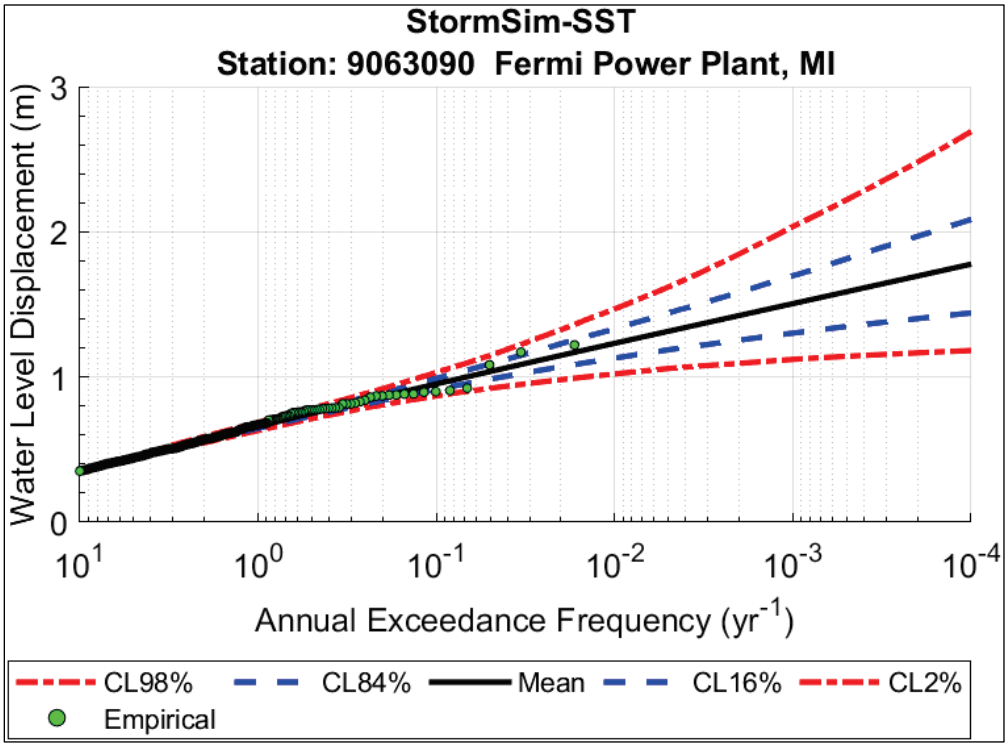

Appendix F: RFA Results Using Combined Hourly Gauge Data

Figure F-1 through Figure F-17 show the RFA results using combined hourly gage data.

Figure F-1. RFA hazard curve (combined hourly data) at Bar Point, Ontario.

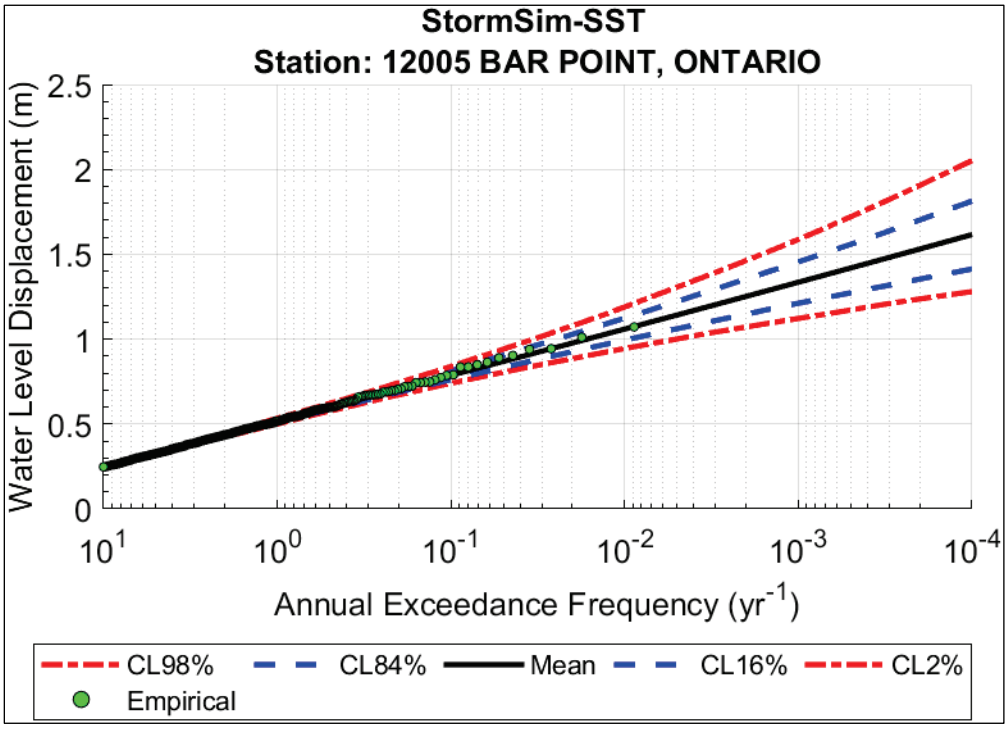

Figure F-2. RFA hazard curve (combined hourly data) at Kingsville, Ontario.

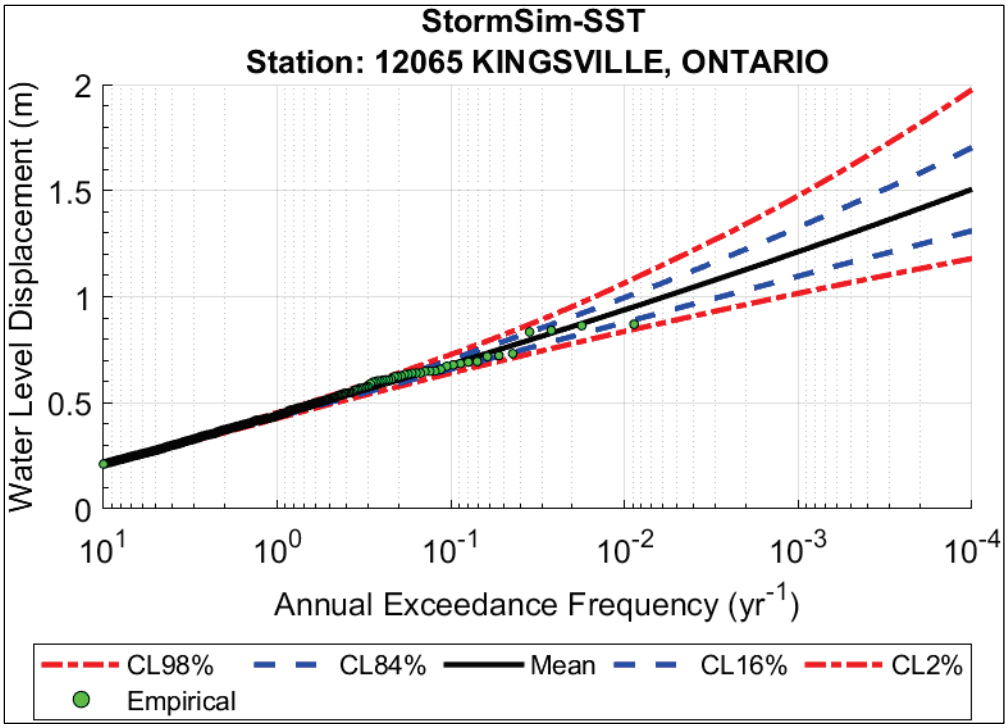

Figure F-3. RFA hazard curve (combined hourly data) at Point Pelee, Ontario.

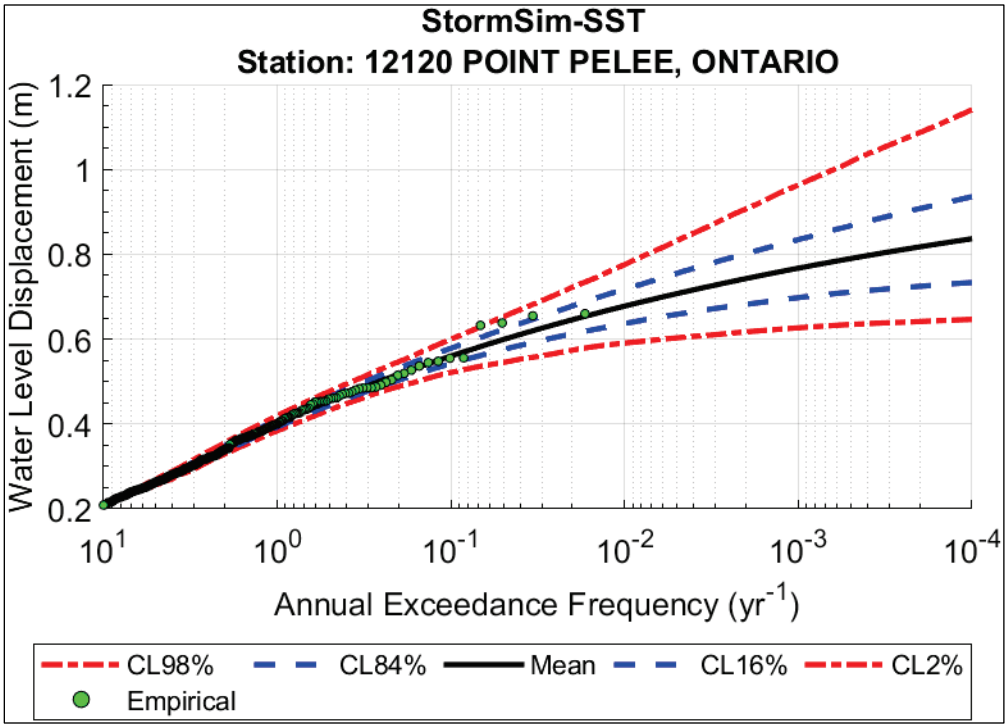

Figure F-4. RFA hazard curve (combined hourly data) at Point Pelee East, Ontario.

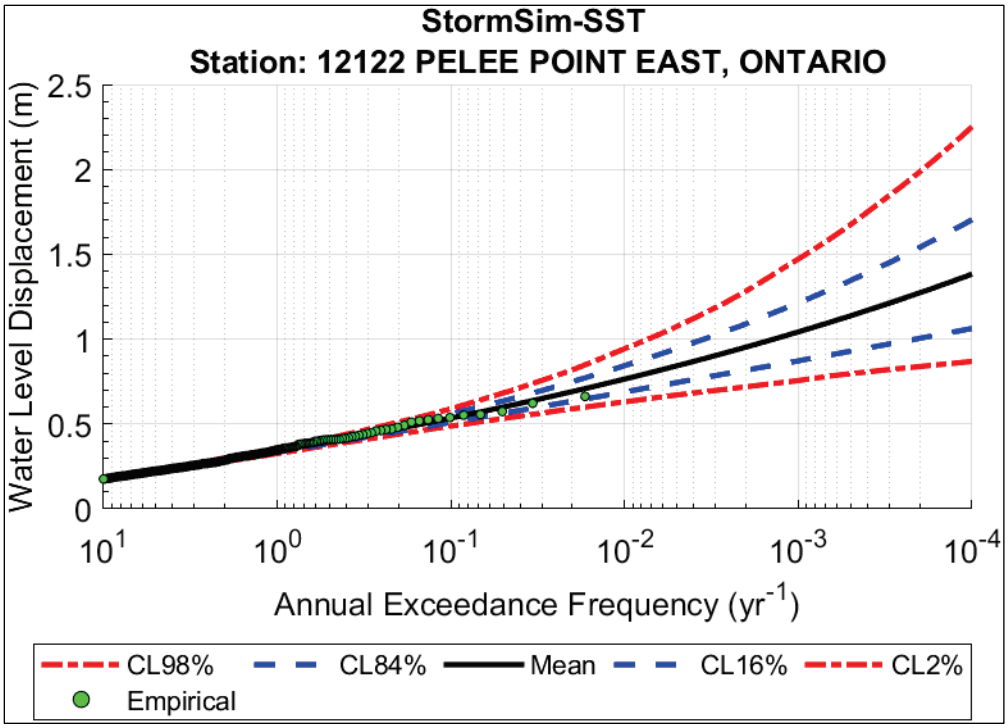

Figure F-5. RFA hazard curve (combined hourly data) at Erieau, Ontario.

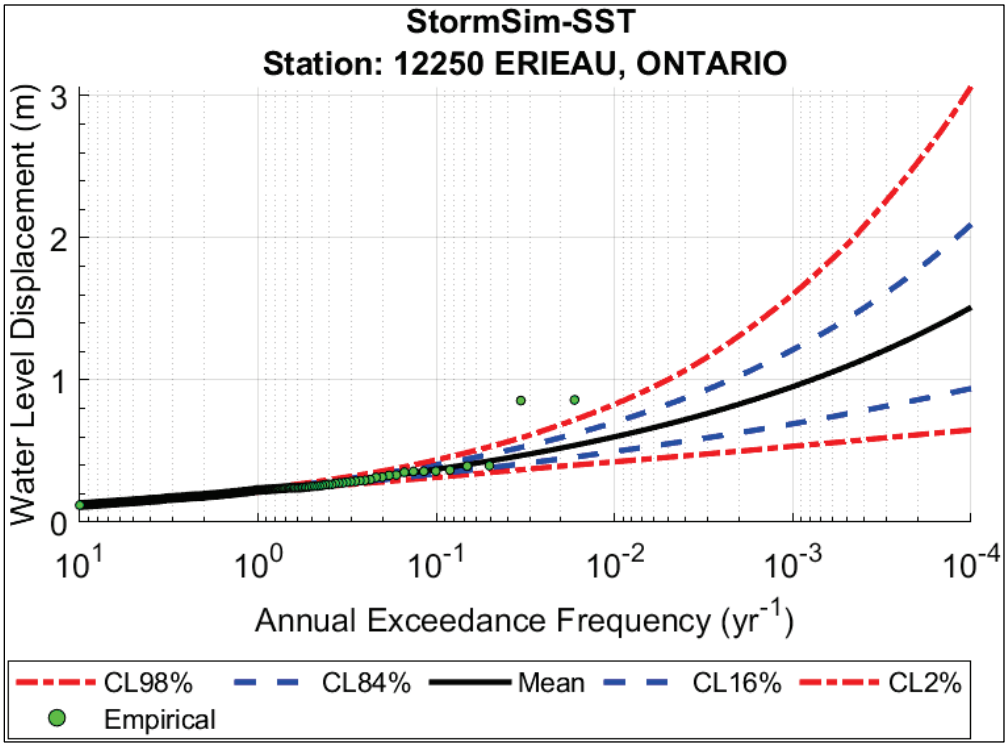

Figure F-6. RFA hazard curve (combined hourly data) at Port Stanley, Ontario.

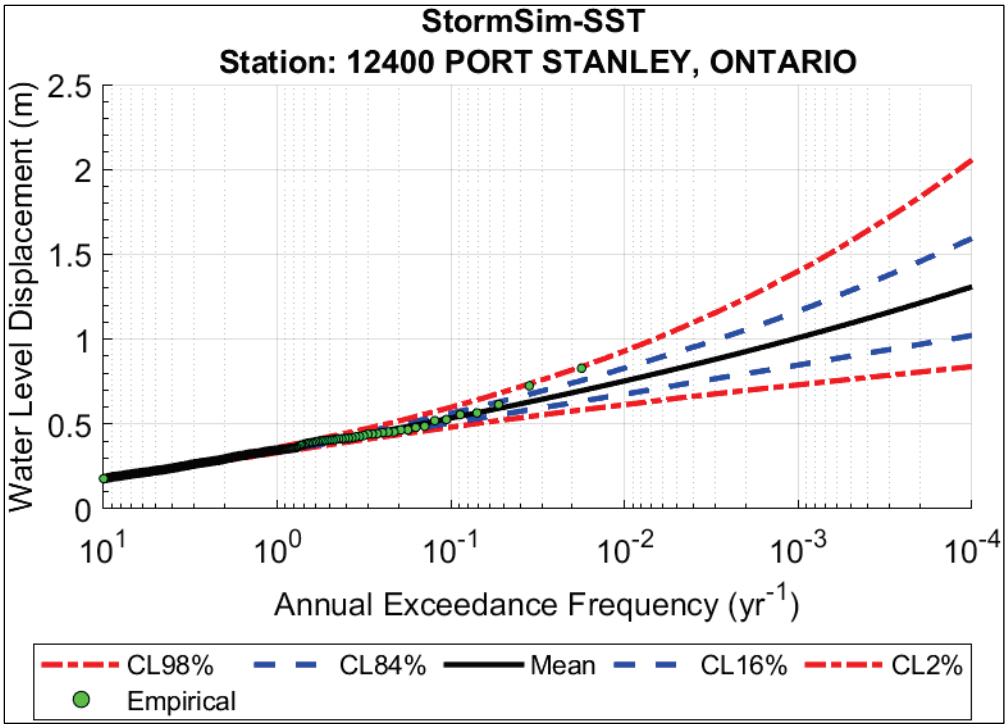

Figure F-7. RFA hazard curve (combined hourly data) at Port Dover, Ontario.

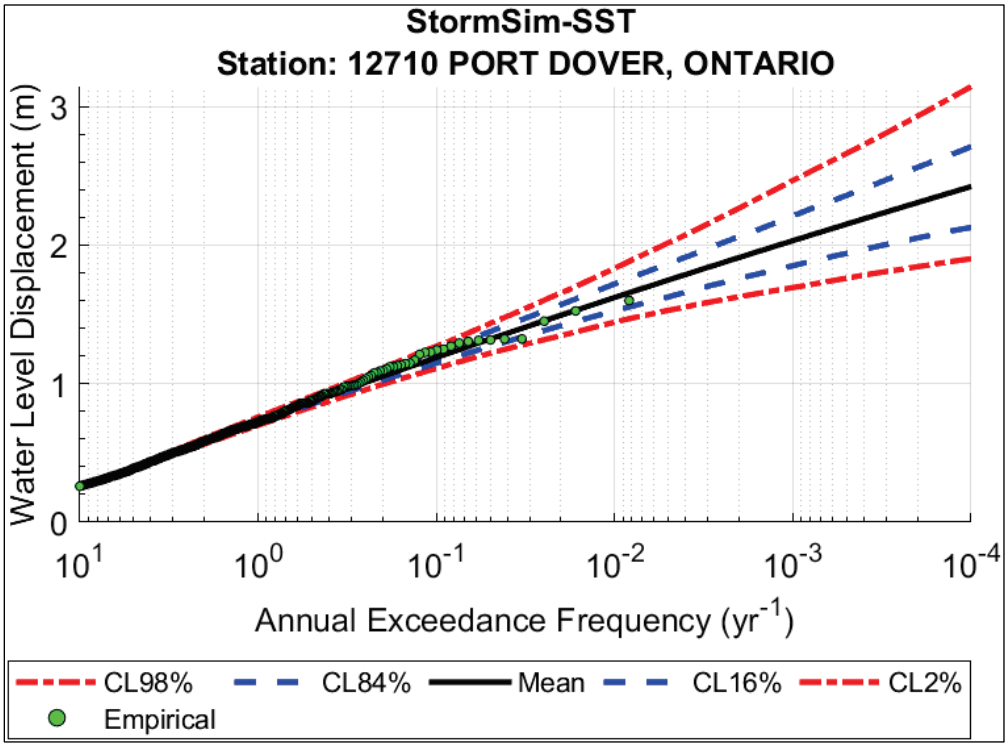

Figure F-8. RFA hazard curve (combined hourly data) at Port Colborne, Ontario.

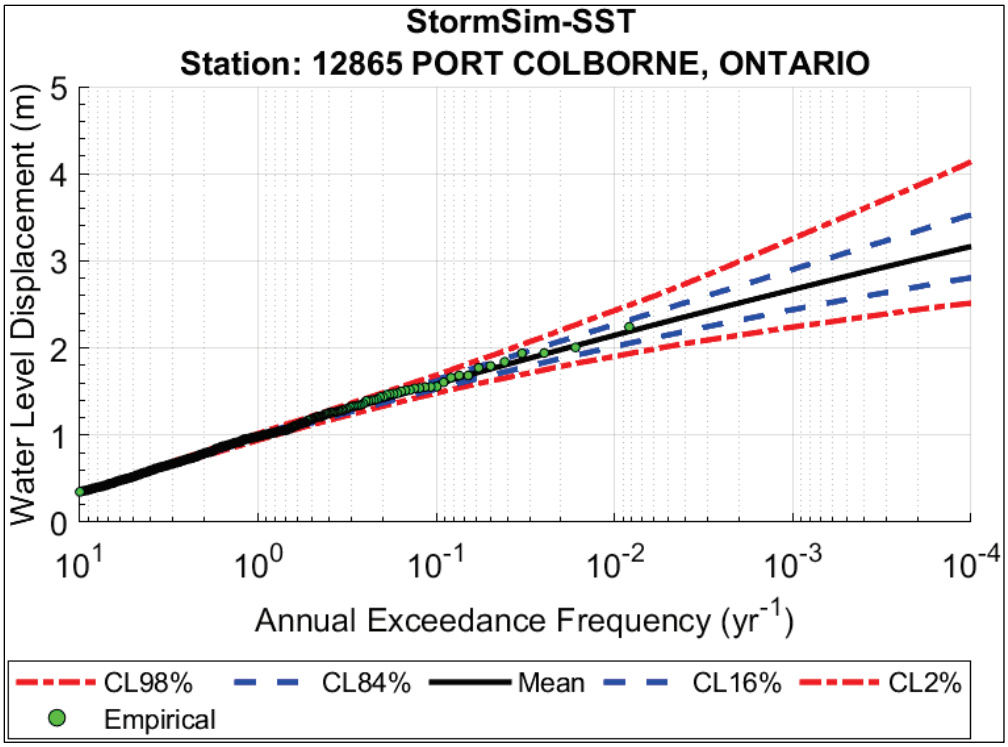

Figure F-9. Hazard curve (combined hourly data) at Gibraltar, Michigan.

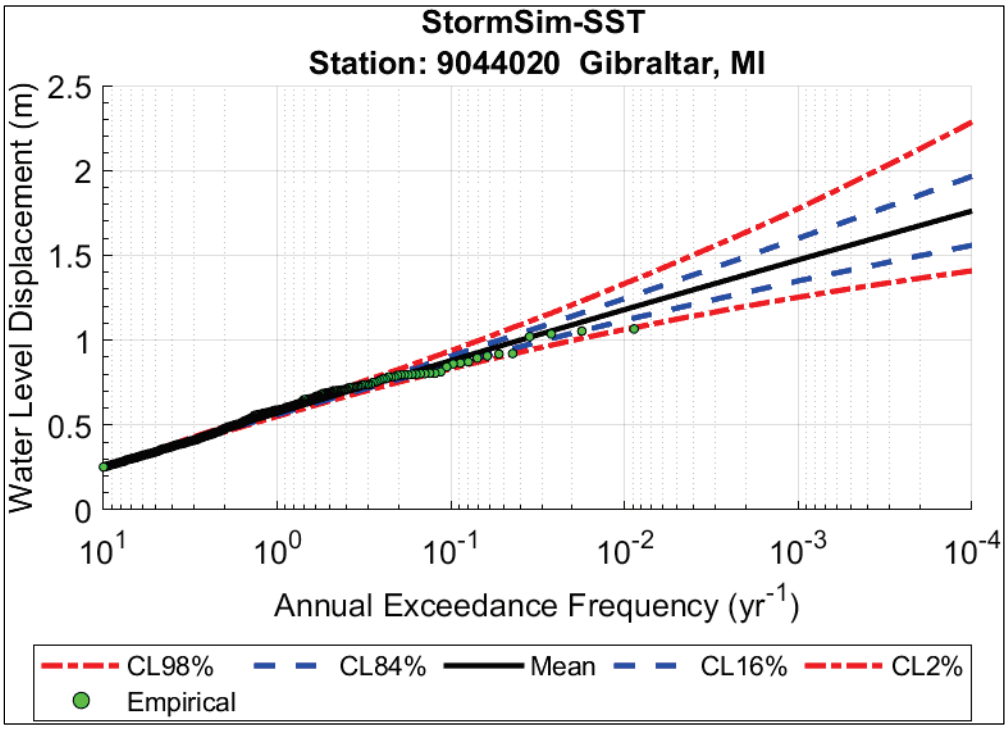

Figure F-10. RFA hazard curve (combined hourly data) at Sturgeon Point, New York.

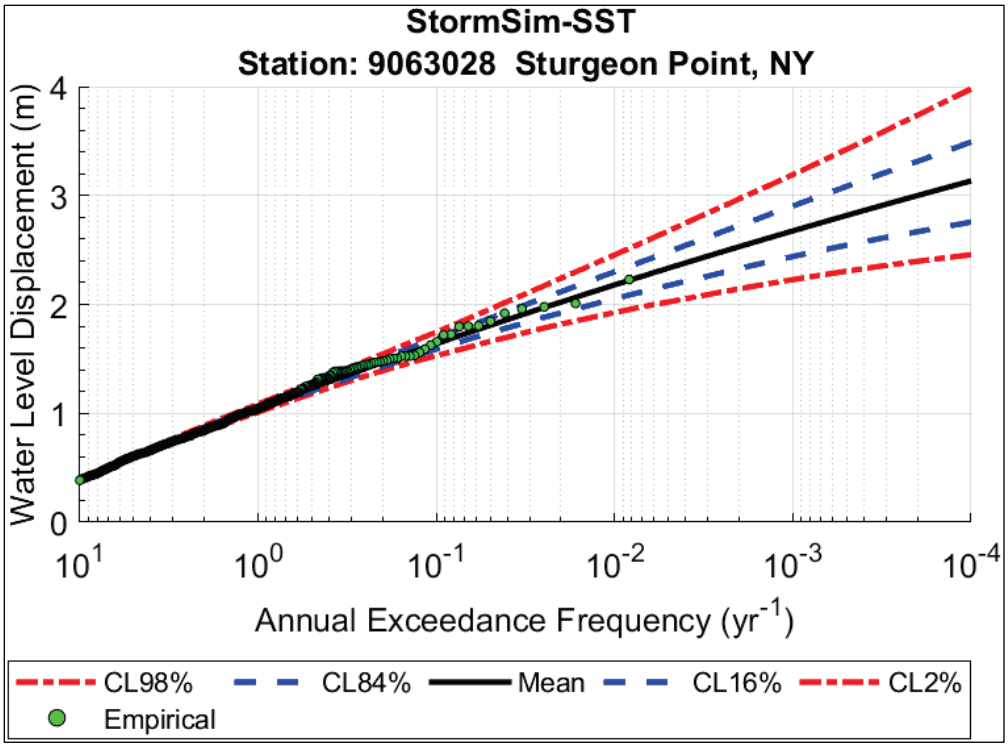

Figure F-11. RFA hazard curve (combined hourly data) at Barcelona, New York.

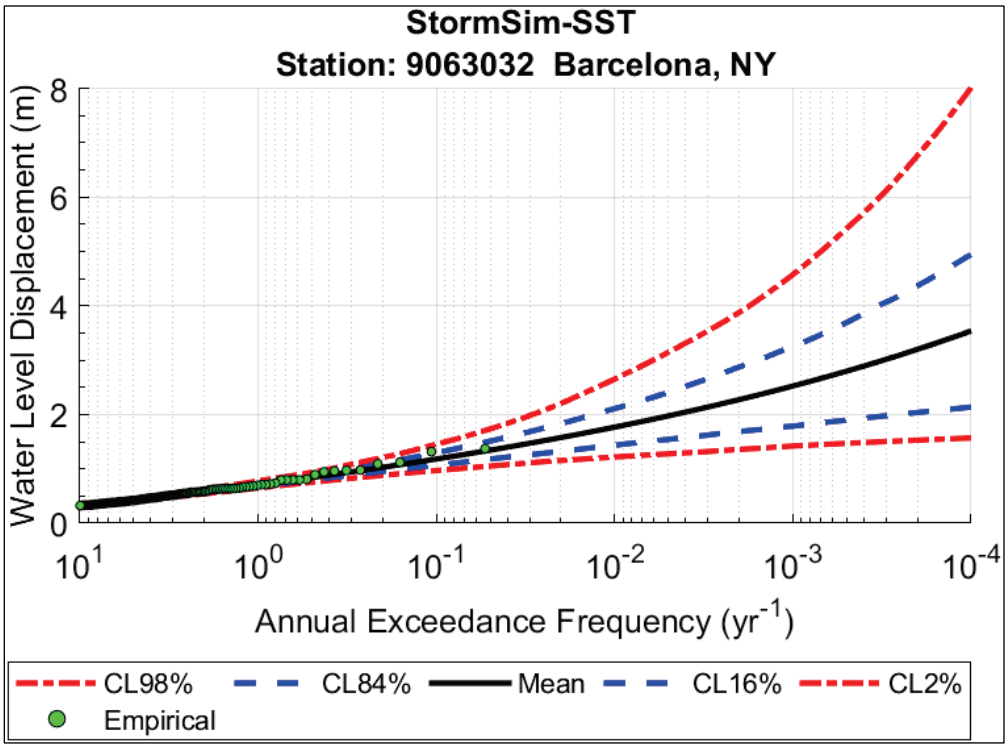

Figure F-12. RFA hazard curve (combined hourly data) at Erie, Pennsylvania.

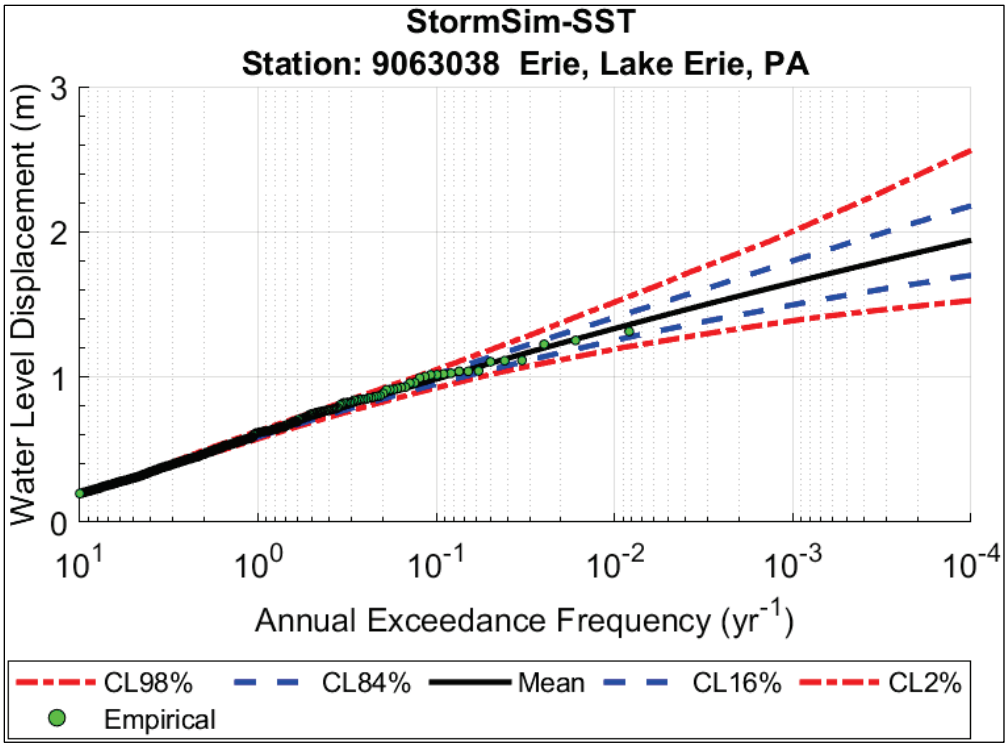

Figure F-13. RFA hazard curve (combined hourly data) at Fairport, Ohio.

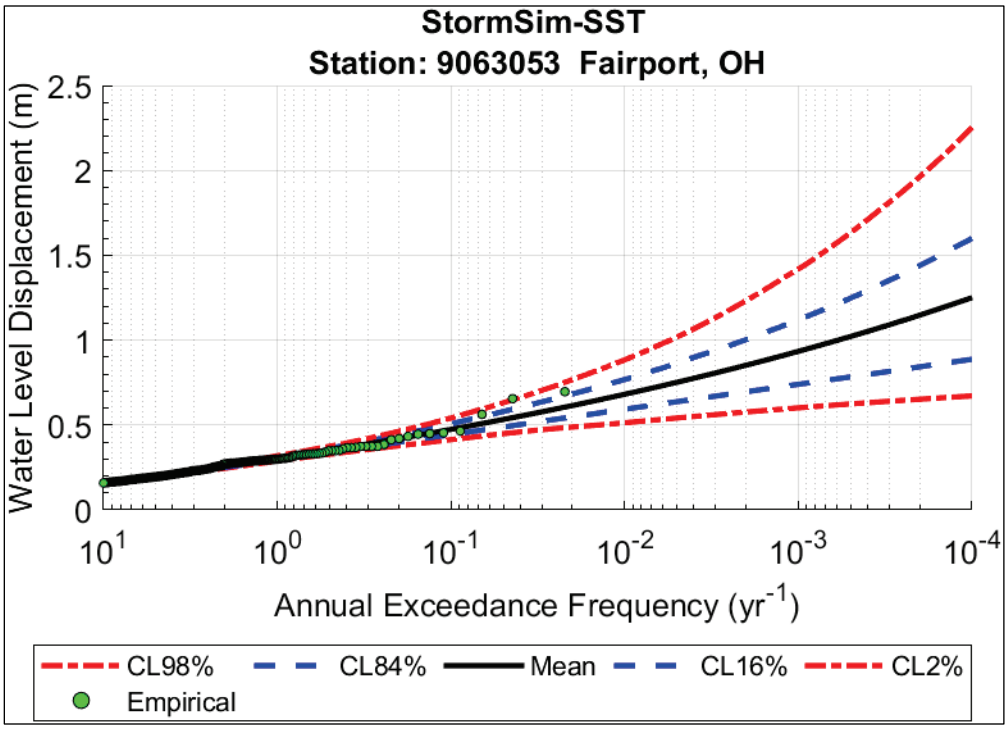

Figure F-14. RFA hazard curve (combined hourly data) at Lorain, Ohio.

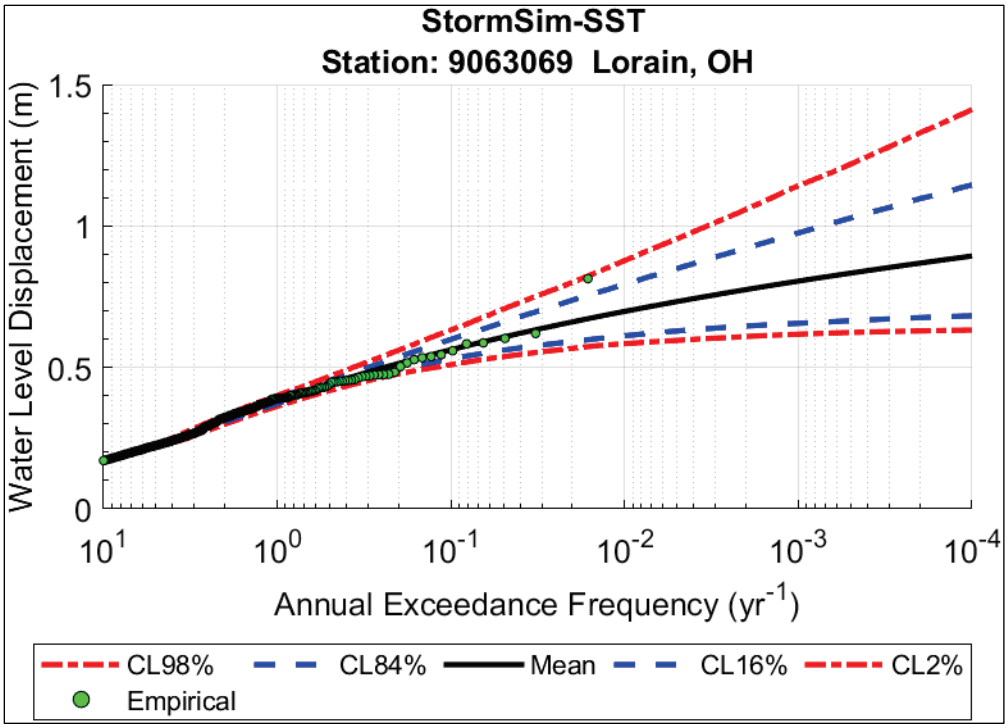

Figure F-15. RFA hazard curve (combined hourly data) at Marblehead, Ohio.

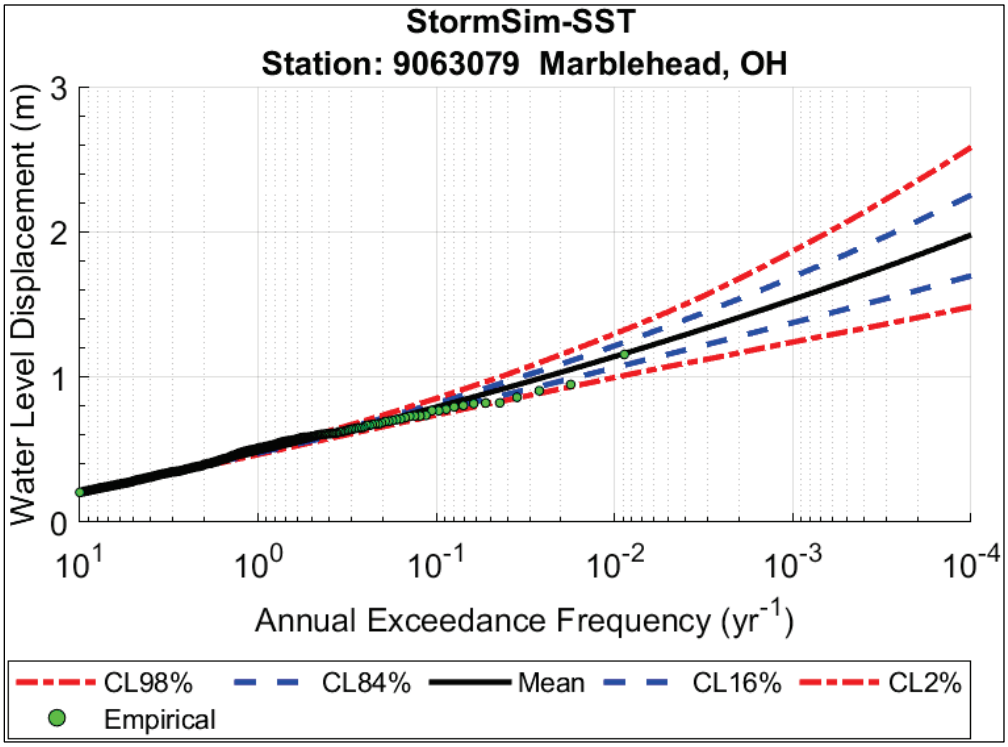

Figure F-16. RFA hazard curve (combined hourly data) at Monroe, Michigan.

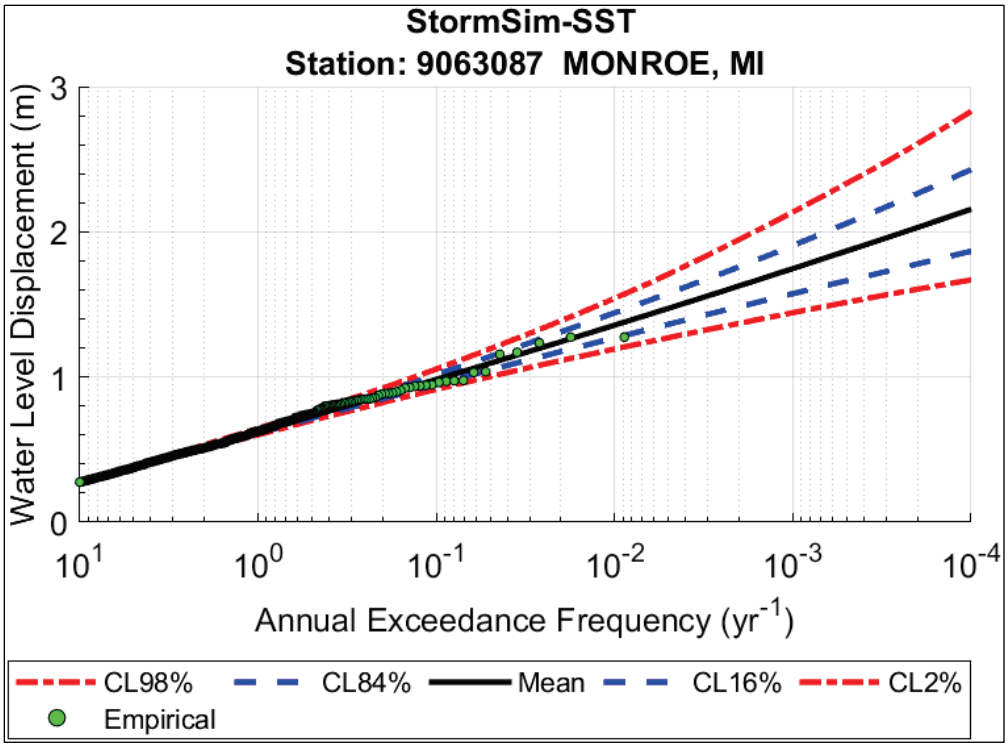

Figure F-17. RFA hazard curve (combined hourly data) at Fermi Power Plant, Michigan.

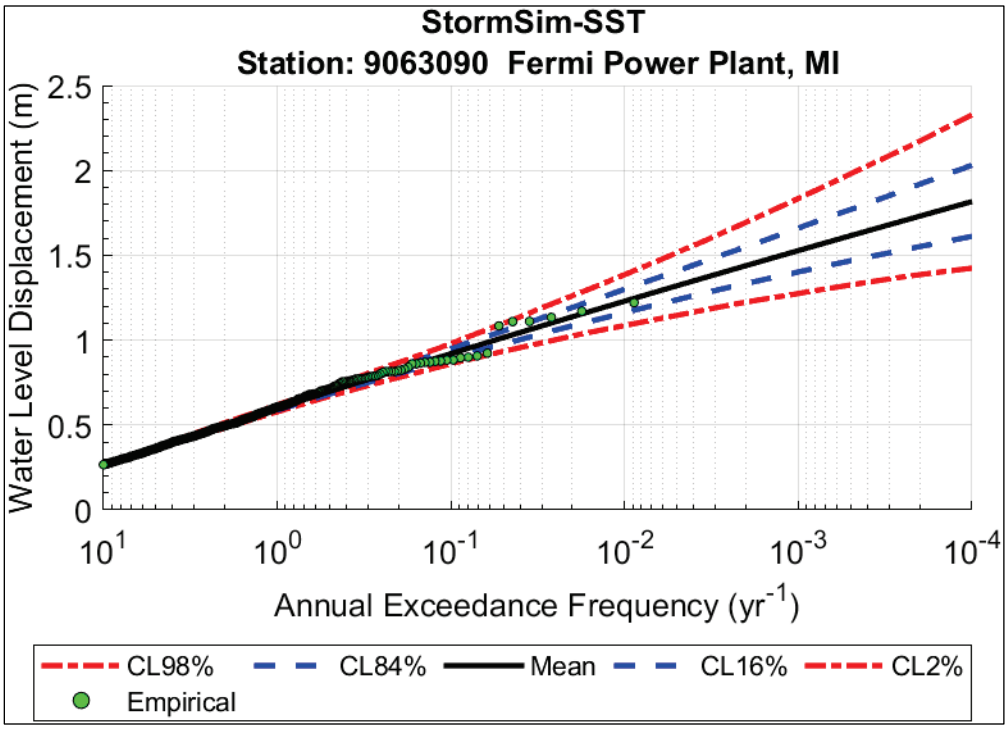

Abbreviations

ADCIRC	Advanced Circulation
AEF	Annual exceedance frequency
AEP	Annual exceedance probability
ARI	Average recurrence interval
CHL	Coastal and Hydraulics Laboratory
CHS	Coastal Hazards System
CI	Confidence interval
CL	Confidence limit
CO-OPS	Center for Operational Oceanographic Products and Services
CPD	Cycles per day
ERDC	US Army Engineer Research and Development Center
ESE	Empirical spatial extremogram
EST	Empirical simulation technique
GLCFS	Great Lakes Coastal Flood Study
GPD	Generalized Pareto distribution
HH	Hourly
HHMM	Combined
ID	Identification
IIR	Infinite impulse response
LFA	Local frequency analysis
MLL	Mean lake level

MRL	Mean residual life
MSL	Mean sea level
PDS	Partial duration series
POT	Peaks-over-threshold
PSD	Power spectral density
PST	Probabilistic Simulation Technique
RFA	Regional frequency analysis
RFM	Regional frequency model
RMSE	Root-mean-square error
SST	Stochastic Simulation Technique
StormSim	Storm Simulation
USACE	US Army Corps of Engineers
WLD	Water-level displacement
WMSE	Weighted mean-square error

REPORT DOCUMENTATION PAGE

1. REPORT DATE	2. REPORT TYPE	3. DATES COVERED	
May 2024	Final Technical Report (TR)	START DATE FY23	END DATE FY24

4. TITLE AND SUBTITLE

Statistical Analysis of Storm Surge and Seiche Hazards for Lake Erie

5a. CONTRACT NUMBER	5b. GRANT NUMBER	5c. PROGRAM ELEMENT
5d. PROJECT NUMBER	**5e. TASK NUMBER**	**5f. WORK UNIT NUMBER**

6. AUTHOR(S)

Efrain Ramos-Santiago, Norberto C. Nadal-Caraballo, Fabian Garcia-Moreno, Luke A. Aucoin, Meredith L. Carr, Madison C. Yawn, and Jeffrey A. Melby

7. PERFORMING ORGANIZATION NAME(S) AND ADDRESS(ES)

US Army Engineer Research and Development Center (ERDC)
Coastal and Hydraulics Laboratory (CHL)
3909 Halls Ferry Road
Vicksburg, MS 39180-6199

8. PERFORMING ORGANIZATION REPORT NUMBER

ERDC/CHL TR-24-12

9. SPONSORING/MONITORING AGENCY NAME(S) AND ADDRESS(ES)

US Army Corps of Engineers (USACE)
Detroit District
477 Michigan Ave.
Detroit, MI 48226

10. SPONSOR/MONITOR'S ACRONYM(S)

11. SPONSOR/MONITOR'S REPORT NUMBER(S)

12. DISTRIBUTION/AVAILABILITY STATEMENT

Distribution Statement A. Approved for public release: distribution is unlimited.

13. SUPPLEMENTARY NOTES

Funded by Labor Charge Code

14. ABSTRACT

Storm surge and seiche events are generally forced by severe storms, initially resulting in a wind-driven super elevation of water level on one or more sides of a lake (surge) followed by a rebound and periodic oscillation of water levels between opposing sides of the lake (seiche). These events have caused flooding along Lake Erie and significant damages to coastal communities and infrastructure. This study builds upon statistical analysis methods initially developed for the 2012 federal interagency Great Lakes Coastal Flood Study. Using the Coastal Hazards System's stochastic Storm Simulation (StormSim) suite of tools, including the Probabilistic Simulation Technique (PST), and a regional frequency model, historical extreme events were assessed in a local frequency analysis and a regional frequency analysis to quantify the annual exceedance frequency (AEF) of WLD events specific to Lake Erie. The objective of this study was to quantify AEFs of storm surge and seiche hazards to provide a better understanding of these events to aid flood mitigation and risk reduction for lakeside properties.

15. SUBJECT TERMS

Erie, Lake; Hydraulic structures; Seiches; Statistics; Storm surges; Water waves

16. SECURITY CLASSIFICATION OF:			17. LIMITATION OF ABSTRACT	18. NUMBER OF PAGES
a. REPORT	b. ABSTRACT	C. THIS PAGE		
Unclassified	Unclassified	Unclassified	SAR	141

19a. NAME OF RESPONSIBLE PERSON	19b. TELEPHONE NUMBER (include area code)